DOCTORAL THESIS

NANOFLUIDS BASED ON METAL NANOPARTICLES WITH OPTIMIZED THERMAL PROPERTIES FOR BEING USED IN THERMOSOLAR INDUSTRY

Roberto Gómez Villarejo

Supervisors:

Dr. Javier Navas Pineda | University of Cadiz

Dra. Elisa Isabel Martín Fernández | University of Seville

Thesis committee:

Dr. David Zorrilla Cuenca | University of Cadiz

Dr. Gaweł Żyła | Rzeszów University of Technology

Dr. Luis Lugo Latas | University of Vigo

External examiners:

Dr. Juan José Nogueira Pérez | The Australian National University

Dr. Nicolás Ramos Berdullas | University of Vienna

UCA | Universidad de Cádiz

Facultad de Ciencias
Departamento de Química Física
Universidad de Cádiz

DOCTORAL THESIS

NANOFLUIDS BASED ON METAL NANOPARTICLES WITH OPTIMIZED THERMAL PROPERTIES FOR BEING USED IN THERMOSOLAR INDUSTRY

The doctoral candidate Mr. Roberto Gómez Villarejo presents the memory of the Doctoral Thesis, supervised by Dr. Francisco Javier Navas Pineda and Dr. Elisa Isabel Martín Fernández, and carried out in the Department of Physical Chemistry of the Faculty of Sciences of University of Cadiz, between 2015-2018 academic years, and ensure that meets all the requirements established by current legislation and assumes the right to obtain of the degree of Doctor from University of Cadiz.

Mr. Roberto Gómez Villarejo

Dr. Francisco Javier Navas Pineda

Dr. Elisa Isabel Martín Fernández

Cádiz, December 2018

Agradecimientos

Agosto de 2015. Me acercaba al centro de Jerez para tomarme un aperitivo inocente con algunos amigos. Tras un año prácticamente en blanco, y preparándome para afrontar la búsqueda de trabajo en Barcelona, recibo una llamada. Y he aquí donde empiezan los agradecimientos…

En primer lugar, estaré eternamente agradecido a D. Francisco Javier Navas, autor de esa llamada, cuya oferta era realizar una Tesis Doctoral. No entraba en mis planes, pero no la pude rechazar. No he podido tener mejor director de Tesis. Haciendo más veces de "poli bueno" que de "poli malo", siempre me he sentido guiado y arropado. *Veeenga* y *paaaper* son palabras que siempre irán conmigo. Un millón de gracias se quedan cortas.

La segunda sorpresa fue saber que mi primer codirector de Tesis Doctoral sería D. Antonio Sánchez Coronilla. Nunca fue mi profesor, pero tenemos un sinfín de anécdotas ferroviarias. Desde estas líneas quiero agradecerte que apostaras por mí en un campo, la Química Teórica, totalmente desconocido para mí. Gracias por apoyarme en todos los sentidos: congresos, estancia, presentaciones,... y por estar siempre con una buena sonrisa. De nuevo, un millón de gracias se quedan cortas.

Mi tercera y grata sorpresa fue conocer a la que actualmente es mi codirectora de Tesis Doctoral, Dª. Elisa Martín. Eli, gracias por tu paciencia, por ayudarme y enfadarte en los momentos claves. A veces uno necesita un toque de atención. Gracias enormemente por mostrarme con mucho cariño, junto a Antonio, una nueva visión de la Química. Os debo mucho a ambos en este aspecto. Otra vez, un millón de gracias se quedan cortas.

Gracias de corazón a D. Rodrigo Alcántara, D. David Zorrilla, Dª. Concha Fernández y Dª. Pilar Martínez. Quién me diría que compartiría y aprendería en las prácticas de laboratorio con ustedes. Aunque no lo parezca, enfrentarme en un laboratorio a unos alumnos universitarios no me fue fácil, pero siempre me sentí protegido por ustedes. Gracias a Desi que, aunque por motivos maternales no haya estado en el final del camino, siempre me dejaste tu rincón para pensar. También me acuerdo de D. Jesús Ayuso, D. Joaquín Martín, D. Jesús Sánchez, Dª. Ana Mena y demás compañeros del departamento, quizás no tengan una mención en la elaboración de esta Tesis Doctoral, pero un "buenos días" y una sonrisa hacen más llevaderos los día a día.

Y aquí seré breve: gracias Tere (Tereee, ¿qué?, naaa), gracias Iván (*aiván*, tu eres mi amigo fiel, *aiván*…), gracias JJ (el i30 NO es coche de mujer), gracias Paloma (¡que desastre!), gracias Fany (nanofluido de cobre/oro/no pongas nada), gracias Miriam (no hay emoticono pulcro y decente, ya sabes), gracias Fran (tose fuerte siempre, amigo), gracias Sara (mi primera presentación en inglés), gracias Mawi (por ese Ford Focus que nunca me compré), y gracias a todos los estudiantes que hicieron su TFG y de una forma u otra compartimos juntos unas cuantas anécdotas. Somos un buen grupo.

Y antes de comenzar con familiares, gracias de corazón a D. Patrice Estellé. Rennes, los idiomas, vivir solo, ...todo ello me generaba inseguridad. La inseguridad se fue al conocerte. Siempre me tendiste la mano, me invitaste a conocer lugares, la gastronomía francesa, disfrutar de la estancia,…sería un placer volver a coincidir contigo.

Mis recuerdos a los que están arriba. Mis cuatro abuelos y mi tío Paco. Desearía saber que estáis orgullosos de verme llegar hasta aquí. Os querré siempre.

A mis padres, Vicente y Pilar. Quién os iba a decir que vuestros dos hijos serían doctores. Sin ustedes no habríamos conseguido nada. No puedo agradeceros lo que soy ahora. No hay palabras. Espero que vuestros (muchos) esfuerzos estén siendo recompensados. Decir que sois los mejores padres que existen es un tópico, decir que sois lo mejor que tengo es una verdad. Merecéis más que un gracias. Os quiero más de lo que os lo demuestro. Quizás debería deciros más veces que os quiero. Os quiero.

A mi hermano, David. Aunque seas mi hermano "menor" eres un referente para mí y aunque te abriera el camino siempre sabía que me adelantarías. Créeme que estoy orgulloso de que mi hermano sea lo que es hoy en día. Espero que tú también lo estés de mí. También tienes tu parte de culpa en esta Tesis Doctoral. Te quiero.

Y gracias de corazón a todos mis familiares. Mis tíos y primos de Madrid: siempre habéis sido mi Familia de Madrid y así os seguiré llamando. A mi madrina Toñi y mis primos Alejandro y Alicia, de Zaragoza: siempre seréis especiales. A mi tío Gonzalo, por ser tan cercano y tener su favoritismo en ausencia de mi hermano; mi tía Gloria y mi prima Patri, no me olvido; mis tíos Salvador y Anabel, mis primos Alejandro e Iván, tampoco os olvido. Os quiero a todos. Sois mi familia, y como dice la película: *la familia es lo más importante*.

INDEX

"Nanofluids based on metal nanoparticles with optimized thermal properties for being used in thermosolar industry"

Chapter 1

Abstract

1. Abstract

The proximity of the end of fossil fuels as our main source of energy, together with the huge demand for energy resulting from the exponential growth of the world's population and high levels of industrial and residential development has led to the commitment to energy from natural, clean and renewable resources becoming, to say the least, a short-term obligation. Taking advantage of new sources of energy from the sun, water or wind, among others, would lead to a rationalization of energy production and a decrease in pollution and the emission of harmful gases.

In recent decades, solar power has been the natural source of energy that has generated most interest, playing a more and more important role in the management and production of energy on a global scale. Within this field, in addition to photovoltaic solar power, an interesting option to emerge is that of concentrating solar power, and in particular thermosolar plants that use parabolic trough mirrors as concentrators of solar radiation. In this kind of plants, sunlight is concentrated in order to heat a fluid, which stores thermal energy to then generate steam in a heat exchanger, which drives a turbine to produce electricity. Spain is one of the world leaders in the production of this kind of energy, which provides the perfect framework for the topic of this Doctoral Thesis.

However, to become a high-yield source of energy with the capacity to store energy without the need for joining forces with other plants or power stations, the overall efficiency of concentrating solar power plants must improve. This can be achieved by optimising some of its components, such as the thermal properties of the heat transfer fluid, which are generally thermal oils that present low thermal conductivity values. One alternative to thermal fluids, discovered over twenty years ago, is based on the suspension of nanometric solid particles, one result of which is an increase in thermal conductivity with regard to the traditional fluids. These new fluids have been known since then as nanofluids.

Metals such as silver, gold and platinum present far greater thermal conductivity than the base fluid commonly used in the thermosolar industry, which is a thermal oil consisting of the eutectic mixture of diphenyl oxide and biphenyl. Therefore, this Doctoral Thesis has established as its main aims to design and prepare nanofluids based on silver, gold and platinum nanoparticles through the use of different methods. The nanofluids prepared were characterized for their temporal stability and a possible increased efficiency as a heat transfer fluid, taking

into consideration their thermal and rheological properties. The results obtained show, amongst other aspects, that metal nanoparticles improve the thermal conductivity of nanofluids (improvements reaching 70% for the gold-based nanofluids and 37% for those based on platinum). Furthermore, despite the fact that the addition of nanomaterial and additives such as surfactants leads to inherent increases in viscosity, which is counter-productive in terms of efficiency, the nanofluids presented significant improvements in the efficiency of heat transfer processes with regard to the base fluid (from 6% in the case of the silver-based nanofluids to 36% for matching nanofluids based on gold). In turn, the nanofluids prepared were shown to reach a level of temporal stability that allows for long-lasting suspension of the nanomaterial, limiting the agglomeration and precipitation phenomena that are inherent to nanomaterials in this kind of colloidal suspension. In this respect, the use of phase transfer agents and surfactants is essential for the nanomaterial to be incorporated into the base fluid and to improve the suspension of the nanomaterial. Finally, it was also shown that applying sonication treatment is vital for ensuring that the greatest possible amount of the nanomaterial is dispersed into the base fluid used. The combination of this treatment and the presence of surfactants has been shown to be a beneficial strategy.

Moreover, with the aim of increasing our knowledge and understanding of these systems, and to complement the experimental study, we proceeded to perform a theoretical, molecular-level analysis of the nanofluid systems by means of Molecular Dynamics simulations. Technological advances and the development of large, efficient computer clusters has enabled studies of real systems using simulations to become more common in the field of chemistry in general, and in the field of nanofluids in particular.

The three nanofluid systems prepared in this Doctoral Thesis were analysed using Molecular Dynamics simulations in order to determine their thermal and transport properties of interest and to understand through the analysis of their structural properties how the molecules of the base fluid and surfactants are organised around the silver, gold and platinum nanoparticles. The results calculated for isobaric specific heat and thermal conductivity show that the addition of metal nanoparticles results in improvements in both properties, in agreement with the trend obtained experimentally. In turn, the analysis of radial and spatial distribution functions reveals the dynamic arrangements of the base fluid and surfactant molecules around the nanoparticles, and how these molecular layouts affect the stability of the nanofluids and the enhancement of thermal properties.

Thus, the study of nanofluids based on silver, gold and platinum nanoparticles and using a thermal oil consisting of the eutectic mixture of diphenyl oxide and biphenyl as the base fluid shows that these new fluids present an adequate level of stability over time and a promising increase in efficiency in heat transfer processes. This is mainly due to a significant increase in thermal conductivity values, which makes their direct application in high temperature concentrating solar power plants to replace the currently used heat transfer fluids recommendable and viable.

Chapter 2

Introduction and justifiction

2. Introduction and justification

2.1. Current energy situation

While the mystery remains about when the first hominids appeared and how they evolved until our species, and although it is impossible to be categorical about the origin of humanity, we can indeed confirm that from those beginnings until now humanity and society have advanced meteorically towards the present day, in which we could define humanity as an anthropophagic and energivorous entity. Humans have become the biggest threat to the planet: overpopulation, a shortage of basic resources, overexploitation of natural sources, pollution on a planetary scale, and uncontrollable energy consumption. A sustainable future for the planet is in the hands of a society that is cradled in its comfort zone and well-being.

The definition of society as energivorous is a term that has been the focus of attention of politicians worldwide for decades. To reduce the pollution produced by generating energy from fossil fuels and the commitment to change to clean and renewable sources of energy are among the most common promises made by governments at the present time. However, this year's Global Status Report (GSR) reveals two truths: the revolution of the energy sector is promoting a change towards a future based on renewable energy, but the transition taking place worldwide is not occurring fast enough [1].

In 2016, modern renewable energy contributed 10.4% of the total final energy consumption worldwide, a larger contribution than that of nuclear and traditional biomass energy, but far below the 79.5% provided by fossil fuels (Figure 2.1.1).

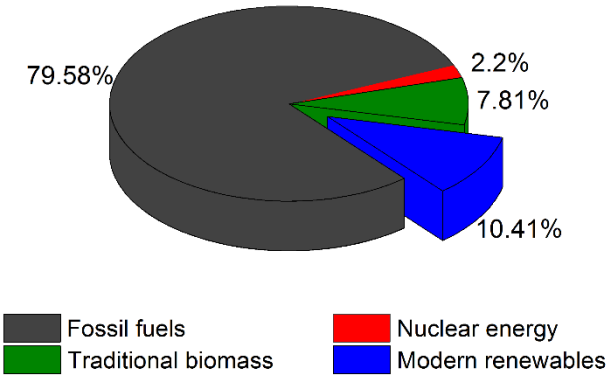

Figure 2.1.1. Participation of energy sources in the total final consumption in 2016 [1].

In 2017, the production capacity of energy from renewable sources increased by 9% with regard to the previous year, largely thanks to a strong commitment to the three most common sources of renewable energy: photovoltaic solar (55%), wind (29%) and hydroelectric (11%).

Although these data indicate that the transition towards renewable energy is possible, the progress made is not the same in all sectors, as shown by Figure 2.1.2. The two main sectors, which consume around 80% of the world's energy, receive very different contributions from renewable energy: the heating and cooling sector represents 48% of the final energy use, of which 27% is supplied by renewable energy, while the transport sector constitutes 32%, of which only 3% comes from renewable sources. Neither of these sectors currently receives a great deal of attention from governments. The remaining 20% is mainly destined to the generation of electricity, of which 25% comes from renewable energy.

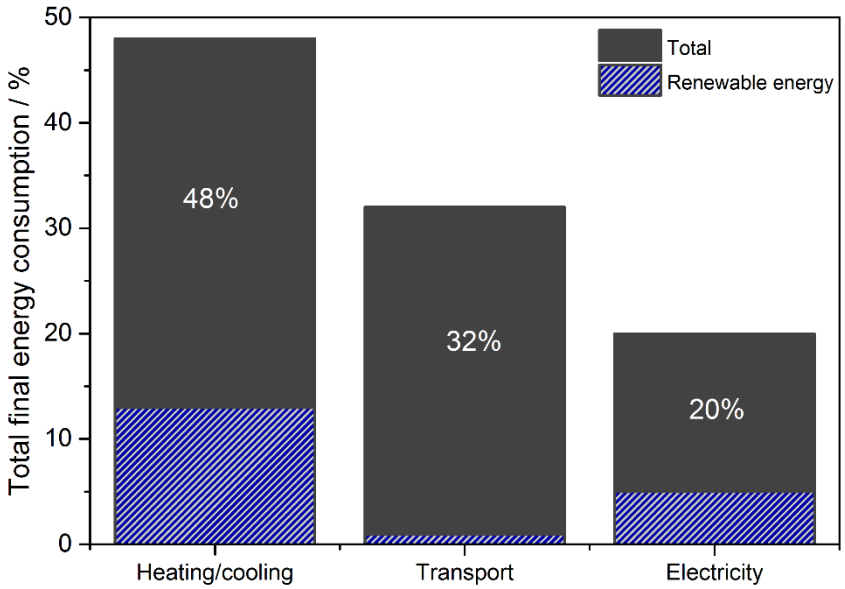

Figure 2.1.2. Contribution of renewable energy by sectors [1].

2.2. Concentrating solar power

Solar power is the cleanest and most abundant renewable resource on the planet and, taking on the role of the most favourable source of energy, it is in a position to play a leading role in supplying the world's energy in the future. There are two kinds of technology that enable electricity to be generated from solar radiation.

On the one hand, photovoltaic solar power converts radiant energy into electrical energy by means of semiconductor materials based on the photovoltaic effect. At present, as Figure 2.2.1 shows, it is the energy with the highest annual growth rate, increasing from 302 GW in 2016 to 402 GW the following year, mainly due to the decrease in market costs, industrial competitiveness and the transfer of capital by companies in the oil sector.

On the other hand, concentrating solar power (CSP) emerged at a later date than photovoltaic solar power, reaching the commercial market in 2007; it is based on the concentration of solar radiation to obtain heat energy. This heat energy is used to generate steam that, after passing through a turbine, produces electricity.

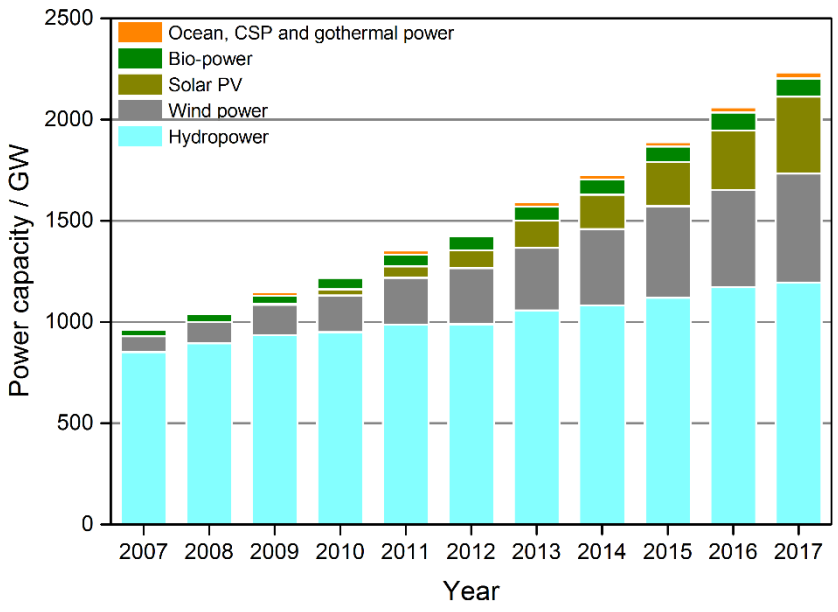

Figure 2.2.1 Annual global capacity of renewable energy [1].

As Figure 2.2.1 shows, the total contribution of this kind of energy reached 5 GW in 2017, a 2% increase on the previous year. The challenge for CSP is to achieve the objectives set by the International Energy Agency (IEA) for 2020 (147 GW) and 2050 (1089 GW) [2], and become the backbone of future energy systems [3].

Photovoltaic solar power systems necessarily consist of two main components: a photovoltaic module (solar panel) and a power inverter that changes direct current to alternating current. Both components are basic elements that are easily accessible, a wide variety being available on the market. However, CSP plants are more complex systems. There are currently four kinds of CSP technology [4], as shown in Figure 2.2.2:

- Parabolic trough collectors or concentrators (PTC): consist of a solar field containing lines of parabolic trough-shaped mirrors that concentrate the incident solar radiation onto an absorber tube through which a heat transfer fluid circulates.

- Central tower receivers: consist of a solar field formed by heliostats that concentrate incident solar radiation onto a receiver located at the top of a tower.

- Linear Fresnel reflectors: use flat or slightly curved mirrors that can rotate around an axis to direct incident solar radiation towards a linear receptor (absorber tube) located above them.

- Stirling parabolic dishes: dishes shaped like a satellite dish that concentrate solar radiation onto a small receptor located on a focal point of the reflector, connected to a small motor (Stirling).

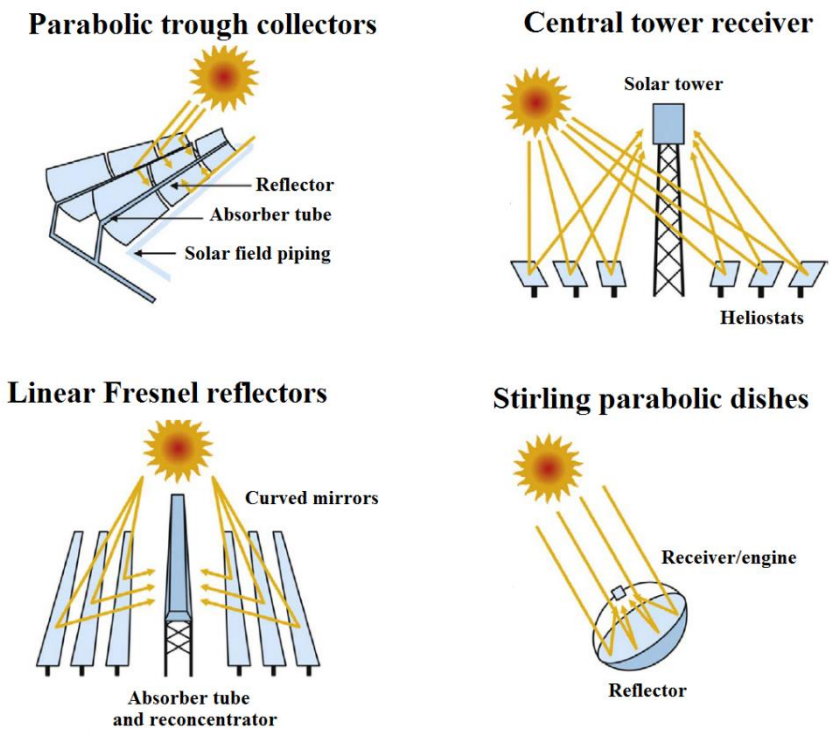

Figure 2.2.2. Types of CSP plants [5].

Although each kind of CSP plant has a different mechanism for concentrating solar radiation, they all share three common elements [6]. Taking as a specific example a CSP plant using parabolic trough technology, shown in Figure 2.2.3, the elements they have in common are:

i. Solar field: where the mirrors, also called heliostats, receptors, collector systems, etc. are to be found.

ii. Heat transfer fluid circuit, which may include a thermal energy storage (TES) unit.

iii. Power block, where the thermal energy obtained from solar power is converted into electrical energy.

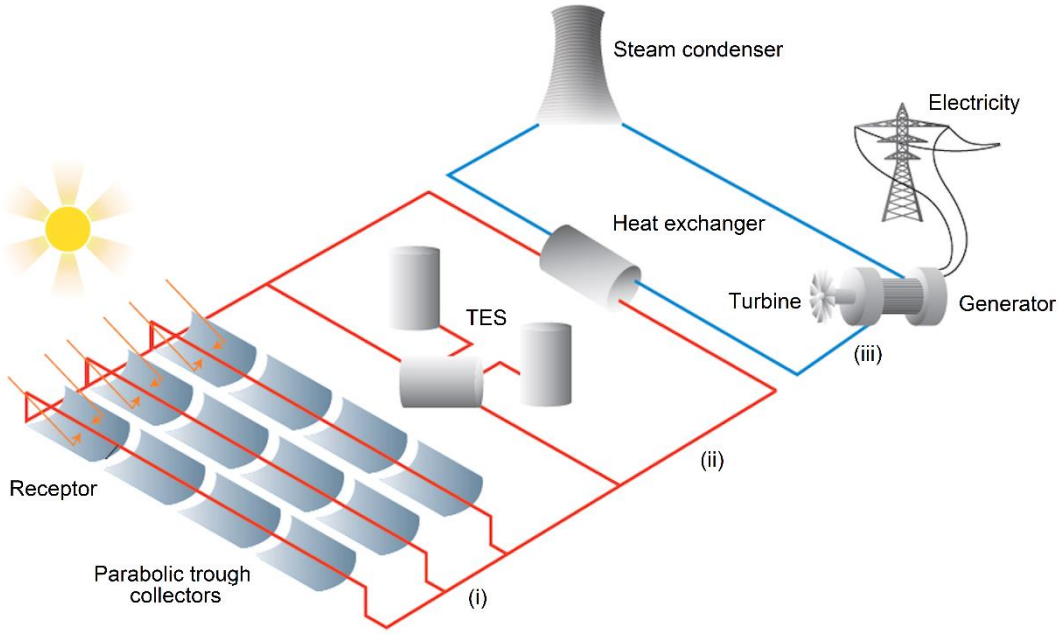

Figure 2.2.3. Image of a parabolic trough collector CSP plant [7], where: (i) is the solar field, (ii) is the heat transfer fluid circuit, and (iii) is the power block.

Thus, the cost of installing and maintaining a photovoltaic system or a CSP plant is clearly different. However, cost of running a parabolic trough-type CSP plant has decreased by 25% in five years, a higher figure than expected and more promising than the case of photovoltaic technology, where costs have decreased by 20.9% in 35 years [7]. In addition, the option of fitting CSP plants with a thermal energy storage system (TES) provides them with greater appeal than other power stations where it is necessary to combine different kinds of technology to obtain a balance between supply and demand [8]. TES units are now being incorporated into all CSP plants, which are providing fossil fuel power stations with tough competition [6, 7].

Spain is one of the world leaders in CSP technology, achieving a record total generation capacity in 2017 (2.3 GW). Together with the USA (with a total generation capacity of 1.7 GW), the two countries represent around 80% of the total capacity worldwide [9], as Figure 2.2.4 shows. In turn, for the second year running, South Africa has been the country with the highest investment in CSP [10], taking third place in this ranking and overtaking emerging countries such as China [11], India [12] and Morocco [13].

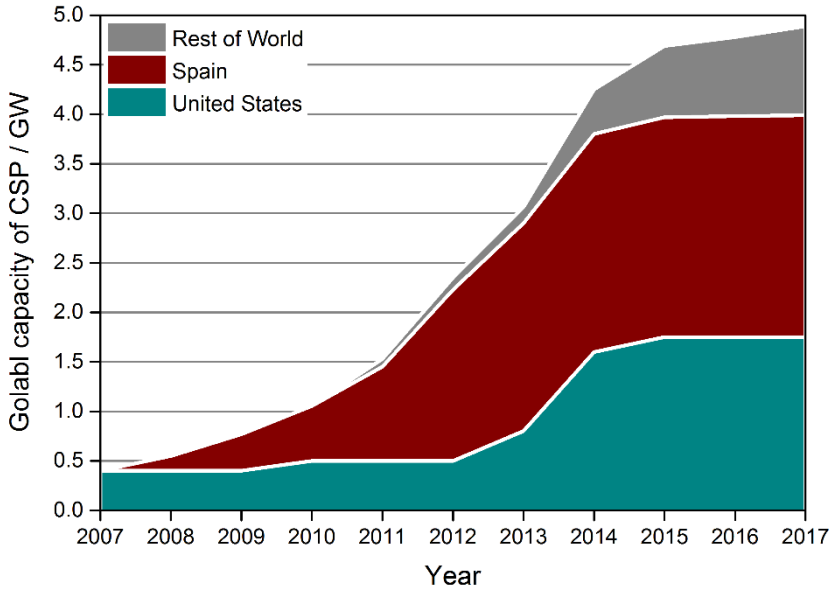

Figure 2.2.4. Contribution of countries to the total capacity of CSP [1].

Regarding the plans for new installations, China (with twenty plants), India, Morocco, Israel, Saudi Arabia, Chile and Australia have projects to build CSP plants, which will be finished in the next few years. In Europe there are plans to develop CSP plants in Denmark and France in 2018 [1]. However, neither Spain nor the USA has created new CSP plants since 2013 and 2015 respectively, and there are no plans to do so in coming years. Spain currently has 50 projects [14], 22 of which are in Andalusia, all based on parabolic trough technology with the exception of three solar towers in Seville. ***Annex 1*** includes a list of the thermosolar projects built in Spain.

2.3. Justification behind the topic of the Doctoral Thesis

To increase the profitability and efficiency of CSP plants, technological advances have focused on three aspects: first, improving the design of the reflector and collector, and the materials used; second, increasing the efficiency of absorption and heat transfer processes, thus increasing the energy output; and finally, minimizing energy losses in heat storage installations [6].

Regarding the second aspect mentioned, the impact exerted by nanoscience in every field of science and technology, including the energy sector, has led to the development of a new generation of heat transfer fluids, which have been given the name “nanofluids” [15].

Nanofluids are colloidal systems created by the dispersion of solid nanometric material into the heart of a base fluid. The presence of this suspended nanomaterial leads to enhanced thermal properties, in particular thermal conductivity [16-18]. Consequently, the development of nanofluids and the optimization of their properties for use in heat transfer processes have become established as the main challenges of numerous research groups worldwide. Figure 2.3.1 shows the growing trend over the last two decades of scientific publications of research that focuses on the word "*nanofluids*" (in the title, abstract and key words) according to the Scopus database, reaching a figure of over 11.000 articles.

During this time, a huge variety of nanomaterials have been used in the preparation of nanofluids: metallic [19, 20] and metallic oxide [21, 22] nanoparticles, two-dimensional [23, 24] and three-dimensional [25, 26] materials, carbides [27], etc.; and a wide range of base fluids: water [28], ethylene glycol [19, 29], methanol [30], thermal oils [31-33], molten salts [34], etc.; the range of applications of these nanofluids has been widened to include different areas connected with heat transfer: solar power [35], cooling [36], thermosyphons [37], automotion [38], micro-electronics [39], medical applications [40-42], safety of nuclear reactors [43], etc.

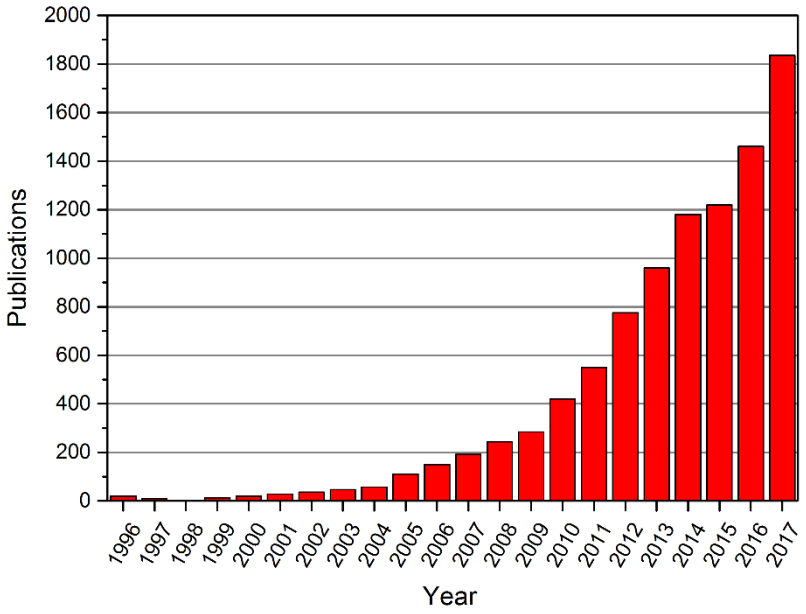

Figure 2.3.1. Publications including the key word "*nanofluids*" in the last two decades.

To reach a better understanding of these complex nanofluid systems, mathematical models and advances in computing have become essential tools in helping basic experimental science to study this kind of systems. Therefore, aiming to reach a compromise between experimental and theoretical approaches, as shown by Figure 2.3.2, simulations open a direct pathway between a macroscopic system and its microscopic properties, making it possible for experimental assays that are difficult to perform in real-world situations to become viable to study and analyse by means of a simulator.

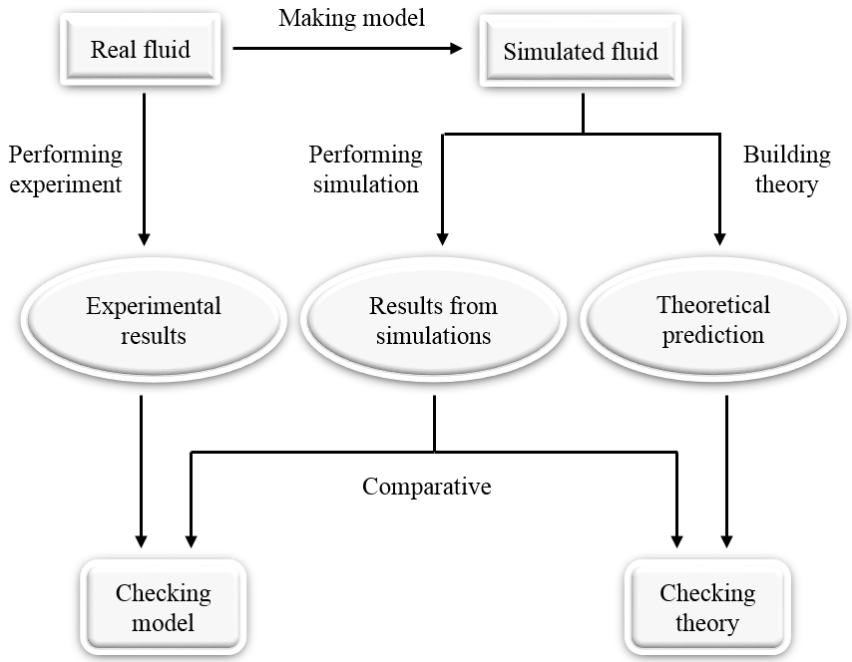

Figure 2.3.2. Flowchart of real system, simulated system and theory [44]**.**

The first simulations within the context of science date back to the fifties, highlighting the emergence of the Monte Carlo methods [45] and molecular dynamics [46]. The connecting link between nanofluids and simulation began during this century [47, 48] and theoretical studies of nanofluids, although quite scarce, have recently caught the attention of many researchers and are now becoming more prevalent. According to the *Scopus* database, of the approximately 11.000 articles published to date containing the word "*nanofluids*" (in the title, abstract and key words), only around 1.200 also contain the topic of "*molecular*

dynamics". However, the increasing popularity of this topic (Figure 2.3.3) is very similar to that of the main topic of nanofluids.

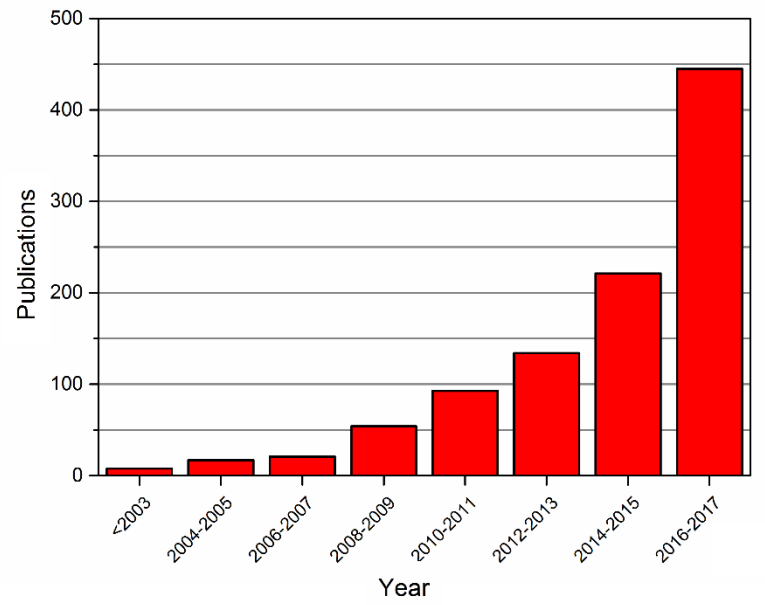

Figure 2.3.3. Publications including the key words "*molecular dynamics*" within the topic of nanofluids.

Thus, in view of the interest generated by this new field of theoretical and experimental research into nanofluids, this Doctoral Thesis will revolve around improving the efficiency of the heat transfer fluids used in thermosolar energy plants by means of the preparation of nanofluids based on metal nanoparticles. The nanofluids prepared will be characterized in depth. Their physical and chemical temporal stability will be determined and an analysis will be performed of their thermal properties, isobaric specific heat and thermal conductivity, which will enable the nanofluids prepared to be assessed for their efficiency as heat transfer fluids. Furthermore, molecular dynamics simulations of the nanofluid systems prepared experimentally will be performed in order to enhance our understanding of how they behave.

2.4. References

[1] Renewables 2018 Global Status Report. ISBN 978-3-9818911-3-3, (Paris: REN21 Secretariat) (2018).

[2] Technology Roadmap.Solar Thermal Electricity, International Energy Agency (IEA) <https://www.iea.org/>, (2014).

[3] P. Gauché, J. Rudman, M. Mabaso, W.A. Landman, T.W. von Backström, A.C. Brent, System value and progress of CSP, Solar Energy 152 (2017) 106-139.

[4] D.A. Baharoon, H.A. Rahman, W.Z.W. Omar, S.O. Fadhl, Historical development of concentrating solar power technologies to generate clean electricity efficiently – A review, Renewable and Sustainable Energy Reviews 41 (2015) 996-1027.

[5] W. Fuqiang, C. Ziming, T. Jianyu, Y. Yuan, S. Yong, L. Linhua, Progress in concentrated solar power technology with parabolic trough collector system: A comprehensive review, Renewable and Sustainable Energy Reviews 79 (2017) 1314-1328.

[6] S. Kuravi, J. Trahan, D.Y. Goswami, M.M. Rahman, E.K. Stefanakos, Thermal energy storage technologies and systems for concentrating solar power plants, Progress in Energy and Combustion Science 39(4) (2013) 285-319.

[7] R. Pitz-Paal, Concentrating solar power: Still small but learning fast, Nature Energy 2(7) (2017) 17095.

[8] G. San Miguel, B. Corona, Economic viability of concentrated solar power under different regulatory frameworks in Spain, Renewable and Sustainable Energy Reviews 91 (2018) 205-218.

[9] M.T. Islam, N. Huda, A.B. Abdullah, R. Saidur, A comprehensive review of state-of-the-art concentrating solar power (CSP) technologies: Current status and research trends, Renewable and Sustainable Energy Reviews 91 (2018) 987-1018.

[10] C.A. Pan, F. Dinter, Combination of PV and central receiver CSP plants for base load power generation in South Africa, Solar Energy 146 (2017) 379-388.

[11] L.E. Vieira de Souza, A.M. Gilmanova Cavalcante, Concentrated Solar Power deployment in emerging economies: The cases of China and Brazil, Renewable and Sustainable Energy Reviews 72 (2017) 1094-1103.

[12] J.P. Bijarniya, K. Sudhakar, P. Baredar, Concentrated solar power technology in India: A review, Renewable and Sustainable Energy Reviews 63 (2016) 593-603.

[13] T. Bouhal, Y. Agrouaz, T. Kousksou, A. Allouhi, T. El Rhafiki, A. Jamil, M. Bakkas, Technical feasibility of a sustainable Concentrated Solar Power in Morocco through an energy analysis, Renewable and Sustainable Energy Reviews 81 (2018) 1087-1095.

[14] Protermosolar,Asociación Española de la Industria Solar Termoeléctrica <https://www.protermosolar.com/> (2018).

[15] S.U.S. Choi, J. A. Eastman, Enhancing thermal conductivity of fluids with nanoparticles, ASME-Publications-Fed 231 (1995) 99-106.

[16] S. Lee, S.U.S. Choi, S. Li, J.A. Eastman, Measuring thermal conductivity of fluids containing oxide nanoparticles, Journal of Heat Transfer-Transactions of the ASME 121(2) (1999) 280-289.

[17] E.V. Timofeeva, A.N. Gavrilov, J.M. McCloskey, Y.V. Tolmachev, S. Sprunt, L.M. Lopatina, J.V. Selinger, Thermal conductivity and particle agglomeration in alumina nanofluids: experiment and theory, Physical Review E 76(6) (2007) 061203.

[18] J.H. Lee, K.S. Hwang, S.P. Jang, B.H. Lee, J.H. Kim, S. Choi, C.J. Choi, Effective viscosities and thermal conductivities of aqueous nanofluids containing of Al_2O_3 low volume concentrations nanoparticles, International Journal of Heat and Mass Transfer 51(11-12) (2008) 2651-2656.

[19] J.A. Eastman, S.U.S. Choi, S. Li, W. Yu, L.J. Thompson, Anomalously increased effective thermal conductivities of ethylene glycol-based nanofluids containing copper nanoparticles, Applied Physics Letters 78(6) (2001) 718-720.

[20] H.E. Patel, S.K. Das, T. Sundararajan, A. Sreekumaran Nair, B. George, T. Pradeep, Thermal conductivities of naked and monolayer protected metal nanoparticle based nanofluids: Manifestation of anomalous enhancement and chemical effects, Applied Physics Letters 83(14) (2003) 2931-2933.

[21] D.H. Yoo, K.S. Hong, H.S. Yang, Study of thermal conductivity of nanofluids for the application of heat transfer fluids, Thermochimica Acta 455(1-2) (2007) 66-69.

[22] M.J. Pastoriza-Gallego, L. Lugo, D. Cabaleiro, J.L. Legido, M.M. Piñeiro, Thermophysical profile of ethylene glycol-based ZnO nanofluids, The Journal of Chemical Thermodynamics 73 (2014) 23-30.

[23] J. Taha-Tijerina, L. Peña-Paras, T.N. Narayanan, L. Garza, C. Lapray, J. Gonzalez, E. Palacios, D. Molina, A. García, D. Maldonado, P.M. Ajayan, Multifunctional nanofluids with 2D nanosheets for thermal and tribological management, Wear 302(1) (2013) 1241-1248.

[24] H. Yarmand, S. Gharehkhani, G. Ahmadi, S.F.S. Shirazi, S. Baradaran, E. Montazer, M.N.M. Zubir, M.S. Alehashem, S.N. Kazi, M. Dahari, Graphene nanoplatelets–silver hybrid nanofluids for enhanced heat transfer, Energy Conversion and Management 100 (2015) 419-428.

[25] S. Jana, A. Salehi-Khojin, W.-H. Zhong, Enhancement of fluid thermal conductivity by the addition of single and hybrid nano-additives, Thermochimica Acta 462(1) (2007) 45-55.

[26] S. Halelfadl, P. Estellé, B. Aladag, N. Doner, T. Maré, Viscosity of carbon nanotubes water based nanofluids: Influence of concentration and temperature, International Journal of Thermal Sciences, 71 (2013) 111-117.

[27] H. Xie, J. Wang, T. Xi, Y. Liu, Thermal conductivity of suspensions containing nanosized SiC particles, International Journal of Thermophysics 23(2) (2002) 571-580.

[28] S.S. Sonawane, R.S. Khedkar, K.L. Wasewar, Study on concentric tube heat exchanger heat transfer performance using Al_2O_3 – water based nanofluids, International Communications in Heat and Mass Transfer 49 (2013) 60-68.

[29] G. Żyła, J. Fal, P. Estellé, The influence of ash content on thermophysical properties of ethylene glycol based graphite/diamonds mixture nanofluids, Diamond and Related Materials 74 (2017) 81-89.

[30] R.M. Mostafizur, M.H.U. Bhuiyan, R. Saidur, A.R. Abdul Aziz, Thermal conductivity variation for methanol based nanofluids, International Journal of Heat and Mass Transfer 76 (2014) 350-356.

[31] W. Yu, E.V. Timofeeva, D. Singh, D.M. France, R.K. Smith, Investigations of heat transfer of copper in Therminol-59 nanofluids, International Journal of Heat and Mass Transfer 64 (2013) 1196-1204.

[32] C. Wang, J. Yang, Y. Ding, Phase transfer based synthesis and thermophysical properties of Au/Therminol VP-1 nanofluids, Progress in Natural Science: Materials International 23(3) (2013) 338-342.

[33] D. Singh, E.V. Timofeeva, M.R. Moravek, S. Cingarapu, W. Yu, T. Fischer, S. Mathur, Use of metallic nanoparticles to improve the thermophysical properties of organic heat transfer fluids used in concentrated solar power, Solar Energy 105 (2014) 468-478.

[34] N. Navarrete, R. Mondragon, D. Wen, M.E. Navarro, Y. Ding, J.E. Julia, Thermal energy storage of molten salt –based nanofluid containing nano-encapsulated metal alloy phase change materials, Energy (2018).

[35] R.A. Taylor, P.E. Phelan, T.P. Otanicar, C.A. Walker, M. Nguyen, S. Trimble, R. Prasher, Applicability of nanofluids in high flux solar collectors, Journal of Renewable and Sustainable Energy 3(2) (2011) 023104.

[36] K.Y. Leong, R. Saidur, S.N. Kazi, A.H. Mamun, Performance investigation of an automotive car radiator operated with nanofluid-based coolants (nanofluid as a coolant in a radiator), Applied Thermal Engineering 30(17) (2010) 2685-2692.

[37] E. Firouzfar, M. Soltanieh, S.H. Noie, S.H. Saidi, Energy saving in HVAC systems using nanofluid, Applied Thermal Engineering 31(8) (2011) 1543-1545.

[38] S.C. Tzeng, C.W. Lin, K.D. Huang, Heat transfer enhancement of nanofluids in rotary blade coupling of four-wheel-drive vehicles, Acta Mechanica 179(1) (2005) 11-23.

[39] C. Tsai, H. Chien, P. Ding, B. Chan, T. Luh, P. Chen, Effect of structural character of gold nanoparticles in nanofluid on heat pipe thermal performance, Materials Letters 58(9) (2004) 1461-1465.

[40] L. Zhang, Y. Jiang, Y. Ding, M. Povey, D. York, Investigation into the antibacterial behaviour of suspensions of ZnO nanoparticles (ZnO nanofluids), Journal of Nanoparticle Research 9(3) (2007) 479-489.

[41] L. Zhang, Y. Ding, M. Povey, D. York, ZnO nanofluids – A potential antibacterial agent, Progress in Natural Science 18(8) (2008) 939-944.

[42] N. Yadav, A.K. Jaiswal, K.K. Dey, V.B. Yadav, G. Nath, A.K. Srivastava, R.R. Yadav, Trimetallic Au/Pt/Ag based nanofluid for enhanced antibacterial response, Materials Chemistry and Physics 218 (2018) 10-17.

[43] J. Buongiorno, L.W. Hu, S.J. Kim, R. Hannink, B. Truong, E. Forrest, Nanofluids for enhanced economics and safety of nuclear reactors: an evaluation of the potential features, issues, and research gaps, Nuclear Technology 162(1) (2008) 80-91.

[44] M.P. Allen, D.J. Tildesley, Computer Simulation of Liquids (Clarendon Press, Oxford, 1987).

[45] N. Metropolis, S. Ulam, The Monte Carlo method, Journal of the American Statistical Association 44(247) (1949) 335-341.

[46] B. Alder, T. Wainwright, Phase transition for a hard sphere system, The Journal of Chemical Physics 27(5) (1957) 1208-1209.

[47] L.A. Pozhar, Structure and dynamics of nanofluids: Theory and simulations to calculate viscosity, Physical Review E - Statistical Physics, Plasmas, Fluids, and Related Interdisciplinary Topics 61(2) (2000) 1432-1446.

[48] J.M.D. McElroy, L.A. Pozhar, S.H. Suh, Self-diffusion in a fluid confined within a model nanopore structure, Colloids and Surfaces A: Physicochemical and Engineering Aspects 187-188 (2001) 493-507.

Chapter 3

Hypothesis and objectives

3. Hypothesis and objectives

The working mechanism of a thermosolar plant involving CSP technology is generally common to any kind of light harvesting technology: the solar radiation incident on the harvesting system is concentrated onto a central tube through which flows a heat transfer fluid; this fluid is pumped through a system of pipes connected to a steam generator, where heat is released to turn water into steam at high pressure, which drives a turbine and produces electricity. The steam from the turbine is condensed in cooling towers into liquid water, which then rejoins the cycle. When there is too much heat energy in the solar field, part of the hot fluid is diverted towards a molten salt heat exchanger where the heat energy can be stored (TES unit). Thus, a heat transfer fluid flows between the harvesting and heat exchanger systems. Depending on the kind of plant, this fluid has the main aim of transferring and accumulating heat. Consequently, using a fluid that is significantly better at capturing and storing heat, and that presents a lower fusion temperature, increased boiling temperature and/or enhanced thermal conductivity would have interesting advantages for its application as a heat transfer fluid in this kind of plant.

A new kind of fluid with enhanced thermal properties are those known as nanofluids, which are an interesting proposition and an attractive alternative with regard to improving the efficiency of concentrating solar power plants. Nanofluids can be optimized by altering parameters such as the nanoparticles used, their proportion, and the addition of surfactants and/or stabilizers, amongst others. This makes it possible to improve the thermal properties of the nanofluids, thus improving the capture and storage of energy from the sun. Thus, the starting hypothesis of this Doctoral Thesis is that the use of nanofluids based on metal nanomaterials in a fluid used in CSP technology with improved thermal properties may lead to the increased overall efficiency of this kind of thermosolar plants.

Consequently, the research proposal presented here focuses on the study, design, characterization and value given to nanofluids with optimized thermal properties that are stable enough to be used to capture and transport heat from the sun's energy, in particular in concentrating solar power, where possible. The study of this proposal will be approached from three interconnected lines of research:

- Design and preparation of nanofluids. Totally experimental line that takes as a starting point the fluid normally used in solar harvesting systems, which is a thermal oil derived from benzenes with alkyl or phenyl-type radicals. In particular, compositions similar to those defined in commercial heat transfer fluids such as the Dowtherm A® line of fluids developed by The Dow Chemical Company© will be taken as references. The Dowtherm A® fluid will be used as the base fluid for the nanofluids in this Doctoral Thesis. Two kinds of metal nanoparticles will be selected: commercial silver nanoparticles; and gold and platinum nanoparticles synthesized during the same preparation process as the nanofluid. Furthermore, mechanisms will be taken into account to improve the dispersion and suspension of the nanoparticles in the heart of the base fluid, such as the use of ultrasound; and mechanisms to improve and maintain the suspension of nanoparticles, such as the used of additives that act as phase transfer agents and/or as surfactants, specifically, tetraoctylammonium bromide (TOAB), dodecylamine (DDA) and 1-octadecanethiol (ODT). Consequently, it is important to take into account the cost-efficiency ratio in the optimal design of the nanofluid in order to exclude any combinations that, despite showing positive properties, cannot be incorporated in large plants.

- Experimental characterization of the main chemical and physical properties of the nanofluids designed. This characterization will include different measurements in order to perform a comprehensive study of the nanofluids prepared, paying special attention to:
    a) Chemical and physical changes that can take place over time; monitoring will be performed of variables such as the particle size and zeta potential, and measurements taken of sedimentation to assess the degree of cluster formation and therefore the stability of the nanofluids over time.
    b) Thermal properties such as heat capacity or thermal conductivity, and rheological properties such as viscosity, which will shed light on the efficiency of the nanofluids in heat transfer processes.
    c) The characterization of the oxidation state, size, shape and crystallinity of the nanomaterial in the cases where they have been synthesized.

- Theoretical modelling of the nanofluid systems using classic Molecular Dynamics (MD). The statistical results obtained by means of the Molecular Dynamics technique will be used to calculate parameters of interest such as thermal conductivity or heat capacity. Likewise, other information obtained will include: dynamic properties such as the diffusion of the nanoparticles in the fluid; structural properties related with how the fluid molecules are arranged around the nanoparticles; and the interaction energy between the nanoparticle and fluid molecules. These results will prove useful for determining how these nanofluids behave in order to make laboratory experiments as effective as possible.

For general technical advice, the research counts on the collaboration of the company Torresol Energy Investments S.A., which has concentrating solar power plants in Seville (Gemasolar, tower-type receptor with molten salts) and in Cadiz (Valle-1 and Valle-2, parabolic trough concentrators). They will provide useful guidelines, information and knowledge at end-user level. Thus, the nanofluids will be prepared with the clear objective of using them in parabolic trough concentrating plants that currently use thermal oils.

Therefore, a series of general and specific objectives are established that will allow the main objective of this Doctoral Thesis to be achieved.

- General objective.

From a purely scientific and technical perspective, the general aim is to develop nanofluids with optimized thermal properties that consequently have a high potential for use in industrial systems involving concentrating solar power. In turn, the in-depth study of this kind of systems may be of interest in many applications, so we will help to increase the scientific knowledge of this topic.

From a social perspective, the launch of a line of research aimed at improving the efficiency of energy sources could entail a decrease in economic costs and an increase in the industrial exploitation of this renewable energy. Additionally, on a national level, this novel line of research may be a driver for new opportunities to carry out R+D in Spain, a country which, as mentioned above, is a world leader in this kind of technology.

- Specific objectives.

On the basis of the hypotheses described, which present the design of a set of nanofluids that are economically viable for use in concentrating solar power, a series of specific objectives are established that are classified according to the two general areas of work: the experimental and theoretical approaches.

The experimental pathway, working hand in hand with the theoretical pathway, establishes the following objectives:

- ✓ To establish the methodology for preparing nanofluids taking into account different factors such as: the nature of the components (fluid and nanoparticle); the size, shape and concentration of nanoparticles; the addition of stabilizers (surfactants); or the separation process (use of ultrasound, homogenization time, temperature, etc.).
- ✓ To synthesize nanoparticles while being able to modulate parameters that improve the efficiency of the nanofluids.
- ✓ To obtain nanofluids with optimized thermal and transport properties, paying special attention to their isobaric specific heat, thermal conductivity and viscosity.
- ✓ To ensure that the nanofluids obtained are stable over time.

The theoretical pathway involves the use of classic Molecular Dynamics (MD), establishing the following objectives:

- ✓ To calculate heat capacity and study variations in this thermodynamic property.
- ✓ To study dynamic transport properties such as thermal conductivity and the auto-diffusion coefficients of the simulated nanofluids in order to enhance our understanding of the macroscopic behaviour of these systems.
- ✓ Analysis of structural parameters. Analyses will be performed of the radial distribution function (RDF) and the spatial distribution function (SDF) in order to determine how the fluid molecules are arranged around the nanoparticles studied, calculating the interaction energy between the nanoparticles and fluid for the most probable structure.

- Main objective.

Achieving these specific objectives leads to fulfilling the main scientific aim of this Doctoral Thesis, which can be summarized as:

To detect nanoparticle and fluid pairs that make it possible to produce stable nanofluids with a high potential for use in high temperature thermosolar power.

Chapter 4

Review of the background

4. Review of the background

One of the challenges to be met by present-day technology is how to improve the thermophysical properties of the fluids commonly used as heat exchangers, especially for their direct application in the solar power industry [1]. Focussing our attention on the thermal properties, in particular the thermal conductivity, of conventional fluids such as water or ethylene glycol, they present vastly inferior values with regard to solids. Consequently, combining a fluid and a solid in dispersion into a single system is the most obvious way to improve the thermal properties of the original fluid. The suspension and dispersion of micrometric solid particles into a fluid modifies its values in terms of thermophysical properties, making it possible to improve heat transfer processes. However, despite this feasible improvement, applying these fluids in practice leads to engineering-related drawbacks due to the abrasive action of the solids and, amongst other problems, blockages in channels and pipelines, erosion of tubes and drops in pressure. Furthermore, due to the considerable size of the particles added, they tend to precipitate quickly, reducing the amount of solid in suspension, and generating rheological problems and high levels of instability in the system. Therefore, although the presence of a solid in suspension improves the thermal properties of a fluid, in practice its use is not viable.

Recent advances in technology have made it possible to take the evolution of materials to a new nanometric dimension, which has led to the development of a new range of materials: nanomaterials. In the last few decades, nanotechnology and nanomaterials have caught the attention of a vast number of groups performing research in fields such as science, electronics, mechanics, health, etc. Nanomaterials have been in increasingly high demand due to the surprising and interesting optical, mechanical, electrical and thermal properties that they present.

4.1. Background

Consequently, nanomaterials and nanotechnology did not go unnoticed for the milestone of improving the thermal properties of heat transfer fluids since they might be able to solve the problems generated by using micrometric solids, as described above. Thus, in 1995, in the Argonne National Laboratory (USA), Choi proposed the word “nanofluid” to describe fluids containing nanomaterial in suspension[2]. Earlier records of work in this field

exist from 1993, such as the German patent of A. Grimm based on heat transfer fluids containing aluminium powder [3], the study by Masuda and co-workers with metallic oxide nanoparticles [4], or the conference by V. Gass [5].

Amongst other characteristics, this new category of heat transfer fluids showed improved stability over time, a decreased tendency of the nanomaterial towards agglomeration and precipitation, a decrease in engineering-type drawbacks and, decisively, they presented dramatic improvements in thermal properties, in particular thermal conductivity, when compared with base fluids and with micrometric solids in suspension.

The following research centred its attention on studying how to improve the thermal conductivity of the nanofluids with regard to the base fluid through the addition of nanoparticles, mainly metallic oxides. The studies showed that thermal conductivity was highly dependent on the nanomaterial and its concentration, and on the base fluid that it was dispersed into. In 1999, Wang and his co-workers [6] studied the thermal conductivity of nanofluids prepared with Al_2O_3 and CuO dispersed into four base fluids: water, ethylene glycol, engineering oil and vacuum pump fluid. They found the same trend in every case for both metallic oxides: thermal conductivity increased with the concentration of nanomaterial. They achieved improvements in thermal conductivity of 26% and 40% with regard to ethylene glycol when the volume concentrations of Al_2O_3 and CuO were 5% and 8%, respectively. In the same year, Lee and co-workers [7] prepared nanofluids based on the same oxides in water and ethylene glycol, showing that for the same nanomaterial the thermal conductivity of the nanofluids prepared with ethylene glycol was always higher than that of the nanofluids prepared with water; they also reported that, using the same base fluid and the same volume concentration, the CuO-based nanofluids presented higher thermal conductivity than those based on Al_2O_3. Thus, for a volume concentration of 4%, and using ethylene glycol as the base fluid, the nanofluid with CuO presented an increase in thermal conductivity of 20%, compared with the 12% improvement for the nanofluid with Al_2O_3.

At this point, a relationship was established between these two studies and the earlier work by Masuda and co-workers [4], who had reported significant changes in the thermophysical properties of a fluid when metal oxide nanoparticles were dispersed into it, and that the fluid had possible applications as a fluid for transferring heat by convection. For a nanofluid based on Al_2O_3 particles in water with a volume concentration of 3%, Masuda

obtained an improvement in thermal conductivity of 20%, Wang of 12% and Lee of 8%. Although each author prepared the nanofluid using a different technique, which affected the morphology of the nanomaterial, and even used additives to keep the nanofluids stable, the main difference between the three nanofluids lay in the size of the nanoparticles: Masuda used Al_2O_3 nanoparticles with a diameter of 13 nm and obtained the most significant improvement; Wang used 28 nm-diameter nanoparticles and achieved an intermediate improvement; and Lee obtained the most discrete enhancement using the largest nanoparticles, which measured 38 nm in diameter. This suggested that thermal conductivity did not only depend on the concentration of the nanomaterials, but that the size of the nanoparticle also had a significant effect.

A year later, Eastman and co-workers [8] obtained, for the same concentration of nanomaterial, a greater increase in thermal conductivity in metallic copper nanofluids (of 10 nm in diameter) than in CuO nanofluids (of 35 nm in diameter), attributing this result to the different particle sizes. They also determined that nanofluids prepared using copper in ethylene glycol showed greater stability and a bigger increase in thermal conductivity when they used thioglycolic acid as a surfactant, obtaining an improvement of 40% in the presence of surfactant, and of 5% in its absence for the same volume concentration of nanomaterial of 0.3%.

Morphology also plays an important role in the improvement in the thermal conductivity of nanofluids. In 2002, Xie and co-workers [9] studied the effect of the morphology of the nanomaterial on thermal conductivity. They prepared and studied SiC-based nanofluids with two morphologies: spherical nanoparticles of 26 nm in diameter and cylindrical nanoparticles of 600 nm and diameter dispersed in water and in ethylene glycol. For the same volume concentration of 4%, they obtained a greater increase in thermal conductivity for the cylindrical nanomaterial (of 23%) than for the spherical nanomaterial (of 15%), despite the smaller particle size. In 2005, Murshed and co-workers [10] prepared nanofluids in water using spherical TiO_2 nanoparticles with a diameter of 15 nm and cylindrical nanoparticles of the same oxide measuring 10x40 nm. They reported the expected trend: the thermal conductivity of each nanofluid increased with the concentration of nanomaterial, and for the same concentration the improvement in thermal conductivity was 32% for the nanofluid with cylinder-shaped nanomaterial compared with an improvement of 29% for the spherical nanomaterial.

This and other research showed how thermal conductivity was dependent on factors related to the kind of nanomaterial used, its size and concentration, and the base fluid that it was dispersed into. However, factors such as temperature, the clustering effect and pH also affect the thermal conductivity of nanofluids. In 2010, Teng and co-workers [11] studied the thermal conductivity of Al_2O_3-based nanofluids of three different sizes (20, 50 and 100 nm in diameter) and its relationship with increases in concentration and temperature. They reported a tendency for thermal conductivity to increase when smaller nanoparticles were used and when both the concentration and temperature increased. In 2006, Hong and co-workers [12] investigated the effect of the clustering of metallic iron nanoparticles of 10 nm in diameter in nanofluids prepared with ethylene glycol. They determined that when the nanofluids were subjected to ultrasound treatment, they presented higher thermal conductivity the longer it was applied; however, once left idle, the nanomaterial presented large particle sizes again due to the formation of clusters, leading to a decrease in thermal conductivity with regard to that obtained moments after the application of ultrasound. The studies by Lee and co-workers [13] and Karthik and co-workers [14] into the influence of pH on the thermal conductivity of CuO nanofluids in water showed that the pH affected the stability of the system by modifying the surface charge of the nanoparticles and therefore the number of no-agglomerated nanoparticles in dispersion, which had a direct effect on thermal conductivity.

Keblinski [15] and Eastman [16] are just two of the researchers that reported the possible mechanisms that might explain the anomalous increase in the thermal conductivity of a fluid due to the presence of a dispersed nanometric solid. To this day, due to the complexity of the systems, the scientific community is yet to reach consensus on this matter [17]. The main mechanisms proposed were:

- The mobility of the nanoparticles (Brownian motion) due to the fluid. The energy exchange arising from the direct contact between nanoparticles when they collide with each other may result in an increase in thermal conductivity. These collisions are a result of the Brownian motion of the nanoparticles, although this is too slow to transport and exchange significant amounts of heat. However, Brownian motion is significantly affected by temperature; when the temperature rises, an increase in the kinetic energy of the particles is produced as their speed increases: the smaller the particles, the greater the momentum they gain and the more collisions taking place, provoking a significant increase in thermal conductivity. Therefore, although

Brownian motion does not lead to a drastic increase in thermal conductivity, it can play an important role, for example, in the formation of clusters, which directly affects thermal properties.

- Liquid/solid interface. Liquid molecules form ordered structures on the surface of solids, forming layers that have different thermophysical properties to the liquid (bulk) and to the solid nanoparticles. These monolayers present intermediate thermal conductivity values, between those found for the liquid and the solid, and an increase in the thermal conductivity of the nanofluid with regard to the base fluid could therefore be expected, although it is true that this increase would not only be a result of this phenomenon.
- Characteristics of heat transfer in nanoparticles. Macroscopic theories suggest that heat transport is produced due to diffusion. In crystalline solids, heat is transported by phonons; that is, by the propagation of reticular vibrations. These phonons are created and spread randomly in all directions and may interact with each other. A phonon involves a group of periodic vibrations with long wavelengths that mainly occur in solids. These vibrations generate energy, which results in a change of temperature and thus in the transfer of heat (known as ballistic heat transport).
- Clustering. If nanoparticles cluster to form lattices, lower resistance thermal pathways are created that have a positive effect on thermal conductivity. For heat flow to exist, physical contact between the particles is not necessary, rather a very short distance, and the clusters formed present a considerable surface area, which results in an unusual improvement in thermal conductivity. However, this has two disadvantages: first, the formation of clusters over a prolonged period gives rise to fairly heavy aggregates that eventually precipitate; and second, at low concentrations of nanomaterial, the clustering creates areas of liquid of high thermal resistance due to the absence of solid material. Both problems would provoke a decrease in thermal conductivity.
- Surface charge. The pH is a factor that has a large impact on the surface charge of the particles, which, in turn, directly affects thermal conductivity. When the pH of the nanofluid moves away from its isoelectric point, the surface charge and charge density increase, prompting electrostatic repulsions and preventing agglomeration phenomena. There would, therefore, be a higher concentration of dispersed nanomaterial, which could result in an increase in thermal conductivity values. On the other hand, when the

nanofluid is found at its isoelectric point, the surface charge is low or zero, resulting in the nanomaterial agglomerating and in the subsequent loss of nanomaterial in suspension. Depending on the nature of the system, this agglomeration may improve other processes such as the formation of clusters or heat transport by phonons, which would lead to improved thermal conductivity.

From a theoretical perspective, models were developed using mathematical formulas that predict or approximate this dramatic increase in thermal conductivity, although no model currently makes totally accurate predictions [17]. Since the first model by Maxwell in 1904 for a mixture of two components, until the most recent approximations, the factors that could have an effect on the increase in thermal conductivity experimentally (stated above) and the factors affecting the nanomaterial (especially morphology) have enhanced the ever more complex formulas.

The first model by Maxwell [18] was proposed for liquid-solid mixtures with large particles. This model (Equation 4.1, Table 4.1) only takes into account the thermal conductivity of the nanomaterial (only with spherical morphology) and the base fluid, and the volume fraction of the solid. When the volume fraction of the solid is high enough, the Maxwell model begins to get predictions of thermal conductivity wrong. In 1962, Hamilton and Crosser [19] proposed a model (Equation 4.2, Table 4.1) based on the Maxwell model that includes the volume fraction of the nanoparticles $\boldsymbol{\phi}$, and considers nanomaterial with a non-spherical morphology by using the empirical constant $\boldsymbol{n}$ given by $n = {}^{3}/_{\psi}$, where $\boldsymbol{\psi}$ is defined as the sphericity of the particle. If this sphericity is equal to 1, the Hamilton-Crosser model is identical to the Maxwell one. However, these considerations limit the accuracy of the predictions made by the classical models, which, in turn, assume that heat is transferred by diffusion in both fluids and solids, which results in good approximations for suspensions with macro- or millimetric particles, but generally underestimates thermal conductivity values in the case of nanofluids [20].

Recently, the theoretical studies performed and the new models proposed have taken into account heat transfer mechanisms that could explain the anomalous increase in thermal conductivity. One of the factors that minimises the difference between experimental results and those predicted theoretically is the use of the effective volume fraction. From the perspective of the mechanisms presented above, the improvement in thermal conductivity

may be due to the formation of a nanolayer structure on a solid-liquid interface, which means it is easier for the liquid molecules to transport heat when they are part of that layer than when they are part of the bulk liquid. This effect is not important for micro- or millimetric particles, but is very significant for nanoparticles. In 2003, Yu and Choi [21] proposed a model (Equation 4.3, Table 4.1) that considered that the nanolayer has nanometric dimensions and semi-solid properties, and that the effective volume fraction $\boldsymbol{\phi_{eff}}$ is estimated by the approximation $\phi_{eff} = \phi(1+\beta)^3$, where $\boldsymbol{\beta}$ is the ratio of the thickness of the nanolayer and the diameter of the nanoparticle. In the same year, Xuan and co-workers [22] proposed a model (Equation 4.4, Table 4.1) that takes into account Brownian motion and the clustering of nanoparticles, and in which the density and isobaric specific heat of the nanoparticles, the apparent radius of the cluster, ($\boldsymbol{r_{cl}}$, estimated experimentally) and the viscosity $\boldsymbol{\mu}$ of the base fluid intervene. The first term in this model is in its entirety the Maxwell model, while the second term is the participation of the Brownian movement of the nanoparticles. In 2004, Koo and Kleinstreuer [23] combined in their model (Equation 4.5, Table 4.1) Brownian motion with the Hamilton-Crosser model, considering the presence of aggregates with regard to their conductivity and diameter (estimated experimentally), a term $\boldsymbol{\beta}$ that depends on the kind of nanoparticles and that is related to the interactions between the nanoparticles and the fluid, and a function $\boldsymbol{f(T,\phi)}$ that is dependent on the temperature and volume fraction.

The incorporation and dispersion of nanomaterial not only affects the thermal properties of the base fluid, but also its rheological properties. Rheology is the study of the physical principles that govern the flow of fluids. Although the pioneers of this branch of science include Isaac Newton and Robert Hooke (with studies into ideal viscous fluids and elastic solids), modern rheology was posited in 1929 by Eugene Cook Bingham [24], and focuses on complex systems that exhibit elastic and viscous behaviour simultaneously, that is, viscoelastic materials such as plastics, fibres, lubricants, suspensions and emulsions. Viscosity is a crucial parameter in the design of nanofluids and their future application as heat transfer fluids, since many engineering-related drawbacks (such as pumping power or pumping pressure) and the heat transfer coefficient depend on this property to a large extent [25]. Therefore, the study of rheological properties, in particular viscosity, is essential in the field of nanofluids.

Table 4.1. Models to predict the effective thermal conductivity k_{eff} of the nanofluids, where k_f, k_p and k_a represent the thermal conductivity of the fluid, the nanoparticle and the aggregate; ϕ and ϕ_{eff} are the volume fraction and the effective volume fraction; n is the empirical factor; ρ_p and $C_{P,np}$ are the density and the isobaric specific heat of the nanoparticles; κ_B is the Boltzmann constant; r_{cl} is the apparent radius of the cluster; μ is the viscosity of the base fluid; d_a is the diameter of the aggregate; the term β depends on the kind of nanoparticle and a function $f(T,\phi)$ dependent on the temperature and the volume fraction.

Eq. Maxwell (1904) [18]

$$k_{eff} = \frac{k_p + 2k_f + 2(k_p - k_f)\phi}{k_p + 2k_f - (k_p - k_f)\phi} k_f \tag{4.1}$$

Eq. Hamilton-Crosser (1962) [19]

$$k_{eff} = \frac{k_p + (n-1)k_f - (n-1)(k_f - k_p)\phi}{k_p + (n-1)k_f + (k_f - k_p)\phi} k_f \tag{4.2}$$

Eq. Yu-Choi (2003) [21]

$$k_{eff} = \frac{k_p + (n+1)k_f - \phi_{eff}(n-1)(k_f - k_p)}{k_p + (n+1)k_f + \phi_{eff}(k_f - k_p)} k_f \tag{4.3}$$

Eq. Xuan (2003) [22]

$$k_{eff} = \frac{k_p + 2k_f - 2\phi(k_f - k_p)}{k_p + 2k_f + \phi(k_f - k_p)} k_f + \frac{\rho_p \phi C_{p_p}}{2k_f} \sqrt{\frac{\kappa_B T}{3\pi r_{cl} \mu_f}} k_f \tag{4.4}$$

Eq. Koo- Kleinstreuer (2004) [23]

$$k_{eff} = \frac{k_a + 2k_f - 2\phi_{eff}(k_f - k_a)}{k_a + 2k_f + \phi_{eff}(k_f - k_a)} k_f + 5 \cdot 10^4 \beta \phi_{eff} \rho_p C_{p_p} \sqrt{\frac{\kappa_B T}{\rho_p d_a}} f(T, \phi) \tag{4.5}$$

Masuda [4] was the first to measure the viscosity of metallic oxide nanofluids in water at temperatures ranging between 20 and 70°C. He found that the viscosity of the nanofluids decreased as the temperature increased, and that at a set temperature the viscosity of the nanofluid increased with the concentration of nanomaterial. Pak and Cho [26] studied the viscosity of Al_2O_3 and TiO_2 nanofluids in a range of volume concentrations between 1-10%, and reported the same trend as that described earlier by Masuda, obtaining a 200% increase in the viscosity for a volume concentration of 10%. Furthermore, they reported a change in the viscous behaviour of the nanofluids, which stopped behaving like a Newtonian fluid when the volume concentration of Al_2O_3 was higher than 3%. Moreover, Wang and co-workers [6] obtained an increase in viscosity of 30% when the volume concentration of Al_2O_3 in water was 3%. They also observed that the degree of dispersion of the nanomaterial within the base fluid also has an effect on variations in viscosity, lower values being found with higher degrees of dispersion.

In 2008, Murshed and co-workers [27] performed research into the effect of temperatures ranging between 20 and 60ºC on the thermal conductivity and viscosity of nanofluids based on aluminium, Al_2O_3 and TiO_2, using cetyltrimethylammonium bromide (CTAB) as the surfactant, and water, ethylene glycol and mineral oil as the base fluids. They concluded that, despite the increase in thermal conductivity with temperature and the concentration of nanomaterial, viscosity showed a similar trend to the base fluid, having negative repercussions in terms of efficiency. In 2009, Duangthongsuk and Wongwises [28], in a study of TiO_2-based nanofluids in water, found that, although viscosity increased with the concentration of nanomaterial and decreased with temperature, in terms of efficiency, the improvement in the heat transfer coefficient varied between 26% and 14% when the volume concentration increased from 1% to 2%. This demonstrated that, despite the increase in thermal conductivity, the change in viscosity played a very important role in the efficiency of the transfer of heat. Later, in 2013, Sundar and co-workers [29] investigated the thermal conductivity and viscosity of nanofluids with magnetic Fe_3O_4 nanoparticles with a diameter of 13 nm in water, and using CTAB be as the surfactant. They observed that for a volume concentration of 2% and a temperature of 60°C, the thermal conductivity of the nanofluid increased by 45% with regard to the base fluid, but there was a threefold increase in the viscosity of the water, which had a negative impact on the efficiency of the nanofluid.

The size and shape of the particles, as occurs with thermal conductivity, also has an effect on viscosity values. In 2008, Nguyen and co-workers [30] studied the effect of particle size on the viscosity of Al_2O_3 nanofluids in water (with particle diameters between 36 and 47 nm). They found that significant effects can only be appreciated when a high concentration of nanomaterial is used. Research by Timofeeva and co-workers in 2009 [31] focused on how the morphology of nanomaterials affects viscosity. Using four different shapes of nanoparticles (platelet, blade, cylindrical and brick shapes) and a mixture of water and ethylene glycol (50/50) as the base fluid, they observed that the Newtonian behaviour of the nanofluid depended on the shape of the particle, which consequently has a significant effect on changes in viscosity.

Thus, the parameters that affect the thermal conductivity of the nanofluid also impact to a large extent on its viscosity. Generally, viscosity decreases with an increase in temperature, and increases with higher concentrations of nanomaterial (and with the presence of surfactants). Moreover, the size and distribution of the nanomaterial has a considerable

impact, whereby, for the same concentration of nanomaterial, the smaller the nanoparticles the greater the viscosity of the nanofluid. In addition, nanofluids with a greater distribution of particle sizes will generate more spaces between the molecules of the base fluid, making the nanofluid flow more and have a lower viscosity value. Finally, in the study of nanofluids, it is also interesting to determine whether they present Newtonian or non-Newtonian fluid behaviour. In a Newtonian fluid, the strain rate is proportional to the tangential force; and the ratio of the two is a constant known as viscosity, which is only dependent on temperature and not on the strain rate or time. Generally, when the concentration of nanomaterial is low, nanofluids present Newtonian behaviour. As the strain rate increases, the interactions between nanoparticles begin to weaken, presenting low viscosity values.

As with thermal conductivity, theoretical models have been developed to predict the viscosity of nanofluids, using formulas for biphasic mixtures. The first theoretical model (Equation 4.6, Table 4.2) was proposed by Einstein [32] in 1906 for nanofluids with a low concentration of particles (<0.02 vol.%) and spherical morphology. Later, models were proposed that took into consideration the phenomena and mechanisms mentioned above for changes in thermal conductivity. Brinkman [33], in 1952, expanded Einstein's model for concentrations of up to 4 vol.% (Equation 4.7, Table 4.2). Batchelor [34], in 1977, took the Brownian motion of the nanoparticles into consideration in his model (Equation 4.8, Table 4.2). More recently in 2007, Nguyen and co-workers [30] proposed a model (Equation 4.9, Table 4.2) to predict the viscosity of nanofluids with nanoparticle concentrations of between 1 and 4 vol.%; and in 2009, Masoumi [35] took into consideration the effect of temperature, the density of the nanoparticles and the physical properties of the base fluid (Equation 4.10, Table 4.2).

Table 4.2. Models for the prediction of the viscosity $\boldsymbol{\mu}$ of nanofluids, where $\boldsymbol{\mu_f}$ is the viscosity of the fluid; $\boldsymbol{\phi}$ is the volume fraction; $\boldsymbol{T}$ is the temperature; $\boldsymbol{C}$ is a correction factor that depends on the size and concentration of the nanomaterial; $\boldsymbol{\rho_p}$ is the density of the nanoparticles; $\boldsymbol{V_B}$ is Brownian velocity; $\boldsymbol{d}$ is the diameter of the nanoparticles, and $\boldsymbol{l}$ is the space between particles.

Eq. Einstein (1906) [32]	$\mu = \mu_f(1 + 2.5\phi)$	(4.6)
Eq. Brinkman (1952) [33]	$\mu = \mu_f \frac{1}{(1-\phi)^{2.5}}$	(4.7)
Eq. Batchelor (1977) [34]	$\mu = \mu_f(1 + 2.5\phi + 6.25\phi^2)$	(4.8)
Eq. Nguyen (2007) [30]	$\mu = \mu_f(1.125 - 0.0007\ T)$	(4.9)
Eq. Masoumi (2009) [35]	$\mu = \mu_f + \frac{\rho_p V_B d^2}{72\ C\ l}$	(4.10)

Other relatively important properties in the study of nanofluids are density and isobaric specific heat, although the number of references and studies related with these properties is somewhat lower in comparison with the studies that focus on thermal conductivity and viscosity.

Since the density of solids is greater than that of liquids, it is to be expected that the addition of nanomaterial and other agents (such as surfactants) will result in an increase in the density of the nanofluid with regard to the original base fluid. This is what is known as the simple rule of mixtures, although this increase is not as dramatic as that of viscosity. Variations of below 5% are estimated for nanofluids with a volume concentration of 1% [16], although some studies, such as the one by Summers and Yerkes [36], report increases of less than 5% with volume concentrations below 5% in Al_2O_3-based nanofluids in propanol. The density of a nanofluid $\boldsymbol{\rho_{nf}}$ is predicted in accordance with the simple rule of mixtures according to Equation 4.11 [26]:

$$\rho_{nf} = \phi\ \rho_{np} + (1 - \phi)\rho_{bf} \tag{4.11}$$

where $\boldsymbol{\rho_{bf}}$ and $\boldsymbol{\rho_{np}}$ are the densities of the base fluid and the nanoparticle respectively, and $\boldsymbol{\phi}$ has been defined above.

On the other hand, solids usually present lower isobaric specific heat values than liquids at the same temperature. Thus, incorporating nanoparticles into the base fluid will result in a decrease in isobaric specific heat, meaning that, for the same increase in temperature, less thermal energy is required for the nanofluid than for the base fluid.

According to the theory of simple mixtures of ideal gases, the isobaric specific heat of nanofluids $\boldsymbol{C_{P,nf}}$ can be estimated according to Equation 4.12, as [26]:

$$C_{P,nf} = \phi\, C_{P,np} + (1-\phi)\, C_{P,bf} \tag{4.12}$$

where $\boldsymbol{C_{P,bf}}$ and $\boldsymbol{C_{P,np}}$ are the isobaric specific heat of the base fluid and the nanoparticles, respectively. This equation was modified by Xuan and Roetzel [37], introducing the density term (Equation 4.13):

$$\rho_{nf}\, C_{P,nf} = \phi\, \rho_{np}\, C_{P,np} + \rho_{bf}\, (1-\phi)\, C_{P,bf} \tag{4.13}$$

Studies in the literature report lower isobaric specific heat values for nanofluids with regard to the base fluid. One such study is that of Eastman and co-workers [16] who found a decrease of approximately 8% in Al_2O_3 nanofluids with a volume concentration of 3% compared with the water used as the base fluid.

However, in opposition to this common trend, cases can also be found of nanofluids presenting an increase in isobaric specific heat when compared with the base fluid. Shin and Banerjee [38, 39] obtained improvements in isobaric specific heat values of 14% for nanofluids with a volume fraction of 0.6% SiO_2 in eutectic chloride salts as a base fluid. They observed that internal sub-structures were formed in the nanomaterial in the form of lattices, which had the properties of a semi-solid, resulting in an improvement in isobaric specific heat. They presented three models to explain this anomalous improvement:

I. Greater surface energy. The atoms found on the surface of the nanoparticles are less limited in terms of bonds, so they vibrate at a lower frequency and greater amplitude, which results in greater surface energy, which, in addition, is more notable the lower the amount of nanomaterial dispersed within the fluid.

II. Fluid-solid interaction energy. Nanoparticles present high surface area per unit of mass values, which creates a great deal of thermal resistance at the interface between the nanoparticles and the liquid molecules, which is insignificant at a macrometric scale. This resistance must act as additional thermal storage, resulting from the interaction between the vibration energy from the nanoparticles and the liquid molecules around them, leading to an increase in the isobaric specific heat.
III. Formation of a semi-solid layer. The liquid molecules create a layer around the nanoparticles whose thickness depends largely on the surface energy of the nanoparticles. This layer has semi-solid properties; that is, higher values than the nanoparticles dispersed in the bulk that contribute to an increase in the isobaric specific heat.

Therefore, incorporating the nanomaterial into the heart of the base fluid modifies a series of properties that can be predicted with greater or lesser accuracy by mathematical approximations, and phenomena and mechanisms are assumed to take place in these systems that mean that nanofluids cannot be considered to be a simple mixture of the two materials.

Experimentation and the use of theoretical models to understand and define any natural phenomenon are not the only methodologies currently being employed. The meteoric developments in computers that have taken place since the fifties, and the use of computers to resolve problems in the field of science, has resulted in substantial improvements in our knowledge thanks to a new methodology: computer simulation.

Presented as a new scientific tool in the early fifties, the new methodology involving computer simulation was first pioneered in a study by Metropolis and co-workers [40], who used a new method base on the generation of random numbers, christened Monte Carlo simulation. Not long after, in 1957, the first study appeared that used Molecular Dynamics (MD) simulations, when Alder and Wainwright [41] used this technique to investigate the phase diagram of a rigid spheres model. The early studies involving Molecular Dynamics include the one in 1960 by Gibson, Vineyard and co-workers [42], who carried out the first MD simulation of a real material composed of 500 copper atoms forming a crystalline structure; and the study by Rahman [43], in 1964, that analysed the attraction and repulsion interactions of a system composed of 864 argon atoms.

From then until now, the amount of scientific research that has simulated real systems using computational techniques has increased constantly, boosted by the improvements in computers (performance, data processing speed, storage capacity, etc.) and by the desire to learn about and understand the world of nanotechnology. Molecular Dynamics simulations have now become a key tool for complementing experimental studies and research in the field of science.

Within the field of nanofluids in particular, simulations using different methods or techniques in general, and Molecular Dynamics in particular, have promoted a greater, more in-depth understanding of these systems and the phenomena taking place within them. The most important studies in this context include the research carried out in 2004 by Xue and co-workers [44] involving MD simulations to investigate the effect of the arrangement of the liquid-solid interface on thermal resistance. They reported that a single-atom layer of base fluid had no effect on heat transport and this mechanism was ruled not to be responsible for the enhancement in the thermal conductivity of the nanofluids; Shenogin and co-workers [45] used classical MD simulations to study the interfacial resistance for the heat flow between a carbon nanotube and liquid octane. They discovered that this resistance presented a high value due to the coupling between the nanotubes and the liquid, which decreases as the length of the nanotubes increases. In 2006, Vladkov and Barrat [46] found with the help of MD simulations that the confinement effect, particle mass and Brownian motion have an effect on the transfer of heat between the base fluid and the nanoparticles, and they showed that in the absence of collective effects, the thermal conductivity of the nanofluid is well described by the classic Maxwell model. In the same year, Prasher and co-workers [47] used MD to study the effect of the formation of clusters on thermal conductivity, showing that these aggregates are responsible for the enhancement in this property. In 2007, Sarkar and Selvam [48] used MD simulations to calculate the thermal conductivity of copper-based nanofluids using liquid argon as the base fluid for a single nanoparticle and for variable volume fractions. They investigated the possible atomic-level mechanisms involved in the transport of heat, reporting that the increase in movement of the liquid molecules in the presence of nanoparticles caused an increase in the thermal conductivity of the nanofluids. In 2008, Sankar and co-workers [49] proposed a theoretical approach based on MD to estimate the improvement in thermal conductivity caused by suspending platinum nanoparticles in water. Their results were in line with existing experimental results and those predicted by conventional theories. Then, in

2012, Kang and co-workers [50] used several nanoparticles within the simulation box to recreate by means of MD how aggregation of the nanomaterial affected thermal conductivity and viscosity. In turn, Babaei and co-workers [51] applied the Green-Kubo Molecular Dynamics procedure on various systems, including nanofluids, without observing a clear difference when the nanomaterial was dispersed well enough; they underlined the importance of correctly defining the mean energies in the assessment of heat transport. In the same year, Dang and co-workers [52] carried out MD simulations to study the effects of solvation and the interactions between metal particles in n-hexane, methanol and water, demonstrating that the methanol and water molecules bind to the coordination sites of the metals, while the n-hexane molecules were significantly influenced by solvated nanoparticles. Finally, Lin and co-workers [53] provided confirmation of the improvement in the thermal conductivity with volume fraction and nanoparticle size by studying nanofluids consisting of copper nanoparticles suspended in ethylene glycol. They revealed the molecular mechanisms that were responsible for these improvements by means of DM.

The number of studies performed into nanofluids since 1995 [2] has not ceased to increase and, while it is true that thermal conductivity and viscosity are the two most studied properties, numerous authors have completed studies that have increased our knowledge and understanding of the nanofluids by means of studies involving: different techniques for preparing nanofluids; the use of a variety of nanomaterials and base fluids; monitoring their stability over time following different procedures; the addition of surfactants; the application of ultrasound treatment; assessment of their density and isobaric specific heat; theoretical perspectives through the use of various simulation methods (Molecular Dynamics, Monte Carlo, DFT, etc.); and widening their application to different and varied fields.

However, among all these alternatives, few studies have been performed to date that focus on how these nanofluids can be applied in concentrating solar power using the heat transfer fluid used in these power plants as the base fluid and characterising the nanofluid from both a theoretical and experimental perspective, studying and monitoring their stability and estimating the efficiency of the heat transfer processes.

A fine example of this kind of publications is the study from 2016 carried out by Navas and co-workers [54] into nanofluids based on commercial copper and nickel nanoparticles dispersed into the heat transfer fluid that is used in CSP plants. These

nanofluids presented good stability over time, with particle sizes that remained stable a few hours after their preparation. Increases in density and viscosity were found for both nanofluids, while the copper-based nanofluids presented higher values for isobaric specific heat (improvement of 15%) and thermal conductivity (improvement of 12.5%) with regard to the base fluid, which led to an improvement in the heat transfer coefficient of 11% at room temperature for a mass concentration of $5 \cdot 10^{-4}$ %. In turn, the nickel nanofluids did not show a significant improvement.

Based on the theoretical approach using MD simulations, the dynamic and thermal properties of both nanofluids were estimated, the same trend being obtained as for that reached experimentally: the copper nanofluids improved the thermal properties of the base fluid, while the nickel nanofluids presented a downward trend. In turn, analyses were performed of the structural properties of both systems to determine how the base fluid molecules were organised around each nanoparticle. It was observed that the base fluid was not organised in the same way in each case, which is categorical evidence of the difference between both systems for transporting heat.

This precedent is of great interest as a model to follow for the studies underpinning this Doctoral Thesis: a line of research focusing on improving the efficiency of stable nanofluids so that they can be used directly in CSP plants, research based on approaches that are both experimental and theoretical, involving Molecular Dynamics simulations.

4.2. References

[1] A.H. Elsheikh, S.W. Sharshir, M.E. Mostafa, F.A. Essa, M.K. Ahmed Ali, Applications of nanofluids in solar energy: A review of recent advances, Renewable and Sustainable Energy Reviews 82 (2018) 3483-3502.

[2] S.U.S. Choi, J.A. Eastman, Enhancing thermal conductivity of fluids with nanoparticles, ASME-Publications-Fed 231 (1995) 99-106.

[3] A. Grimm, Powdered aluminum-containing heat transfer fluids, German Patent DE 4131516 A 1 (1993).

[4] H. Masuda, A. Ebata, K. Teramae, N. Hishinuma, Alteration of thermal conductivity and viscosity of liquid by dispersing ultra-fine particles. Dispersion of Al_2O_3, SiO_2 and TiO_2 ultra-fine particles, Netsu Bussei 7(4) (1993) 227-233.

[5] V. Gass, Nanofluid handling by micro-flow-sensor based on drag force measurements, Proceedings IEEE Micro Electro Mechanical Systems, Fort Lauderdale, USA, (1993) 167-172.

[6] X. Wang, X. Xu, S.U. S. Choi, Thermal conductivity of nanoparticle-fluid mixture, Journal of Thermophysics and Heat Transfer 13(4) (1999) 474-480.

[7] S. Lee, S.U.S. Choi, S. Li, J.A. Eastman, Measuring thermal conductivity of fluids containing oxide nanoparticles, Journal of Heat Transfer-Transactions of the ASME 121(2) (1999) 280-289.

[8] J.A. Eastman, S.U.S. Choi, S. Li, W. Yu, L.J. Thompson, Anomalously increased effective thermal conductivities of ethylene glycol-based nanofluids containing copper nanoparticles, Applied Physics Letters 78(6) (2001) 718-720.

[9] H. Xie, J. Wang, T. Xi, Y. Liu, Thermal conductivity of suspensions containing nanosized SiC particles, International Journal of Thermophysics 23(2) (2002) 571-580.

[10] S.M.S. Murshed, K.C. Leong, C. Yang, Enhanced thermal conductivity of TiO_2—water based nanofluids, Int. J. Therm. Sci. 44(4) (2005) 367-373.

[11] T.P. Teng, Y.H. Hung, T.C. Teng, H.E. Mo, H.G. Hsu, The effect of alumina/water nanofluid particle size on thermal conductivity, Applied Thermal Engineering 30(14) (2010) 2213-2218.

[12] K.S. Hong, T.K. Hong, H.S. Yang, Thermal conductivity of Fe nanofluids depending on the cluster size of nanoparticles, Applied Physics Letters 88(3) (2006).

[13] D. Lee, J.W. Kim, B.G. Kim, A new parameter to control heat transport in nanofluids: surface charge state of the particle in suspension, The Journal of Physical Chemistry B 110(9) (2006) 4323-4328.

[14] R. Karthik, R.H. Nagarajan, B. Raja, P. Damodharan, Thermal conductivity of CuO–DI water nanofluids using 3-ω measurement technique in a suspended micro-wire, Experimental Thermal and Fluid Science 40 (2012) 1-9.

[15] P. Keblinski, S. Phillpot, S. Choi, J. Eastman, Mechanisms of heat flow in suspensions of nano-sized particles (nanofluids), International Journal of Heat and Mass Transfer 45(4) (2002) 855-863.

[16] J.A. Eastman, S. Phillpot, S. Choi, P. Keblinski, Thermal transport in nanofluids, Annual Review of Materials Research 34 (2004) 219-246.

[17] M. Hadadian, S. Samiee, H. Ahmadzadeh, E.K. Goharshadi, Nanofluids for heat transfer enhancement – a review, Physical Chemistry Research 1 (2013) 1-33.

[18] J.C. Maxwell, J.J. Thompson, A treatise on electricity and magnetism, Clarendon (1904).

[19] R.L. Hamilton, O.K. Crosser, Thermal conductivity of heterogeneous two-component systems, Industrial & Engineering Chemistry Fundamentals 1(3) (1962) 187-191.

[20] C. Kleinstreuer, Y. Feng, Experimental and theoretical studies of nanofluid thermal conductivity enhancement: a review, Nanoscale Research Letters 6(1) (2011) 229.

[21] W. Yu, S.U.S. Choi, The role of interfacial layers in the enhanced thermal conductivity of nanofluids: a renovated Maxwell model, Journal of Nanoparticle Research 5(1) (2003) 167-171.

[22] Y. Xuan, Q. Li, W. Hu, Aggregation structure and thermal conductivity of nanofluids, AIChE Journal 49(4) (2003) 1038-1043.

[23] J. Koo, C. Kleinstreuer, A new thermal conductivity model for nanofluids, Journal of Nanoparticle Research 6(6) (2004) 577-588.

[24] A. Nadai, Eugene Cook Bingham, Journal of Colloid Science 2(1) (1947) 1-5.

[25] S. Halelfadl, T. Maré, P. Estellé, Efficiency of carbon nanotubes water based nanofluids as coolants, Experimental Thermal and Fluid Science 53 (2014) 104-110.

[26] B.C. Pak, Y.I. Cho, Hydrodinamic and heat transfer study of dispersed fluids with submicron metallic oxide particles, Experimental Heat Transfer 11(2) (1998) 151-170.

[27] S.M.S. Murshed, K.C. Leong, C. Yang, Investigations of thermal conductivity and viscosity of nanofluids, International Journal of Thermal Sciences, 47(5) (2008) 560-568.

[28] W. Duangthongsuk, S. Wongwises, Measurement of temperature-dependent thermal conductivity and viscosity of TiO_2-water nanofluids, Experimental Thermal and Fluid Science 33(4) (2009) 706-714.

[29] L. Syam Sundar, M.K. Singh, A.C.M. Sousa, Investigation of thermal conductivity and viscosity of Fe_3O_4 nanofluid for heat transfer applications, International Communications in Heat and Mass Transfer 44 (2013) 7-14.

[30] C.T. Nguyen, F. Desgranges, G. Roy, N. Galanis, T. Maré, S. Boucher, H. Angue Mintsa, Temperature and particle-size dependent viscosity data for water-based nanofluids – Hysteresis phenomenon, International Journal of Heat and Fluid Flow 28(6) (2007) 1492-1506.

[31] E.V. Timofeeva, J.L. Routbort, D. Singh, Particle shape effects on thermophysical properties of alumina nanofluids, Journal of Applied Physics 106(1) (2009) 014304.

[32] A. Einstein, Eine neue Bestimmung der Moleküldimensionen, Annalen der Physik 324(2) (1906) 289-306.

[33] H. Brinkman, The viscosity of concentrated suspensions and solutions, The Journal of Chemical Physics 20(4) (1952) 571-571.

[34] G. Batchelor, Journal Fluid Mechanical 83 (1977) 97.

[35] N. Masoumi, N. Sohrabi, A. Behzadmehr, A new model for calculating the effective viscosity of nanofluids, Journal of Physics D: Applied Physics 42(5) (2009) 055501.

[36] A.D. Sommers, K.L. Yerkes, Experimental investigation into the convective heat transfer and system-level effects of Al_2O_3-propanol nanofluid, Journal of Nanoparticle Research 12(3) (2010) 1003-1014.

[37] Y. Xuan, W. Roetzel, Conceptions for heat transfer correlation of nanofluids, International Journal of heat and Mass transfer 43(19) (2000) 3701-3707.

[38] D. Shin, D. Banerjee, Enhancement of specific heat capacity of high-temperature silica-nanofluids synthesized in alkali chloride salt eutectics for solar thermal-energy storage applications, International Journal of Heat and Mass Transfer 54(5-6) (2011) 1064-1070.

[39] D. Shin, D. Banerjee, Enhanced specific heat capacity of nanomaterials synthesized by dispersing silica nanoparticles in eutectic mixtures, Journal of Heat Transfer-Transactions of the ASME 135(3) (2013).

[40] N. Metropolis, S. Ulam, The Monte Carlo method, Journal of the American Statistical Association 44(247) (1949) 335-341.

[41] B. Alder, T. Wainwright, Phase transition for a hard sphere system, The Journal of Chemical Physics 27(5) (1957) 1208-1209.

[42] J. Gibson, A.N. Goland, M. Milgram, G. Vineyard, Dynamics of radiation damage, Physical Review 120(4) (1960) 1229.

[43] A. Rahman, Correlations in the motion of atoms in liquid argon, Physical Review 136(2A) (1964) A405.

[44] L. Xue, P. Keblinski, S.R. Phillpot, S.U.S. Choi, J.A. Eastman, Effect of liquid layering at the liquid–solid interface on thermal transport, International Journal of Heat and Mass Transfer 47(19) (2004) 4277-4284.

[45] S. Shenogin, L. Xue, R. Ozisik, P. Keblinski, D.G. Cahill, Role of thermal boundary resistance on the heat flow in carbon-nanotube composites, Journal of Applied Physics 95(12) (2004) 8136-8144.

[46] M. Vladkov, J.L. Barrat, Modeling transient absorption and thermal conductivity in a simple nanofluid, Nano Letters 6(6) (2006) 1224-1228.

[47] R. Prasher, W. Evans, P. Meakin, J. Fish, P. Phelan, P. Keblinski, Effect of aggregation on thermal conduction in colloidal nanofluids, Applied Physics Letters 89(14) (2006) 143119.

[48] S. Sarkar, R.P. Selvam, Molecular dynamics simulation of effective thermal conductivity and study of enhanced thermal transport mechanism in nanofluids, Journal of Applied Physics 102(7) (2007) 074302.

[49] N. Sankar, N. Mathew, C.B. Sobhan, Molecular dynamics modeling of thermal conductivity enhancement in metal nanoparticle suspensions, International Communications in Heat and Mass Transfer 35(7) (2008) 867-872.

[50] H. Kang, Y. Zhang, M. Yang, L. Li, Molecular dynamics simulation on effect of nanoparticle aggregation on transport properties of a nanofluid, Journal of Nanotechnology in Engineering and Medicine 3(2) (2012) 021001.

[51] H. Babaei, P. Keblinski, J.M. Khodadadi, Equilibrium molecular dynamics determination of thermal conductivity for multi-component systems, Journal of Applied Physics 112(5) (2012) 054310.

[52] L.X. Dang, H.V. Annapureddy, X. Sun, P.K. Thallapally, B.P. McGrail, Understanding nanofluid stability through molecular simulation, Chemical Physics Letters 551 (2012) 115-120.

[53] Y.S. Lin, P.Y. Hsiao, C.C. Chieng, Thermophysical characteristics of ethylene glycol-based copper nanofluids using nonequilibrium and equilibrium methods, International Journal of Thermal Sciences, 62 (2012) 56-60.

[54] J. Navas, A. Sanchez-Coronilla, E.I. Martin, M. Teruel, J.J. Gallardo, T. Aguilar, R. Gomez-Villarejo, R. Alcantara, C. Fernandez-Lorenzo, J.C. Pinero, J. Martin-Calleja, On the enhancement of heat transfer fluid for concentrating solar power using Cu and Ni nanofluids: An experimental and molecular dynamics study, Nano Energy 27 (2016) 213-224.

Chapter 5

Methodology

5. Methodology

Before addressing the main results obtained, it is useful to outline the methodology followed and the equipment and techniques used for measuring the different properties.

From an experimental perspective, a methodology was established consisting of three stages that have directly guided the study towards the achievement of the objectives proposed (see ***Chapter 3 – Hypothesis and objectives***). The stages that make up the experimental approach are:

- Design and preparation of nanofluids.
- Study and monitoring over time of the stability of the nanofluids prepared.
- Characterization of the rheological and thermal properties of the nanofluids prepared and the assessment of their efficiency.

Likewise, the theoretical approach and the parameters used for the Molecular Dynamics simulations will be described.

5.1. Definition of the base fluid

Concentrating solar power (CSP) plants work with heat exchanger fluids based on molten salts or thermal oils [1]. Examples of these are the Dowtherm range of fluids produced by The Dow Chemical Company© or Therminol, produced by the Eastman Chemical Company©. For their potential application in the concentrating solar power industry based on parabolic trough technology, all the nanofluids studied in this Doctoral Thesis were prepared using the heat transfer fluid commonly used in this kind of plants, supplied by the company Torresol Energy Investments S.A. This heat transfer fluid (HTF) is a thermal oil from the Dowtherm-A range that is composed of a eutectic mixture of two stable aromatic compounds (Figure 5.1.1): diphenyl oxide (or diphenyl ether, with the molecular formula $C_{12}H_{10}O$) and biphenyl (or phenylbenzene, with the molecular formula $C_{12}H_{10}$), in proportions of 73.5% and 26.5%, respectively. Eutectic mixture means the mixture of two or more liquid components in proportions so that their melting point or vaporisation point is lower than that of any of its components in a pure state.

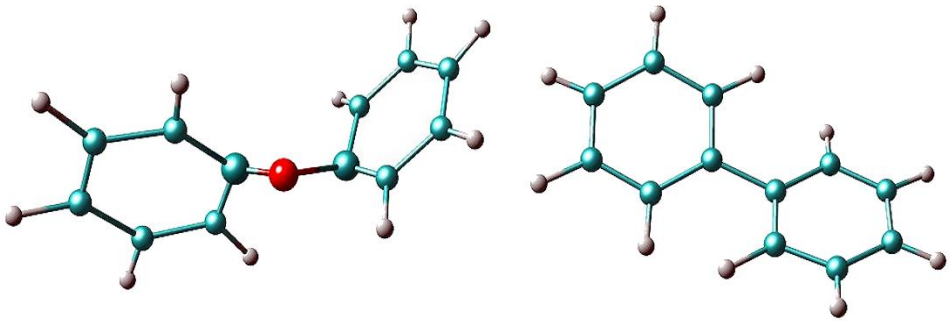

Figure 5.1.1. Image of the molecules that form the base fluid: diphenyl oxide (left) and biphenyl (right).

The main aim of nanofluids is to be more efficient at exchanging or transferring heat since than the currently-used fluids, which present relatively low efficiency values. The isobaric specific heat values of solids such as copper (383 J kg^{-1} K^{-1}) or gold (129 J kg^{-1} K^{-1}) at room temperature are known to be considerably lower than those of liquids. In our case, the eutectic mixture presented a specific heat of 1573 J kg^{-1} K^{-1}. However, also at room temperature, copper (401 W m^{-1} K^{-1}) or gold (318 W m^{-1} K^{-1}) present significantly higher thermal conductivity values than the eutectic mixture (0.13 W m^{-1} K^{-1}). Figure 5.1.2 shows the isobaric specific heat and thermal conductivity values in a temperature range between 300 and 360 K for the eutectic mixture Dowtherm-A.

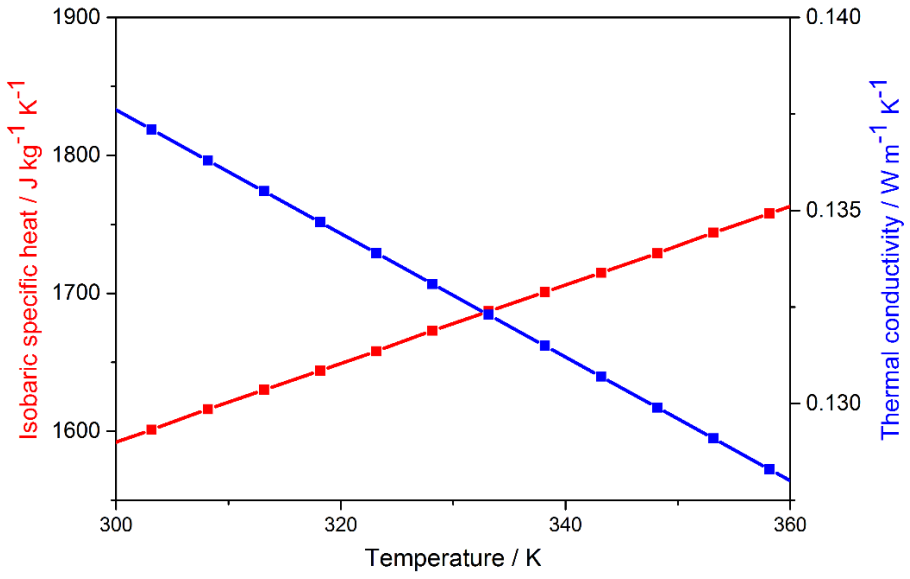

Figure 5.1.2. Isobaric specific heat values (in red) and thermal conductivity (in blue) for the eutectic mixture Dowtherm-A.

Therefore, if the addition of nanoparticles in suspension produces an improvement in these properties, and this leads to an increase in the efficiency of the heat transfer processes, nanofluids acquire interesting advantages and become an alternative to the base fluid for application as heat transfer fluids in CSP plants.

This Doctoral Thesis presents the results obtained for nanofluids based on the Dowtherm-A base fluid and using metallic nanoparticles of silver, gold and platinum as the nanomaterial. All the nanofluids were studied to determine their stability over time, and characterized experimentally by measuring their thermal and rheological properties to assess the degree of improvement in their efficiency as heat transfer fluids. In turn, by means of Molecular Dynamics simulations, dynamic and thermal properties were calculated to compare the theoretical results with those obtained experimentally, while structural properties were analysed to determine and understand the molecular arrangement of this kind of systems in order to rationalise what is known about them with regard to heat transfer mechanisms.

5.2. Design and preparation of nanofluids

There are basically two ways or methods for preparing nanofluids:

- One-step preparation method. In this method, the nanomaterial is synthesized and directly dispersed into the nanofluid in the same preparation process as the nanofluid. This method generally produces nanofluids with remarkable stability and efficiency as it avoids problems that are inherent in nanomaterials, which tend to agglomerate during the drying, storage and transport stages, leading to problems in the dispersion stage [2-6].
- Two-step preparation method. This method consists of two steps: first the nanomaterial is synthesized before being dispersed into the base fluid in the second stage. This method has become the most common way of preparing nanofluids [7-13] thanks to the large variety of methods of synthesis and the wide range of commercial nanomaterials currently on the market.

One of the challenges to be met in the preparation of nanofluids is to minimize the natural tendency of the particles to agglomerate and precipitate due to the attractive interactions between molecules that are favourable to the interactions between the particles and the fluid molecules. This tendency modifies the amount of nanomaterial in suspension and has a direct impact on the stability and thermal properties of the nanofluids [3,14], generating unstable nanofluids that do not possess significantly-enhanced thermal properties. The characteristics of the suspended particles and the base fluid, such as their morphology, chemical structure or degree of agglomeration, are factors that have a strong effect on the stability of a nanofluid [15].

Chemical and physical methods exist make it possible to prepared stable nanofluids. The most commonly used mechanisms are:

- To control the surface charge of the nanomaterial by pH modification. The stability of a nanofluid is directly related with electrostatic interactions as repulsive forces can stabilize material in dispersion [16-18]. The isoelectric point of a colloidal system is the pH value at which the concentration of ions results in a zero net charge, or the pH at which the ζ potential is zero, and therefore the charge on the surface of the nanomaterial is zero. This means that to obtain stable nanofluids it is necessary to set the pH at the furthest possible distance from the isoelectric point without encouraging the reactivity of any of the species involved in the system; in other words, high ζ potential values are required [19, 20]. It is generally agreed that for water-based nanofluids a greater ζ potential value, 30 mV in absolute terms, leads to a stable colloidal suspension [21].
- Modification of the particle surface by adding surfactants. This is the most widely used method for obtaining stable nanofluids [22]. Surfactants are substances that have an effect on the interface between the surface of a particle and the medium [23], preventing the agglomeration of the nanomaterial by altering the hydrophobicity of the surface of the particle, decreasing the surface energy, generating repulsion energy, etc. Some of the most commonly used surfactants are sodium dodecyl sulphate or SDS [24], sodium dodecyl benzenesulfonate or SDBS [25], cetyltrimethylammonium bromide or CTAB [26], or polyvinylpyrrolidone or PVP [10], amongst others. Although the addition of surfactants makes nanofluids more stable, it may limit their

application at high temperatures as the bonds between the nanomaterial and the surfactant may be affected [27, 28], as well as the stability of the surfactant itself.

- Ultrasound treatment. This mechanism allows the break-up of any agglomerates formed during the process of preparing the nanofluids. This leads to a greater concentration of nanomaterial in suspension without the formation of large agglomerates [12, 16, 29, 30].

The present Doctoral Thesis shows the preparation of nanofluids based on both commercial and synthesized nanoparticles using both methods of preparation, an example of which can be seen in Figure 5.2.1. A combination of the mechanisms described above is usually used to obtain stable nanofluids, so a variety of additives were used to act as phase transfer agents and surfactants, and ultrasound treatment was applied in the preparation of the nanofluids to facilitate the suspension of the nanomaterial.

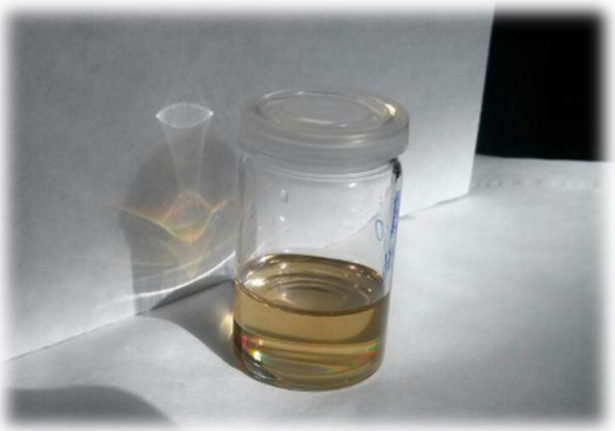

Figure 5.2.1. Final appearance of a nanofluid.

5.2.1. Preparation of silver nanofluids

The nanofluids based on silver nanoparticles were prepared using the two-step method. The nanomaterial used was commercial silver nanoparticles (purity ≥ 99%, density: 10490 kg m^{-3} at 298 K, Sigma-Aldrich©) with a particle size below 100 nm, which were dispersed into the base fluid (eutectic mixture Dowtherm-A). Three nanofluids were prepared varying the concentration of the nanomaterial, $0.5 \cdot 10^{-4}$, $1.0 \cdot 10^{-4}$ y $5.0 \cdot 10^{-4}$ wt.%, and the same percentage of polyethylene glycol (molecular weight: 400; Sigma-Aldrich©), which acted as a surfactant. The mixture underwent sonication treatment (three hours, with a final

power applied of 50 W) in a thermostatically-controlled water bath at 298 K to achieve the best possible dispersion of the nanomaterial.

5.2.2. Preparation of gold nanofluids

In this section it is essential to distinguish between two different preparation methods for the gold nanofluids.

The first nanofluid system based on gold nanoparticles was prepared using the one-step method. The experimental procedure for preparing these nanofluids can be summarised as:

1) A solution of 10 mM of the gold precursor, tetrachloroauric acid ($HAuCl_4$, purity ≥ 99.9%, Sigma-Aldrich©) is mixed into an aqueous solution with a base fluid solution (eutectic mixture Dowtherm-A) and tetraoctylammonium bromide ($[(C_8H_{17})_4N]Br$, commonly known as TOAB, purity ≥ 98%, Sigma-Aldrich©), with double the weight percent in comparison with the quantity of gold. The TOAB acts first of all as a phase transfer agent causing the metal precursor to migrate from the aqueous phase to the organic phase, according to the reaction:

$$AuCl_4^-{}_{(aq)} + N(C_8H_{17})_4^+{}_{(bf)} \rightarrow N(C_8H_{17})_4^+ AuCl_4^-{}_{(bf)}$$

2) After an initial liquid/liquid extraction, an aqueous solution of 50 mM of sodium borohydride ($NaBH_4$, purity ≥ 98%, Fluka Sigma-Aldrich©) is gradually added to the organic phase and left under magnetic stirring. The colour of the solution is seen to change from dark green to brown as a result of the reduction of the tetrachloroauric anion to metallic gold, as indicated by the reaction:

$$m\,AuCl_4^-{}_{(bf)} + 3m\,e^-{}_{(bf)} \rightarrow 4m\,Cl^-{}_{(bf)} + Au_{m(bf)}$$

   At this moment, the TOAB additive plays a second role, acting as a surfactant to prevent the recently-formed gold nanoparticles from agglomerating.

3) A final liquid/liquid extraction is performed: the organic phase is considered to be the gold nanofluid and the aqueous phase, which has a transparent appearance, is discarded.

4) Three nanofluids were prepared varying the concentration of gold nanoparticles, 0.0025, 0.005 and 0.01 wt.%, with double the percentage by weight of TOAB and with five times the molar proportion of sodium borohydride.

The second gold nanofluid system was designed in order to perform a comparison with the silver nanofluids described above. To this end, gold nanofluids were prepared following the two-step method under the same conditions as those explained above for the silver nanofluids, but in this case commercial nanoparticles were not used. Instead, gold nanoparticles were synthesised by reduction (by means of sonication [31]) with sodium citrate ($C_6H_5Na_3O_7 \cdot 2H_2O$, purity ≥ 99%, PanReac AppliChem©) and the same gold precursor, tetrachloroauric acid ($HAuCl_4$). The nanofluids were prepared using the eutectic mixture Dowtherm-A as the base fluid.

Three nanofluids were prepared with the same concentrations as the silver nanofluids, $0.5 \cdot 10^{-4}$, $1.0 \cdot 10^{-4}$ and $5.0 \cdot 10^{-4}$ wt.%, and the same percentage of polyethylene glycol. The mixture underwent sonication treatment (three hours, with a final power applied of 50 W) in a thermostatically-controlled water bath at 298 K to achieve the best possible dispersion of the nanomaterial.

5.2.3. Preparation of platinum nanofluids

The nanofluids based on platinum nanoparticles were prepared following the two-step method. The platinum nanoparticles were synthesized in an aqueous solution beginning with a 14 mM solution with a metallic precursor, hexachloroplatinic acid (H_2PtCl_6, purity ≥ 38% in platinum, Sigma-Aldrich©), which was reduced by the reducing agent sodium borohydride ($NaBH_4$, purity ≥ 98%, Fluka Sigma-Aldrich©), at a weight ratio of 1:10 with regard to the platinum. The reaction took place in a low-power ultrasound bath by slowly adding the reducing agent to control the formation of agglomerates. The reduction of the platinum can be deduced from the change in colour from orange (original solution) to black (final solution), through the reaction:

$$H_2PtCl_6 + 6NaBH_4 \rightarrow 6NaCl + Pt + 3(BH_3)_2 + 4H_2$$

Next, this aqueous solution is added to the base fluid solution (Dowtherm-A) together with dodecylamine ($CH_3(CH_2)_{11}NH_2$, commonly known as DDA, purity ≥ 98%, Sigma-Aldrich©), which acts as a phase transfer agent, at a weight ratio of 1:2 with regard to the original platinum. The resulting solution is kept under gentle magnetic stirring for one hour and, after a liquid/liquid extraction, the aqueous phase, which has a transparent appearance (unmistakable sign that the platinum has transferred to the organic phase) is discarded.

In this research, two mechanisms were studied for improving the stability of the nanofluids: the addition of surfactants and the application of ultrasound. To this end, following the methodology described above, three nanofluids were prepared with a platinum concentration of 0.005 wt.%. Two of them were treated with ultrasound (with impulses every two seconds for 45 minutes at 30% power, stopping for four seconds to prevent a dramatic increase the temperature, and a total energy transmitted of approximately 11 kJ). Second surfactant, 1-Octadecanethiol ($CH_3(CH_2)_{17}SH$, commonly known as ODT, purity ≥ 98%, Sigma-Aldrich©) was added to the third nanofluid and to one of the two nanofluids treated with ultrasound at a weight ratio of 1:3 with regard to the original platinum. Finally, the three nanofluids were left under magnetic stirring for one hour in a thermostatically-controlled water bath at 298 K.

5.3. Experimental characterization

The stability of the nanofluids and the improvement in the efficiency of heat transfer processes, together with economic viability, are the indicators to be taken into account ahead of the potential use of the nanofluids in the thermosolar industry. Therefore, it is essential to obtain nanofluids that are stable over time as a preliminary and limiting step before subsequently characterizing their thermal and rheological properties in order to study possible improvements in efficiency.

5.3.1. Stability

The Derjaguin-Landau-Verwey-Overbeek (DLVO) theory [32, 33] of colloidal interactions dictates that a colloidal system will remain stable if and only if the repulsive electrostatic forces, which stem from the net charge on the surfaces of the particles, are greater than the Van der Waals attraction force; otherwise, the colloidal particles will group together and form clusters and aggregates. Furthermore and in parallel, a nanofluid can be described as stable when the concentration of nanomaterial in suspension remains constant over time [34].

Although the stability of nanofluids is incredibly important when they are put into use, there are a limited number of studies that estimate the stability of a suspension, and even fewer in the field of nanofluids. In the present Doctoral Thesis, an assessment has been made of the stability of all the nanofluids by means of different techniques:

- Ultraviolet-visible spectroscopy: a simple and direct technique that makes it possible to study the suspension of the nanomaterial in the heart of the fluid and to monitor it over time [35]. As well as being quick and easy to use, it provides the option of assessing and estimating the concentration of nanomaterial in suspension, although it is not suitable or advisable for nanofluids with a high concentration of nanomaterial [36]. In addition, by comparing the absorption bands of the spectra of the nanofluids and the base fluid, it is possible to observe whether chemical changes have taken place in the base fluid due to the addition of the nanomaterial.
- Measurements of particle size and their distribution using light dispersion methods: analysing the size of the particles enables the formation of agglomerates and their behaviour over time to be studied [37, 38], nanofluids being considered more stable when the particle size remains constant and they present a narrow distribution of sizes. The particle sizes were analysed using the dynamic light scattering (DLS) technique. This technique is based on illuminating a sample with a laser beam and detecting the fluctuations in the intensity of the light when it strikes the particles, which are in constant movement due to Brownian motion [39, 40].

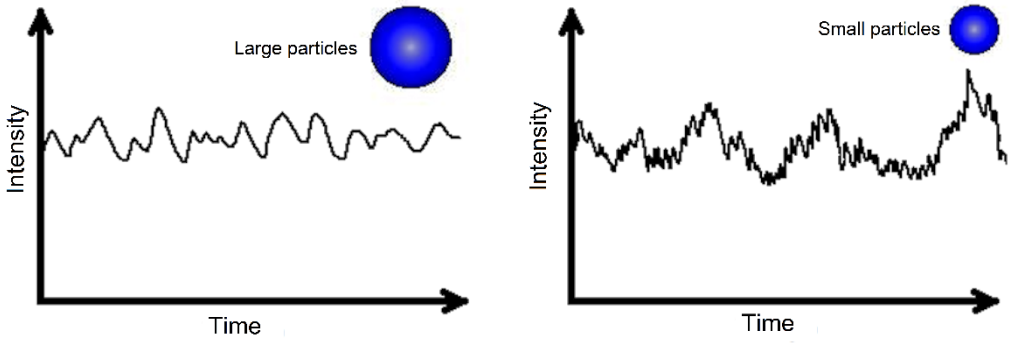

Figure 5.3.1. Fluctuations in the particle size observed in the DLS technique.

These fluctuations in intensity (Figure 5.3.1) are related to the translational diffusion coefficient $\boldsymbol{D}$ and to the diameter of the particles by means of the Stokes-Einstein equation (Equation 5.3.1), which establishes that the translational diffusion coefficient of a spherical particle depends on its size and the temperature and viscosity of the medium, but not on the density and composition of the nanoparticle:

$$R_H = \frac{kT}{6\pi\mu D} \tag{5.3.1}$$

where $\boldsymbol{k}$ is the Boltzmann constant, $\boldsymbol{T}$ and $\boldsymbol{\mu}$ the temperature and viscosity of the medium, and $\boldsymbol{R_H}$ the hydrodynamic radius of the particle (or Stokes radius). However, this radius is the sum of the size of the particle and the layer of ions and molecules bonded to it; thus, the DLS technique slightly overestimates the real size of a particle (Figure 5.3.2).

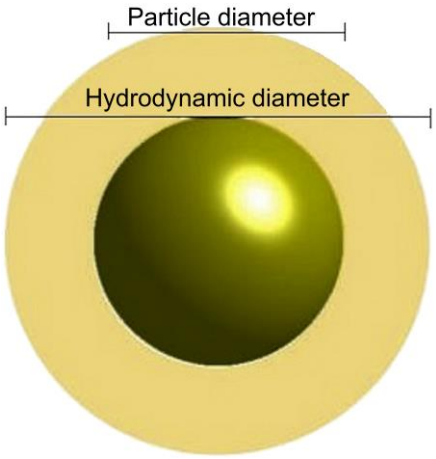

Figure 5.3.2. Illustration of the hydrodynamic diameter and diameter of a particle.

The real size of a particle is analysed using transmission electron microscopy (TEM), which is a procedure that complements DLS in cases where it is necessary to obtain an accurate result of the nominal size of the nanoparticles, for example in the study of the size and morphology of a nanomaterial after synthesis, or for observing modifications in the size and shape of the nanoparticles after applying a series of heat cycles to the nanofluid.

- Measurements of ζ potential: a commonly-used technique in the field of colloidal chemistry that enables the measurement of the electrostatic (or charge) repulsion or attraction between the particles, a fundamental parameter that affects stability and provides information about the degree of dispersion or agglomeration of the nanomaterial within the fluid [41, 42]. A high ζ potential value indicates that the electrostatic interaction between the particles of the system is greater that the Van der Waals forces, which leads to a high degree of stability. The published literature concludes that a water-based colloidal system is considered to be stable if it presents absolute ζ potential values above 30 mV [21, 43]. The ζ potential can be obtained indirectly by measuring electrophoretic mobility using the combined technique of laser Doppler microelectrophoresis and phase analysis light scattering (PALS), a similar technique to DLS. In this case, the sample is submitted to an electric field that provokes the movement of charged particles towards the oppositely charged pole with a velocity that is related to electrophoretic mobility $\boldsymbol{\mu_e}$ ($\mu_e = {}^{V}/_{E}$, where $\boldsymbol{V}$ is the particle velocity and $\boldsymbol{E}$ the electric field), which is in turn related to the ζ potential through the Henry equation (Equation 5.3.2):

$$\mu_e = \frac{2\,\varepsilon\,Z\,f(ka)}{3\mu} \tag{5.3.2}$$

where $\boldsymbol{\varepsilon}$ is the dielectric constant of the medium, $\boldsymbol{Z}$ the ζ potential and $\boldsymbol{f(ka)}$ Henry's function, which measures the ratio of the particle radius and the thickness of the electrical double layer, to which the Smoluchowski approach was applied: $f(ka) = 1.5$ [44, 45].

To study the stability of each nanofluid prepared in this Doctoral Thesis, each of the properties of the samples mentioned above were monitored for a week, taking several measurements every day to obtain representative mean values. To this end, the following equipment was used:

- A system consisting of a DH-2000-Bal deuterium-halogen light source with a USB200+ spectrometer, supplied by Ocean Optics©, to record the ultraviolet-visible spectra in the wavelength range of 350-880 nm, using glass cuvettes and recording the spectra in triplicate every day for a week.
- A Malvern© Zetasizer Nano ZS to perform the measurements of DLS and ζ potential. Both measurements were performed in glass cuvettes and in the case of the ζ potential in particular using a platinum electrode, recording both analyses in triplicate every day for a week.

5.3.2. Efficiency

Once the physical and chemical stability of the nanofluids had been determined, the next step of the study focused on changes in the rheological and thermal properties of the base fluid due to the incorporation of the nanomaterial, and whether these changes improved its efficiency in heat transfer processes with regard to the base fluid with a view to using the nanofluids in the thermosolar industry. According to Timofeeva and co-workers [46], for a nanofluid to be used as a heat transfer fluid, a rather complex study is required that explains the changes produced in all the thermophysical properties of the base fluid after the addition of nanomaterials, from the interactions between the particles and the fluid to a large number of factors: concentration and type of nanomaterial, its size and shape, the properties of the base fluid, the presence of surfactants, etc.

Therefore, the efficiency of the fluids in heat transfer processes was assessed according to the heat transfer coefficient, $\boldsymbol{h}$, which is defined as $h = (k^a \rho^b C_p^c)/(\mu^d \sigma^e)$, where $\boldsymbol{k}$ is thermal conductivity, $\boldsymbol{\rho}$ density, $\boldsymbol{C_p}$ the isobaric specific heat, $\boldsymbol{\mu}$ viscosity and $\boldsymbol{\sigma}$ surface tension [47]. The exponents are empirical and theoretical constants that depend on the boundary conditions of the system under study; *e,* normally being zero when no phase change takes place [48]. In this Doctoral Thesis, the fluids in concentrating solar power plants are

considered to be found under conditions of turbulent flow and the enhancement in the efficiency of the nanofluids with regard to the base fluid has therefore been estimated in accordance with the Dittus-Boelter equation [49], which gives the ratio of the heat transfer coefficients of the nanofluid and the base fluid, and is considered to be a Figure of Merit. According to this equation, efficiency is considered to increase if the ratio of the heat transfer coefficients between the nanofluid and the base fluid is $\left(h_{nf}/h_{bf}\right) > 1$. The heat transfer coefficient is calculated by means of this equation taking into consideration the previous expression, according to Equation (5.3.3):

$$FoM = \frac{h_{nf}}{h_{bf}} = \left(\frac{\rho_{nf}}{\rho_{bf}}\right)^{0.8} \left(\frac{k_{nf}}{k_{bf}}\right)^{0.6} \left(\frac{C_{p(nf)}}{C_{p(bf)}}\right)^{0.4} \left(\frac{\mu_{nf}}{\mu_{bf}}\right)^{-0.4} \tag{5.3.3}$$

defining the nanofluid and the base fluid under the subscripts nf and bf.

A similar equation to that developed by Dittus-Boelter is the Mouromtseff equation [50, 51]. In this Equation (5.3.4), the heat transfer coefficient, represented by the Mouromtseff number, M_O, is estimated using the same thermophysical properties used for the Dittus-Boelter equation. A nanofluid is considered to be more efficient when the ratio of the Mouromtseff number of the nanofluid to the base fluid is higher $\left(M_{o_{nf}}/M_{o_{bf}}\right)$.

$$M_o = \frac{\rho^{0.8} k^{0.67} {C_p}^{0.33}}{\mu^{0.47}} \tag{5.3.4}$$

Other authors, such as Prasher and co-workers[52], suggest that under laminar flow conditions the efficiency of a nanofluid will depend only and to a large extent on two properties: viscosity and thermal conductivity. Thus, if the increase in dynamic viscosity is less than four times the increase in the thermal conductivity, the nanofluid is considered to be efficient, in accordance with ratio (5.3.5):

$$\frac{DVI}{TCE} = \frac{\left(\mu_{nf} - \mu_{bf}\right)/\mu_{bf}}{\left(k_{nf} - k_{bf}\right)/k_{bf}} \leq 4 \tag{5.3.5}$$

Therefore, to be able to apply these models, it is necessary to study the properties that they are comprised of:

- Density: is a physical property that relates the mass of a substance to its volume. Since the density of solids is greater than that of liquids, generally speaking, adding nanomaterial to the base fluid will produce an increase in its density value. In turn, materials with high density values make heat transfer processes more efficient [47].
- Viscosity: a rheological property that can be defined, in simple terms, as the greater or lesser resistance of a fluid to flow freely. However, as seen in the equations that define the efficiency of a nanofluid, an increase in viscosity values is counter-productive in terms of efficiency and must therefore be controlled and kept to a minimum. The natural tendency produced by incorporating nanomaterial into the base fluid is an increase in viscosity values as the concentration of nanomaterial increases and the temperature decreases [28, 53].
- Isobaric specific heat: defined as the amount of heat required per unit mass to raise the temperature by one degree. Solids present lower isobaric specific heat values than liquids, so, for the same temperature increase, less thermal energy is required by the nanofluid than the base fluid, and thus the nanofluid will present a lower isobaric specific heat value [54, 55]. However, the opposite trend is also plausible and some studies have reported that nanofluids may present improvements in this property [56, 57].
- Thermal conductivity: refers to the ability of a material to transfer heat, and is the most important intrinsic parameter for demonstrating the potential for improvements in heat transfer in nanofluids. Solids present much higher thermal conductivity values than liquids. Therefore, incorporating nanomaterial into a fluid leads to nanofluids presenting high thermal conductivity values than the base fluid. In addition, amongst other factors, an increase in the concentration of nanomaterial and in temperature generally involves an increase in thermal conductivity values [58-60].

In order to perform the measurements of the density, viscosity, isobaric specific heat and thermal conductivity values of the nanofluids and the base fluid, the following equipment and techniques were used:

- The density was determined by means of pycnometry at room temperature, performing the number of measurements required to obtain a representative mean value. The values for density at high temperature were estimated using the curve plotted by the

base fluid, obtained from the data sheet of the manufactured product and shown in Figure 5.3.3.

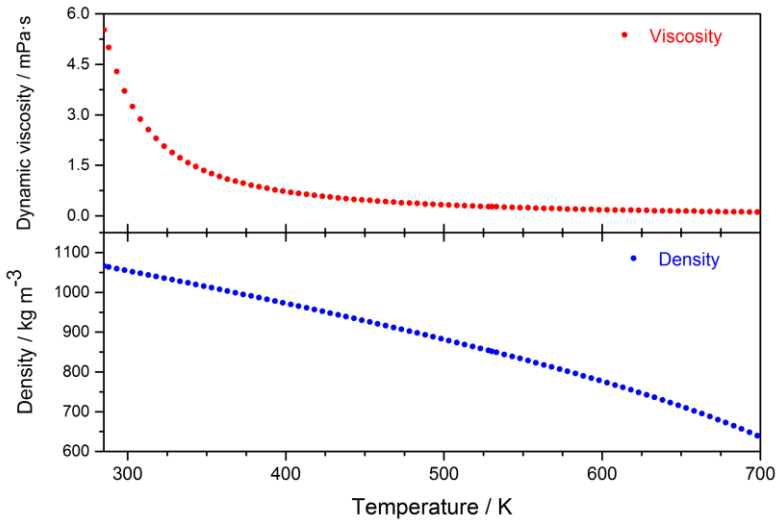

Figure 5.3.3. Density values (in blue) and viscosity (in red) for the eutectic mixture Dowtherm-A.

- Viscosity was analysed by means of a vibration system, the Vibro Viscosimeter SV-10 from A&D Company©, coupled to a temperature sensor and a thermal bath set a room temperature. To perform the measurements, two sensor plates were placed into the fluid and submitted to a constant vibration frequency (30 Hz), generating a current between the two sensor plates proportional to the viscous drag of the fluid; this ratio is used to calculate the viscosity value. The required number of measurements of viscosity at room temperature were performed to obtain a representative mean, while the viscosity values at high temperature were estimated in the same way as those of density, described above (Figure 5.3.3).

- Isobaric specific heat was determined by means of the temperature-modulated differential scanning calorimetry (TMDSC) technique, using a Q-20 calorimeter supplied by TA Instruments©. To carry out the measurements, a procedure was developed that can be summarised in the following steps: first, the temperature was equilibrated to 341 K to eliminate contaminants and impurities, and isothermal conditions were maintained for 10 minutes; next, the temperature was lowered to 301 K and then increased to 391 K at a rate of 1 K/min; then, a modulation was

programmed around the temperatures studied with a amplitude of ±1 K and a period of 120 seconds; finally, cooling took place at a rate of 1 K/min. To check the accuracy of the procedure and the equipment, the isobaric specific heat of the base fluid was measured and these values compared with the data provided by the supplier. The isobaric specific heat of each nanofluid was measured in triplicate.

- Thermal conductivity was calculated by means of the light flash analysis (LFA) technique, using the LFA-1600 device supplied by Linseis Thermal Analysis©. This technique measures thermal diffusivity, which is the thermophysical property that defines the rate of heat propagation by conduction during changes in temperature and which is related to thermal conductivity through Equation 5.3.6 [61]:

$$k(T) = D(T) \cdot C_P(T) \cdot \rho(T) \tag{5.3.6}$$

To measure thermal diffusivity, $\boldsymbol{D}$, the sample is placed in an oven at a set temperature. An energy pulse (laser or xenon flash) programmed to that temperature heats the lower side of the sample. This pulse generates a homogeneous increase in the energy across the whole sample and the increase in temperature of the other side of the sample is measured using a high-speed infra-red detector. Thermal diffusivity is calculated taking into consideration the thickness of the sample and the mean time of the amplitude of the temperature signal. Thermal conductivity $\boldsymbol{k}$ is estimated according to Equation 5.3.6, having previously determined the isobaric specific heat $\boldsymbol{C_P}$ and the density $\boldsymbol{\rho}$. To check the accuracy of the equipment, the thermal conductivity of the base fluid was measured and these values were compared with the data provided by the supplier. The thermal conductivity of each nanofluid was measured in triplicate.

5.4. Theoretical modelling

5.4.1. Molecular Mechanics

Electrons are a key element in quantum mechanics, making it possible to study structures and calculate their properties through the distribution of electrons and chemical reactivity. However, quantum mechanics calculations cannot be applied to systems with a large number of atoms. However, molecular mechanics ignores electrons and focuses solely on the arrangement or the atomic nuclei in molecules, which makes it possible to study macromolecular systems. Molecular mechanics calculations are based on the Born-Oppenheimer approximation [62, 63], which, by considering that the nuclei move more slowly than the electrons due to the difference in their masses, makes it possible to distinguish the movements of nuclei and electrons. Thus, the baseline energy state of a molecule can be considered as a function of the coordinates of the atomic nuclei, this function being known as the force field.

5.4.1.1. Definition of force field

A force field is composed of a set of empirically-determined equations that define how the potential energy varies with the position of the atoms of a molecule. Most force fields used for molecular systems are composed of two main components that describe the bonding and non-bonding interactions of the system:

$$E_{Total} = E_{bond} + E_{angle} + E_{dihedral} + E_{VdW} + E_{Coulomb} \quad (5.4.1)$$

The first three terms correspond to bonding interactions (covalent bonds, valence angles and dihedral angles), while the remaining terms belong to non-bonding interactions, which are defined as Lennard-Jones attractive and repulsive terms (Van der Waals forces) and Coulomb electrostatic interactions (Figure 5.4.1).

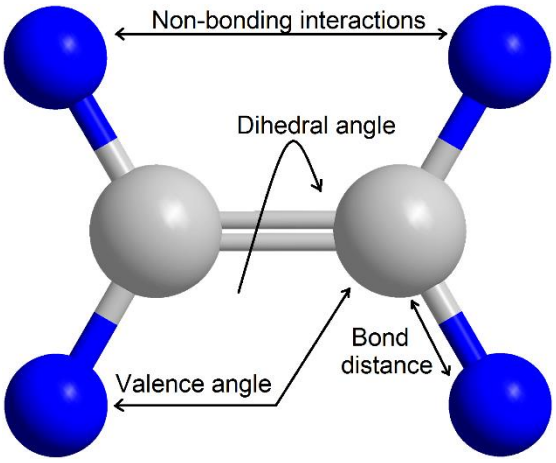

Figure 5.4.1. Schema of the bonding and non-bonding interactions.

5.4.1.2. TraPPE force field

The Transferable Potentials for Phase Equilibria (TraPPE) family of force fields is a collection of functional forms and interaction parameters that are useful for modelling complex chemical systems with molecular mechanics simulation techniques. TraPPE maintains a high degree of accuracy in the prediction of thermophysical properties when applied to a range of different compounds, different state points, different compositions, and different properties. This makes TraPPE one of the few force fields generally suitable for materials and industrial applications. TraPPE force fields consider that molecules interact in pairs via Lennard Jones centres located in the atoms they are composed of, while the Coulomb electrostatic and induction interactions are modelled with punctual charge distributions (Equation 5.4.2):

$$U(r_{ij}) = 4\varepsilon_{ij}\left[\left(\frac{\sigma_{ij}}{r_{ij}}\right)^{12} - \left(\frac{\sigma_{ij}}{r_{ij}}\right)^{6}\right] + \frac{q_i q_j}{4\pi\varepsilon_0 r_{ij}} \qquad (5.4.2)$$

where i and j are the interaction centres and $\boldsymbol{r_{ij}}$ is the distance at which the Lennard-Jones potential between both centres is zero (which gives an idea of the minimum separation distance); $\boldsymbol{\varepsilon_{ij}}$ and $\boldsymbol{\sigma_{ij}}$ are the Lennard-Jones well depth and diameter; $\boldsymbol{q_i}$ and $\boldsymbol{q_j}$ are the partial charges in the interaction centres i and j; and $\boldsymbol{\varepsilon_0}$ the vacuum permittivity.

To model the fluid and to describe the inter- and intramolecular interactions between the diphenyl oxide and biphenyl molecules, the TraPPE-Explicit Hydrogen (TraPPE-EH)

force field model was used [64]. This model, which is specific to aromatic compounds, considers the rings and bonds as rigid entities and involves geometric constraints for the H-C-H and H-C-C angles, although it allows the biphenyl rings freedom of rotation around the C1-C1' bonds.

In turn, to model alkane-type compounds, as in the case of surfactants that contain a heteroatom at any end of the chain, the TraPPE-United Atom (TraPPE-UA) model was used [65]. This model allows for total flexibility as it treats each of the Lennard-Jones interaction centres of the hydrocarbon chain located in the middle of the C-H bonds as pseudoatoms; meanwhile, the interaction centres of the heteroatoms (nitrogen atom of the TOAB and DDA amine group, and sulphur atom of the ODT thiol group) and the carbon atoms directly linked to them are treated as rigid units.

For the description of the metallic nanoparticles, the parameters used in our simulations were adapted to the Non-bonded Dummy model, in which six particles, known as dummy atoms, are located around a central metallic particle in an octahedral geometry. The geometry of the complex is kept rigid by the by the imposition of large force constants on the metal-dummy bonds. However, since there are no bonds between the dummy atoms of the complex, these can rotate around the central metal atom. Therefore, the coordination geometry is not restricted so the system is free to exchange ligands.

5.4.2. Classical Molecular Dynamics

Classical Molecular Dynamics is a computer simulation technique that makes it possible to analyse the properties of systems of particles in equilibrium that interact with each other via a certain potential and evolve over time following the classical equations of motion. It is known as a deterministic approach, since the state of one point of the trajectory makes it possible to predict the state of the following one.

The classical Molecular Dynamics technique has its origins in statistical mechanics, based on the definition of a classical system according to the $\vec{\boldsymbol{r}}$ coordinate and the $\vec{\boldsymbol{p}}$ momentums from the classical Hamiltonian $\boldsymbol{H}$, expressed as:

$$H = H(\vec{r},\vec{p}) = K(\vec{p}) + U(\vec{r}) = \sum_i \frac{p_i^2}{2m_i} + U(\vec{r}) \tag{5.4.3}$$

where $\boldsymbol{K(\vec{p})}$ corresponds to kinetic energy, $\boldsymbol{U(\overrightarrow{r})}$ to potential energy, $\boldsymbol{\vec{p}}$ to the linear moment and $\boldsymbol{m}$ to mass, for all *i* particles.

Thus, by means of a set of $\{\vec{r},\vec{p}\}$ values that correspond to a point of the phase space defined on the basis of coordinates and momentums, we can characterize and simulate the microscopic behaviour of a system and obtain values for different macroscopic properties, both statistical and dynamic.

In mechanic statistics, thermodynamic properties are calculated by taking averages of the statistical set of the states of the system that configure the configuration or phase space of the system. Nevertheless, simultaneously determining all the possible states of the system has a high computational cost. To reduce this cost, the alternative method is based on following the dynamics of one point of the configuration through the phase space instead of taking a mean of all the configuration points in all the configuration space.

Therefore, to determine a property taking into consideration all the configuration points of the configuration space we calculate the mean known as the thermodynamic mean value < A > of a thermodynamic property A ($\vec{r}$,$\vec{p}$) by:

$$< A(\vec{r},\vec{p}) >_z = \int_V \int_{-\infty}^{\infty} \rho(\vec{r},\vec{p}) A(\vec{r},\vec{p})\, d\vec{r} d\vec{p} \tag{5.4.4}$$

where $\boldsymbol{\rho(\vec{r},\vec{p})}$ is the probability distribution given by the Boltzmann distribution, in which the partition function $\boldsymbol{Z}$ is the system phase space integral of the exponential factor e:

$$\rho(\vec{r},\vec{p}) = \frac{e^{-H(\vec{r},\vec{p})/k_b T}}{Z} \tag{5.4.5}$$

Furthermore, if we follow the dynamics of a configuration point across the phase space over time, the mean calculated is the dynamic mean value < A >, defined for any thermodynamic property A ($\vec{r}$,$\vec{p}$) from its trajectory:

$$< A(\vec{r},\vec{p}) >_{\tau} = \frac{1}{\tau}\int_{0}^{\tau} A(\vec{r}(t),\vec{p}(t))\, dt \tag{5.4.6}$$

$\boldsymbol{\tau}$ being the duration of the simulation.

As established by the ergodic hypothesis of statistical mechanics [66], the orbit of a representative point of a system goes through all the representative points of the phase space in the course of infinite time. If this is this case, for trajectories of infinite simulations, the dynamic mean value converges with the thermodynamic mean value. This means that the system reaches equilibrium and underpins the argument that Molecular Dynamics simulations can be used to calculate the thermodynamic mean values of a system, and both dynamic (determined by time correlation functions) and statistical (not dependent on time) properties.

5.4.2.1. Newton's equation of motion

Molecular Dynamics simulations assume that particle motion is governed by Newton's second law of motion (classical mechanics) [67, 68], which is a second order differential equation that, for a system of $\boldsymbol{N}$ particles, is expressed as:

$$\vec{F}(\vec{r}_1 \ldots \vec{r}_N) = m_i \frac{d^2\vec{r}_i}{dt^2} \tag{5.4.7}$$

where $\boldsymbol{m_i}$, $\vec{\boldsymbol{r}}_i$ and $\vec{\boldsymbol{F}}_{\boldsymbol{i}}$ are, respectively, the mass, the vector position and the net force acting on the particle *i*. In accordance with all the coordinates $\vec{\boldsymbol{r}}$ of the system, this force is determined by the gradient of the potential energy $\boldsymbol{U}(\vec{\boldsymbol{r}})$:

$$\vec{F} = -\nabla_i U(\vec{r}_1 \ldots \vec{r}_N) = -\frac{\partial U(\vec{r}_1 \ldots \vec{r}_N)}{\partial \vec{r}_i} \tag{5.4.8}$$

As it is impossible to find a mathematical expression that represents the system's evolution over time, numerical methods are required that provide an approximation to the solution that is as accurate as possible. In the endeavour to achieve the highest levels of accuracy using the lowest number of possible operations, several methods, known as algorithms, have been developed with different features in terms of accuracy and complexity.

5.4.2.2. Verlet integration algorithm

The Verlet algorithm [69] is one of the most popular in the study of Molecular Dynamics for the integration of the centre of mass of one or more particles in motion. From the positions and velocities of the particles at a time $\boldsymbol{t}$, it is necessary to obtain those positions and velocities with sufficient accuracy for a time $(t + \Delta t)$, from the Taylor expansion series:

$$\begin{aligned}\vec{r}(t + \Delta t) &= \vec{r}(t) + \frac{d\vec{r}}{dt}(t)\Delta t + \frac{1}{2}\frac{d^2\vec{r}}{dt}(t)\Delta t^2 + \cdots \\ &= \vec{r}(t) + \vec{v}(t)\Delta t + \frac{1}{2}\vec{a}(t)\Delta t^2 + \cdots\end{aligned} \tag{5.4.9}$$

where $\vec{\boldsymbol{v}}(\boldsymbol{t})$ is the vector velocity and $\vec{\boldsymbol{a}}(\boldsymbol{t})$ is the vector acceleration. If we use $\vec{\boldsymbol{r}}_{\boldsymbol{n}}$ to indicate the position in step $\boldsymbol{n}$ and at time $\boldsymbol{t}$, and use $\vec{\boldsymbol{r}}_{\boldsymbol{n+1}}$ for the step *n+1*, at time $(t + \Delta t)$, and truncating the Taylor series in the second order term, we obtain:

$$\vec{r}_{n+1} = \vec{r}_n + \vec{v}_n\Delta t + \frac{1}{2}\left(\frac{\vec{F}_n}{m}\right)\Delta t^2 + O(\Delta t^3) \tag{5.4.10}$$

Which allows us to know the velocity $\vec{\boldsymbol{v}}_{\boldsymbol{n+1}}$ at step *n+1*:

$$\vec{v}_{n+1} = (\vec{r}_{n+1} - \vec{r}_n)/\Delta t \tag{5.4.11}$$

Therefore, if we know position $\vec{\boldsymbol{r}}_{\boldsymbol{n}}$, the velocity $\vec{\boldsymbol{v}}_{\boldsymbol{n}}$ and the force $\vec{\boldsymbol{F}}_{\boldsymbol{n}}$ at step $\boldsymbol{n}$, we can calculate the position $\vec{\boldsymbol{r}}_{\boldsymbol{n+1}}$ and the velocity $\vec{\boldsymbol{v}}_{\boldsymbol{n+1}}$ at step *n+1*, by means of Equations 5.4.10 and 5.4.11, which constitute the integration algorithm.

To indicate the position at step *n-1*, using $\vec{\boldsymbol{r}}_{\boldsymbol{n-1}}$ for a time $(t + \Delta t)$, and again truncating the Taylor series at the second order term, we obtain:

$$\vec{r}_{n-1} = \vec{r}_n - \vec{v}_n\Delta t + \frac{1}{2}\left(\frac{\vec{F}_n}{m}\right)\Delta t^2 - O(\Delta t^3) \tag{5.4.12}$$

Combining expressions 5.4.10 and 5.4.12, we obtain a new algorithm that makes it possible to know the position (5.4.13) and calculate the velocity (5.4.14):

$$\vec{r}_{n+1} = 2\vec{r}_n - \vec{r}_{n-1} + \left(\frac{\vec{F}_n}{m}\right)\Delta t^2 + O(\Delta t^4) \tag{5.4.13}$$

$$\vec{v}_n = \frac{\vec{r}_{n+1} - \vec{r}_{n-1}}{2\Delta t} + O(\Delta t^3) \tag{5.4.14}$$

Consequently, a new algorithm is obtained that is known as the Verlet algorithm, which can numerically solve second order differential equations, especially applicable to Molecular Dynamics.

A variation of the Verlet algorithm is known as the leap frog (LF) algorithm [70], which results from defining the velocity at the midpoint of the integration step, for *n+1/2* and *n-1/2* according to the expressions:

$$\vec{v}_{n+1/2} = (\vec{r}_{n+1} - \vec{r}_n)/\Delta t \tag{5.4.15}$$

$$\vec{v}_{n-1/2} = (\vec{r}_n - \vec{r}_{n-1})/\Delta t \tag{5.4.16}$$

Taking the difference between the two equations and applying the expression from the Verlet algorithm (5.4.14), we obtain:

$$\vec{v}_{n+1/2} = \vec{v}_{n-1/2} + \frac{\vec{F}_n}{m}\Delta t \tag{5.4.17}$$

This variant has the advantage of allowing us to know explicitly the velocity at a different moment for which the position is known, so to find the velocity at time $\boldsymbol{t}$, it can be approximated as:

$$\vec{v}_n = \frac{\vec{v}_{n+1/2} + \vec{v}_{n-1/2}}{2} \tag{5.4.18}$$

Another variant, known as the Verlet with explicit velocities or the Verlet Velocity algorithm (VV) [71], proposes the benefits of calculating the position and velocity at the time $\boldsymbol{t}$, beginning with two stages: in the first (5.4.19), the position is calculated at a given step, and in the second (5.4.20), the velocity is calculated at the midpoint of the step:

$$\vec{r}_{n+1} = \vec{r}_n + \vec{v}_n \Delta t + \frac{1}{2}\left(\frac{\vec{F}_n}{m}\right)\Delta t^2 \tag{5.4.19}$$

$$\vec{v}_{n+1/2} = \vec{v}_n + \frac{1}{2}\left(\frac{\vec{F}_n}{m}\right)\Delta t \tag{5.4.20}$$

From there, the force is obtained $\vec{\boldsymbol{F}}\,(t + \Delta t)$, with which the velocity is calculated at the step under consideration:

$$\vec{v}_{n+1} = \vec{v}_{n+1/2} + \frac{1}{2}\left(\frac{\vec{F}_{n+1}}{m}\right)\Delta t \tag{5.4.21}$$

These three algorithms are equivalents, generating identical trajectories, the difference between them lying in the computation time, the memory used and the accuracy of each one.

5.4.2.3. Choice of integration time step

It is of extremely important to choose the appropriate time step since it affects the magnitude of the error associated with the algorithm used, so there is a strong relationship between its accuracy and its evolution. To verify the stability of the simulation with regard to selected time step, it is necessary to ensure that the fluctuation of the Hamiltonian of the system $\Delta \boldsymbol{H}$ with regard to the absolute value is: $(\Delta H/H) < 10^{-4}$.

5.4.2.4. Choice of ensemble

The aim of Molecular Dynamics simulations is to be able to study the average behaviour of a system of particles by performing a numerical calculation of the evolution of the system over time, from which it is possible to calculate time averages, which do not depend on the initial conditions. Thus, the time average of a property is equal to the ensemble average. The MD technique was originally used for the study over time of classical systems consisting of $\boldsymbol{N}$ particles in a volume $\boldsymbol{V}$. In these simulations, the equations of motion conserve energy $\boldsymbol{E}$ (established as the sum of kinetic and potential energy), so the properties calculated using the time average from the simulation belong to the macrocanonical statistical

ensemble (NVE). Later, more degrees of freedom were added to the system to perform simulations under other ensembles: the canonical statistical ensemble (NVT), associated with the Helmholtz free energy; and the isothermal-isobaric ensemble (NPT), associated with the Gibbs free energy. The choice of ensemble for carrying out a simulation is governed by the problem under consideration and is vitally important when trying to calculate the mean square fluctuations of thermodynamic magnitudes. In the case of this Doctoral Thesis, the calculation of the heat capacity at constant volume of the nanofluids led to the choice of the NVT ensemble as the best option.

NVT ensemble

Under the NVT ensemble, in which the number of particles remains constant $\boldsymbol{N}$, in a volume $\boldsymbol{V}$, the temperature is established as the mean temperature rather than the instantaneous temperature so the mean temperature of the system is kept constant during the simulation, $\langle T \rangle = T_0$. The particle velocities of the system are stepped by a factor $\lambda = (T_0/T)^{1/2}$ every few steps so the temperature of the system is kept constant at $\boldsymbol{T_0}$, $\boldsymbol{T}$ being the instantaneous temperature. The NVT canonical ensemble is performed by connecting the system in a large bath (thermostat) that sets the desired temperature $\boldsymbol{T_0}$ and enables the particle velocities to be rescaled. Among the most widely-used thermostats is the one used in this Doctoral Thesis, namely the Nosé-Hoover thermostat [72, 73].

Nosé-Hoover thermostat

This algorithm modifies Newton's equations by introducing the friction coefficient of the thermostat, $\boldsymbol{\chi_n}$:

$$\frac{d\vec{v}_n}{dt} = \frac{\vec{F}_n}{m} - \chi_n \vec{v}_n \tag{5.4.22}$$

This coefficient is controlled by the first order differential equation:

$$\frac{d\chi_n}{dt} = \frac{N_f k_b}{Q}(T - T_0) \tag{5.4.23}$$

where $\boldsymbol{Q}$ is the effective mass of the thermostat, $\boldsymbol{N_f}$ is the number of degrees of liberty of the system, $\boldsymbol{T}$ is the instantaneous temperature and $\boldsymbol{T_0}$ the temperature required in the simulation.

5.4.2.5. Phases of a Molecular Dynamics simulation

- Thermalization: the initial positions and velocities of each particle are specified. In systems in equilibrium, these positions and velocities are assigned randomly taking into consideration a Boltzmann distribution thermalized to the temperature of the system, given by the principle of equal energy sharing. During this stage, the velocities of all the particles are repeatedly rescaled to take the system to the required temperature and achieve net linear momentum for dynamic equilibrium.
- Equilibration: the system reaches ergodicity after a given time and, after a significant number of simulation steps, in which it is not necessary to rescales the velocities, the Hamiltonian of the system remains constant and the system is in equilibrium.
- Production: configurations are generated numerically integrating the classical equations of motion that govern the system through the use of different algorithms. The results (position, velocity, force, etc.) are stored for later analysis. An assessment is made of the time averages from the different configurations, which, calculated over a long enough period of time, correspond with the statistical averages from which the statistical and dynamic properties of interest are extracted.

5.4.2.6 Boundary conditions

Molecular Dynamics simulations involve a relatively small number of particles with regard to the order of magnitude of particles in a macroscopic system. This means that the cell volume must be chosen very carefully in order to match the theoretical density of the system to the experimental density and thus prevent the particles from being surrounded by a vacuum. Therefore, to simulate what takes place macroscopically in the heart of the fluid, it is necessary to choose boundary conditions that reproduce an infinite environment of particles surrounding the system, thus minimizing edge effects from the simulation box; that is, the behaviour of atoms found at the outer limits of the system deviates with regard to those in the heart of it. To achieve this, periodic boundary conditions (PBC) are used, whereby the simulation box, which is generally cubic, is considered to be a primitive cell from an infinite

and periodic network of identical cells. Thus, if a particle leaves its cell during the simulation, it is replaced by an identical particle entering through the opposite side of the system (Figure 5.4.2). Thus, any specific particle interacts periodically with both the rest of the particles in the simulation box and all its repeated images in the simulation box.

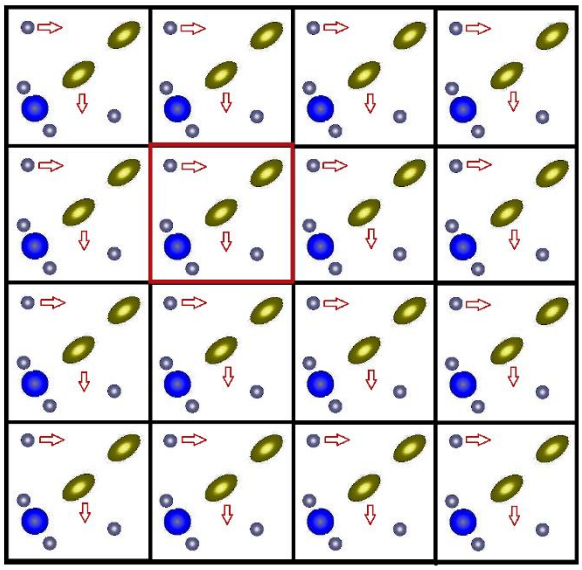

Figure 5.4.2. Image of periodic boundary conditions (PBC).

Therefore, the correct treatment of the boundary conditions and the outer limits of the simulation system are extremely important for the simulation methods to be able to estimate macroscopic properties with a relatively small number of particles.

5.4.2.7. Short- and long-range intermolecular interactions

Intermolecular interactions arise from attractive and repulsive interactions between different molecules, the result of which affects the macroscopic properties of the matter. These interactions may be classified into short- and long-range interactions.

Short-range interactions:

They derive from the short-range overlap of the different electron densities existing in every atom. The interaction energy presents exponential behaviour with the distance between the particles that interact: e^{-kR}, $\boldsymbol{k}$ being a constant.

Long-range interactions:

They stem from the electrostatic contribution derived from the Coulomb force, induction and dispersion forces or the London dispersion force. The interaction energy has an inverse relationship with distance: R^{-n}.

In Molecular Dynamics simulations, it is necessary to know what forces are acting on each particle in the system. Taking into consideration that a particle interacts with the other particles of the system and the images of itself, included due to the periodic boundary conditions, we obtain a high number of non-bonding terms in the calculation. In the case of Van der Waals non-bonding interactions, the Lennard-Jones potential decays rapidly with distance, so the calculation of this interaction cannot be justified for atoms a sufficient distance away, which means that only the interactions between particles included within a certain radius are calculated. This approximation is called the minimum image criterion [74], and it establishes a short radius $\boldsymbol{r_{cut}}$ with the aim of ignoring interactions separated by large distances, so the calculation of the interaction potential, $\boldsymbol{U_{(r)}}$, only includes those terms that are within the cut-off radius, taking interactions outside the cut-off distance as null values. This $\boldsymbol{r_{cut}}$ generally considers values between 8 and 12 Å, and introducing it makes it possible to reduce the computational cost of assessing the potential energy of the system.

5.4.2.8. Ewald summation method

The incorrect treatment of long-range interactions can result in the system being rather unstable [75]. To this end, the Ewald summation method [76] allows for the interaction of a particle with both the other particles in the simulation cell and with the images of itself in a periodic, infinite system of cells. The procedure involves transforming the sum of all the possible electrostatic interactions, which converges slowly and conditionally, into the sum of two terms that converge much more quickly, plus a constant term.

The Ewald summation method is based on the Coulomb expression:

$$U_{Coulomb} = \frac{1}{4\pi\varepsilon_0} \sum_{|n|=0} \sum_{i=1}^{N} \sum_{j=i+1}^{N} \frac{q_i q_j}{|r_{ij} + n|} \tag{5.4.24}$$

where $\boldsymbol{N}$ is the number of particles contained by each cell, $\boldsymbol{q}$ are the charges associated with the particles i and j, $\boldsymbol{r}$ is the distance separating the two particles, and $\boldsymbol{n}$ the number of vectors of a periodic network $n = (n_x L_x, n_y L_y, n_z L_z)$, $\boldsymbol{L_i}$ being the length of each dimension (x,y,z) of the cell.

This equation is conditionally convergent, meaning that its result depends on the order in which the terms are added, and as mentioned above, it has a slow convergence rate. The Ewald summation method separates the sum into two series, one in real space and the other in reciprocal space:

$$\frac{1}{r} = \frac{f(r)}{r} + \frac{1 - f(r)}{r} \tag{5.4.25}$$

The first term corresponds physically to surrounding each charge in the system with a neutralizing distribution of charges with equal magnitude and the opposite sign. This distribution corresponds to a Gaussian function that converges quickly and is responsible for interactions in real space:

$$U_{real} = \frac{1}{4\pi\varepsilon_0} \sum_{|n|=0} \sum_{i=1}^{N} \sum_{j=i+1}^{N} q_i q_j \frac{erfc\,(\alpha|r_{ij} + n|)}{|r_{ij} + n|} \tag{5.4.26}$$

$\boldsymbol{erfc}$ being the complementary error function:

$$1 - erfc(x) = \frac{2}{\pi^{1/2}} \int_{\pi}^{\infty} e^{-t^2} dt \tag{5.4.27}$$

The second term counteracts the neutralizing distribution of the first by means of an imaginary charge distribution of opposite sign to those of the real space. The series changes slightly with distance so its Fourier transform may be used (5.4.28). This sum is performed in reciprocal space and also converges more quickly than the original sum.

$$U_{recip} = \frac{1}{\varepsilon_0 V} \sum_{k>0} \frac{1}{k^2} e^{-\frac{k^2}{4\alpha^2}} \left| \sum_{j=1}^{N} q_j e^{-ikr_j} \right|^2 \tag{5.4.28}$$

where $\boldsymbol{k}$ are the reciprocal vectors given by $k = 2\pi n/L$ and $\boldsymbol{L}$ is the wavelength of the cell. The value of $\boldsymbol{\alpha}$ determines the amplitude of the Gaussian. Its value must be chosen within a range that is high enough for many of the terms of the real space series to be negligible above a certain cut-off radius and low enough for the number of terms in the reciprocal space to be reduced.

In addition, three terms are added due to the different contributions. The first term $\boldsymbol{U_{self}}$ is added to eliminate the interaction of the Gaussian with itself that takes place in the sum in real space:

$$U_{self} = (\alpha/\pi)^{1/2} \sum_{i=1}^{N} \frac{q_i^2}{4\pi\varepsilon_0} \tag{5.4.29}$$

The second term $\boldsymbol{U_{dip}}$ is added in the event of the system being in vacuum to counter the dipole moment of the unit cell as it is not neutralized by image charges on the surface:

$$U_{dip} = \frac{1}{6V\varepsilon_0} \left| \sum_{i=1}^{N} q_i r_i \right|^2 \tag{5.4.30}$$

The final term $\boldsymbol{U_{charge}}$ is added when working with closed systems to correct the lack of neutrality of the system:

$$U_{charge} = \frac{1}{8\pi V \alpha^2 \varepsilon_0} \left| \sum_{i=1}^{N} q_i \right|^2 \tag{5.4.31}$$

By incorporating these terms, the general expression of the Coulomb electrostatic potential becomes the sum of five contributions:

$$U_{Coulomb} = U_{real} + U_{recip} + U_{self} + U_{dip} + U_{charge} \tag{5.4.32}$$

The Ewald summation method is the most accurate way to include all the long-range effects, although it is computationally expensive. Formally, it is of $\boldsymbol{N^2}$ order, although if the value of $\boldsymbol{\alpha}$, the number of vectors $\boldsymbol{k}$ and the truncation of the pairs in real space are adjusted appropriately, it could be reduced to an $N^{3/2}$ order.

5.4.3. Analysis of the Molecular Dynamics simulations

The interest in determining the properties of a system by means of Molecular Dynamics simulations lies in comparing the results obtained with the experimental ones for the same properties. Thus, from the statistical averages obtained for the different configurations, calculated using the time averages over a sufficiently long simulation time, it is possible to analyse the structural, dynamic, transport and thermal properties of the simulated systems.

5.4.3.1. Analysis of structural properties

The analysis of structural properties by means of Molecular Dynamics simulations enables us to know how the base fluid molecules are arranged around the nanomaterial. Two structural properties were analysed:

I. The radial distribution function (RDF), $\boldsymbol{g_{\alpha\beta}(r)}$, can be defined as the likelihood of finding a particle α at a distance $\boldsymbol{r}$ from another particle β taken as the origin with regard to the likelihood in a homogeneous distribution [77, 78]:

$$g_{\alpha\beta}(r) = \frac{1}{4\pi r^2 \rho_\alpha} \frac{dN_{\alpha\beta}(r)}{dr} \tag{5.4.33}$$

where $\boldsymbol{\rho_\alpha}$ is the density of α atoms, and $\boldsymbol{N_{\alpha\beta}}$ represents the number of α atoms within a sphere with radius $\boldsymbol{r}$ whose centre is the β atom.

From the position of each atom, a simulation calculates the distance at which all the neighbouring atoms are found, repeating the procedure for all the atoms. Thus, the integration on a sphere with a specific radius will give an average of the number of neighbouring particles each atom has (Figure 5.4.3). The same information can be obtained experimentally using x-ray diffraction techniques [79].

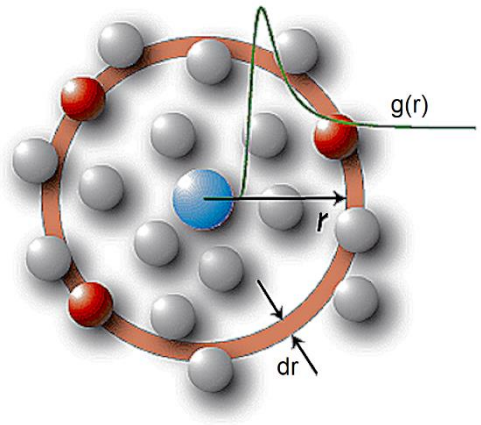

Figure 5.4.3. Radial distribution function (RDF) plot [80].

The number of central atoms of a specific type around another chosen as the centre can be calculated using the integration number $\boldsymbol{N_{\alpha\beta}(r)}$, resulting from the integration of the RDF signals:

$$N_{\alpha\beta}(r) = \int_0^r g_{\alpha\beta}(r) 4\pi r^2 \rho_\alpha \, dr \tag{5.4.34}$$

II. The spatial distribution function (SDF) $\boldsymbol{g_\alpha(\vec{r})}$ provides information about the spatial distribution of the atoms and affords a view of the regions where there is a high probability of finding a type of atom α in a point of space defined by the vector $\vec{\boldsymbol{r}}$ [81]:

$$g_\alpha(\vec{r}) = \frac{\rho_\alpha(\vec{r})}{\rho_\alpha} \tag{5.4.35}$$

where $\boldsymbol{\rho_\alpha}$ and $\boldsymbol{\rho_\alpha(\vec{r})}$ correspond to the density of the atoms α in a homogeneous distribution and to the density of the atoms α in the position defined by the vector $\vec{\boldsymbol{r}}$ in a system of specific spatial coordinates.

5.4.3.2. Analysis of dynamic or transport properties

Transport properties define the way a system responds to perturbation. When the concentration gradient is responsible for this perturbation, it is related with the movement of a particle through a medium, namely diffusion. Therefore, it is possible to calculate the diffusion coefficient of a particle, or translational diffusion coefficient, $\boldsymbol{D}$, using Einstein's equation (5.4.36), taking into consideration the position of a particle i over time $\vec{\boldsymbol{r}}(\boldsymbol{t})$:

$$D_i = \lim_{t\to\infty} \frac{\langle|\vec{r_i}(t) - \vec{r_i}(0)|^2\rangle}{6t} \tag{5.4.36}$$

the term $\langle|\vec{r_i}(t) - \vec{r_i}(0)|^2\rangle$ being the mean square displacement (MSD).

This theoretically-calculated diffusion coefficient is related with the diffusivity obtained experimentally, defined as the velocity at which heat can be transferred from one molecule to a neighbouring one.

5.4.3.3. Analysis of thermal properties

Thermal or heat energy spreads through a system due to the temperature gradient. Specific heat relates this change in temperature with the amount of heat stored inside a substance, specific heat being defined as the amount of energy (heat) required to raise the temperature of a unit mass by one degree. If we consider conditions at constant pressure, the property studied will be the isobaric specific heat. Therefore, from this definition, Molecular Dynamics simulations are used to estimate the total energy of the system at certain temperatures, and from these temperatures the isobaric specific heat of each system can be obtained.

The results obtained for the diffusion coefficient and isobaric specific heat values are of use for calculating thermal conductivity, $\boldsymbol{k}$, by means of Equation 5.3.6.

5.5. References

[1] G. Peiró, J. Gasia, L. Miró, C. Prieto, L.F. Cabeza, Influence of the heat transfer fluid in a CSP plant molten salts charging process, Renewable Energy 113 (2017) 148-158.

[2] V.V. Srdić, M. Winterer, A. Möller, G. Miehe, H. Hahn, Nanocrystalline zirconia surface-doped with alumina: chemical vapor synthesis, characterization, and properties, Journal of the American Ceramic Society 84(12) (2001) 2771-2776.

[3] H.T. Zhu, Y.S. Lin, Y.S. Yin, A novel one-step chemical method for preparation of copper nanofluids, Journal of Colloid and Interface Science 277(1) (2004) 100-103.

[4] A.K. Singh, V.S. Raykar, Microwave synthesis of silver nanofluids with polyvinylpyrrolidone (PVP) and their transport properties, Colloid and Polymer Science 286(14) (2008) 1667-1673.

[5] S.A. Kumar, K.S. Meenakshi, B. Narashimhan, S. Srikanth, G. Arthanareeswaran, Synthesis and characterization of copper nanofluid by a novel one-step method, Materials Chemistry and Physics 113(1) (2009) 57-62.

[6] N. Nikkam, M. Ghanbarpour, M. Saleemi, E.B. Haghighi, R. Khodabandeh, M. Muhammed, B. Palm, M.S. Toprak, Experimental investigation on thermo-physical properties of copper/diethylene glycol nanofluids fabricated via microwave-assisted route, Applied Thermal Engineering 65(1) (2014) 158-165.

[7] M.S. Liu, C.C.L. Mark, I.T. Huang, C.C. Wang, Enhancement of thermal conductivity with carbon nanotube for nanofluids, International Communications in Heat and Mass Transfer 32(9) (2005) 1202-1210.

[8] S. Suresh, K.P. Venkitaraj, P. Selvakumar, M. Chandrasekar, Synthesis of Al_2O_3–Cu/water hybrid nanofluids using two step method and its thermo physical properties, Colloids and Surfaces A: Physicochemical and Engineering Aspects 388(1) (2011) 41-48.

[9] M. Chopkar, S. Kumar, D.R. Bhandari, P.K. Das, I. Manna, Development and characterization of Al_2Cu and Ag_2Al nanoparticle dispersed water and ethylene glycol based nanofluid, Materials Science and Engineering: B 139(2) (2007) 141-148.

[10] H. Zhu, C. Zhang, Y. Tang, J. Wang, B. Ren, Y. Yin, Preparation and thermal conductivity of suspensions of graphite nanoparticles, Carbon 45(1) (2007) 226-228.

[11] M. Kole, T.K. Dey, Enhanced thermophysical properties of copper nanoparticles dispersed in gear oil, Applied Thermal Engineering 56(1) (2013) 45-53.

[12] Y. Hwang, J.K. Lee, J.K. Lee, Y.M. Jeong, S. Cheong, Y.C. Ahn, S.H. Kim, Production and dispersion stability of nanoparticles in nanofluids, Powder Technology 186(2) (2008) 145-153.

[13] S. Lee, S.U.S. Choi, S. Li, J.A. Eastman, Measuring thermal conductivity of fluids containing oxide nanoparticles, Journal of Heat Transfer-Transactions of the ASME 121(2) (1999) 280-289.

[14] S. Chakraborty, I. Sarkar, K. Haldar, S.K. Pal, S. Chakraborty, Synthesis of Cu–Al layered double hydroxide nanofluid and characterization of its thermal properties, Applied Clay Science 107 (2015) 98-108.

[15] D.H. Yoo, K.S. Hong, H.S. Yang, Study of thermal conductivity of nanofluids for the application of heat transfer fluids, Thermochimica Acta 455(1-2) (2007) 66-69.

[16] D. Lee, J.W. Kim, B.G. Kim, A new parameter to control heat transport in nanofluids: surface charge state of the particle in suspension, The Journal of Physical Chemistry B 110(9) (2006) 4323-4328.

[17] D. Zhu, X. Li, N. Wang, X. Wang, J. Gao, H. Li, Dispersion behavior and thermal conductivity characteristics of Al_2O_3–H_2O nanofluids, Current Applied Physics 9(1) (2009) 131-139.

[18] X. Wei, H. Zhu, T. Kong, L. Wang, Synthesis and thermal conductivity of Cu_2O nanofluids, International Journal of Heat and Mass Transfer 52(19) (2009) 4371-4374.

[19] H. Xie, J. Wang, T. Xi, Y. Liu, F. Ai, Q. Wu, Thermal conductivity enhancement of suspensions containing nanosized alumina particles, Journal of Applied Physics 91(7) (2002) 4568-4572.

[20] H. Chang, C. Jwo, P. Fan, S. Pai, Process optimization and material properties for nanofluid manufacturing, The International Journal of Advanced Manufacturing Technology 34(3-4) (2007) 300-306.

[21] S.K. Das, S.U.S. Choi, W. Yu, T. Pradeep, Nanofluids: science and technology John Wiley & Sons (2007).

[22] W. Yu, H. Xie, L. Chen, Y. Li, Investigation of thermal conductivity and viscosity of ethylene glycol based ZnO nanofluid, Thermochimica Acta 491(1) (2009) 92-96.

[23] J.-Y. Jung, C. Cho, W.H. Lee, Y.T. Kang, Thermal conductivity measurement and characterization of binary nanofluids, International Journal of Heat and Mass Transfer 54(9) (2011) 1728-1733.

[24] L. Jiang, L. Gao, J. Sun, Production of aqueous colloidal dispersions of carbon nanotubes, Journal of Colloid and Interface Science 260(1) (2003) 89-94.

[25] X.J. Wang, D.S. Zhu, S. Yang, Investigation of pH and SDBS on enhancement of thermal conductivity in nanofluids, Chemical Physics Letters 470(1) (2009) 107-111.

[26] M.J. Assael, I.N. Metaxa, J. Arvanitidis, D. Christofilos, C. Lioutas, Thermal conductivity enhancement in aqueous suspensions of carbon multi-walled and double-walled nanotubes in the presence of two different dispersants, International Journal of Thermophysics 26(3) (2005) 647-664.

[27] D. Wu, H. Zhu, L. Wang, L. Liu, Critical issues in nanofluids preparation, characterization and thermal conductivity, Current Nanoscience 5(1) (2009) 103-112.

[28] S.M.S. Murshed, K.C. Leong, C. Yang, Investigations of thermal conductivity and viscosity of nanofluids, International Journal of Thermal Sciences, 47(5) (2008) 560-568.

[29] W. Duangthongsuk, S. Wongwises, Comparison of the effects of measured and computed thermophysical properties of nanofluids on heat transfer performance, Experimental Thermal and Fluid Science 34(5) (2010) 616-624.

[30] W. Yu, H. Xie, L. Chen, Y. Li, Enhancement of thermal conductivity of kerosene-based Fe_3O_4 nanofluids prepared via phase-transfer method, Colloids and Surfaces A: Physicochemical and Engineering Aspects 355(1) (2010) 109-113.

[31] L.M. Cubillana-Aguilera, M. Franco-Romano, M.L.A. Gil, I. Naranjo-Rodríguez, J.L. Hidalgo-Hidalgo de Cisneros, J.M. Palacios-Santander, New, fast and green procedure for the synthesis of gold nanoparticles based on sonocatalysis, Ultrasonics Sonochemistry 18(3) (2011) 789-794.

[32] B. Derjaguin, L. Landau, Theory of the stability of strongly charged lyophobic sols and of the adhesion of strongly charged particles in solutions of electrolytes, Progress in Surface Science 43(1) (1993) 30-59.

[33] E.J.W. Verwey, J.T.G. Overbeek, Theory of the stability of lyophobic colloids, Courier Corporation (1999).

[34] W. Yu, H.Q. Xie, A Review on Nanofluids: Preparation, Stability Mechanisms, and Applications, Journal of Nanomaterials (2012) 17.

[35] W.S. Sarsam, A. Amiri, M.N.M. Zubir, H. Yarmand, S.N. Kazi, A. Badarudin, Stability and thermophysical properties of water-based nanofluids containing triethanolamine-treated graphene nanoplatelets with different specific surface areas, Colloids and Surfaces A-Physicochemical and Engineering Aspects 500 (2016) 17-31.

[36] A. Ghadimi, R. Saidur, H. Metselaar, A review of nanofluid stability properties and characterization in stationary conditions, International Journal of Heat and Mass Transfer 54(17-18) (2011) 4051-4068.

[37] R.C. Murdock, L. Braydich-Stolle, A.M. Schrand, J.J. Schlager, S.M. Hussain, Characterization of nanomaterial dispersion in solution prior to In vitro exposure using dynamic light scattering technique, Toxicological Sciences 101(2) (2008) 239-253.

[38] S. Angayarkanni, J. Philip, Review on thermal properties of nanofluids: Recent developments, Advances in Colloid and Interface Science 225 (2015) 146-176.

[39] H. Cummins, N. Knable, Y. Yeh, Observation of diffusion broadening of Rayleigh scattered light, Physical Review Letters 12(6) (1964) 150.

[40] R.D. Pecora, Doppler shifts in light scattering from pure liquids and polymer solutions, The Journal of Chemical Physics 40(6) (1964) 1604-1614.

[41] P. Vadasz, Heat conduction in nanofluid suspensions, Journal of Heat Transfer 128(5) (2006) 465-477.

[42] K.S. Suganthi, K.S. Rajan, Temperature induced changes in ZnO–water nanofluid: Zeta potential, size distribution and viscosity profiles, International Journal of Heat and Mass Transfer 55(25) (2012) 7969-7980.

[43] J.H. Lee, K.S. Hwang, S.P. Jang, B.H. Lee, J.H. Kim, S. Choi, C.J. Choi, Effective viscosities and thermal conductivities of aqueous nanofluids containing of Al_2O_3 low volume concentrations nanoparticles, International Journal of Heat and Mass Transfer 51(11-12) (2008) 2651-2656.

[44] I.M. Tucker, J.C.W. Corbett, J. Fatkin, R.O. Jack, M. Kaszuba, B. MacCreath, F. McNeil-Watson, Laser Doppler Electrophoresis applied to colloids and surfaces, Current Opinion in Colloid & Interface Science 20(4) (2015) 215-226.

[45] S. Bhattacharjee, DLS and zeta potential–What they are and what they are not?, Journal of Controlled Release 235 (2016) 337-351.

[46] E.V. Timofeeva, J.L. Routbort, D. Singh, Particle shape effects on thermophysical properties of alumina nanofluids, Journal of Applied Physics 106(1) (2009) 014304.

[47] M. Chandrasekar, S. Suresh, T. Senthilkumar, Mechanisms proposed through experimental investigations on thermophysical properties and forced convective heat transfer characteristics of various nanofluids - A review, Renewable & Sustainable Energy Reviews 16(6) (2012) 3917-3938.

[48] D. Wen, G. Lin, S. Vafaei, K. Zhang, Review of nanofluids for heat transfer applications, Particuology 7(2) (2009) 141-150.

[49] F.W. Dittus, L.M.K. Boelter, University California Publications Eng. 2 (1930) 443-461.

[50] R. Simons, calculation corner: comparing heat transfer rates of liquid coolants using the Mouromtseff number, Electronics Cooling 12(2) (2006) 10.

[51] S. Bobbo, L. Fedele, A. Benetti, L. Colla, M. Fabrizio, C. Pagura, S. Barison, Viscosity of water based SWCNH and TiO_2 nanofluids, Experimental Thermal and Fluid Science 36 (2012) 65-71.

[52] R. Prasher, D. Song, J. Wang, P. Phelan, Measurements of nanofluid viscosity and its implications for thermal applications, Applied Physics Letters 89(13) (2006) 133108.

[53] W. Duangthongsuk, S. Wongwises, Measurement of temperature-dependent thermal conductivity and viscosity of TiO_2-water nanofluids, Experimental Thermal and Fluid Science 33(4) (2009) 706-714.

[54] N.S.S. Mousavi, S. Kumar, Effective heat capacity of ferrofluids - Analytical approach, International Journal of Thermal Sciences, 84 (2014) 267-274.

[55] D. Cabaleiro, C. Gracia-Fernandez, J.L. Legido, L. Lugo, Specific heat of metal oxide nanofluids at high concentrations for heat transfer, International Journal of Heat and Mass Transfer 88 (2015) 872-879.

[56] D. Shin, D. Banerjee, Enhanced specific heat capacity of nanomaterials synthesized by dispersing silica nanoparticles in eutectic mixtures, Journal of Heat Transfer-Transactions of the ASME 135(3) (2013).

[57] D. Shin, D. Banerjee, Specific heat of nanofluids synthesized by dispersing alumina nanoparticles in alkali salt eutectic, International Journal of Heat and Mass Transfer 74 (2014) 210-214.

[58] J.A. Eastman, S.U.S. Choi, S. Li, W. Yu, L.J. Thompson, Anomalously increased effective thermal conductivities of ethylene glycol-based nanofluids containing copper nanoparticles, Applied Physics Letters 78(6) (2001) 718-720.

[59] T.P. Teng, Y.H. Hung, T.C. Teng, H.E. Mo, H.G. Hsu, The effect of alumina/water nanofluid particle size on thermal conductivity, Applied Thermal Engineering 30(14) (2010) 2213-2218.

[60] D. Singh, E.V. Timofeeva, M.R. Moravek, S. Cingarapu, W. Yu, T. Fischer, S. Mathur, Use of metallic nanoparticles to improve the thermophysical properties of organic heat transfer fluids used in concentrated solar power, Solar Energy 105 (2014) 468-478.

[61] S.K. Das, N. Putra, P. Thiesen, W. Roetzel, Temperature dependence of thermal conductivity enhancement for nanofluids, Journal of Heat Transfer 125(4) (2003) 567-574.

[62] M. Born, J. R. Oppenheimer, Ann. Physik 84 (1927) 457.

[63] J. Goodisman, Diatomic interaction potential theory: applications, Academic Press (2013).

[64] N. Rai, J.I. Siepmann, Transferable potentials for phase equilibria. 9. Explicit hydrogen description of benzene and five-membered and six-membered heterocyclic aromatic compounds, Journal of Physical Chemistry B 111(36) (2007) 10790-10799.

[65] M.G. Martin, J.I. Siepmann, Transferable potentials for phase equilibria. 1. United-atom description of n-alkanes, Journal of Physical Chemistry B 102(14) (1998) 2569-2577.

[66] M. Kotelyanskii, D.N. Theodorou, Simulation methods for polymers, CRC Press (2004).

[67] S. Singh, M. Chopra, J.J. de Pablo, Density of states–based molecular simulations, Annual Review of Chemical and Biomolecular Engineering 3 (2012) 369-394.

[68] M. Tuckerman, Statistical mechanics: theory and molecular simulation, Oxford University Press (2010).

[69] L. Verlet, Computer experiments on classical fluids. I. Thermodynamical properties of Lennard-Jones molecules, Physical Review 159(1) (1967) 98.

[70] R.W. Hockney, J.W. Eastwood, Computer simulation using particles, CRC Press (1988).

[71] W.C. Swope, H.C. Andersen, P.H. Berens, K.R. Wilson, A computer simulation method for the calculation of equilibrium constants for the formation of physical clusters of molecules: Application to small water clusters, The Journal of Chemical Physics 76(1) (1982) 637-649.

[72] S. Nosé, A unified formulation of the constant temperature molecular dynamics methods, The Journal of Chemical Physics 81(1) (1984) 511-519.

[73] W.G. Hoover, Physical Review A 31 (1985) 1695.

[74] D. Frenkel, B. Smit, Understanding molecular simulations: from algorithms to applications, Academic Press (2002).

[75] M. Allen, D. Tildesley, Computer Simulation of Liquids (Clarendon Press, Oxford, 1987).

[76] P. Ewald, Evaluation of optical and electrostatic lattice potentials, Ann. Phys. 64 (1921) 253-287.

[77] P. Ahlström, A. Wallqvist, S. Engström, B. Jönsson, A molecular dynamics study of polarizable water, Molecular Physics 68(3) (1989) 563-581.

[78] F. Li, J.S. Lannin, Radial distribution function of amorphous carbon, Physical Review Letters 65(15) (1990) 1905-1908.

[79] J.M. Sorenson, G. Hura, R.M. Glaeser, T. Head-Gordon, What can x-ray scattering tell us about the radial distribution functions of water?, The Journal of chemical physics 113(20) (2000) 9149-9161.

[80] http://www.chimica.unipd.it/federico.rastrelli/pubblica/experimental_nmr.html.

[81] D.L. Bergman, L. Laaksonen, A. Laaksonen, Visualization of solvation structures in liquid mixtures, Journal of Molecular Graphics and Modelling 15(5) (1997) 301-306.

Chapter 6

Analysis and discussion of the results obtained

6. Analysis and discussion of the results obtained

An analysis is presented below of the results obtained for the nanofluids prepared in this Doctoral Thesis. These pertain to the experimental characterization and address, first, the monitoring of stability over time, and then the degree of improvement in the efficiency of heat transfer processes by means of studying their thermal and rheological properties. Furthermore, an evaluation will be carried out of the results of the theoretical analysis using Molecular Dynamics (MD) simulations to estimate thermal and transport properties, and structural properties to discover how the molecules of both the base fluid and the various surfactants are arranged around the metal nanoparticles. All the nanofluids studied were prepared using the eutectic mixture Dowtherm-A as the base fluid, the objective being to improve the thermal properties of this fluid that is commonly used in CSP plants.

Thus, the first section presents the results for nanofluids based on commercial silver nanoparticles prepared following the two-step method. These nanofluids were analysed experimentally and theoretically and the results obtained were published in May 2017 under the title "**Ag-based nanofluidic system to enhance heat transfer fluids for concentrating solar power:** ***Nano-level insights****"*, in the journal *Applied Energy*, whose impact factor in 2017 was 7.900, according to *Journal Citation Reports* (JCR). This article is shown in ***Annex 2*** of this Doctoral Thesis.

In the second section, a study was performed of nanofluids prepared following a one-step method, synthesizing the gold nanoparticles and preparing the nanofluid in a single process. The nanomaterial synthesized was characterized to verify that gold nanoparticles had indeed been obtained. In turn, the nanofluids were characterized using both experimental and theoretical approaches. In this nanofluid system, tetraoctylammonium bromide (TOAB) was used as a surfactant and phase transfer agent, and its participation in the system was studied by analysing the structural properties obtained with MD simulations. The results obtained for the nanofluids based on gold nanoparticles were published in May 2017 under the title "***Preparation of Au nanoparticles in a non-polar medium: obtaining high-efficiency nanofluid for Concentrating Solar Power. An experimental and theoretical perspective****",* in the *Journal of Material Chemistry A*, whose impact factor in 2017 was 9.931, according to *Journal Citation Reports* (JCR). This article is shown in ***Annex 3*** of this Doctoral Thesis.

The next section focuses on the nanofluids prepared following the two-step method and based on synthesized platinum nanoparticles. The nanomaterial was also characterized to check that the desired material had been synthesized, and then the nanofluids were analysed experimentally and theoretically. In this particular case, the application of ultrasound treatment and the combined use of the surfactants dodecylamine (DDA) and 1-octadecanethiol (ODT) were analysed experimentally, and the participation of the surfactants was studied by analysing the structural properties obtained through MD simulations. The results obtained for the nanofluids based on platinum nanoparticles were published in October 2018 under the title "***Towards the improvement of the global efficiency of Concentrating Solar Power plants by using Pt-based nanofluids: The internal molecular structure effect***", in the journal *Applied Energy*, whose impact factor in 2017 was 7.900, according to *Journal Citation Reports* (JCR). This article is shown in ***Annex 4*** of this memory.

The final nanofluid system prepared was based on synthesised gold nanoparticles but, unlike the previous nanofluid, a different preparation method was followed, this time using the two-step method and the same preparation procedure to that used for the silver based nanofluids. The results obtained from the comparison of the nanofluids based on gold and silver nanoparticles were published in December 2018 under the title "***Experimental characterization and theoretical modelling of Ag and Au-nanofluids: A comparative study of their thermal properties***", in the *Journal of Nanofluids*, whose impact factor in 2015 was 0.900, according to *Journal Citation Reports* (JCR). This article is shown in ***Annex 5*** of this Doctoral Thesis. In this section, a comparison was also performed of nanofluids prepared following the same procedure but varying the nanomaterial synthesized: gold and silver, mentioned above, and copper and nickel nanofluids, reported in the literature.

The final section presents the relationship of the results obtained for all the nanofluids prepared and studied in this Doctoral Thesis, and an analysis of the system presenting the best features with regard to its potential use as a heat transfer fluid in CSP plants.

6.1. Nanofluids based on silver nanoparticles

These nanofluids were prepared based on commercial silver nanoparticles (with a particle size smaller than 100 nm) that were dispersed into the eutectic mixture Dowtherm-A used as the base fluid. Using the two-step preparation method (see ***Section 5.2***), three nanofluids were prepared varying concentrations of nanomaterial (see ***Section 5.2.1***). Each nanofluid was characterised experimentally, studying its chemical stability over time and its thermal and rheological properties in order to assess the degree of improvement in their efficiency in heat transfer processes. Furthermore, a theoretical analysis of the nanofluid system was performed by means of Molecular Dynamics simulations to estimate its transport and thermal properties, as well as its structural properties to determine how the molecules from the base fluid are organised around the silver nanoparticles.

The nomenclature used to refer to the nanofluids will be **$0.5 \cdot 10^{-4}$ wt.% Ag**, **$1.0 \cdot 10^{-4}$ wt.% Ag** y **$5.0 \cdot 10^{-4}$ wt.% Ag**, and **Dowtherm-A** to refer to the base fluid.

6.1.1. Monitoring of stability

The results obtained by means of the study using visible and near-infrared spectroscopy, Vis-NIR, (that is, between 400 nm and 1800 nm) show that the addition of silver nanoparticles does not produce modifications in the base fluid and therefore does not have a negative impact on the stability of the system. Figure 6.1.1 shows the Vis-NIR spectra for the nanofluids and the base fluid. At low wavelengths, a wide band appears in the spectra for the nanofluids, which is typical of colloidal systems due to the light dispersion caused by the presence of nanoparticles [1, 2]

Furthermore, the analysis of particle sizes, shown in Figure 6.1.2, reveals that the nanomaterial tends to agglomerate from the time when the nanofluids are prepared until, after approximately the second day, the particle size values start to become fairly constant, suggesting that these nanofluids reach a stable condition after a few days.

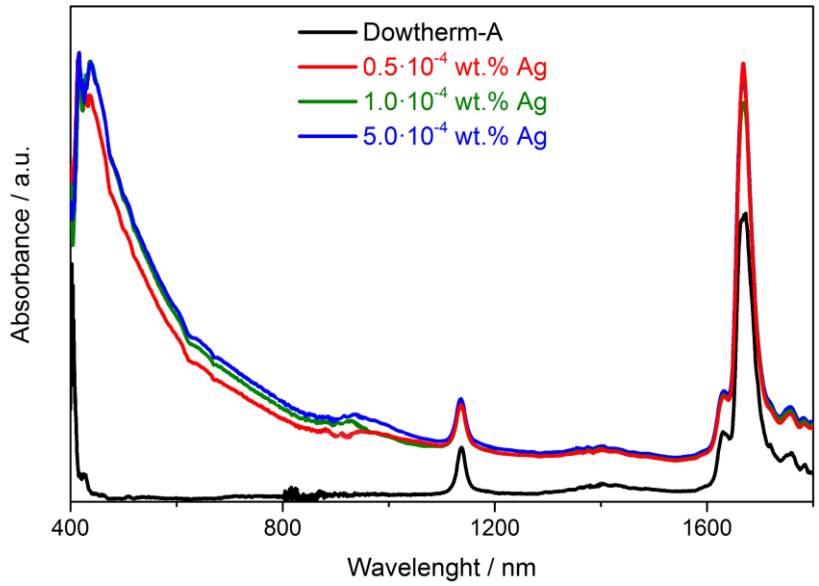

Figure 6.1.1. Vis-NIR spectra for the silver nanofluids and the base fluid.

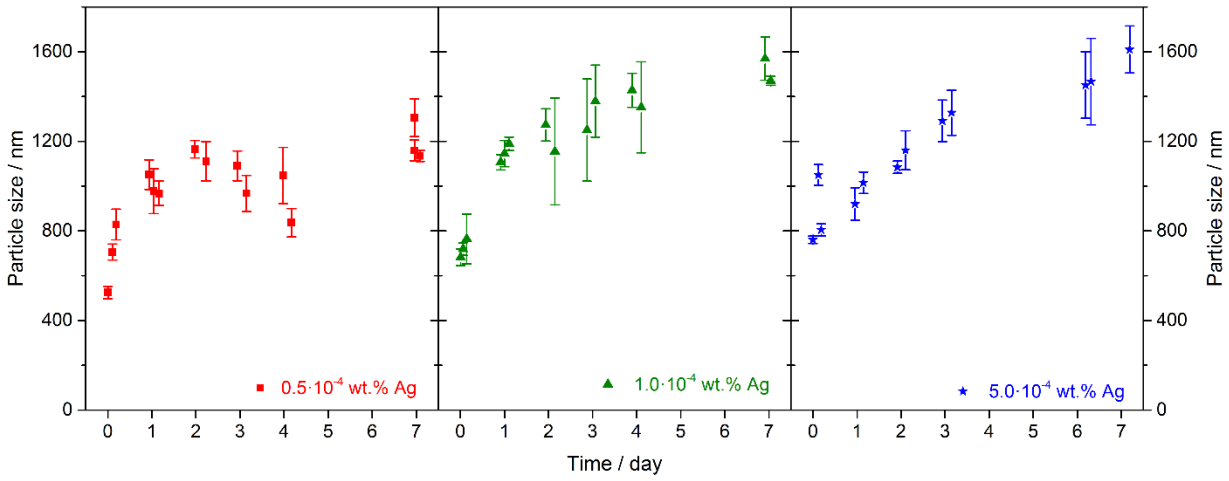

Figure 6.1.2. Particle size measurements of the silver nanofluids using the DLS technique.

6.1.2. Study of efficiency

Table 6.1 shows the results obtained at room temperature for density and viscosity, and the differences observed with regard to the base fluid. As expected, the incorporation of the nanomaterial leads to an increase in the values of both properties with regard to the base fluid, greater increases being observed when more nanomaterial is added. [3]. The increase in density was very slight, with a maximum increase of 0.22% for the nanofluid with the highest concentration of nanomaterial. In turn, greater variations were found in the viscosity values,

up to 4.5%, but this increase is acceptable for the application being considered here, as will be discussed below.

Table 6.1. Density and viscosity values obtained and the variation in each for the silver nanofluids and the base fluid.

Sample	*ρ / kg·m^{-3}*	*variation in density / %*	*μ / mPa·s*	*variation in viscosity / %*
Dowtherm-A	1056.0 ± 1.5	-	4.02 ± 0.06	-
0.5 ·10^{-4} wt.% Ag	1057.5 ± 0.5	0.14	4.14 ± 0.07	2.98
1.0 ·10^{-4}wt.% Ag	1057.9 ± 0.5	0.18	4.17 ± 0.06	3.77
5.0 ·10^{-4}wt.% Ag	1058.3 ± 1.5	0.22	4.21 ± 0.08	4.54

The isobaric specific heat and thermal conductivity of the nanofluids based on silver nanoparticles and the base fluid were measured in a temperature range between room temperature and 360 K. As Figure 6.1.3 shows, the presence of silver nanoparticles leads to the nanofluids presenting higher values than the base fluid for both properties. At 350 K, the nanofluid with the highest concentration of nanomaterial presents an improvement of around 7.4% in isobaric specific heat and of approximately 5.7% in thermal conductivity.

(A)

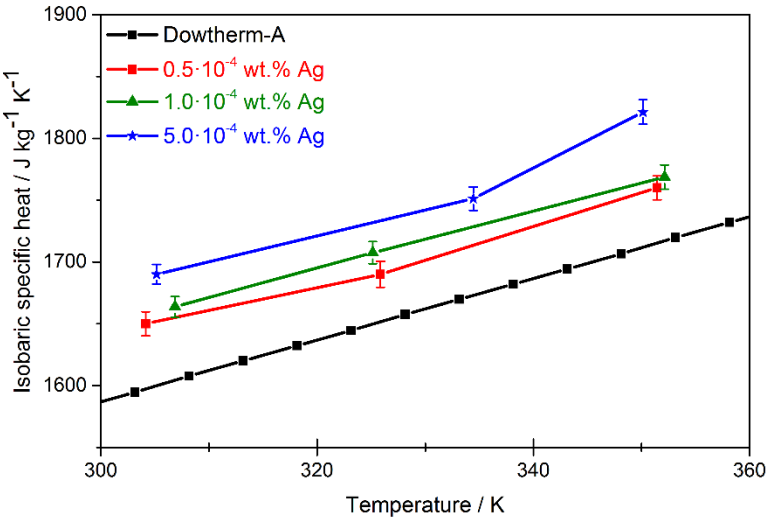

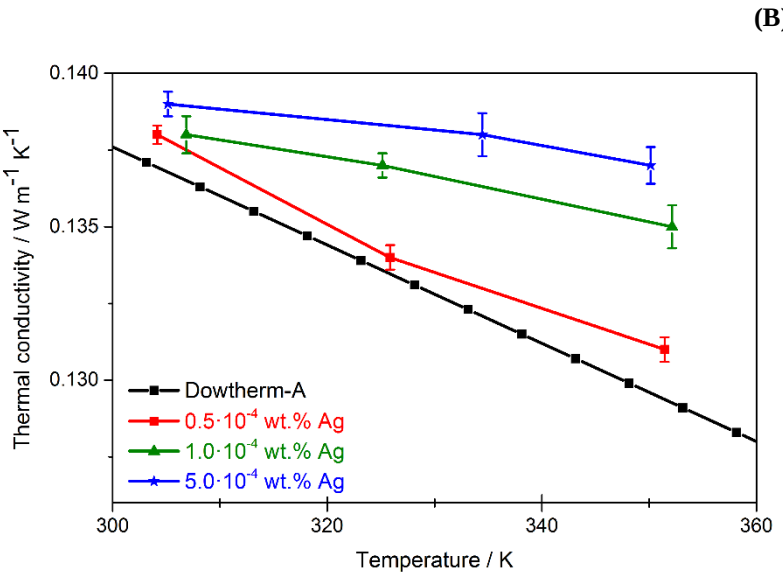

Figure 6.1.3. Values for (A) isobaric specific heat and (B) thermal conductivity for the silver nanofluids and the base fluid.

With the values obtained experimentally for these four properties, an estimation was made of the degree of improvement in the efficiency of heat transfer processes using the Dittus-Boelter equation (Equation 5.3.3), which has been defined above (see ***Section 5.3.2***). The ratio of the heat transfer coefficients of the nanofluids and the base fluid are shown in Figure 6.1.4. An improvement can be observed of approximately 5.3% at 350 K for the nanofluid with the highest concentration of silver nanoparticles.

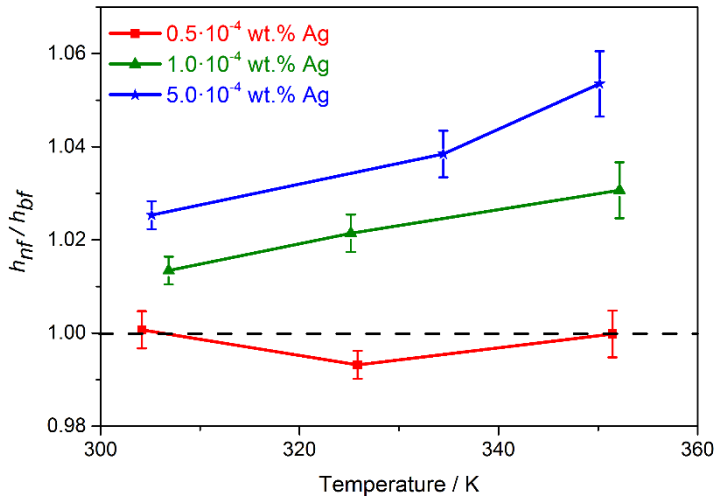

Figure 6.1.4. Ratio of heat transfer coefficients of the silver nanofluids and the base fluid.

6.1.3. Theoretical analysis

For the purpose of comparison with the results obtained experimentally, Molecular Dynamics simulations were performed to estimate thermodynamic properties (isobaric specific heat, thermal diffusivity and thermal conductivity), and to determine the structural properties related with the arrangement of the base fluid molecules around the silver nanoparticles.

6.1.3.1. Molecular Dynamics simulations

The Molecular Dynamics simulations were performed with the DL POLY code [4], using the NVT canonical ensemble, the Nosé-Hoover thermostat and periodic boundary conditions. The initial configuration was built with the PACKMOL code [5], generating a cubic box with such dimensions to enable the experimental density of the base fluid to remain constant at 298 K (1056 kg m^{-3}), for which a representative concentration of $5.0 \cdot 10^{-4}$ wt.% Ag was chosen, taking into consideration computational costs. The time step chosen was 0.5 fs, saving the structures generated every 100 time-steps, with a simulation time of 1 ns. To apply the Ewald summation [6], 9 Å was chosen as the cut-off distance, taking into account electrostatic interactions.

As explained earlier in this Doctoral Thesis (see ***Section 5.4.1.2***), the intra- and intermolecular interactions of the base fluid molecules were described using the TraPPE force field. The parameters used to represent the silver nanoparticle were adapted to the non-bonded dummy model, with six dummy atoms located around a central silver nanoparticle in an octahedral geometry [7].

6.1.3.2. Analysis of dynamic and thermal properties

To estimate the isobaric specific heat value, calculations were performed of the total energy of the system at temperatures ranging from 50 to 500 K. The plot of total energy versus temperature presents a linear trend, where the value of the slope corresponds with the isobaric specific heat value for both the nanofluid and the base fluid (Figure 6.1.5). For the base fluid, the value of the slope is $1.94 \cdot 10^{3}$ J kg^{-1} K^{-1}, while the slope value obtained for the

nanofluid was $2.15 \cdot 10^3$ J kg^{-1} K^{-1}. Although these values are somewhat higher than those obtained experimentally, qualitatively the theoretical results follow the same trend ($C_{P_{nf}} > C_{P_{bf}}$) as that observed experimentally, whereby the silver nanofluids presented a higher isobaric specific heat value than the base fluid.

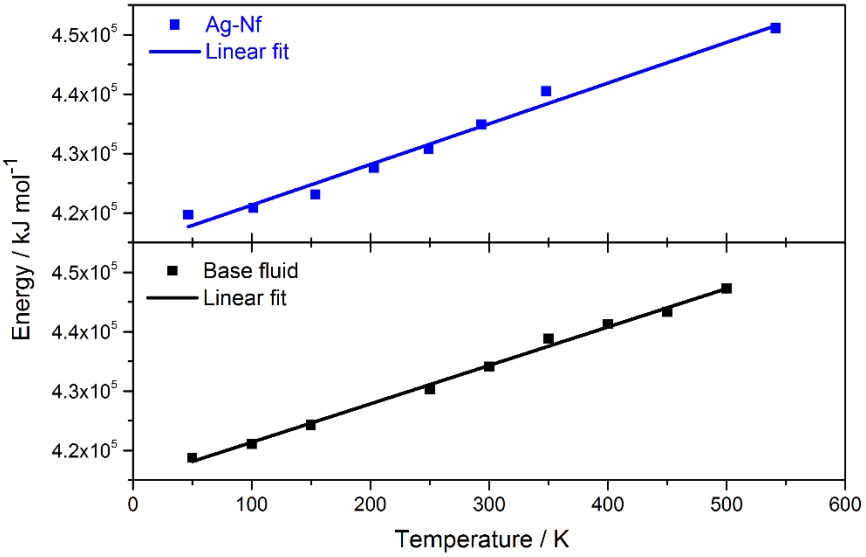

Figure 6.1.5. Plot and linear fit of the theoretical values obtained for total energy versus temperature for the silver nanofluid and the base fluid.

In turn, and following the procedure described in ***Section 5.4.3.2***, in order to calculate thermal conductivity, it is necessary to estimate thermal diffusivity beforehand. To this end, and in accordance with Einstein's equation (Equation 5.4.36), the translational diffusion coefficient is calculated using the mean square displacement (MSD). The plots of MSD versus time for the three directions of space for both the nanofluid and the base fluid at 300 K are shown in Figure 6.1.6. In both cases, the mean MSD follows a linear relationship with time after approximately 3 ps. We can extract the diffusion coefficient value from the slope of this line and, by applying Equation 5.3.6; we obtain a thermal conductivity value of 0.125 W m^{-1} K^{-1} for the nanofluid, and 0.107 W m^{-1} K^{-1} for the base fluid. The values obtained theoretically are slightly lower than the experimental values [8, 9], but qualitatively the same trend is followed in both cases: the nanofluid presents a higher thermal conductivity value than the base fluid ($k_{nf} > k_{bf}$).

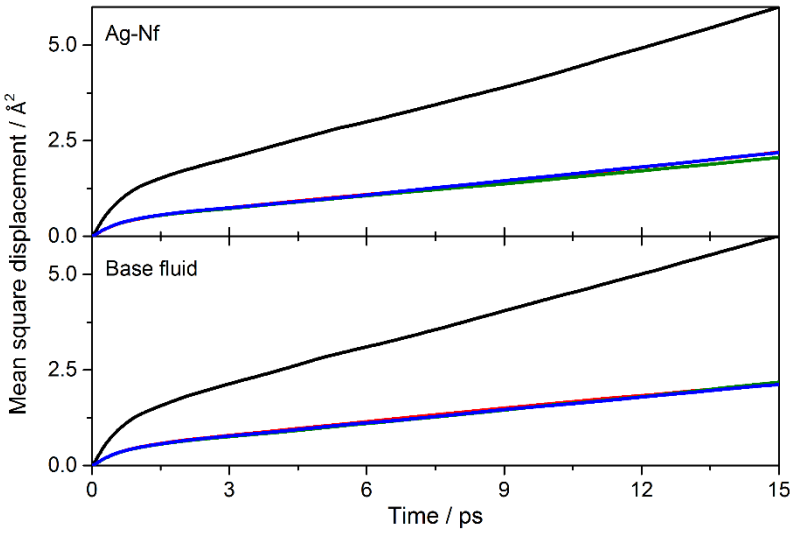

Figure 6.1.6. Mean square displacement (MSD) obtained theoretically for the silver nanofluid and the base fluid. The MSD for the three directions in space x, y, z are described by the colours red, green and blue respectively, while the resulting MSD is described in the colour black.

6.1.3.3. Analysis of structural properties

The interaction between the silver nanoparticle and the oxygen of the diphenyl oxide was analysed in a temperature range between 100 and 500 K in order to observe any movement of the diphenyl oxide molecules around the silver nanoparticle. Figure 6.1.7 shows the RDFs for the Ag-O pair. The change in temperature can be observed not to affect the position of the band centred at 2.2 Å, which corresponds with a strong Ag-O interaction. Thus, a set temperature of 300 K was used for the theoretical study of this system.

To determine how many diphenyl oxide and biphenyl molecules were found around the silver nanoparticle, an analysis was carried out of the RDFs of the Ag-O and Ag-C interactions at 300 K, shown in Figure 6.1.8. In the case of the Ag-O pair, an intense, well-defined peak is observed centred around 2.2 Å that is assigned to two oxygen atoms, so the silver nanoparticle is surrounded by two diphenyl oxide molecules. This sharp peak indicates a strong affinity of the oxygen towards the metal atom [10]. In turn, the study of the Ag-C pair presents three peaks: a sharp peak at a distance of 2.9 Å, and two more gentle ones at 4.2 Å and 5.2 Å, which are assigned to 8, 16 and 8 carbon atoms, respectively. This presupposes the presence of the two expected diphenyl oxide molecules (closer to the metal) and a biphenyl molecule.

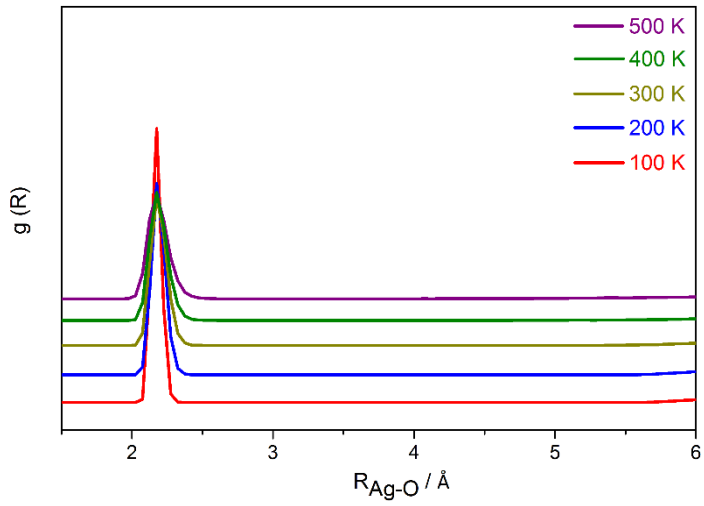

Figure 6.1.7. RDFs obtained for the Ag-O pair in the temperature range 100-500 K.

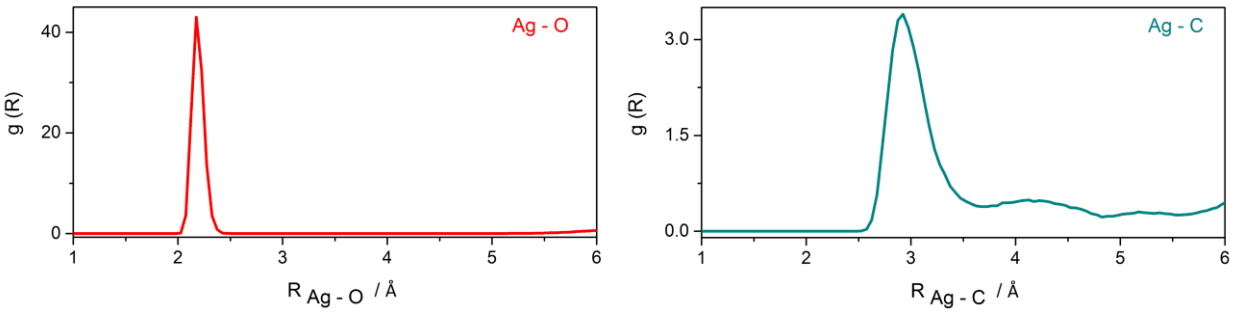

Figure 6.1.8. RDFs obtained for the Ag-O pair (red) and Ag-C pair (turquoise) at 300 K.

In turn, by analysing the SDF, a more specific three-dimensional vision was obtained of how the base fluid molecules are distributed in an inner layer around the silver nanoparticle at a distance of 6 Å. The SDF (Figure 6.1.9.A) reveals the presence of two diphenyl oxide molecules and a biphenyl molecule around the silver nanoparticle (central atom in blue colour). The oxygen atoms are shown in red colour, oriented towards the silver nanoparticles with the carbon atoms bonded directly to them in the blue colour, the aromatic carbons in turquoise and the hydrogen atoms in grey. Figure 6.1.9.B shows a plot of this result to show how the molecules described above are arranged.

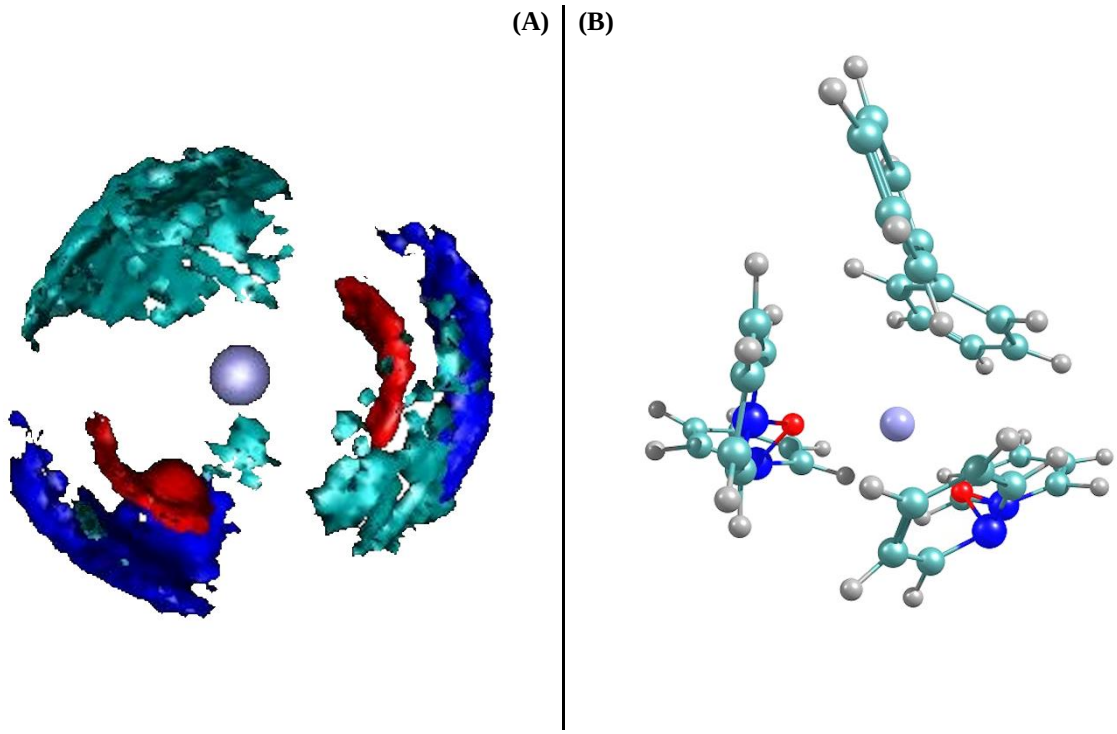

Figure 6.1.9. (A) SDF of the silver nanofluid system. (B) Three-dimensional model of the SDF. The silver nanoparticle is represented in the colour blue, the oxygen from the diphenyl oxide in red, the carbon atom from the aromatic rings directly bonded to the oxygen in blue, and the remaining carbon atoms from the aromatic rings in turquoise, with the hydrogen atoms in grey.

According to the background and previous studies [11], the presence of diphenyl oxide molecules generating a certain organisation around the nanoparticle could be the reason for the enhanced heat transfer processes observed experimentally. In this case, the silver nanoparticle interacts with the two diphenyl oxide molecules and with only one from the biphenyl and it is plausible that this organisation entails a slight improvement in the efficiency of the transfer of heat, in accordance with the results obtained after the experimental characterization.

6.2. Nanofluids based on gold nanoparticles

With the aim of using a different method of preparation to the previous case (one-step method) and to start the studies into the participation of the surfactants, the study of these new nanofluids based on gold nanoparticles was proposed.

To prepare the nanofluids based on gold nanoparticles following a one-step method (see ***Section 5.2***), it was necessary to first synthesize the gold nanoparticles, and then characterize them to confirm that the nanomaterial had indeed been synthesized as expected. It was then dispersed into the eutectic mixture Dowtherm-A used as the base fluid. Following the one-step method, three nanofluids were prepared varying the concentration of the nanomaterial and using tetraoctylammonium bromide (TOAB) as both the surfactant and phase transfer agent, as described above (see ***Section 5.2.2***). This was the first approach to using this kind of stabilizing additives. Thus, each nanofluid prepared and the action of the surfactant were studied and characterised experimentally, addressing their physical and chemical stability over time and their thermal and rheological properties with the purpose of assessing the degree of improvement in their efficiency in heat transfer processes. Furthermore, a theoretical analysis of the nanofluid system was performed by means of Molecular Dynamics simulations to estimate its transport, thermal and structural properties to determine how the molecules from both the base fluid and the surfactant are organised around the gold nanoparticles, and to learn about the role that the surfactant plays in the system.

The nomenclature used to refer to the nanofluids will be **$0.25 \cdot 10^{-2}$ wt.% Au**, **$0.50 \cdot 10^{-2}$ wt.% Au** and **$1.00 \cdot 10^{-2}$ wt.% Au**, and **Dowtherm-A** to refer to the base fluid.

6.2.1. Characterization of gold nanoparticles

As a preliminary step, it is essential to characterize the synthesized nanomaterial "in situ" during the nanofluid preparation process itself to confirm that the expected nanomaterial has indeed been obtained. Below, the results obtained with the techniques used to characterize the synthesized gold nanoparticles are shown.

X-ray photoelectron spectroscopy (XPS) was used to analyse the oxidation state and the chemical bonding state of the gold atoms. The result, shown in Figure 6.2.1, reveals the presence of two peaks at bonding energy values between 83.8 and 87.5 eV, which correspond to the $4f_{7/2}$ and $4f_{5/2}$ orbitals of the gold. The difference between the two signals is at around 3.7 eV, which confirms the presence of gold in the zero-oxidation state, that is, metallic gold nanoparticles [12, 13].

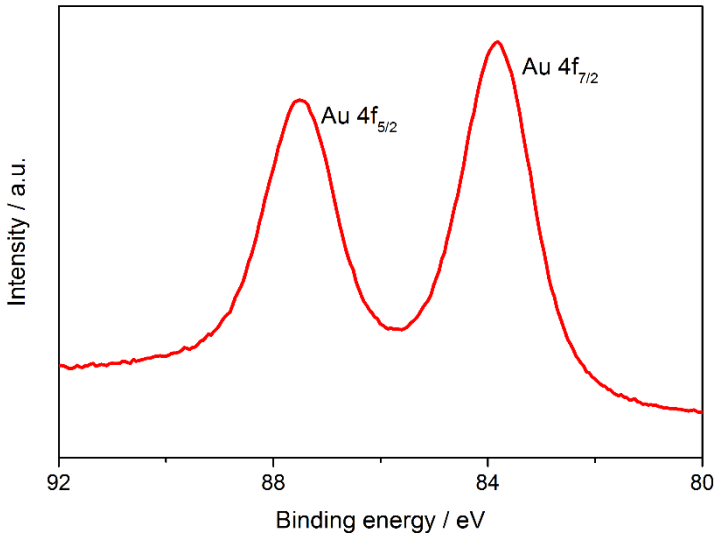

Figure 6.2.1. Signal obtained for the 4f orbital of the gold by XPS.

Moreover, the synthesized nanomaterial was analysed using x-ray diffraction (XRD) to obtain information about its crystalline structure. Figure 6.2.2 shows the XRD pattern obtained. Of note is the presence of three peaks at 2θ values of 38.24, 44.45 and 76.67º, which are characteristic of metallic gold and are assigned to the (111), (200) and (220) families of planes respectively, which correspond with the Fm-3m cubic space group [14, 15].

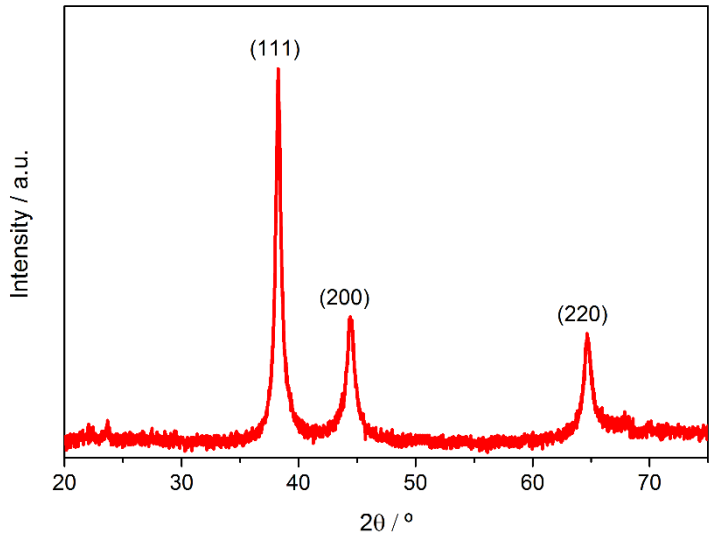

Figure 6.2.2. XRD pattern obtained for the synthesized gold nanoparticles.

Transmission electron microscopy (TEM) was used to analyse the size and shape of the nanoparticles. Figure 6.2.3.A. presents the distribution of sizes found, showing particle sizes between 5 and 25 nm with a mainly spherical morphology [16], as seen in Figure 6.2.3.B.

(A)

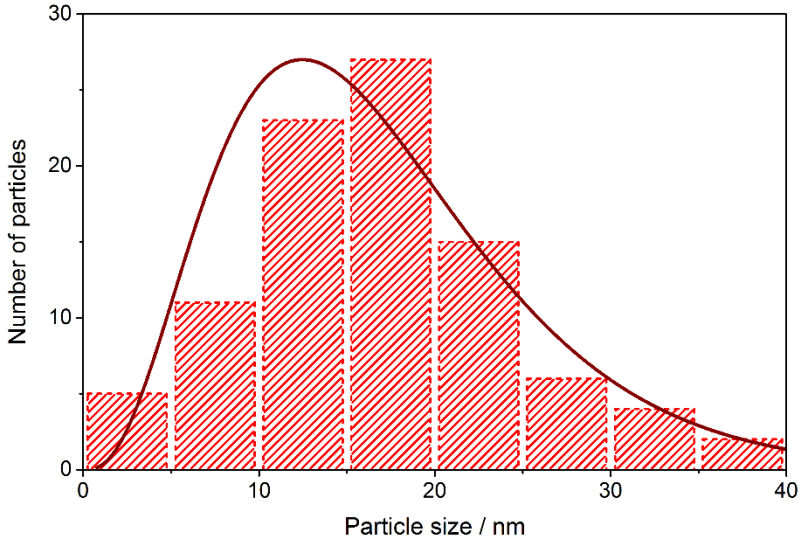

(B)

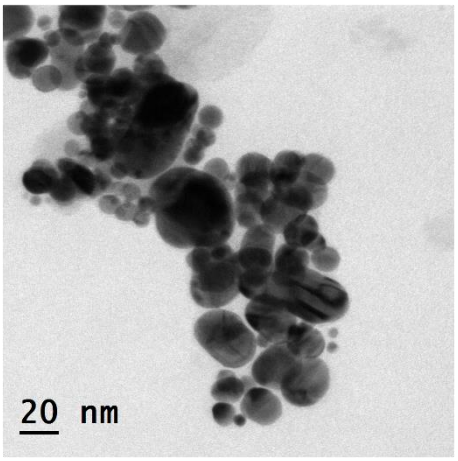

Figure 6.2.3. (A) Size distribution and (B) TEM image of the synthesized gold nanoparticles.

6.2.2. Monitoring of stability

Immediately after each nanofluid was prepared, UV-Vis spectra were recorded in the wavelength interval between 400 and 900 nm. Figure 6.2.4 shows the spectra recorded, those of the nanofluids being clearly different to those of the base fluid as a result of photonic absorption and light scattering processes caused by the presence of the gold nanoparticles in suspension [1, 17].

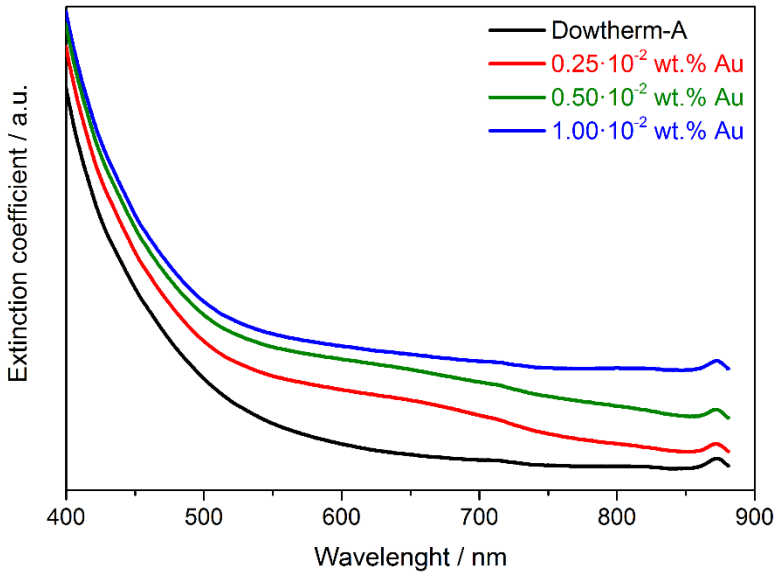

Figure 6.2.4. UV-Vis spectra of the base fluid and the gold nanofluids at time zero.

In addition, the variation in the intensity of the signal obtained at λ=520 nm was studied for one week for all the nanofluids, the results being shown in Figure 6.2.5. A decrease can be observed in the extinction coefficient values obtained during the first few days, which suggests that agglomeration and precipitation phenomena take place that lead to a reduction in the amount of suspended nanomaterial. This decrease in the extinction coefficient is more marked in the case of the two nanofluids with the highest concentration of nanomaterial. In turn, from the third day on, when the signal remains practically constant, these nanofluids can be considered to be stable. In the case of the nanofluid with the lowest concentration of nanomaterial, the decrease takes place more slowly over time, possibly due to the agglomeration processes slowing down since there is less material in the medium when it is prepared. The decay in the extinction coefficient is seen to be gentler over time.

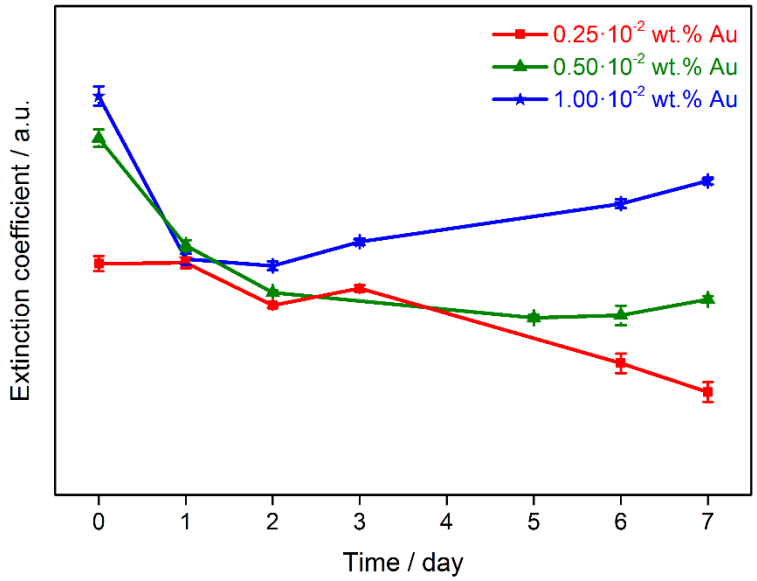

Figure 6.2.5. Variation in the extinction coefficient of the gold nanofluids at λ=520 nm versus time.

In turn, the particle size measurements are shown in Figure 6.2.6. Small variations in the particle size are observed for the nanofluid with the lowest concentration of nanomaterial, with a slight tendency to increase due to agglomeration processes, which, in accordance with the previous study, indicates that this nanofluid undergoes continual change. The nanofluid with the highest concentration of nanomaterial presents sequences of increased and decreased particle size, which suggests successive agglomeration and precipitation processes, possibly due to the high concentration of nanomaterial. These processes, however, maintain the particle size fairly constant after the first few days, during which the larger sized nanomaterial precipitates. This would be in agreement with the relatively stable extinction coefficient observed in the previous section. In the case of the nanofluid with an intermediate concentration of nanomaterial, a greater dispersion of sizes is observed but the values are centred on 900 nm.

Consequently, agglomeration and precipitation phenomena are common features of these nanofluids, which is normal since they are dynamic systems producing variations in the size of the particles, which affects the amount of nanomaterial in suspension and the stability of the nanofluids. However, it is possible to state that after a week the nanofluids seem to present acceptable stability, since no dramatic changes take place in either the extinction coefficient or the particle size.

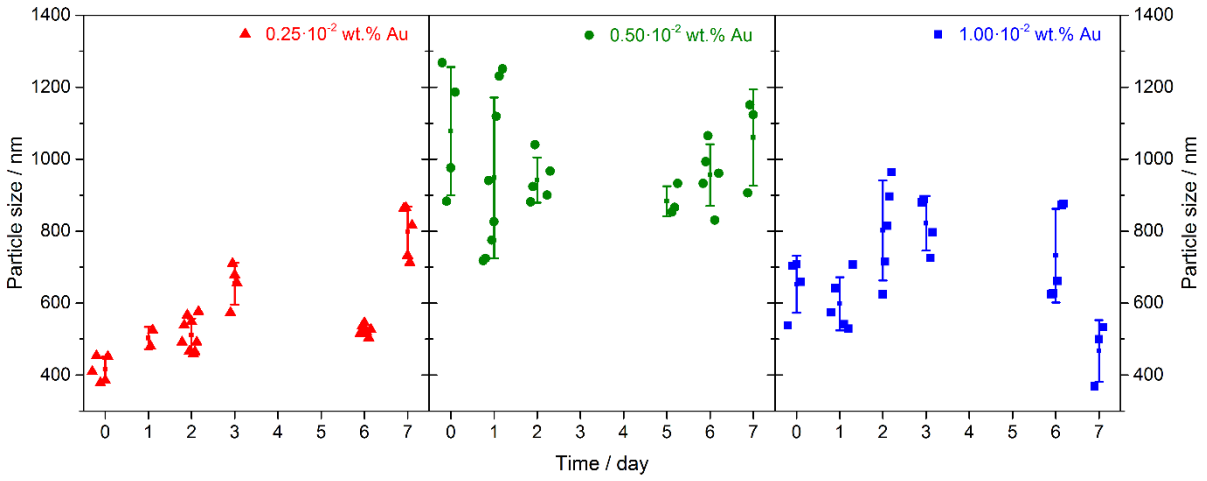

Figure 6.2.6. Particle size measurements of the gold nanofluids using the DLS technique.

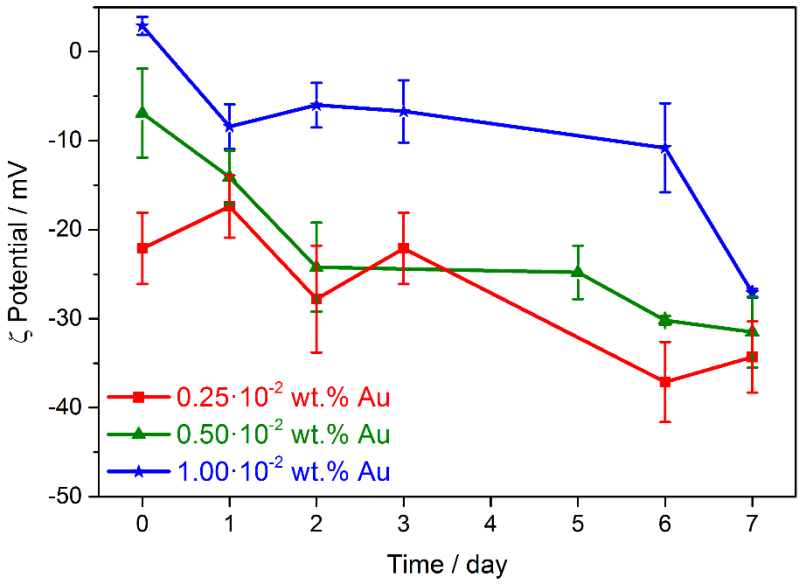

Figure 6.2.7. ζ potential values obtained for the gold nanofluids versus time.

Finally, Figure 6.2.7 shows the results obtained for the ζ potential of each nanofluid. At the end of the week of characterisation, the nanofluids present a ζ potential value of around -30 mV. This is the value commonly used in the literature as the threshold value for stability in water-based colloidal systems [18], which are considered stable when the absolute ζ potential value is higher than 30 mV. Thus, the ζ potential values are seen to decrease throughout the week until reaching values of around or lower than -30 mV, which is indicative of the nanofluids prepared reaching a stable state. This is in agreement with the

results from the measurements of extinction coefficient and particle size. However, the time required to reach that stable state is not the same in every case: the nanofluids with the highest concentration of nanomaterial require a longer time for the repulsive electrostatic interactions to be significant enough as to confer stability on the system.

6.2.3. Study of efficiency

The density values for each nanofluid, measured at room temperature, and the increase observed with regard to the base fluid are presented in Table 6.2 and in Figure 6.2.8.A. Table 6.2 shows that the addition of gold nanoparticles and surfactant produces a slight increase in the density values, greater increases being seen when more nanomaterial is added, from an increase of 0.04% for the nanofluid with the lowest concentration of nanomaterial to a variation of 0.16% for the fluid containing the highest amount of nanomaterial. Figure 6.2.8.A shows how the density of the nanofluids and the concentration of nanomaterial have a linear relationship. Therefore, in this system, to relate the concentration of nanomaterial with the thermal properties in a more reliable way, volume fractions $\boldsymbol{\phi}$ were estimated using the density values by means of the equation $\Phi = (\rho_{nf} - \rho_{bf})/(\rho_{np} - \rho_{bf})$, where $\boldsymbol{\rho}$ is the density and the subscripts $\boldsymbol{nf}$, $\boldsymbol{bf}$ and $\boldsymbol{np}$ correspond to the nanofluid, base fluid and nanoparticle, respectively; the latter with a value of 19380 kg·m^{-3} [19]. However, as observed in the stability analysis, it is clear to see that the nanofluids prepared present agglomeration phenomena, so it is more appropriate to define the system by means of its effective volume fraction $\boldsymbol{\phi_{eff}}$ [20], which is defined as $\Phi_{eff} = \Phi(a_0/a)^{3-D}$, $\boldsymbol{a_0}$ being the radius of the agglomerates and $\boldsymbol{a}$ the radius of the original nanoparticles (both values obtained by DLS and TEM), and $\boldsymbol{D}$, the fractal index, normally 1.8 for nanofluids [20-22]. The results of the calculation of volume fraction and effective volume fraction are shown in Table 6.2.

Table 6.2. Values obtained for density, variation with regard to the base fluid, the estimation of volume fraction and effective volume fraction for the gold nanofluids and the base fluid.

Sample	*ρ / kg·m^{-3}*	*variation in density / %*	*Φ / vol.%*	*$Φ_{eff}$ / vol.%*
Dowtherm-A	1059.5 ± 0.3	-	0	0
0.25 ·10^{-2} wt.% Au	1059.9 ± 0.3	0.04	0.0022	**0.34**
0.50 ·10^{-2} wt.% Au	1060.5 ± 0.2	0.09	0.0079	**1.55**
1.00 ·10^{-2} wt.% Au	1061.2 ± 0.3	0.16	0.0098	**0.86**

(A) **(B)**

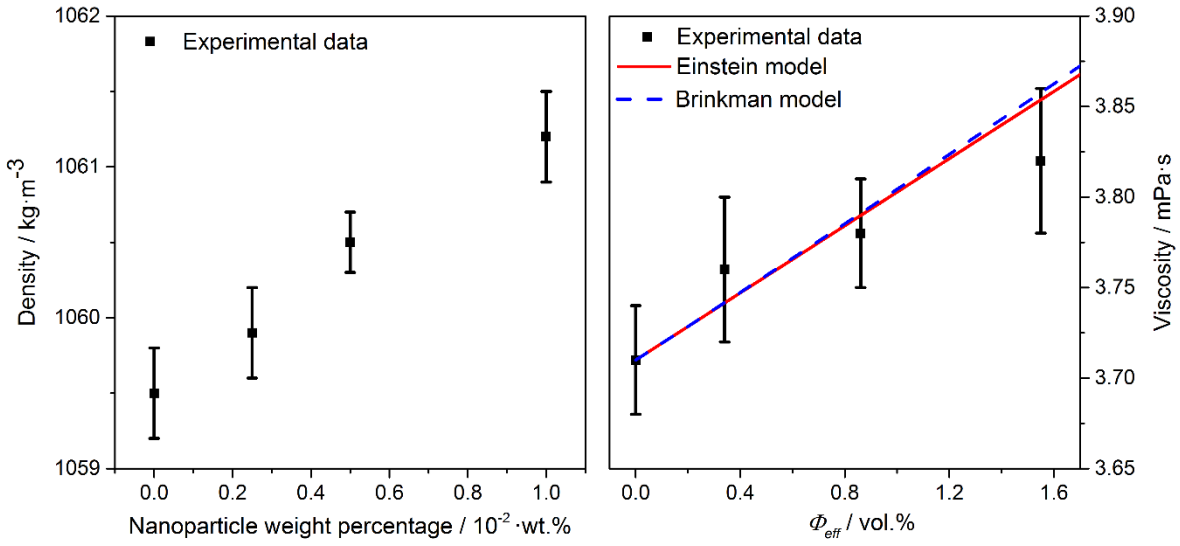

Figure 6.2.8. (A) Density and (B) viscosity values obtained for the gold nanofluids and the base fluid, and the fitted theoretical models.

Thus, from this moment on, the nomenclature used to refer to the nanofluids will be related to the effective volume fraction and, thereby, the nanofluids **0.25·10^{-2} wt.% Au**, **0.50·10^{-2} wt.% Au** and **1.00·10^{-2} wt.% Au** will hereinafter be called ***$Φ_{eff}$* = 0.34 vol. % Au**, ***$Φ_{eff}$* = 1.55 vol. % Au** y ***$Φ_{eff}$* = 0.86 vol. % Au**.

Furthermore, dynamic viscosity was measured since it is a property of particular interest in applications involving heat transfer such as concentrating solar power. The viscosity values measured for the nanofluids and how these varied with regard to the base fluid values, also measured at room temperature, are shown in Table 6.3. It shows that the

nanofluid with the highest effective volume fraction presents viscosity values that are 3% lower, which is a positive result if we take into account that, despite containing more nanomaterial than the silver nanofluids mentioned above, the gold nanofluids present smaller changes in viscosity, which is advantageous in terms of their efficiency.

Table 6.3. Viscosity values obtained for the gold nanofluids and the difference with regard to the base fluid.

Sample	*μ / mPa·s*	*variation in viscosity / %*
Dowtherm-A	3.71 ± 0.03	-
Φ_{eff} = 0.34 vol.% Au	3.76 ± 0.04	1.35
Φ_{eff} = 1.55 vol.% Au	3.82 ± 0.04	2.96
Φ_{eff} = 0.86 vol.% Au	3.78 ± 0.03	1.88

Figure 6.2.8.B shows the dynamic viscosity values obtained versus the effective volume fraction in addition to their fit to Einstein's viscosity model (Equation 4.6) and to Brinkman's model (Equation 4.7), both defined in ***Chapter 4: Review of the background***. A deviation from both models is observed at high volume concentrations due to an increase in the interactions between the particles as a result of the high level of agglomeration, which is not taken into consideration in both the studied models. At low volume concentrations, the experimental values show a good fit to the models.

Furthermore, isobaric specific heat was measured at temperatures ranging between approximately 298 K and 360 K. This property is, together with thermal conductivity, of particular interest in these systems. The isobaric specific heat values obtained are shown in Figure 6.2.9. It shows that only the nanofluid with an intermediate volume concentration presents values above that of the base fluid, an improvement of approximately 5.3% being found at 365 K.

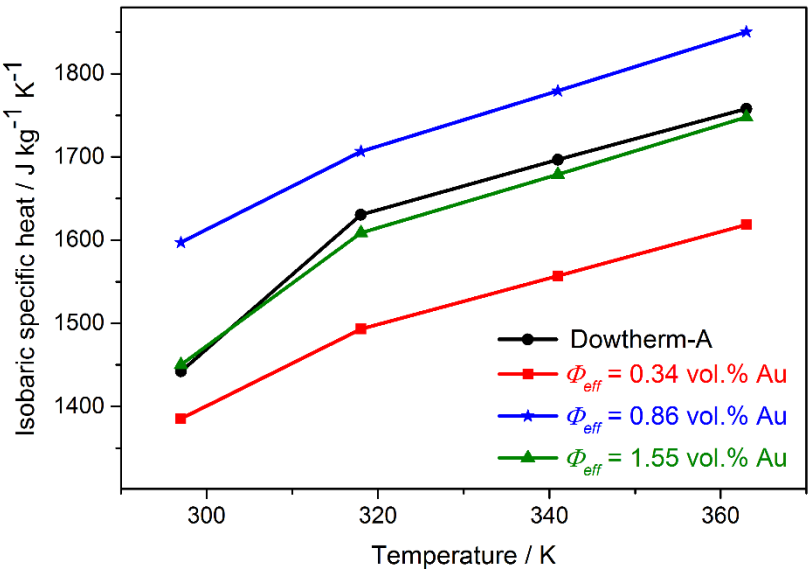

Figure 6.2.9. Isobaric specific heat values obtained for the gold nanofluids and the base fluid.

Studies exist in the literature that report that nanofluids present enhanced isobaric specific heat values with regard to the base fluid, although this behaviour is unusual because lower values for this property are generally found in solids than in liquids [23-25]. However, studies have reported that some nanofluid systems give rise to certain internal structures produced by interactions between the metal and base fluid molecules that can lead to improvements in this property [26, 27]. In this case, we can deduce that there is an optimal concentration of nanomaterial in suspension that facilitates the formation of an internal structure that creates ideal conditions with regard to the number of interactions between particles and that results in an increase in the specific heat.

In turn, with regard to the thermal conductivity results obtained, we can confirm that, in general terms, the three nanofluids present significantly improved thermal conductivity values with regard to the base fluid, as shown in Figure 6.2.10.A, and that the thermal conductivity shows a tendency to increase with temperature and with the effective volume concentration. In addition, Figure 6.2.10.B shows the values of the ratio k_{nf}/k_{bf}, a dramatic improvement in thermal conductivity of up to 70% at 363 K being obtained for the nanofluid with the highest effective volume fraction.

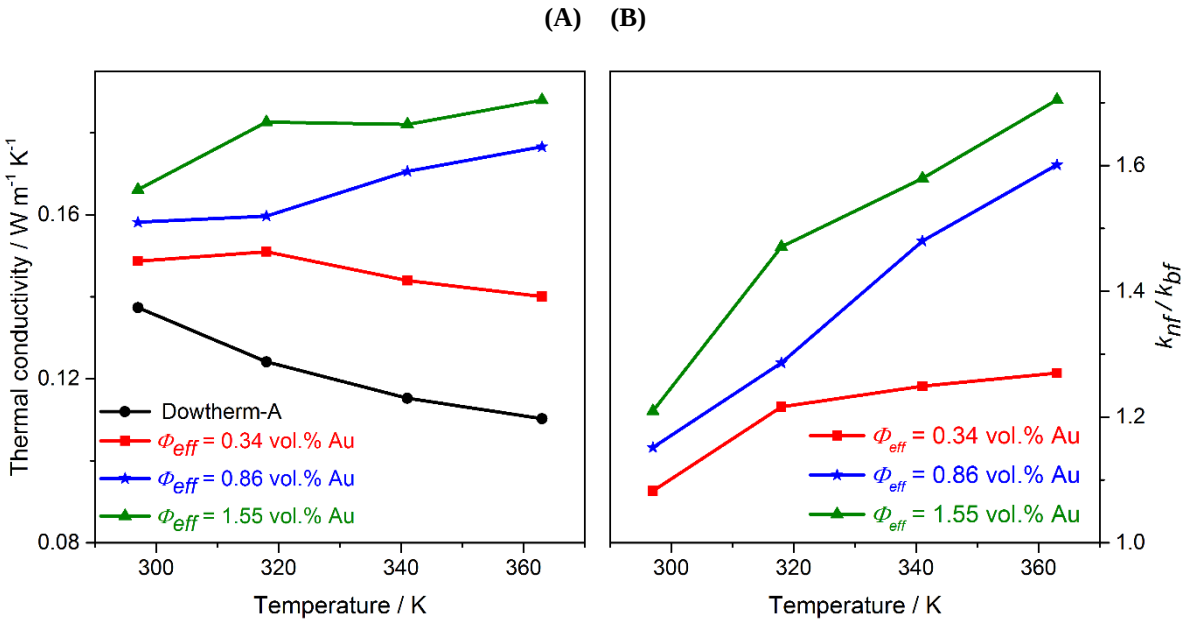

Figure 6.2.10. Values obtained for (A) thermal conductivity and (B) the ratio with regard to the base fluid for the gold nanofluids.

In turn, the thermal conductivity results obtained were analysed in accordance with the effective volume fraction with several theoretical models (see ***Chapter 4. Review of the background***), as shown in Figure 6.2.11. This analysis suggests the formation of aggregates may not be solely responsible for the increase in thermal conductivity. The values obtained experimentally are rather different to those predicted by the classical model by Hamilton and Crosser (Equation 4.2) and by the modified model when aggregates of nanomaterial are included (Equation 4.3). However, the experimental results show a better fit when we use the Koo and Kleinstreuer model (Equation 4.5), which takes into consideration the effect of Brownian motion on the nanoparticles, as reflected in Figure 6.2.11. This suggests that the participation of Brownian motion may be largely responsible for the dramatic improvement in thermal conductivity observed in these nanofluids experimentally.

Finally, to assess the improvement in efficiency of the nanofluids with regard to the base fluid, three criteria were used that have been define previously in this thesis (see ***Section 5.3.2***): the Dittus-Boelter equation (Equation 5.3.3) and the ratio of the Mouromtseff number of the two fluids (Equation 5.3.2), suggested for systems under turbulent flow conditions; and the Prasher criterion (Equation 5.3.4) used for laminar flow conditions.

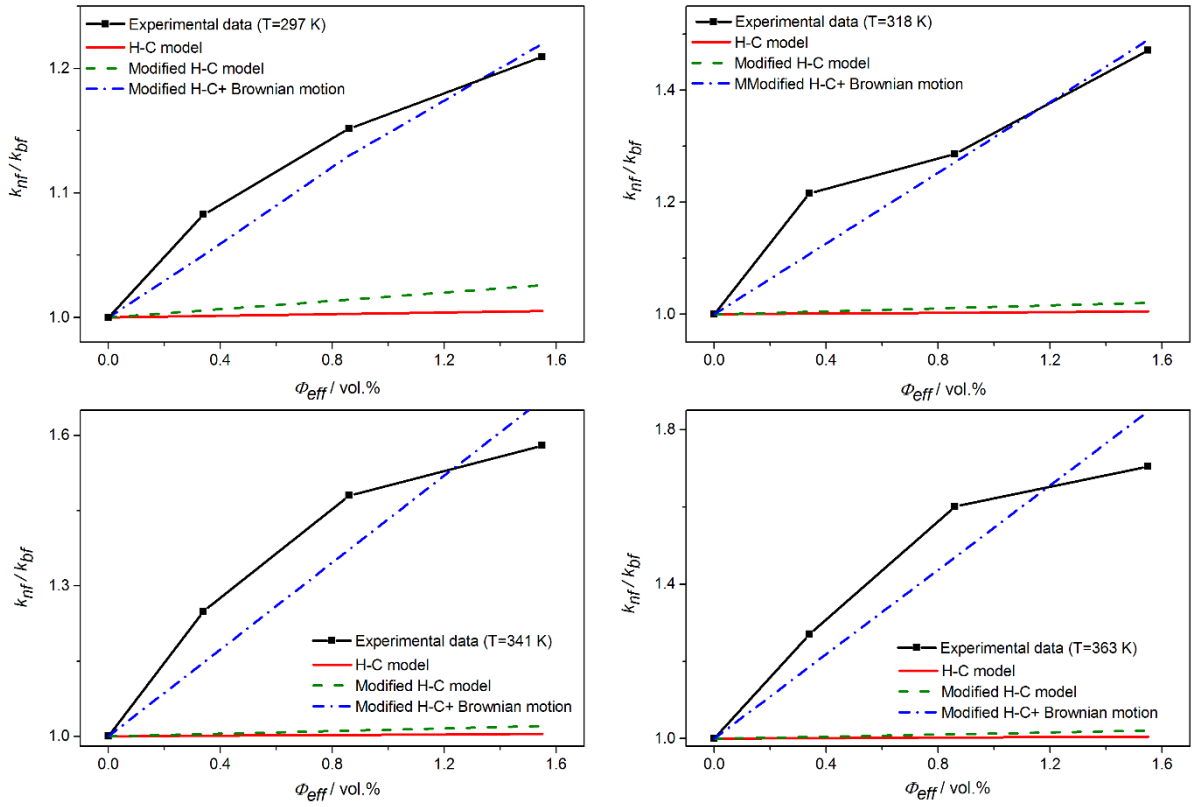

Figure 6.2.11. Thermal conductivity values obtained experimentally and the values predicted by the models presented.

The ratio of the heat transfer coefficients of the nanofluids and the base fluid versus temperature in accordance with the Dittus-Boelter equation are shown in Figure 6.2.12.A. It shows that all the gold nanofluids present an improvement in efficiency in heat transfer processes and that the nanofluid with the highest effective volume fraction is the most suitable for use as a heat transfer fluid, achieving an improvement of up to 36% in the heat transfer coefficient. Using the ratio of the Mouromtseff number of each fluid provides very similar results to those obtained by means of the Dittus-Boelter equation. Figure 6.2.12.B shows that improvement in the heat transfer efficiency of the gold nanofluid with the highest volume fraction is approximately 40%.

Finally, Prasher's criterion considers that a nanofluid presents improved efficiency when the increase in viscosity is less than four times the improvement in thermal conductivity. According to this approximation, all the nanofluids meet this criterion, as can be seen in Figure 6.2.12.C.

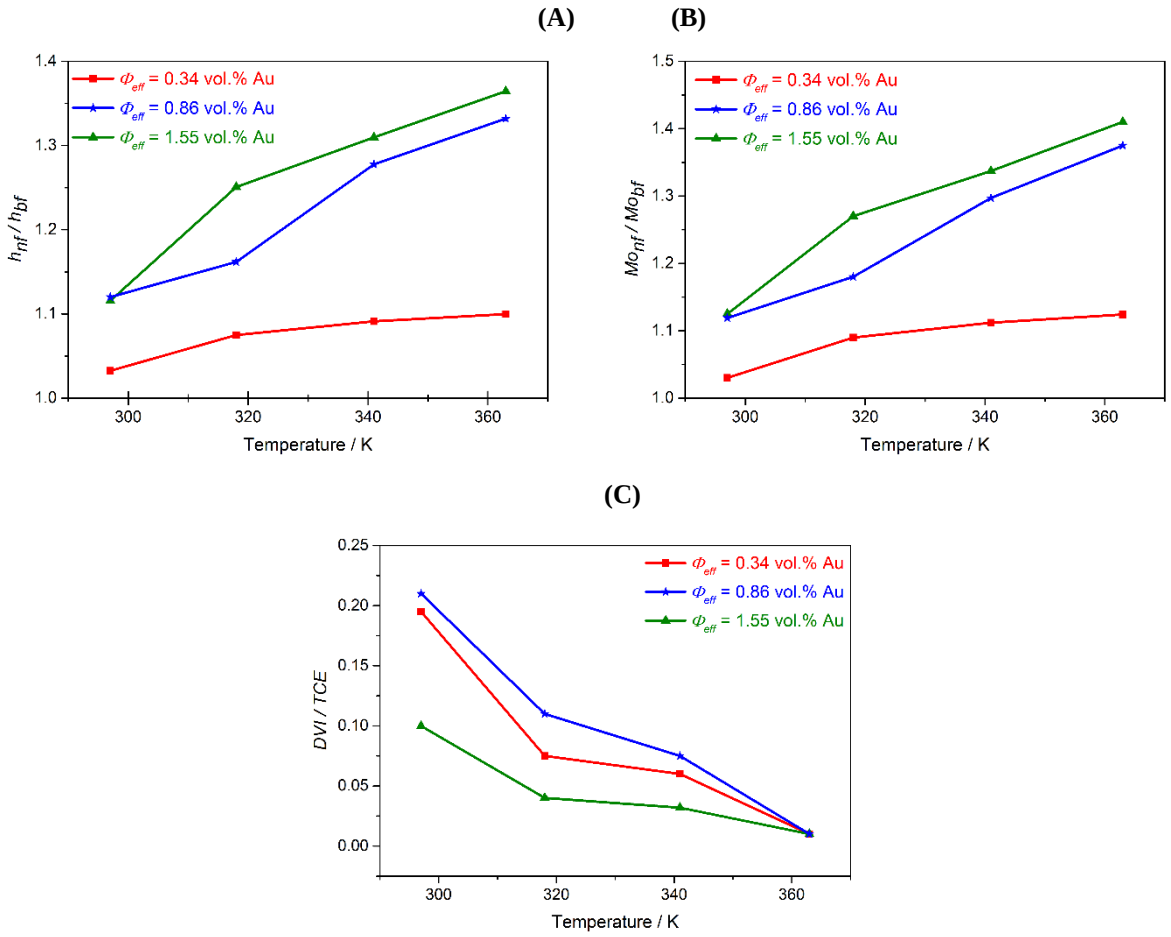

Figure 6.2.12. Estimation of the degree of efficiency of the gold nanofluids using (A) the Dittus-Boelter equation, (B) the Mouromtseff number and (C) Prasher's criterion.

6.2.4. Theoretical analysis

The study of this nanofluid system by means of Molecular Dynamics simulations focused on two matters: (A) the estimation of the thermal properties of interest to compare them with the experimental data; and (b) the study of the role played by the surfactant in this system by analysing structural properties, providing a better understanding of how the base fluid and surfactant molecules are arranged around the gold nanoparticles.

6.2.4.1. Molecular Dynamics simulations

The Molecular Dynamics simulations were performed with the DL POLY code [4], using the NVT canonical ensemble, the Nosé-Hoover thermostat and applying periodic

boundary conditions. The initial configuration was built with the PACKMOL code [5], generating cubic boxes with such dimensions to enable the experimental density of the base fluid to remain constant at 298 K (1056 kg m^{-3}), for which a representative concentration of $0.1 \cdot 10^{-2}$ wt.% Au was chosen, taking into consideration computational costs. The time of each simulation was 1 ns, setting a time-step of 0.5 fs and saving the structures generated for the analysis of trajectories every 100 time-steps. In each case, a cut-off distance of 9 Å was established and the Ewald summation method was applied [6] for the electrostatic reactions.

The TraPPE-EH force field was used to describe the intra- and intermolecular interactions between the base fluid molecules, while the TraPPE-UA force field was used for the interactions of the TOAB surfactant (see ***Section 5.4.1.2***).The parameters of the non-bonded force field that describe the gold nanoparticle, represented by fourteen gold atoms arranged in a symmetrical space group (Fm-3m), were adapted from earlier studies [28].

6.2.4.2. Analysis of dynamic and thermal properties

An analysis of the slope of the plot of the total energy of the system at temperatures ranging from 50 to 600 K shows the isobaric specific heat value of both the nanofluid and the base fluid (Figure 6.2.13). For the base fluid, the slope value $1.94 \cdot 10^{3}$ J kg^{-1} K^{-1}, while a slope value of $3.70 \cdot 10^{3}$ J kg^{-1} K^{-1} was obtained for the gold nanofluid. Although these values are higher than those obtained experimentally, they follow the same trend: $(C_{P_{nf}} > C_{P_{bf}})$.

Thermal conductivity was estimated following the procedure described in ***Section 5.4.3.2***. To this end, the translational diffusion coefficient was calculated from the mean square displacement (MSD) using Einstein's equation (Equation 5.4.36). The diffusion coefficient values for the gold nanofluid and the base fluid were calculated for temperatures ranging between 50 and 600 K. Figure 6.2.14 shows the thermal conductivity values obtained from the diffusion coefficient values using Equation 5.3.6. At temperatures above 100 K, an improvement is produced in the thermal conductivity values of the gold nanofluid with regard to the base fluid, values four times higher being observed at high temperatures. Therefore, the same trend is obtained theoretically and experimentally: the gold nanofluid presents higher thermal conductivity values than the base fluid $(k_{nf} > k_{bf})$.

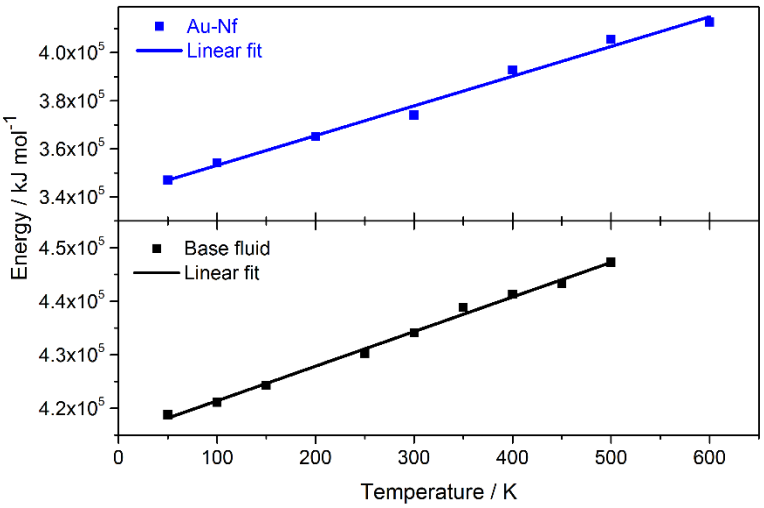

Figure 6.2.13. Plot and linear fit of the theoretical values obtained for total energy versus temperature for the gold nanofluid and the base fluid.

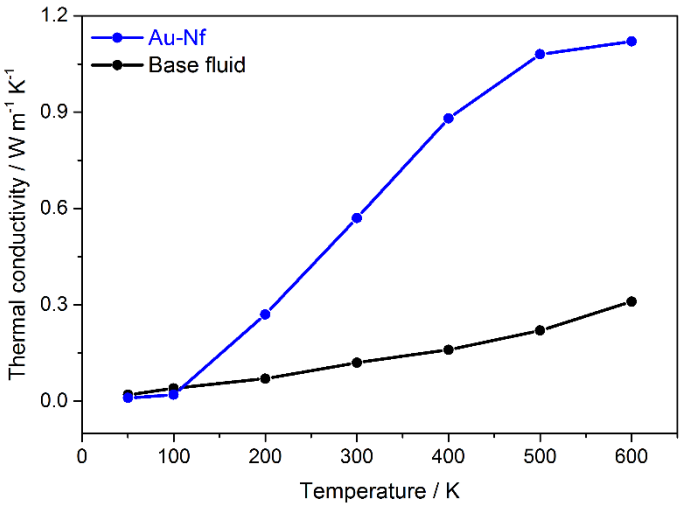

Figure 6.2.14. Thermal conductivity values obtained theoretically for the gold nanofluids and the base fluid.

6.2.4.3. Analysis of structural properties

To know how all the molecules in the system are arranged around the gold nanoparticles, the RDFs of three interactions of the gold were analysed: with the oxygen from the diphenyl oxide (Au-O), with the carbon atoms from the aromatic rings (Au-C), and with

the nitrogen atoms from the amine group of the TOAB surfactant (Au-N). These interactions were studied at a range of temperatures between 50 and 600 K and up to a cut-off distance of 10 Å, which corresponds to an inner layer around the gold nanoparticle. Figure 6.2.15 shows the RDFs studied. In the case of the Au-O pair, a dynamic movement of diphenyl oxide molecules is observed. The first peak for diphenyl oxide appears after 100 K and is centred at a distance of around 5 Å with regard to the gold nanoparticle. When the temperature increases, the number of diphenyl oxide molecules changes: there are two molecules between 100 and 300 K and four at temperatures from 400 to 600 K. For the Au-C interaction, the intense peak is centred at 5.8 Å for the complete range of temperatures. The peak begins to lose its well-defined structure as the temperature increases. Finally, the Au-N interaction shows that two surfactant molecules move closer to the gold nanoparticle at low temperature, a sharp peak being visible at 7.4 Å at 300 K. However, when the temperature rises, the peak moves further away and there is a decrease in the number of surfactant molecules, only one remaining at a distance of 8.5 Å at temperatures between 400 and 600 K.

The results of the RDFs clearly show the effects on the system of the temperature, which produces a rearrangement of both the base fluid and the surfactant molecules. At 300 K, the first movement takes place in the system, both the surfactant and diphenyl oxide molecules moving closer to the metal and forming an inner layer with two molecules of each species. When the temperature increases even more, the molecules move for a second time: the interaction between the gold nanoparticle and the surfactant loses intensity in the inner layer, only one surfactant molecule remaining and four diphenyl oxide molecules. This increase in the number of diphenyl oxide molecules is positive in terms of efficiency, giving rise to an increase in the thermal properties observed experimentally and theoretically. The surfactant, therefore, plays a vital role in the heat transfer process: its closer proximity to the nanoparticles when the temperature increases facilitates the entry of more diphenyl oxide molecules into an inner layer.

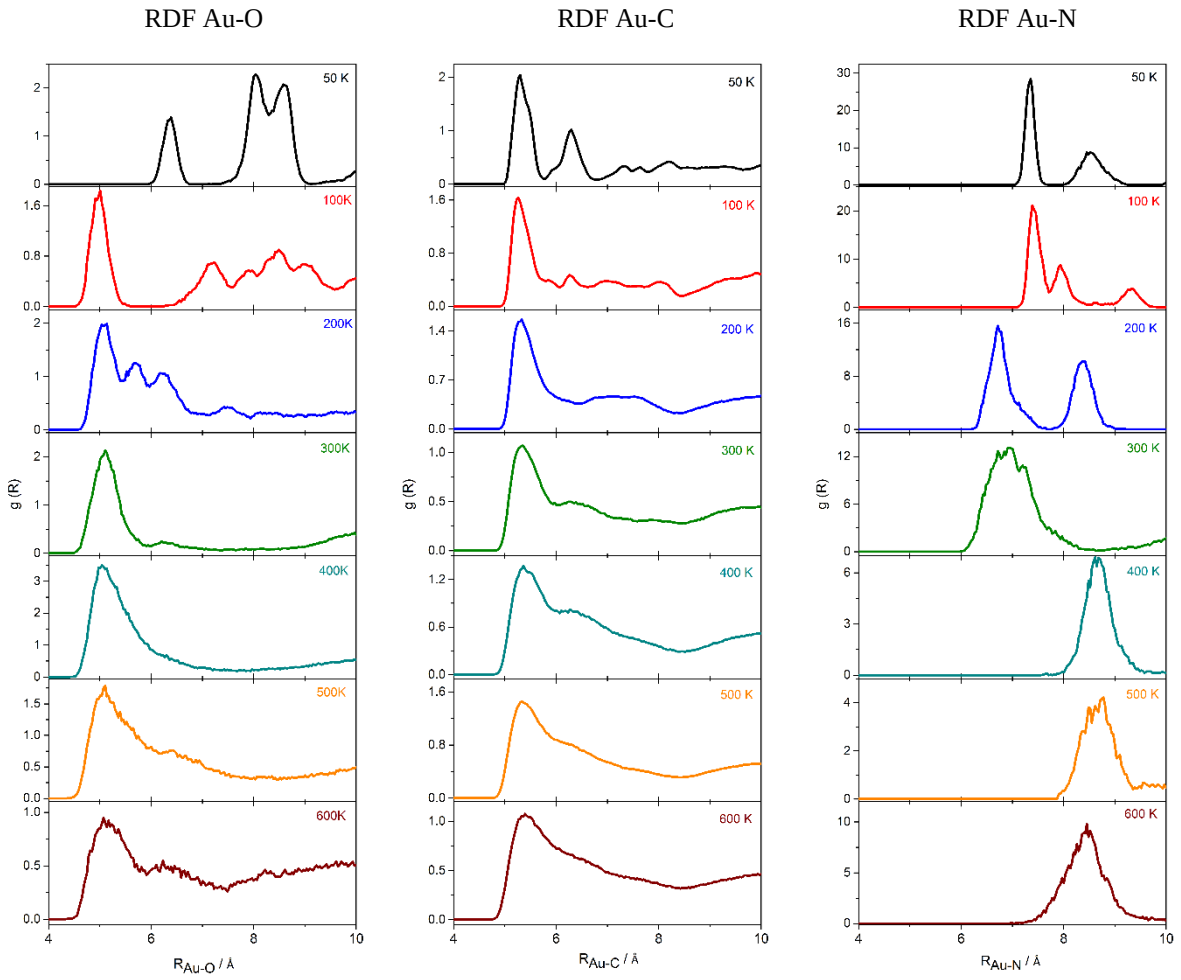

Figure 6.2.15. RDFs obtained for the Au-O, Au-C and Au-N pairs at different temperatures.

To gain a clearer understanding of the system, its spatial distribution function (SDF) was calculated. Figure 6.2.16 shows the SDFs and the three-dimensional image of the arrangement of the molecules in an inner layer at 10 Å at 300 K and 600 K, representative temperatures of the dynamics of the system. The gold nanoparticle (gold colour) is surrounded by diphenyl oxide and biphenyl molecules (the image shows oxygen atoms in red bonded to carbon atoms in blue, and aromatic carbon atoms in turquoise) and surfactant molecules (grey chain with the nitrogen of the amine group in orange). At 300 K, the arrangement of the diphenyl oxide and surfactant molecules around the gold nanoparticle is 2/2, while the ratio at 600 K is 4/1.

T = 300 K **(A)** **(B)** T = 600 K

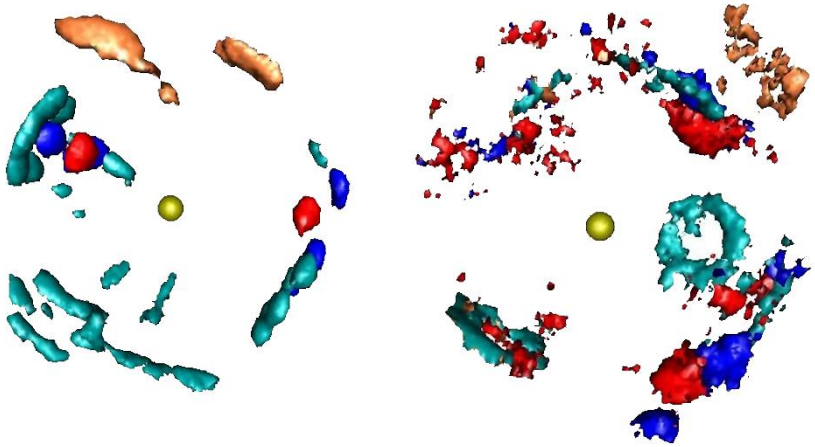

T = 300 K **(C)** **(D)** T = 600 K

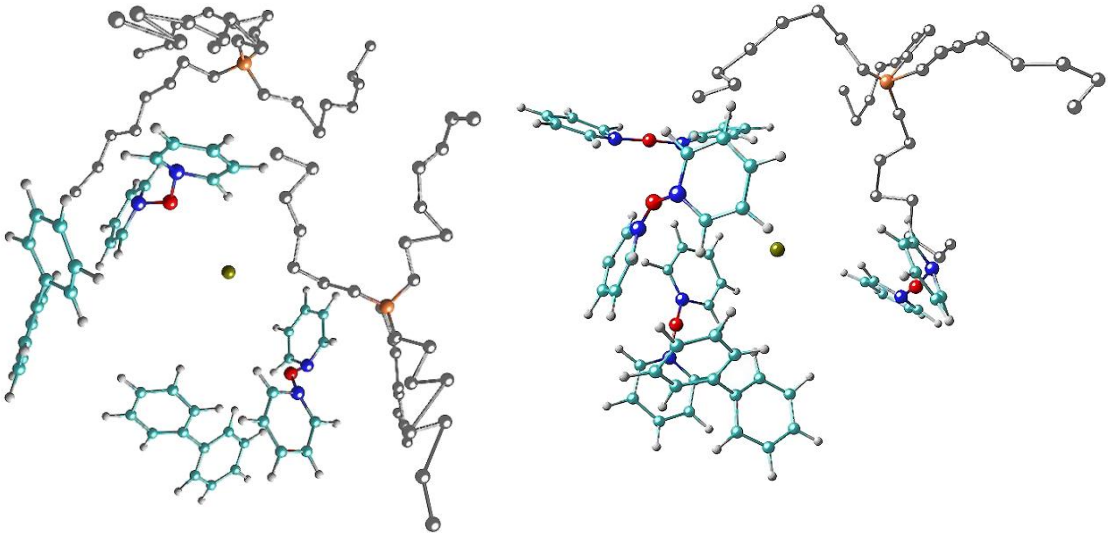

Figure 6.2.16. SDFs of the gold nanofluid system at (A) 300 K and (B) 600 K. Three-dimensional image of the SDF at (C) 300 K and (D) 500 K. The gold nanoparticle is shown in gold, the oxygen atoms of the diphenyl oxide molecules in red (with the carbon atoms from the aromatic ring bonded directly to them in blue), the remaining aromatic carbon atoms in turquoise, with the hydrogen atoms in grey, while the surfactant chain is represented by the colour silver, with the nitrogen from the amine group of the TOAB surfactant in orange.

The movement of the surfactant molecules at a wide range of temperatures (50 - 600 K) is shown below (Figure 6.2.17). At low temperatures, there are more surfactant molecules and they are located very close to the central metal atom. At 300 K, two surfactant molecules surround the gold cell. This is the temperature at which the surfactant molecules are closest to the gold nanoparticle, providing a high level of stability. When the temperature rises, the number of surfactant molecules decreases and they move away from the metal, allowing the diphenyl oxide molecules to enter.

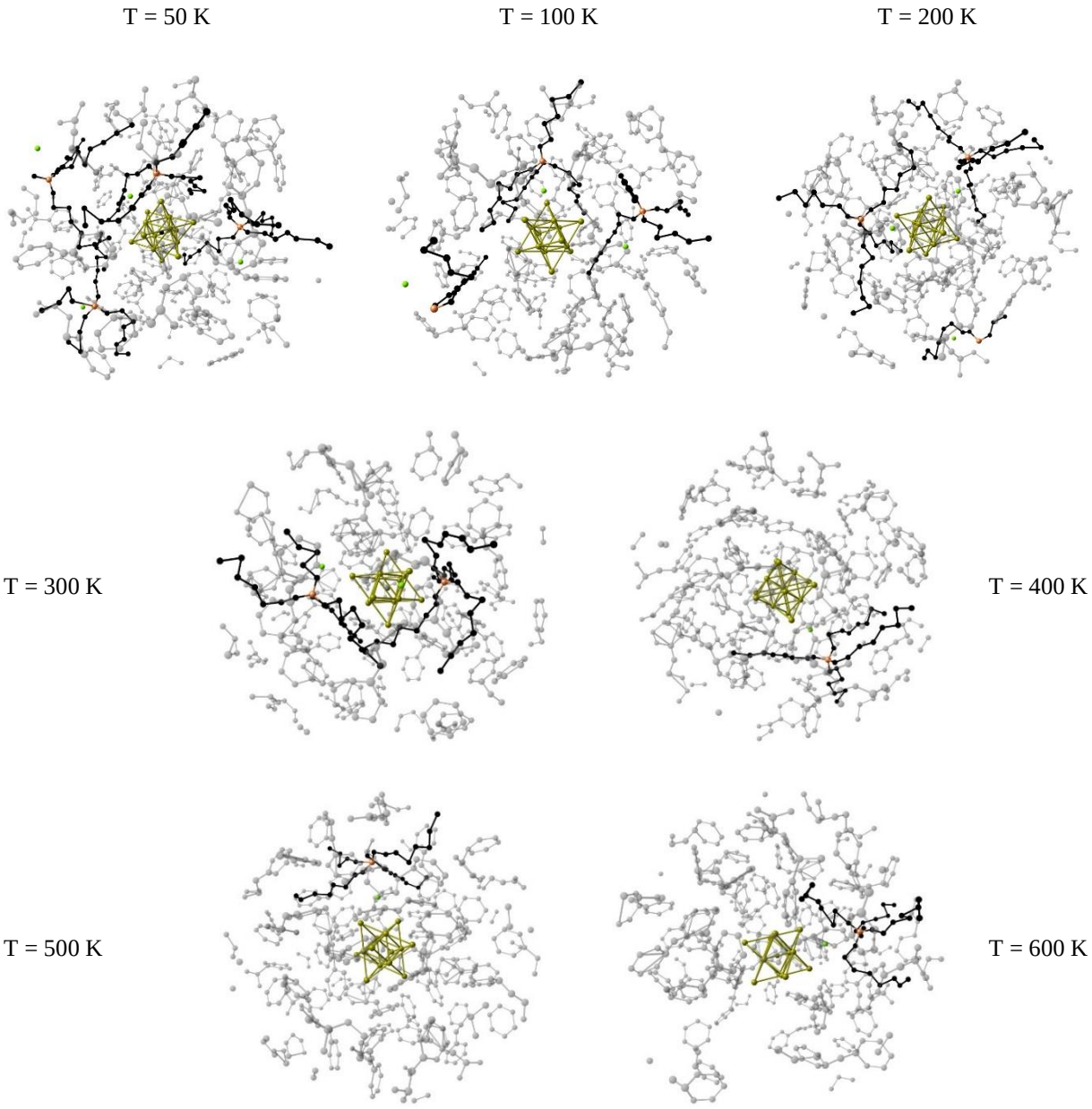

Figure 6.2.17. Movement of the TOAB surfactant around the gold nanoparticle at different temperatures.

Therefore, among all the possible mechanisms that can affect thermal conductivity, it would be logical to think that Brownian motion plays an important role in the dramatic increase obtained, and that the participation of the surfactant affects the free movement of the nanomaterial at low temperatures, leading to a lower number of collisions between particles and more energy being required to increase the temperature of the system. This would explain the isobaric specific heat values obtained by the nanofluid with regard to the base fluid. However, high temperatures promote the rearrangement of the surfactant molecules,

liberating the nanomaterial and facilitating its movement, which leads to an increase in thermal conductivity. This is consistent with the results obtained experimentally, the thermal conductivity of the nanofluids showing a tendency to increase with temperature.

6.3. Nanofluids based on platinum nanoparticles

The nanofluid system based on platinum nanoparticles was prepared following the two-step method (see ***Section 5.2***). The platinum nanoparticles were synthesised and characterised to confirm that the nanomaterial was synthesized as expected. The nanoparticles were then dispersed into the eutectic mixture of diphenyl oxide and biphenyl used as the base fluid. In this study, in light of the positive results obtained with the gold nanofluids where the use of surfactants was analysed, three nanofluids were prepared with the same concentration of nanomaterial but with modifications of two parameters: the surfactants, in this case using ODT and DDA (which also acts as a phase transfer agent); and the application of ultrasound treatment (see ***Section 5.2.3***). Table 6.4 shows the nomenclature established to refer to each nanofluid and the treatment applied to them. Thus, each nanofluid prepared was studied and characterised experimentally, taking into account its physical and chemical stability and its thermal and rheological properties with the purpose of assessing the degree of improvement in its efficiency in heat transfer processes and validating the action of each surfactant and/or the ultrasound treatment. In addition, the theoretical analysis by means of MD simulations was based on analysing the structural properties of the nanofluid system when only one surfactant was used and when the two were used in combination in order to study the molecular organisation of each surfactant and of the base fluid molecules around the platinum nanoparticles.

Table 6.4. Platinum nanofluids prepared and the treatment applied to each.

Nanofluid	*Dowtherm-A + DDA*	*ODT*	*Ultrasound*
Pt-Nf + DDA + ODT	✓	✓	x
Pt-Nf + DDA + U	✓	x	✓
Pt-Nf + DDA + ODT + U	✓	✓	✓

6.3.1. Characterization of platinum nanoparticles

The platinum nanoparticles were synthesised in a previous step to the preparation of the nanofluid. Thus, it was essential to characterise the particles to confirm that the nanomaterial obtained was synthesized as expected. The results obtained by means of the techniques used to characterize the synthesized platinum nanoparticles are shown below.

An analysis was performed using XPS of the oxidation state and the chemical bonding state of the platinum nanomaterial synthesized. Figure 6.3.1 shows the spectrum obtained, revealing the presence of two peaks at binding energy values between 70.8 and 74.2 eV, which correspond to the $4f_{7/2}$ and $4f_{5/2}$ orbitals of the platinum. The difference between the two peaks at 3.4 eV suggests that the solid obtained is platinum in a zero oxidation state; that is, metallic platinum nanoparticles, as has been reported previously [29].

In turn, the x-ray diffraction results provided information about the crystalline structure of the platinum nanoparticles synthesized. Figure 6.3.2 shows the XRD pattern obtained. Of note is the presence of three peaks at 2θ angles of 40.25, 46.81 and 68.36º, which are characteristic of platinum nanoparticles and are assigned to the (111), (200) and (220) families of planes respectively, belonging to the Fm-3m cubic space group [30, 31].

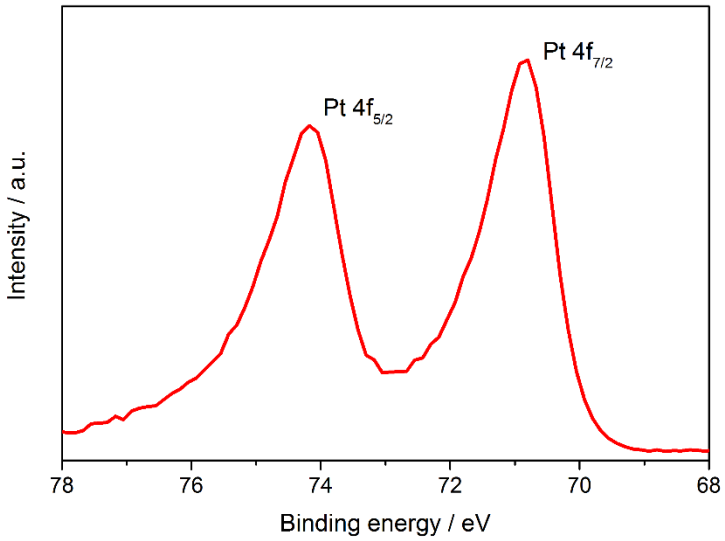

Figure 6.3.1. Signal obtained for the 4f orbital of the platinum by XPS.

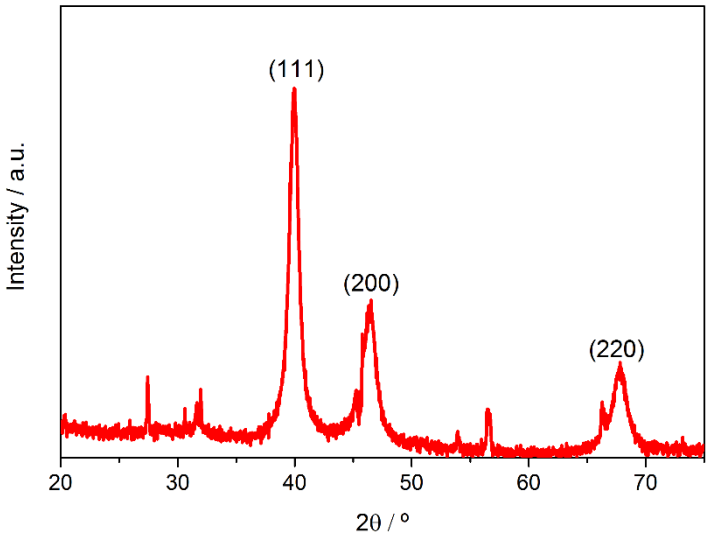

Figure 6.3.2. XRD pattern obtained for the platinum nanoparticles synthesized.

Finally, the size and shape of the platinum nanomaterial was analysed by means of TEM. Figure 6.3.3. shows that the nanomaterial is mainly spherical in shape, the particles ranging in size between 5 and 35 nm. We can therefore conclude that the method of synthesis used produced spherical metallic platinum nanoparticles.

(A)

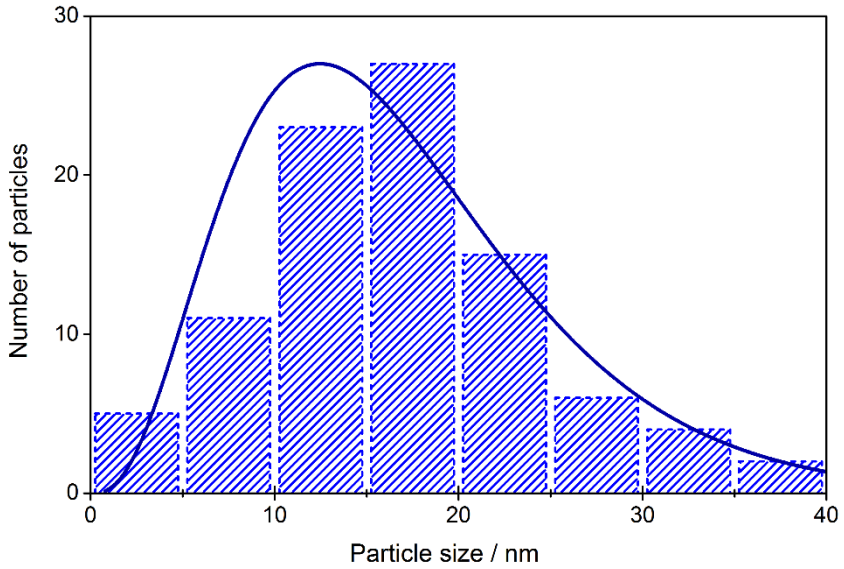

(B)

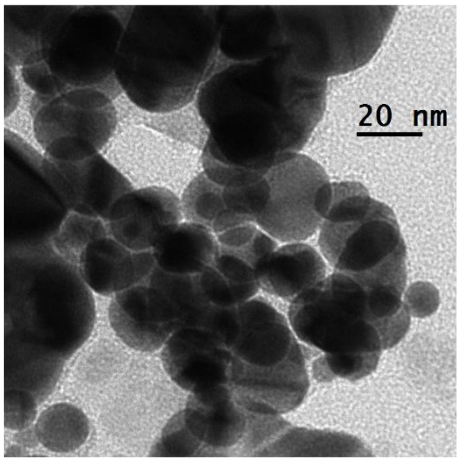

Figure 6.3.3. (A) Size distribution and (B) TEM image of the synthesized platinum nanoparticles.

6.3.2. Monitoring of stability

The UV-vis spectra recorded immediately after preparing each nanofluid suggest the presence of platinum nanomaterial in suspension in the cases where ultrasound treatment was used, shown by the band at 400 nm in Figure 6.3.4.A. In turn, Figure 6.3.4.B shows the spectra of the nanofluids without the base fluid spectrum. The nanofluids treated with ultrasound present a band at approximately 390-500 nm with a higher intensity than the base fluid due to the highly dispersed nanomaterial in suspension as a result of the ultrasound treatment [1, 2]. In turn, the nanofluid that did not undergo ultrasound treatment does not present this signal, which suggests that the nanomaterial in this fluid was not dispersed and that the application of ultrasound is vitally important for these nanofluids.

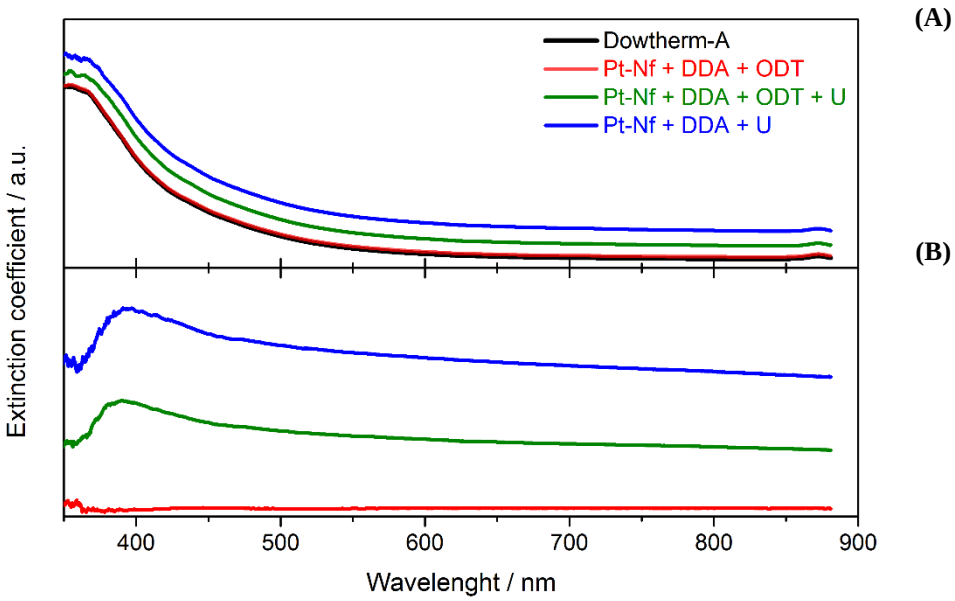

Figure 6.3.4. (A) UV-Vis spectrum of the platinum nanofluids and the base fluid at time zero; (B) UV-Vis spectrum of the platinum nanofluids without the base fluid spectrum at time zero.

In turn, the analysis of the radiation extinction coefficient at a set wavelength (λ=390 nm, the most intense peak) for one week is shown in Figure 6.3.5. It shows that in the case of the two nanofluids treated with ultrasound, the extinction value remains constant after the second day, indicative of the amount of nanomaterial in suspension remaining constant. The nanofluid prepared without ODT, however, presented a sharp decay in the extinction value between the first and second days, suggesting that the presence of a second surfactant prevents the sudden agglomeration and precipitation of the nanomaterial immediately after the nanofluid is prepared. After this time, the concentration of suspended material remains fairly unchanged. Furthermore, the nanofluid that was not treated with ultrasound does not present nanomaterial in suspension, so a second surfactant is totally unnecessary in this case. Therefore, the ultrasound treatment is essential in order to disperse the nanomaterial more effectively, and following this treatment the presence of a second surfactant (ODT) helps the system to maintain the nanomaterial in suspension.

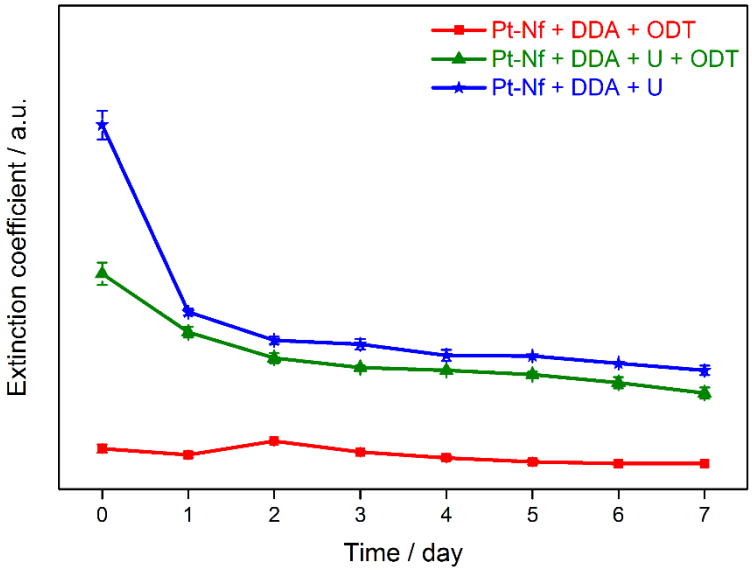

Figure 6.3.5. Variation in the extinction coefficient of the platinum nanofluids at λ=390 nm versus time.

In the study of the size of the particles (Figure 6.3.6) of the Pt- Nf + DDA + ODT nanofluid, highly dispersed data is observed, with sizes ranging between 500 and 2000 nm after the fifth day, which illustrates that the small amount of suspended nanomaterial in the system generates signals of high dispersion. In turn, the application of ultrasound to the other two nanofluids generated aggregates of a constant size of approximately 600-800 nm (larger in the case of the Pt-Nf + DDA + U + ODT nanofluid) after the second day, which would suggest that these two nanofluids reach a stable condition.

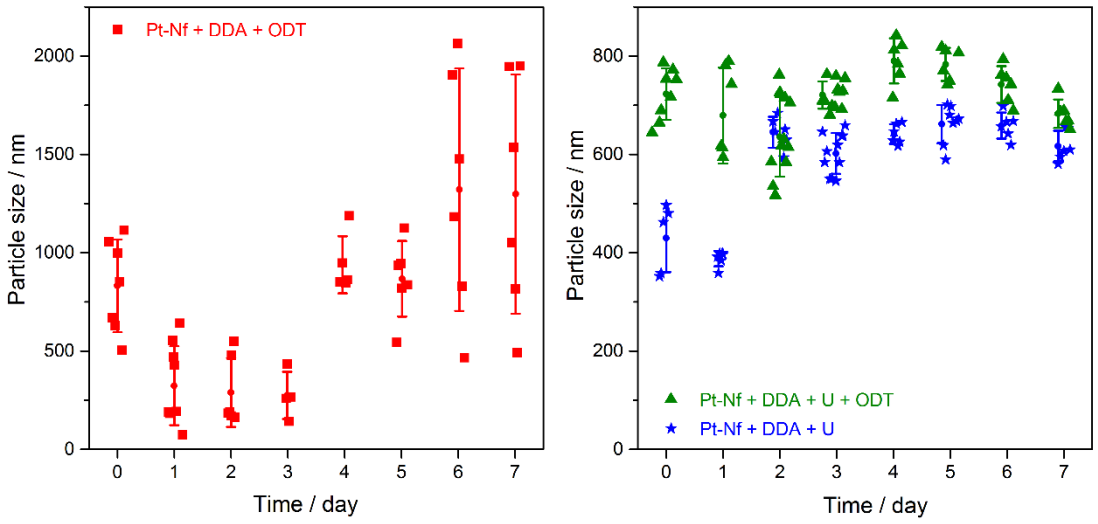

Figure 6.3.6. Particle size measurements of the platinum nanofluids using the DLS technique.

To complete the study of stability, Figure 6.3.7 shows the ζ potential values obtained for each nanofluid during one week. The nanofluid that did not undergo ultrasound treatment presents ζ potential values of around 0 mV, which, once again, is clear evidence that this nanofluid system is unstable. The other two nanofluids present ζ potential values of 30 mV for Pt-Nf + DDA + U and around 60 mV for Pt-Nf + DDA + U + ODT, which shows that both systems present good stability as a result of the nanomaterial being well dispersed by the ultrasound treatment and due to the surfactants preventing its agglomeration and precipitation.

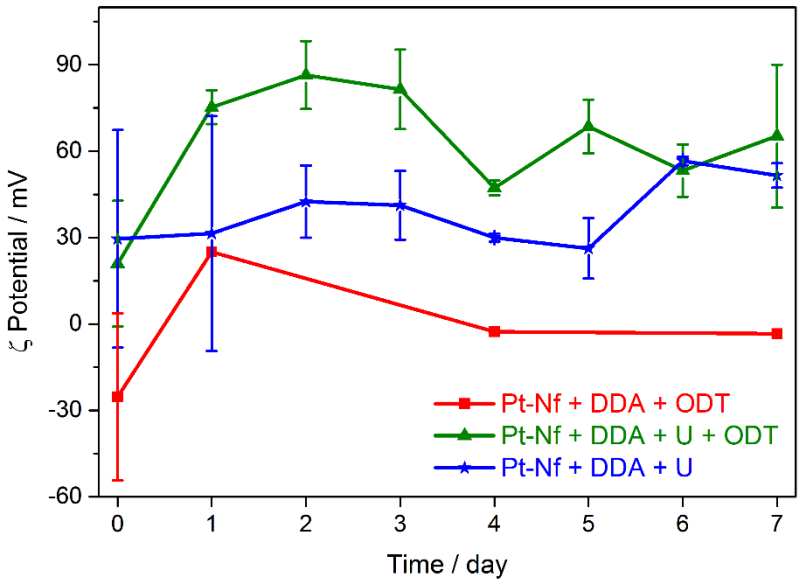

Figure 6.3.7. ζ potential values obtained for the platinum nanofluids versus time.

Thus, from the characterization performed, the two nanofluids treated with sonication were considered to be stable and were therefore characterized for their thermal properties and analysed from a theoretical perspective. On the other hand, the results of the UV-Vis spectra, particle size and ζ potential values showed that the Pt-Nf + DDA + ODT nanofluid is totally unstable and, therefore, it was not characterized for its thermal and rheological properties.

6.3.3. Study of efficiency

The density and viscosity values, measured at room temperature, are shown in Table 6.5. The two nanofluids contain the same amount of both the platinum nanomaterial (0.005 wt.%) and DDA, but one also contains ODT, the second surfactant. Both nanofluids present the same slight increase in density of around 0.18%. The nanofluid prepared using the two surfactants, DDA and ODT, presents a greater increase in viscosity, of 3.9%. Meanwhile, the one containing only DDA shows an increase of 3.2% in viscosity compared with the base fluid.

Table 6.5. Density and viscosity values obtained and the variation in each for the platinum nanofluids and the base fluid.

Sample	*ρ / kg·m^{-3}*	*variation in density / %*	*μ / mPa·s*	*variation in viscosity / %*
Dowtherm-A	1058.8 ± 0.8	-	3.76 ± 0.03	-
Pt-Nf + DDA + U	1060.8 ± 0.4	0.19	3.88 ± 0.03	3.19
Pt-Nf + DDA + U + ODT	1060.3 ± 0.6	0.18	3.91 ± 0.02	3.98

Furthermore, the isobaric specific heat and thermal conductivity were measured at temperatures ranging between room temperature and 363 K. Figure 6.3.8 shows a slight increase in isobaric specific heat for the Pt- Nf + DDA + U + ODT nanofluid with regard to the base fluid, giving a mean improvement value of approximately 1.2% for the whole range of temperatures. However, the Pt-Nf + DDA + U nanofluid presents isobaric specific heat values that are much lower than those of the base fluid, an expected trend according to the literature [24, 25]. The difference between the two nanofluids is the presence of ODT, which somehow generates an internal structure within the solid (and let us remember a smaller particle size), which produces a tendency to show the properties of a semi-solid, resulting in its isobaric specific heat values being higher than those of the base fluid [26, 27].

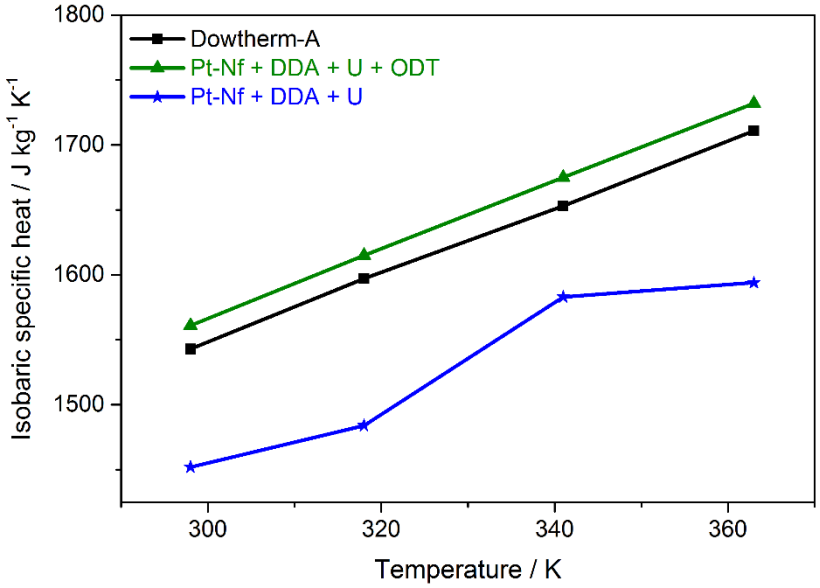

Figure 6.3.8. Isobaric specific heat values obtained for the platinum nanofluids and the base fluid.

Figure 6.3.9 shows the thermal conductivity values obtained and the ratio k_{nf}/k_{bf}. It shows that at temperatures above about 325 K both nanofluids present thermal conductivity values higher than the base fluid. At high temperature (363 K), the Pt-Nf + DDA + U nanofluid presents an improvement of 17%, while the Pt-Nf + DDA + U + ODT nanofluid would seem to be more promising as a heat transfer fluid as it achieves a significant improvement of approximately 37%.

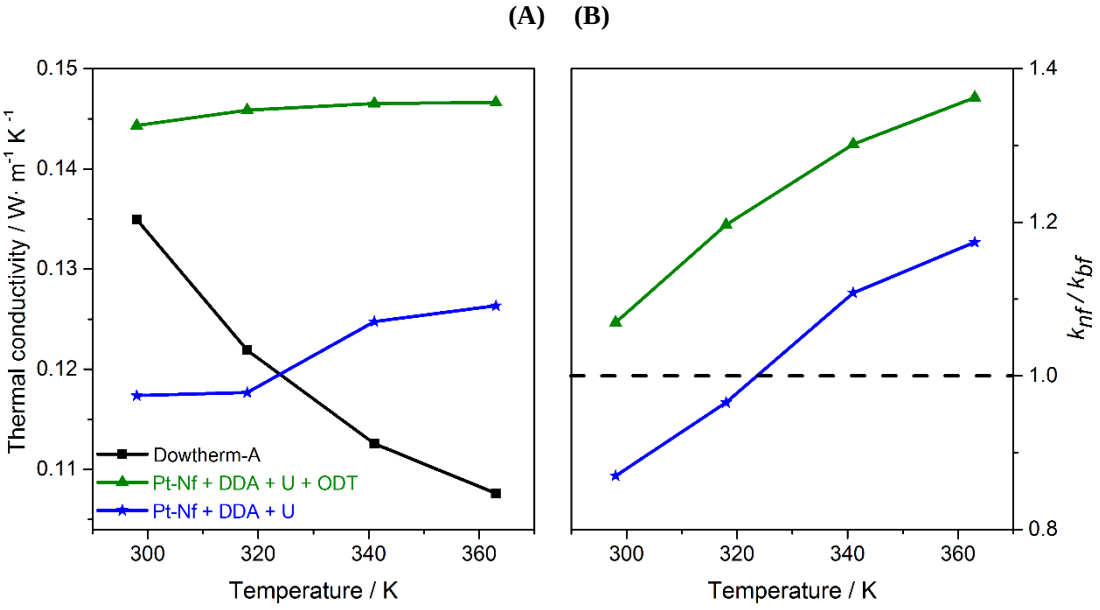

Figure 6.3.9. Values obtained for (A) thermal conductivity and (B) the ratio with regard to the base fluid for the platinum nanofluids.

The estimation of the improvement in efficiency was performed using the ratio of the heat transfer coefficients of the nanofluid and the base fluid in accordance with the Dittus-Boelter equation (Equation 5.3.3), typical for systems in turbulent flow conditions. Figure 6.3.10 shows that, at 363 K, the Pt-Nf + DDA + U system achieves an improvement in efficiency of 5%, while the Pt-Nf + DDA + U + ODT system presents an improvement of 20%. Hence, the conclusion can be drawn that the presence of ODT has a significant, positive effect on the heat transfer coefficient, and consequently on the efficiency of the nanofluid with regard to the base fluid.

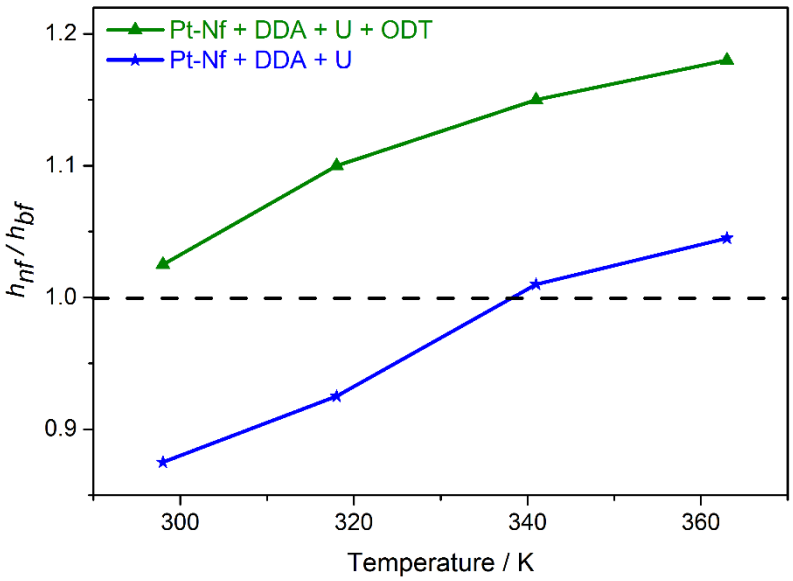

Figure 6.3.10. Estimation of the degree of efficiency of the platinum nanofluids using the Dittus-Boelter equation.

6.3.4. Theoretical analysis

The main advantage of the theoretical analysis of this nanofluid system revolves around determining how each surfactant participates and influences the increase in thermal properties. To this end, Molecular Dynamics simulations were used to study and analyse the structural properties of these systems in order to determine how the surfactant and base fluid molecules are arranged around the platinum nanoparticles, and to discover how the organisation of the molecules changes with temperature.

6.3.4.1. Molecular Dynamics simulations

The Molecular Dynamics simulations were performed with the DL POLY code [4], using the NVT canonical ensemble, the Nosé-Hoover thermostat and applying periodic boundary conditions. The initial configuration was built with the PACKMOL code [5], generating cubic boxes with such dimensions to enable the experimental density of the base fluid to remain constant at 298 K (1056 kg m^{-3}), for which a representative concentration of 0.005 wt.% of platinum was chosen, taking into consideration computational costs. The time-step established was 0.5 fs, saving the generated structures to analyse the trajectories every 100 time-steps, the time for each simulation being 1 ns. In each case, a cut-off distance of 9 Å was established and the Ewald summation method was applied [6] for the electrostatic reactions.

The TraPPE-EH force field was used to describe the intra- and intermolecular interactions between the base fluid molecules, while the TraPPE-UA force field was used for the interactions of each surfactant (DDA and ODT) (see ***Section 5.4.1.2***).

The representation of the metal nanoparticle is based on fourteen platinum atoms arranged in a Fm-3m symmetrical space group [32], while the non-bonded force field parameters were adapted from previously set parameters [33].

6.3.4.2. Analysis of structural properties

In this section, Molecular Dynamics simulations are used to analyse the possible structures formed within the nanofluid system due to the presence of one surfactant (DDA) or the two together (DDA + ODT), and how these structures are related with the increase in the thermal property values.

- Analysis of the structure of the Pt-Nf + DDA system

This nanofluid system was studied to analyse the participation in isolation of the DDA surfactant and how it is arranged, together with molecules from the base fluid, around the platinum. To this end, the interactions were analysed of the platinum (established as the centre of mass of a unit cell) with the oxygen from the diphenyl oxide (Pt-O) and with the nitrogen (accepting that the interaction is produced by the amine group) from the DDA surfactant (Pt-

N) at three temperatures: 100, 300 and 500 K. These interactions were studied up to a cut-off distance of 9 Å, which corresponds with an inner layer around the platinum nanoparticle. The Pt-O and Pt-N interactions at the three temperatures mentioned above are shown in Figure 6.3.11.

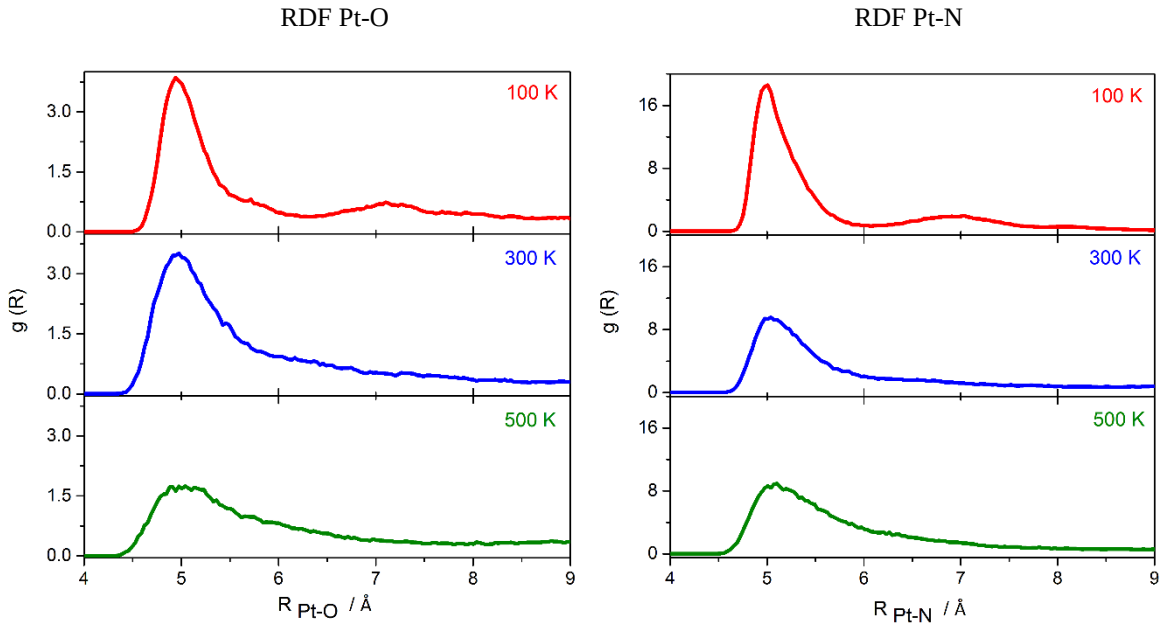

Figure 6.3.11. RDFs obtained for the Pt-O and Pt-N pairs of the Pt-Nf + DDA nanofluid system at different temperatures.

In the case of the Pt-O pair, at 100 K, a sharp peak is seen centred at 5 Å and a second gentle peak at 7 Å, both of which are assigned to a total of six oxygen atoms corresponding to six diphenyl oxide molecules. When the temperature rises to 300 K, the two peaks combine, the new peak corresponding to a total of seven oxygen atoms belonging to seven diphenyl oxide molecules. However, at 500 K the peak is less intense, the number of diphenyl oxide molecules around the platinum nanoparticle decreasing from seven to five. The Pt-N interaction reveals that the peak centred at 5 Å becomes less intense as the temperature rises, which is a result of the number of surfactant atoms, and therefore the number of surfactant molecules, around the platinum nanoparticle. At 100 K and 300 K, the peak consists of six nitrogen atoms; hence six surfactant molecules are surrounding the nanomaterial in a first layer. However, at 500 K, a seventh surfactant molecule is incorporated.

The analysis of the SDFs (Figure 6.3.12) of this system show how as the temperature rises the surfactant molecules (defined by the nitrogen atoms in orange) encapsulate the

platinum nanoparticle (grey atom) impeding its interaction with the diphenyl oxide molecules (the oxygen is shown in red and the carbon from the aromatic ring bonded to it in blue). In addition, the increase in temperature leads to decreased resolution of the image due to the movement of molecules, a reflection of the change in intensities of the RDFs, which is indicative of a dynamic system.

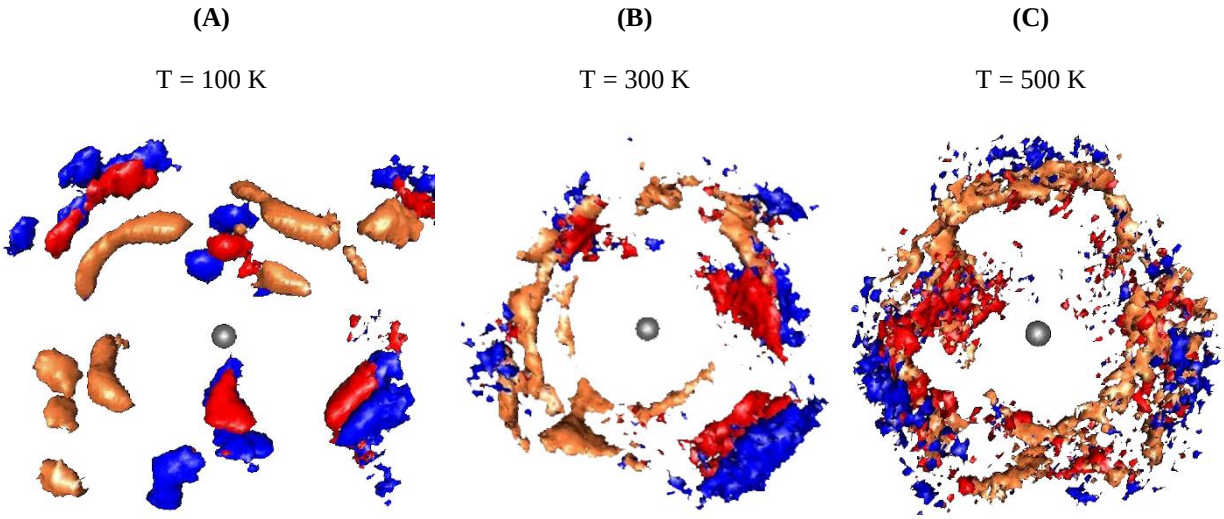

Figure 6.3.12. SDFs of the Pt-Nf + DDA nanofluid system at different temperatures. The platinum nanoparticle is shown in grey, the oxygen molecules from the diphenyl oxide in red (with the carbon atoms from the aromatic ring directly bonded to them on blue) and the nitrogen from the amine group of the DDA surfactant in orange.

When the nanofluid system is prepared with only one surfactant (DDA), the favourable interaction between the platinum and the nitrogen leads to the surfactant molecules predominating a first layer around the nanomaterial, limiting the interaction with the diphenyl oxide molecules responsible for heat transfer. This produces a slight increase in the values of the thermal properties of the nanofluid with regard to the base fluid. Figure 6.3.3. shows how the presence of the chains of DDA molecules located around the platinum generates significant steric hindrance effects that make it difficult for the diphenyl oxide molecules to approach the metal, which would appear to limit the flow of heat.

(A) T = 100 K

(B) T = 300 K

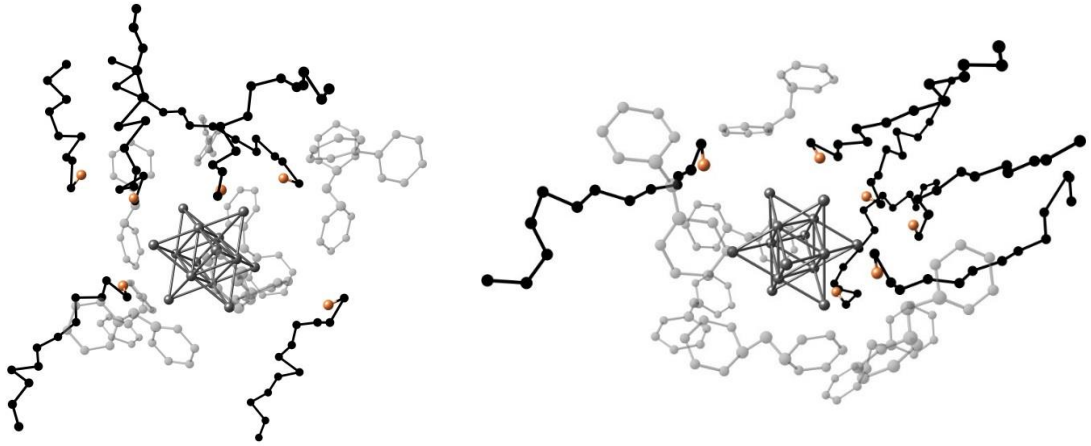

(C) T = 500 K

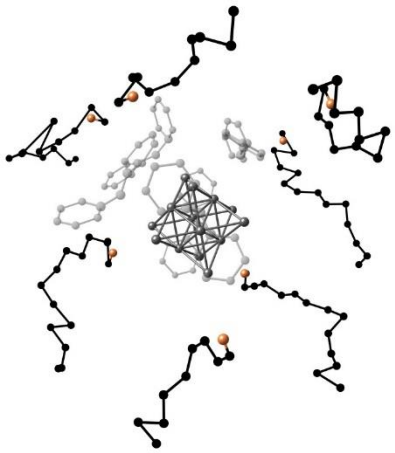

Figure 6.3.13. Movement of the surfactant molecules of the Pt-Nf + DDA nanofluid system at different temperatures. The chain of the DDA surfactant is shown in black with the nitrogen from the amine group in orange.

- Analysis of the structure of the Pt-Nf + DDA + ODT system

When the second surfactant was incorporated into the system, an analysis was performed of the interactions between the platinum nanoparticle (established as the centre of mass of a unit cell) and the atoms from the base fluid molecules and both surfactants at the same temperatures as in the previous case. Thus, the study included the Pt-O interaction between the platinum and the oxygen from the diphenyl oxide of the base fluid, and the interaction between the nanomaterial and the surfactants by means of the Pt-N pair (accepting that the interaction is with the nitrogen from the amine group of the DDA) and the Pt-S pair

(accepting that the interaction is with the sulphur from the thiol group of the ODT). These interactions were studied up to a distance of 9 Å, corresponding with an inner layer around the platinum nanoparticle. The radial distribution functions for the Pt-O, Pt-N and Pt-S pairs at the three temperatures stated above are shown in Figure 6.3.14.

In the case of the Pt-O pair, at 100 K, a first sharp peak can be seen centred at 5 Å, which corresponds to two oxygen atoms, followed by a series of less intense peaks. Up to a distance of 9 Å, seven oxygen atoms can be counted, so seven diphenyl oxide molecules can be found in a first layer around the platinum nanoparticle. As the temperature increases, the peak at 5 Å loses intensity, becomes wider and the series of peaks is combined with it, resulting in a total of six and seven diphenyl oxide molecules at 300 K and 500 K respectively.

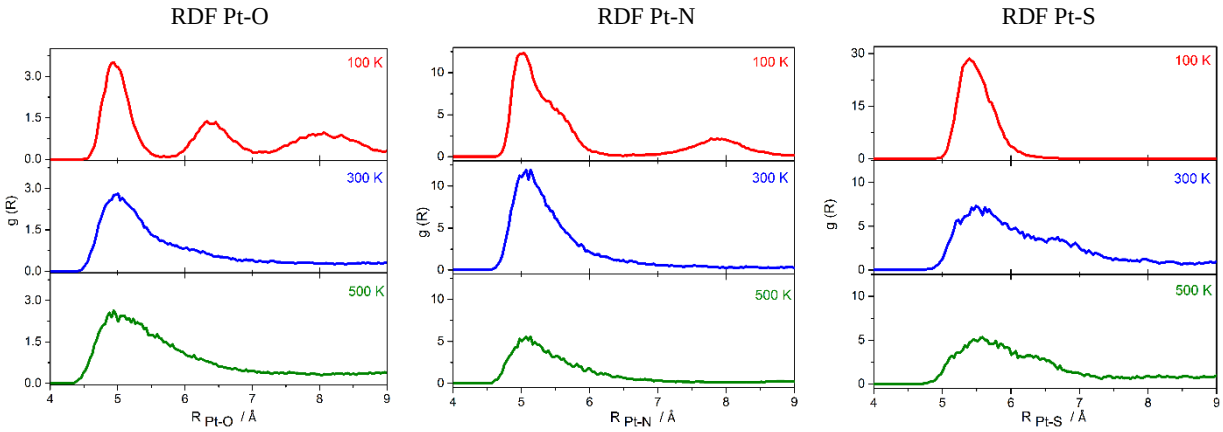

Figure 6.3.14. RDFs obtained for the Pt-O, Pt-N and Pt-S pairs of the Pt-Nf + DDA + ODT nanofluid system at different temperatures.

Regarding the Pt-N interaction, at 100 K, there is a sharp, well-defined peak at 5 Å and another centred at 8 Å, corresponding to a total of three DDA molecules. At 300 K, the second peak disappears and the signal at 5 Å corresponds to three nitrogen atoms, meaning that at this temperature the three DDA molecules are all at the same distance from the nanomaterial. However, at 500 K, this peak quickly loses intensity, meaning the number of DDA molecules around the nanomaterial decreases to two.

The Pt-S interaction, to study the participation of the second surfactant, follows a similar trend to the Pt-N pair. At 100 K, the RDF shows a sharp, well-defined peak centred at

5.4 Å corresponding to three sulphur atoms from three ODT molecules. The signal becomes less intense as the temperature rises, revealing three sulphur atoms at 300 K and two at 500 K.

The analysis of the SDFs (Figure 6.2.15) makes it possible to see how the presence and participation of the DDA (shown in orange) and ODT (shown in yellow) surfactants diminishes as the temperature increases, which is indicative of a dynamic system.

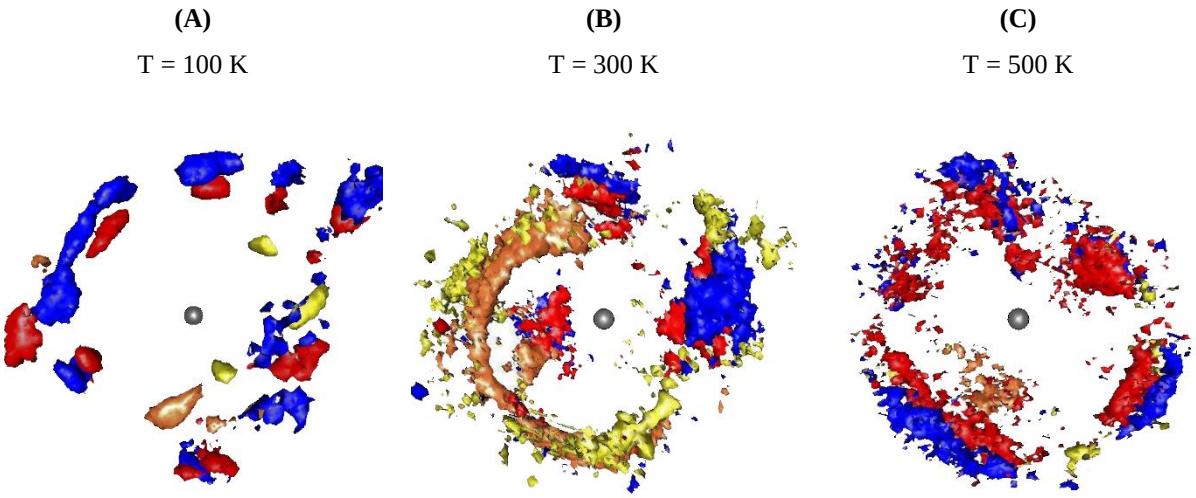

Figure 6.3.15. SDFs of the Pt-Nf + DDA + ODT nanofluid system at different temperatures. The platinum nanoparticle is shown in grey, the oxygen molecules from the diphenyl oxide in red (with the carbon atoms from the aromatic ring directly bonded to them on blue), the nitrogen from the amine group of the DDA surfactant in orange, and the sulphur from the thiol group of the ODT in yellow.

The results are in agreement with those observed in the RDFs, when the peaks become broader as the temperature increases. In this case, the ODT chains are longer than the DDA chains and therefore the number of DDA molecules in this system decreases considerably in comparison with the previous system. The web of chains formed by the molecules of the two surfactants may create "free spaces" that make it easier for the diphenyl oxide molecules (the oxygen atoms shown in red and the carbon atoms from the aromatic rings bonded to the oxygen atoms in blue) to move closer to the platinum. This would create certain directionality in the structures, which, as stated in the literature [11], is related with the improvement in the thermal properties of this kind of nanofluid systems.

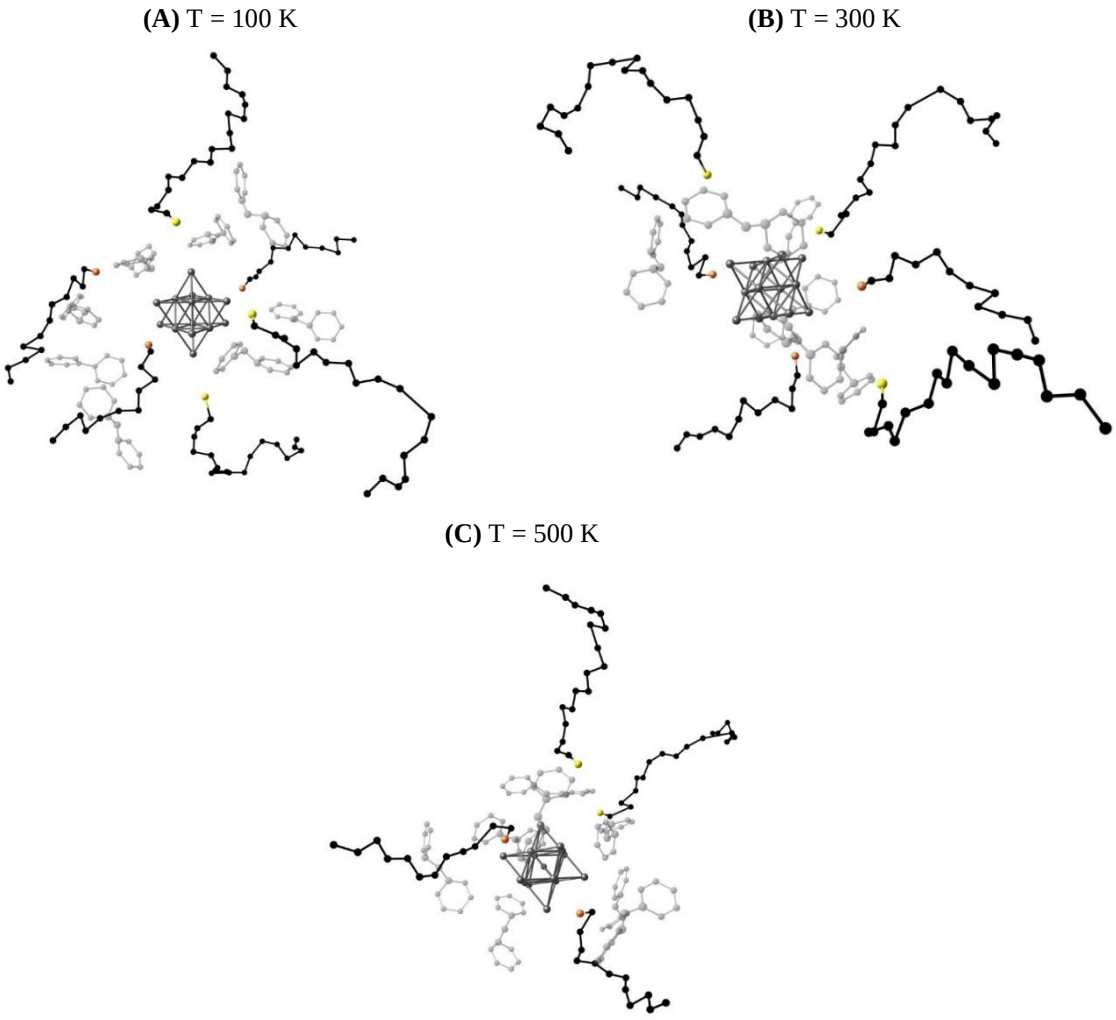

Figure 6.3.16. Movement of the surfactant molecules of the Pt-Nf + DDA + ODT nanofluid system at different temperatures. The surfactant chains are shown in black, the nitrogen from the amine group of the DDA in orange, and the sulphur from the thiol group of the ODT in yellow.

Figure 6.3.16 shows how, as the temperature rises, the presence of the surfactant chains (in black) poses an impediment to interact with other surfactant molecules, but does not impede the active participation of more diphenyl oxide molecules. Therefore, it has been shown theoretically that at high temperatures the presence of two surfactants generates stable structures in which diphenyl oxide molecules, responsible for a possible improvement in the thermal properties, are predominant. These results are in agreement with those obtained experimentally, where the use of two surfactant generated nanofluids that are stable over time and the present significant improvements in efficiency with regard to the base fluid, which means that this nanofluid is potentially of great interest for use as a heat transfer fluid in concentrating solar power plants.

6.4. Comparison of nanofluids prepared following the two-step method

After observing the positive performance of the nanofluids based on gold nanoparticles, in the sense that they quickly become stable over time and present significant increases in thermal conductivity and efficiency as heat transfer fluids, it was decided to simplify the system described in ***Section 6.2***. Thus, a nanofluid system was prepared based on gold nanoparticles but, in this case, following the two-step preparation method with gold nanoparticles synthesized in an aqueous medium before being dispersed into the base fluid (and not in situ in the heart of the base fluid as described in ***Section 6.2***) and without using the TOAB surfactant. In turn, in order to be able to compare the two nanofluid systems, the same procedure described for the nanofluids based on silver nanoparticles was followed (see ***Section 5.2.1***) to prepare these new nanofluids based on gold nanoparticles.

Thus, to prepare these nanofluids, gold nanoparticles were synthesized in an aqueous medium and then dispersed into the eutectic mixture Dowtherm-A, used as the base fluid (see ***Section 5.2***). Thus, three nanofluids were prepared, varying the concentration of nanomaterial (see ***Section 5.2.2***).

The nomenclature established to refer to the nanofluids will be **Au 0.5**, **Au 1.0** and **Au 5.0**, and **Dowtherm-A** to refer to the base fluid.

6.4.1. Monitoring of stability

The chemical stability of these nanofluids was analysed after their preparation by means of UV-Vis spectroscopy in the range between 400 and 900 nm. Figure 6.4.1 shows the UV-Vis spectra for the nanofluids and the base fluid. It is possible to observe that the addition of gold nanoparticles does not modify the base fluid and consequently does not have a negative effect on the chemical stability of the system. The presence of the nanoparticles is observed as a wide band predominantly at low wavelengths, typical of colloidal nanoparticle suspensions [1, 2].

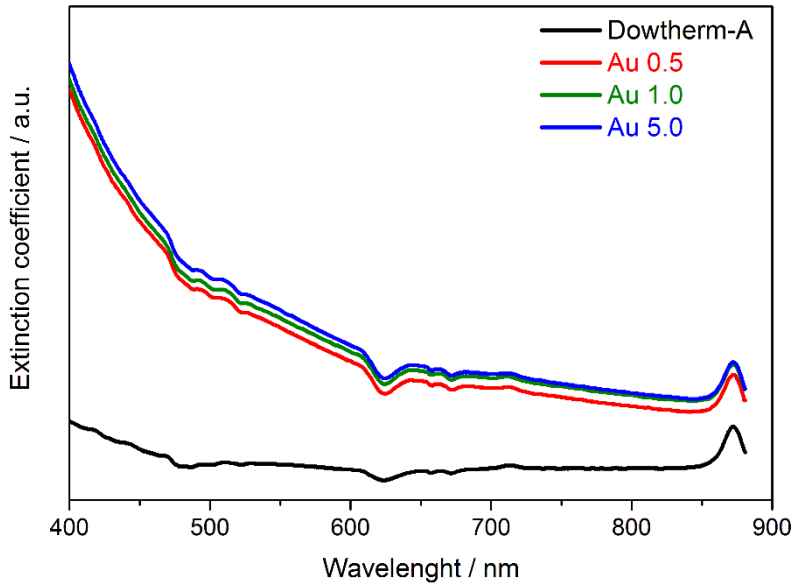

Figure 6.4.1. UV-Vis spectra of the base fluid and the gold nanofluids at time zero.

The analysis of particle size, shown in Figure 6.4.2, suggests the strong agglomeration of the nanomaterial in all the nanofluids, values of 1600 nm being obtained with a wide range of sizes, which makes these nanofluids rather unstable.

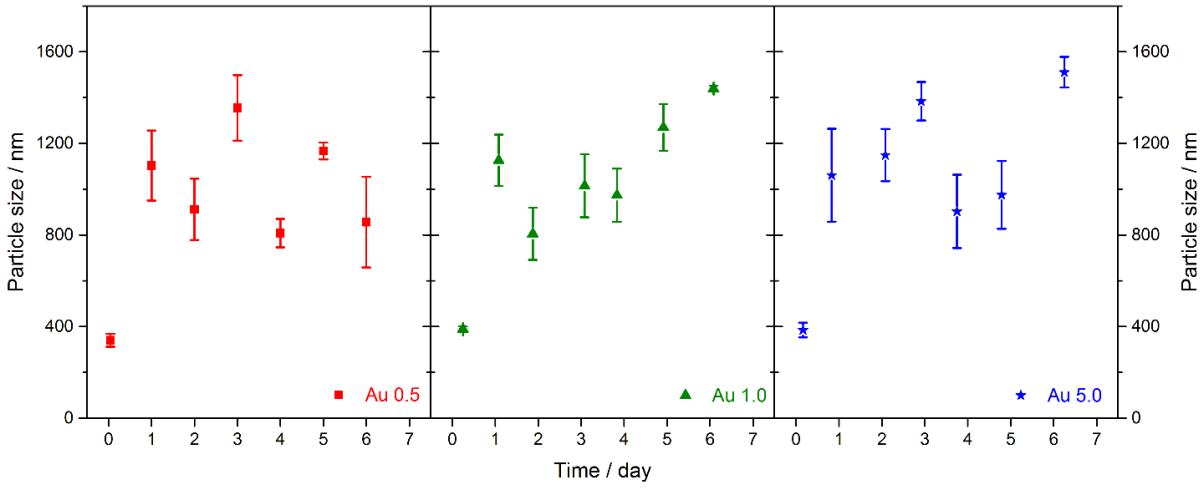

Figure 6.4.2. Particle size measurements of the gold nanofluids using the DLS technique.

6.4.2. Study of efficiency

As in the previous cases, to analyse the efficiency of the nanofluids, their density, dynamic viscosity, isobaric specific heat and thermal conductivity were measured. Table 6.6 show the density and viscosity values obtained for the gold nanofluids prepared and the variation with regard to the base fluid. It is clear that the addition of nanomaterial produces an increase in the values of both properties, which are higher when greater amounts of nanomaterial are added [3]. In comparison with the results described above for the nanofluids based on silver nanoparticles, a significant increase of around 1.3% is seen in density for the nanofluid with the highest concentration of gold nanoparticles. In addition, the increase in viscosity is very similar to that observed in the silver nanofluids, the values rising by 4.3% in the case of the nanofluid with the highest concentration of nanomaterial.

Table 6.6. Density and viscosity values obtained and the variation in each for the gold nanofluids and the base fluid.

Sample	*ρ / kg·m^{-3}*	*variation in density / %*	*μ / mPa·s*	*variation in viscosity / %*
Dowtherm-A	1056.0 ± 1.5	-	4.025 ± 0.006	-
Au 0.5	1065.7 ± 0.4	0.92	4.116 ± 0.006	2.26
Au 1.0	1068.4 ± 0.5	1.17	4.143 ± 0.004	2.93
Au 5.0	1069.6 ± 0.6	1.28	4.201 ± 0.004	4.37

Measurements were taken of the isobaric specific heat and thermal conductivity of the nanofluids based on gold nanoparticles and the base fluid at temperatures ranging between room temperature and 360 K. As Figure 6.4.3.A shows, the values of the isobaric specific heat of nanofluids are close to the values for the base fluid, without improving them, a trend previously reported in the literature [24, 25].

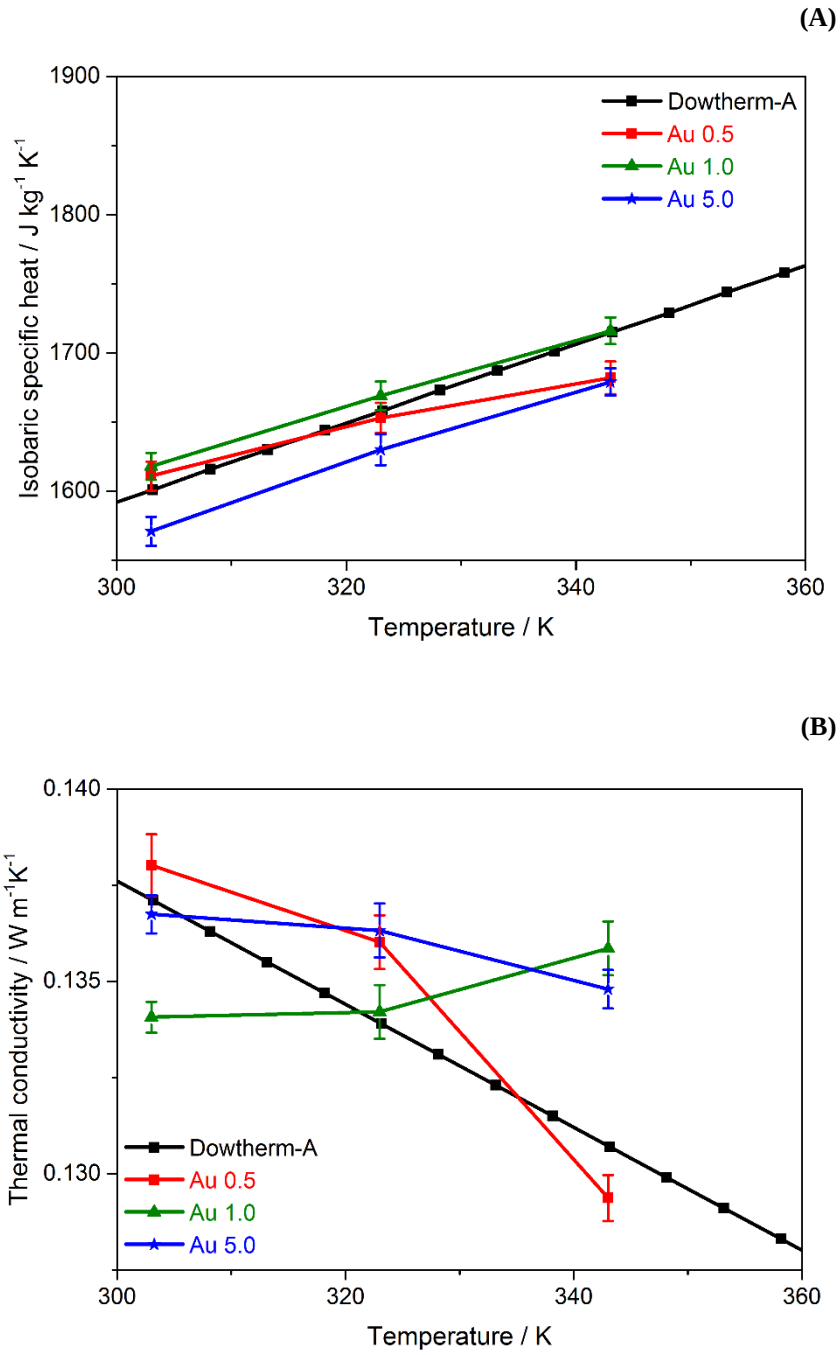

Figure 6.4.3. Values obtained for (A) isobaric specific heat and (B) thermal conductivity for the gold nanofluids and the base fluid.

Regarding thermal conductivity (Figure 6.4.3.B), the nanofluids present a slight improvement with regard to the base fluid, although the behaviour observed is erratic, possibly due to the low levels of stability of these nanofluids. A declining trend is also

observed with temperature, similar to the base fluid. For the nanofluid with the highest concentration, an improvement is obtained of approximately 3% at 343 K.

The efficiency as a heat transfer fluid of the nanofluids based on gold nanoparticles with regard to the base fluid is estimated using the ratio of the heat transfer coefficients in accordance with the Dittus-Boelter equation (Equation 5.3.3). Figure 6.4.4 shows the results obtained, and in this case the addition of gold nanoparticles does not lead to an improvement in the efficiency, as none of the nanofluids comply with $(h_{nf}/h_{bf}) > 1$.

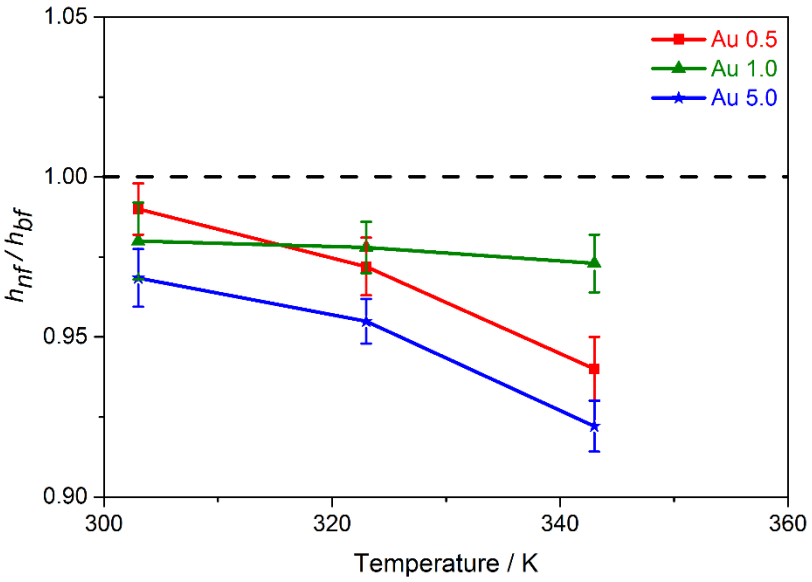

Figure 6.4.4. Values of the ratio of heat transfer coefficients of the gold nanofluids and the base fluid.

6.4.3. Theoretical analysis

In order to perform a comparison with the silver-based nanofluids from a theoretical approach too, Molecular Dynamics simulations were performed to estimate their thermal (isobaric specific heat) and structural properties to understand the how the base fluid molecules are arranged around the gold nanoparticles.

6.4.3.1. Molecular Dynamics simulations

The parameters and conditions established for these simulations are the same as those used in ***Section 6.1.3.1***, including the representative concentration of gold nanoparticles ($5.0 \cdot 10^{-4}$ wt.% Au).

6.4.3.2. Analysis of thermal properties

To determine the isobaric specific heat value, calculations were performed of the total energy of the system at a range of temperatures between 50 and 500 K. The plot of both magnitudes presents a linear relationship where the value of the slope corresponds to the isobaric specific heat value. Figure 6.4.5 shows this linear trend, for both the nanofluid and the base fluid, with slope values of $2.01 \cdot 10^3$ J kg^{-1} K^{-1} and $1.94 \cdot 10^3$ J kg^{-1} K^{-1}, respectively. Although these values are higher than those obtained experimentally, the values obtained theoretically and experimentally follow the same trend: ($C_{P_{nf}} > C_{P_{bf}}$).

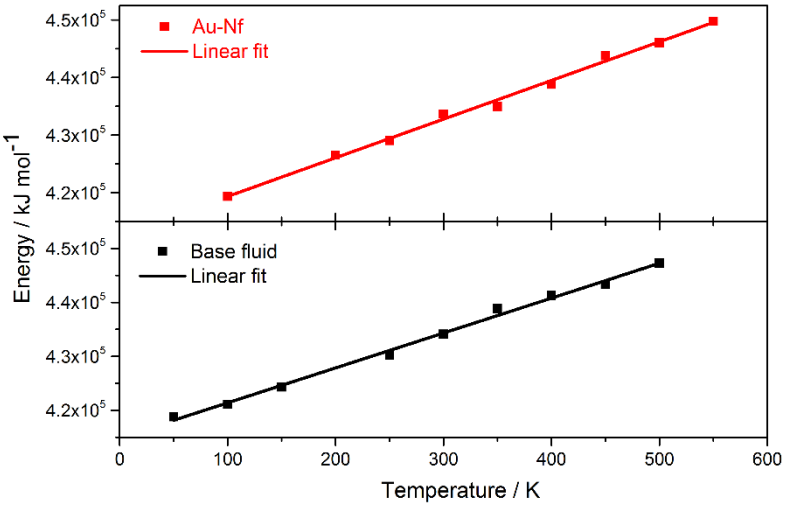

Figure 6.4.5. Plot and linear fit of the theoretical values obtained for total energy versus temperature for the gold nanofluid and the base fluid.

6.4.3.3. Analysis of structural properties

To determine the number of diphenyl oxide and biphenyl molecules arranged around the gold nanoparticle, the RDFs of the Au-O and Au-C interactions at 300 K were analysed. Figure 6.4.6 shows both RDFs and, in the case of the Au-O pair, a sharp, well-defined peak is

observed centred around 2.2 Å that is assigned to a single oxygen atom, so the gold nanoparticle is surrounded by only one diphenyl oxide molecule. However, a smaller peak appears at a distance of approximately 5.7 Å corresponding to another oxygen atom belonging to another diphenyl oxide molecule found on the border of the first and second layer. In turn, the RDF of the Au-C pair presents three peaks: a sharp peak at a distance of 2.9 Å, and two smaller ones at 4.2 Å and 5.7 Å, which are assigned to 8, 16 and 8 carbon atoms, respectively. This presupposes that there are two diphenyl oxide molecules (one in the first layer closer to the metal and another in an intermediate layer) and two biphenyl molecules.

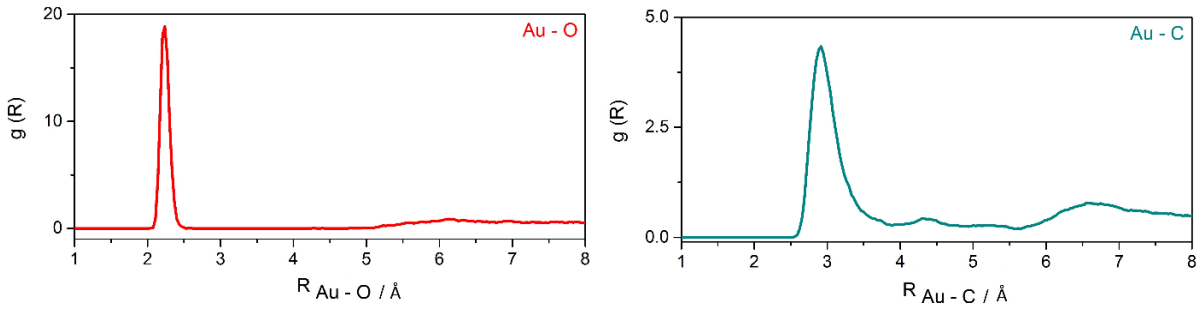

Figure 6.4.6. RDFs obtained for the Au-O (red) and Au-C (turquoise) pairs at 300 K.

In turn, by analysing the SDF, a three-dimensional, more precise view was obtained of how the base fluid molecules are distributed around the gold nanoparticle, deduced from the analysis of the RDFs at a distance of 8 Å. The SDF (Figure 6.4.7) shows the presence of two diphenyl oxide molecules (at varying distances) and another two biphenyl molecules around the gold nanoparticle (central atom in gold). The oxygen atoms are shown in red, oriented towards the gold nanoparticles with the carbon atoms bonded to them in blue, the aromatic carbons in turquoise and the hydrogen atoms in grey. Figure 6.4.7.B shows an image of this result to show how the molecules described above are arranged.

The arrangement of the diphenyl oxide molecules, oriented towards the metal nanoparticle, may be responsible for the possible improvement in heat transfer processes [11]. In this case, the gold nanoparticle interacts with a diphenyl oxide molecule in a first layer and with another molecule in an intermediate layer. This arrangement does not appear to be a favourable distribution for improving the efficiency of the heat transfer process, and is in agreement with the results obtained after the experimental characterization.

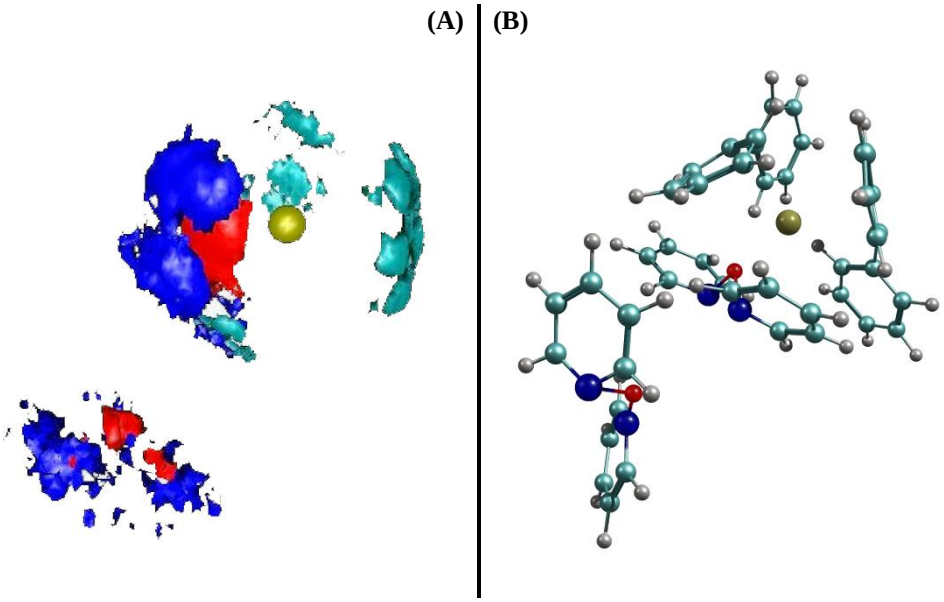

Figure 6.4.7. (A) SDF of the gold nanofluid system. (B) Three-dimensional model of the SDF. The gold nanoparticle is shown in gold, the oxygen from the diphenyl oxide in red, the carbon atom from the aromatic rings directly bonded to the oxygen in blue, and the remaining carbon atoms from the aromatic rings in turquoise, with the hydrogen atoms in grey.

6.4.4. Comparative analysis of the Ag/Au and Cu/Ni nanofluid systems

At this point it is interesting to carry out a comparative analysis (considering the experimental procedure, stability, efficiency of the nanofluids and the theoretical study) of the results obtained for the nanofluids based on gold nanoparticles and those based on silver nanoparticles (see ***Section 6.1*** and ***Section 6.4***) prepared using the two-step method, and the results reported in the earlier study by Navas and co-workers into copper and nickel nanofluids [34]. Navas et al. prepared the nanofluids following the same procedure and the study was performed within the same research group as this Doctoral Thesis.

All the nanofluids were prepared with the same method, concentrations, addition of additives and the application of sonication (see ***Section 5.2.1***). The nomenclature established to refer to the nanofluids according to the nanomaterial will be **Cu- Nf**, **Ag-Nf**, **Ni-Nf** and **Au-Nf**, and according to the concentration of nanomaterial **(Cu/Ag/Ni/Au) 0.5**, **(Cu/Ag/Ni/Au) 1.0** and **(Cu/Ag/Ni/Au) 5.0**, and **Dowtherm-A** to refer to the base fluid.

6.4.4.1. Monitoring of stability

In addition, Figure 6.4.8 shows the results of the particle size analysis obtained for all the nanofluids. The nanofluids based on copper and silver nanoparticles present an exponential growth in the particle size, which remains constant after the second / third day with a small range of particle sizes. However, the nanofluids based on nickel nanoparticles present large and fairly homogeneous particle sizes, while the gold-based nanofluids present quite large but very disperse particles sizes. This suggests that agglomeration and precipitation phenomena are more acute in these two systems than in the previous ones. In view of these results, the nanofluids based on copper and silver nanoparticles present greater stability than those based on gold and nickel.

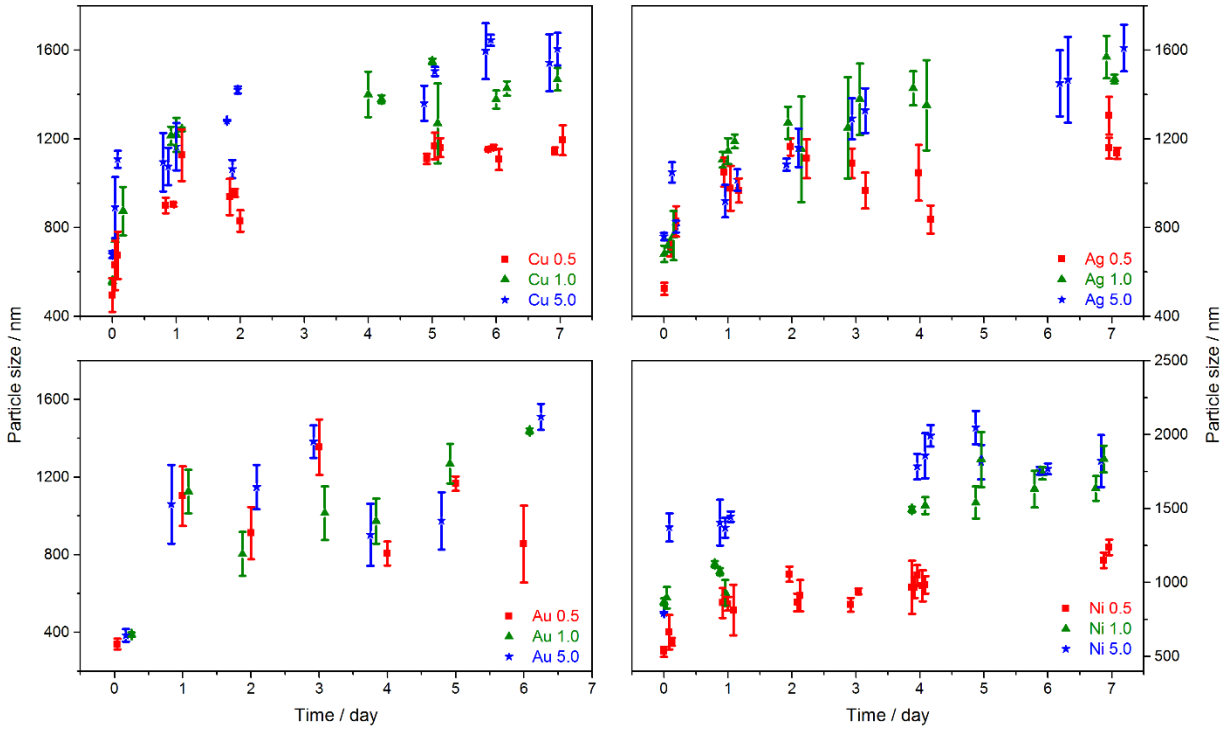

Figure 6.4.8. Particle size measurements of the nanofluids based on copper, silver, gold and nickel nanoparticles using the DLS technique [34].

6.4.4.2. Study of efficiency

Figure 6.4.9 shows the density and viscosity results obtained. In the case of density (Figure 6.4.9.A), an increase of approximately 0.2% was obtained with regard to the base fluid for the nanofluids with the highest concentration of silver, copper and nickel nanoparticles. However, in the case of the gold-based nanofluids, the increase is approximately 1.2%, which is in agreement with the density values for pure metals, as gold has a density value that is approximately double. With regard to viscosity (Figure 6.4.9.B), a similar trend is observed among the four nanofluids: the more nanomaterial added, the greater the increase in viscosity. In the case of the nanofluids with the highest concentration of each metal nanomaterial, a variation of around 4.5% was obtained for the gold and silver nanofluids, the nickel nanofluid presented a change in viscosity of approximately 6.1%, while the copper nanofluid achieved an increase of 7.9%.

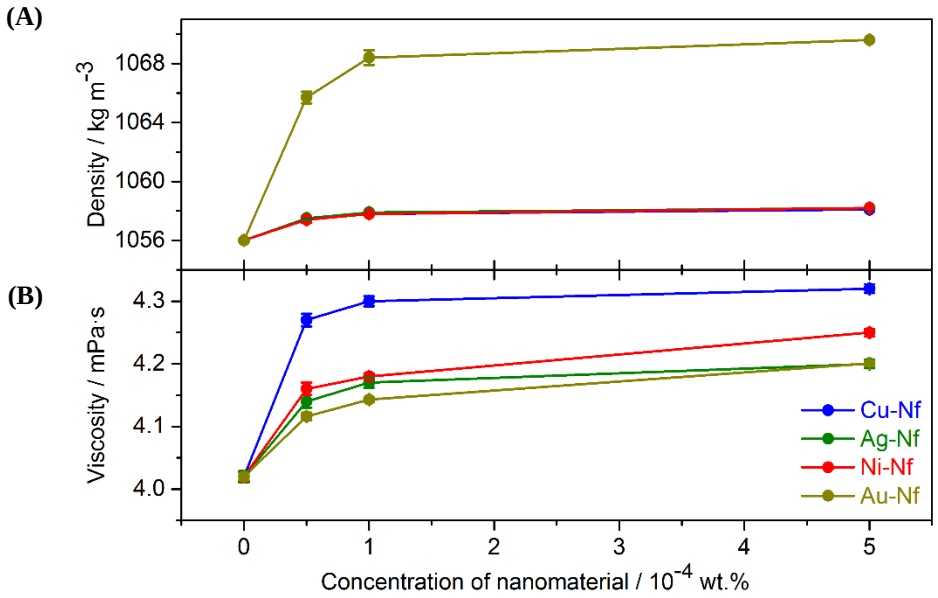

Figure 6.4.9. Values obtained for (A) density and (B) viscosity for the nanofluids based on copper, silver, gold and nickel nanoparticles [34].

Regarding their thermal properties, isobaric specific heat and thermal conductivity were measured at temperatures ranging between room temperature and 360 K. Figure 6.4.10 shows the results obtained for the isobaric specific heat of all the nanofluids. The nanofluids based on copper and silver nanoparticles present values higher than those of the base fluid,

with improvements of approximately 15% and 7.4% respectively for the nanofluids with the highest concentration of nanoparticles at approximately 350 K. However, the nanofluids based on gold and nickel nanoparticles present isobaric specific heat values that are similar to the base fluid, and no improvement in this property was found. The experimental trend obtained was:

$$C_{P_{Cu-Nf}} > C_{P_{Ag-Nf}} > C_{P_{bf}} > C_{P_{Au-Nf}} > C_{P_{Ni-Nf}}$$

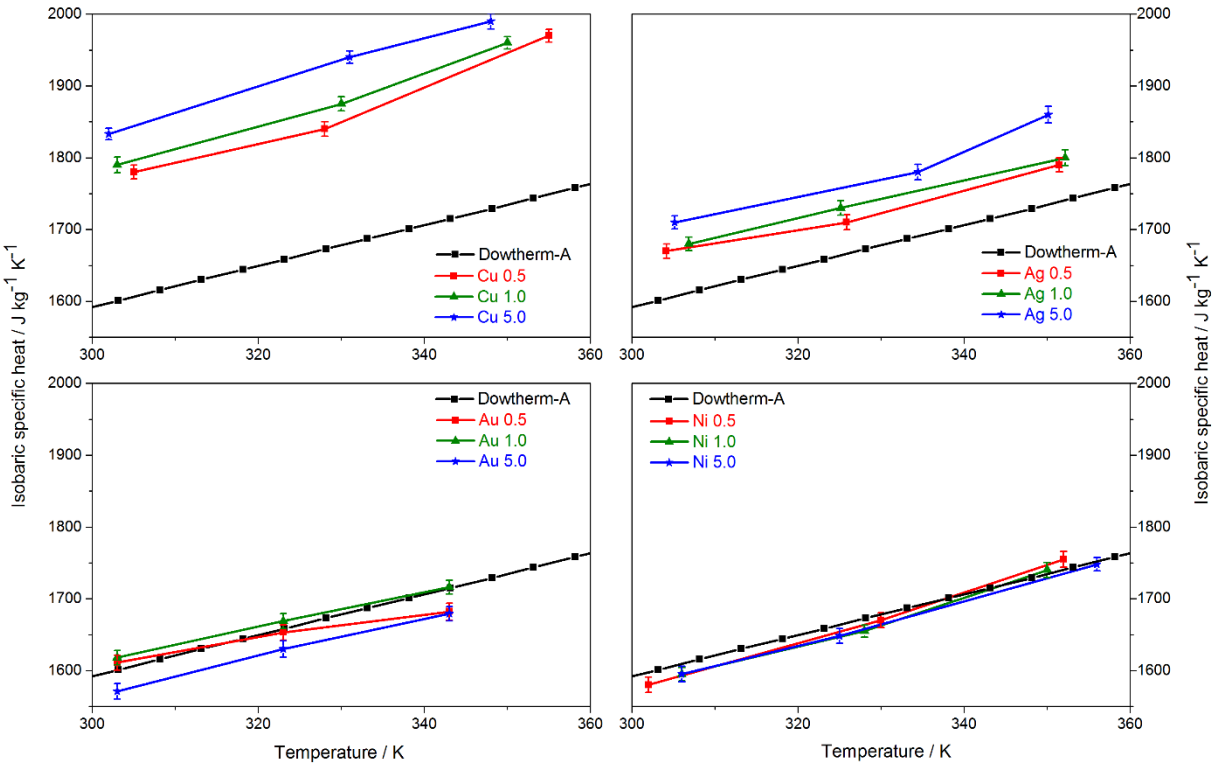

Figure 6.4.10. Isobaric specific heat values obtained for the nanofluids based on copper, silver, gold and nickel nanoparticles [34].

In addition, Figure 6.4.11 shows the thermal conductivity results obtained for all the nanofluids. The nanofluids based on copper nanoparticles show a significant increase in thermal conductivity with regard to the base fluid, as do the gold- and silver-based nanofluids, whose increases are not as pronounced. In the case of the nanofluids with the highest concentration of nanoparticles, an improvement was obtained at 350 K of approximately 14% for copper and 5.7% in the case of silver. The nanofluid with the highest concentration of gold nanoparticles presented an improvement of 3.1% at 343 K. Finally, the nickel-based

nanofluids, far from presenting values similar to those of the base fluid, have thermal conductivity values that are notably worse. The experimental trend obtained was:

$$k_{Cu-Nf} > k_{Ag-Nf} > k_{Au-Nf} > k_{bf} > k_{Ni-Nf}$$

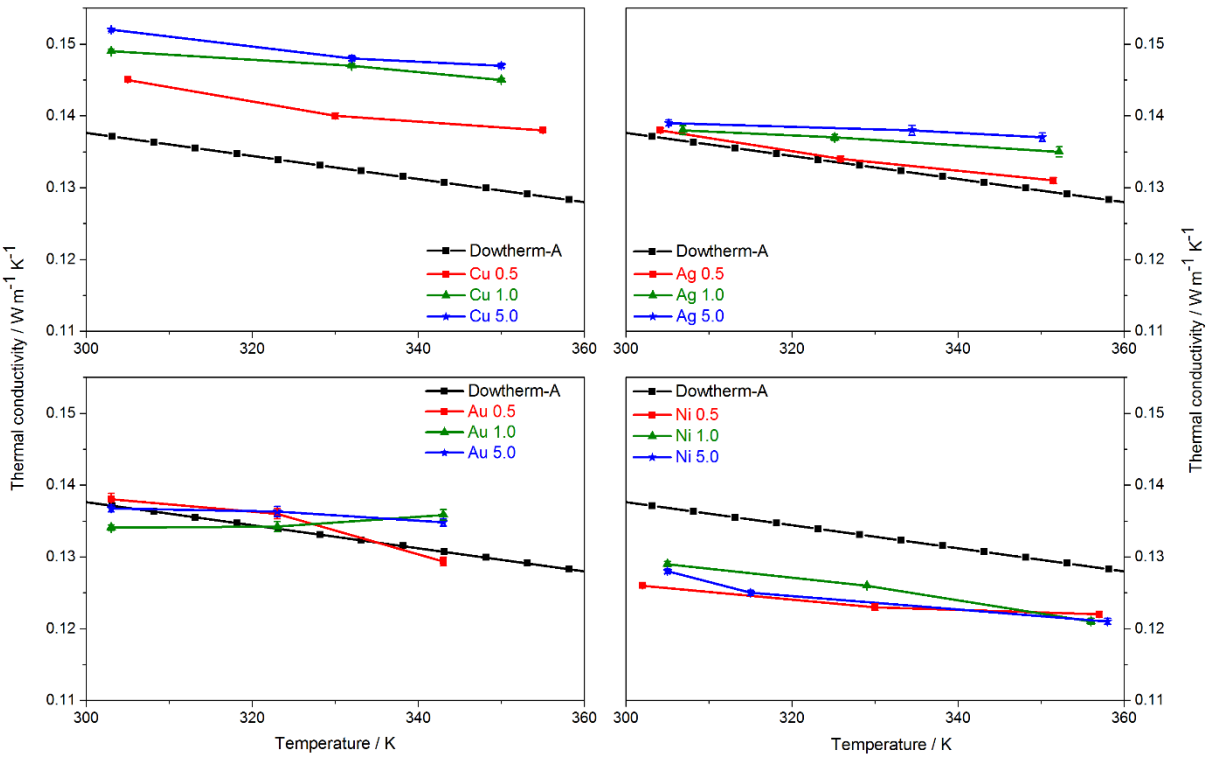

Figure 6.4.11. Thermal conductivity values obtained for the nanofluids based on copper, silver, gold and nickel nanoparticles [34].

Finally, to estimate the efficiency, the ratio of the heat transfer coefficient of the nanofluid and the base fluid was used, in accordance with the Dittus-Boelter equation (Equation 5.3.3). The results shown in Figure 6.4.12 pertain to the data obtained at room temperature. Only the nanofluids based on copper nanoparticles present a significant improvement (of approximately 11%) in their heat transfer coefficient, and thus their efficiency. The nanofluids based on silver nanoparticles present practically no improvement (not reaching 3%) at this temperature, although enhancements are found at high temperatures (see Figure 6.1.4). Meanwhile, the nanofluids based on gold and nickel nanoparticles do not improve the efficiency of the base fluid in any cases, and therefore they are not suitable for use as heat transfer fluids. Thus, according to the experimental results we can establish the following sequence:

$$h_{Cu-Nf} > h_{Ag-Nf} > h_{bf} > h_{Au-Nf} > h_{Ni-Nf}$$

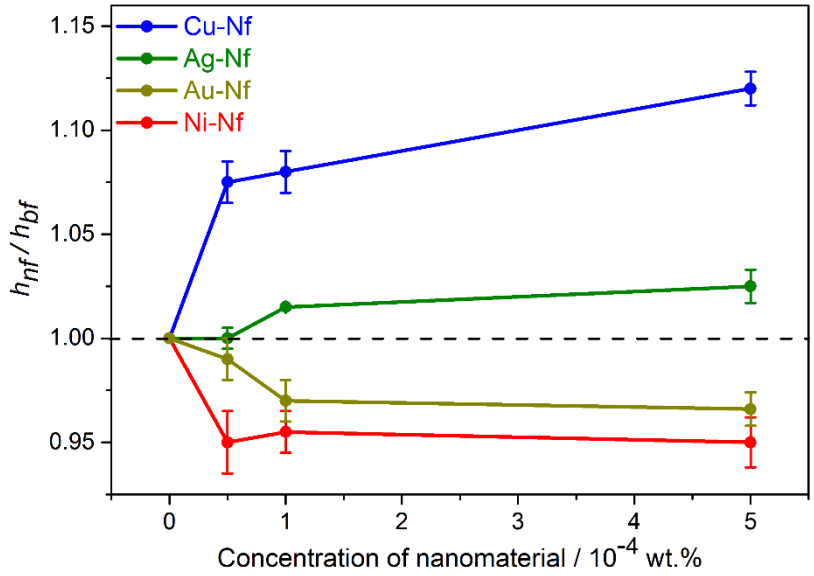

Figure 6.4.12. Values obtained for the ratio between the heat transfer coefficients of the nanofluids based on copper, silver, gold and nickel nanoparticles at room temperature [34].

6.4.4.3. Theoretical analysis: structural properties

For each nanofluid system, a study was conducted of the RDFs of the interactions of each metal with the diphenyl oxide and biphenyl molecules of the base fluid (see Figure 6.1.8 and Figure 6.4.6) [34]. Then, by analysing the RDFs and SDFs, we obtain a view of how the base fluid molecules are arranged around each metal, as shown by the image in Figure 6.4.13.

The literature reports that the directionality in the interaction between a metal and the oxygen from diphenyl oxide may benefit heat transfer processes [11]. If we take into account the diphenyl oxide/biphenyl ratio, Figure 6.4.13 shows that the arrangement of base fluid molecules around the copper atom is 3/1, and 2/1 in the case of silver. The cases of gold and silver may a priori seem to be the same; however, the presence of a diphenyl oxide molecule in an intermediate layer between the first and the second layers creates a more favourable situation for the gold (2/2) than for the nickel (1/1).

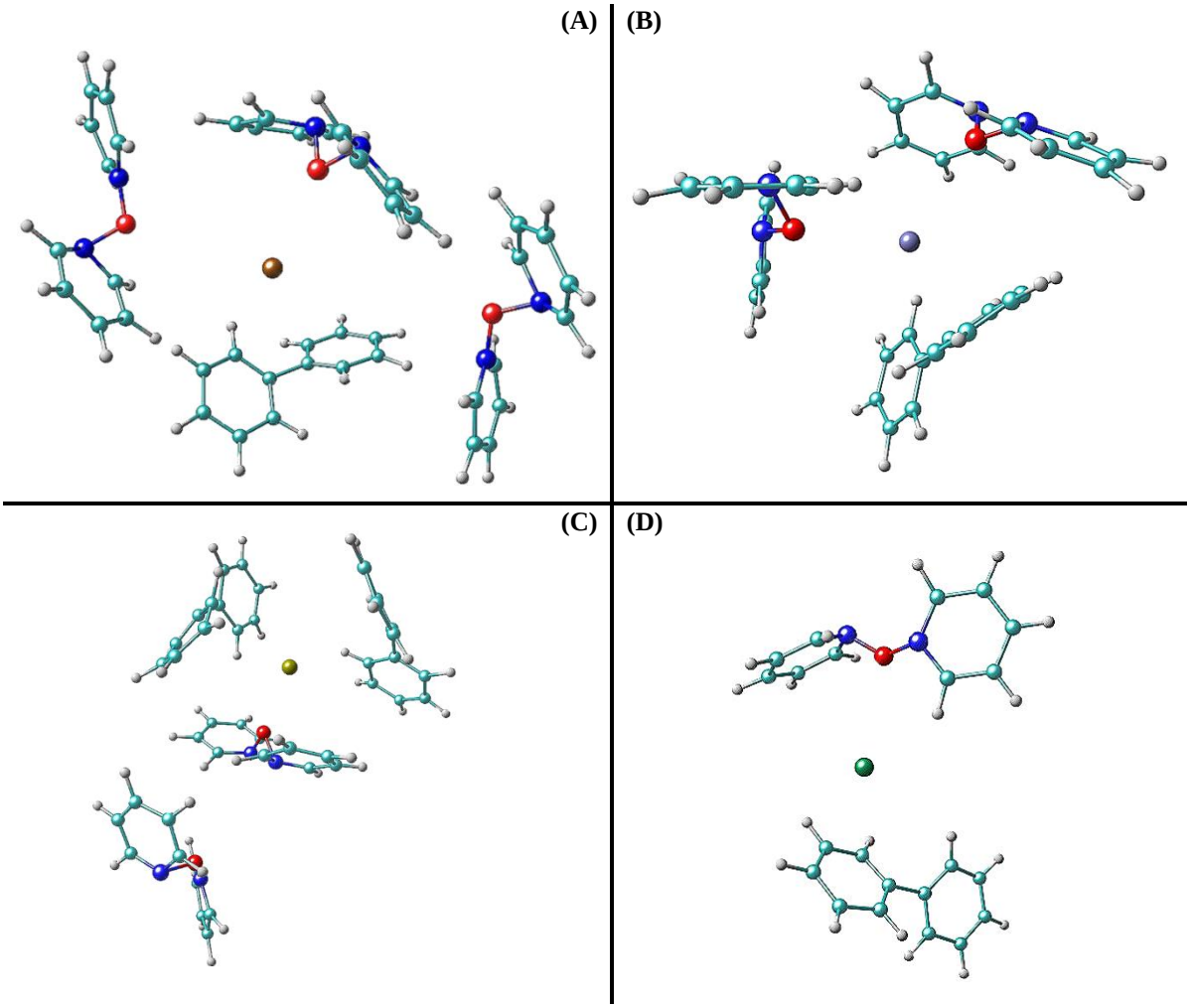

Figure 6.4.13. Three-dimensional image of the SDFs of the nanofluids based on (A) copper, (B) silver, (C) gold and (D) nickel nanoparticles at 300 K. The metal nanoparticles are shown by the colours brown (copper), rock blue (silver), gold (gold) and green (nickel), the oxygen from the diphenyl oxide in red, the carbon from the aromatic rings bonded directly to the oxygen in blue, and the remaining carbon atoms from the aromatic rings in turquoise, with the hydrogen atoms in grey [34].

Therefore, according to the theoretical study and taking into account this arrangement, the order of the nanofluid systems with regard to the most promising situation for heat transfer processes is:

$$Cu - Nf > Ag - Nf > Au - Nf > Ni - Nf$$

And this sequence is the same as the one obtained for the estimation of the heat transfer coefficient using the experimental results. Thus, both approaches (experimental and theoretical) used to analyse these nanofluid systems are in agreement in terms of the results reached. This result indicates that the nanofluid based on copper nanoparticles and prepared in

the eutectic mixture of diphenyl oxide and biphenyl is a promising system for use as a heat transfer fluid in concentrating solar power.

6.5. Ratio of the nanofluids prepared: analysis as heat transfer fluids

As explained in ***Section 6.1***, the nanofluids based on commercial silver nanoparticles were prepared following the two-step method, which is the simplest and most direct way of obtaining nanofluids. These nanofluids, despite presenting good stability, present an increase in efficiency with regard to heat transfer processes of approximately 5.3% at 350 K in the case of the nanofluid with the highest concentration of silver nanoparticles. This increase is negligible, limiting its possible application in the thermosolar industry.

Similar to the case of the silver-based nanofluids in terms of the preparation procedure, control parameters and the nanomaterial concentration, a study was conducted into gold-based nanofluids, prepared in this case by synthesizing the nanomaterial in an aqueous medium before dispersing it into the base fluid, as dictated by the two-step preparation method. However, these nanofluids did not present either the levels of stability or same improvements in efficiency as the previous nanofluids, resulting in them not being recommendable for use.

In addition, the nanofluids based on platinum nanoparticles were also prepared following the two-step method: the platinum nanoparticles were synthesized in an aqueous medium before being dispersed into the base fluid. In addition, this case involved the use of surfactants (DDA and ODT), which enhanced the stability of the nanomaterial, and sonication treatment to facilitate the dispersion of the nanomaterial into the base fluid. Thus, the nanofluids based on synthesized platinum nanoparticles presented a significant increase in thermal conductivity (at high temperatures, the nanofluid named Pt-Nf + DDA + U presented an improvement of 17%, while the Pt-Nf + DDA + U + ODT nanofluid showed an increase of approximately 37%), which entailed a substantial improvement in their efficiency: at 363 K, the Pt-Nf + DDA + U system showed an improvement of 5%, compared with approximately 20% for the Pt-Nf + DDA + U + ODT system. The conclusion can be drawn that the presence of ODT clearly has a beneficial impact on the heat transfer coefficient, and therefore the efficiency of the nanofluid with regard to the base fluid. Consequently, the use of these

nanofluids as heat transfer fluid in the thermosolar industry would appear to be of great interest.

However, when the gold nanoparticles are synthesized in the same preparation process as the nanofluid, in situ within the base fluid (one-step method) and the TOAB surfactant is also added, the nanofluids present optimal temporal stability and a dramatic increase in thermal conductivity: an improvement of approximately 70% at 363 K for the nanofluid with the highest effective volume fraction of gold nanoparticles. This has a direct effect on the efficiency of heat transfer processes, resulting from an improvement of up to 36% in the heat transfer coefficient, meaning that these nanofluids present the most positive properties for their application in CSP plants as heat transfer fluids.

This result is evidence that the one-step method, whereby the nanomaterial is synthesized in situ in the heart of the base fluid, is the best way to prepare nanofluids. Regarding the role of the surfactants, both the experimental results and those provided by the theoretical approach in the cases of the gold- and platinum-based nanofluids are confirmation that the presence of some kind of additive is necessary to improve the stability of the nanofluids. Their use results in a greater amount of nanomaterial in suspension, which consequently improves the efficiency of the heat transfer processes.

Thus, for the gold-based nanofluids prepared following the one-step method to be of greater interest for use as a heat exchange fluid, it was necessary to study ways of modifying their stability after successive heat cycles that are as similar as possible to those they would be subjected to in a CSP plant. The nanofluid with the highest volume concentration of gold nanoparticles was subjected to thermal cycles of up to 573 K, after which it was cooled to room temperature. After each cycle, the nanomaterial agglomeration processes were analysed using UV-Vis spectroscopy and the particle sizes by means of the DLS and TEM techniques.

Increases in temperature produce a higher number of collisions between the nanofluid particles, breaking up the agglomerates that may have formed at room temperature and generating an increase in the extinction coefficient as a result of the greater amount of nanomaterial in suspension (Figure 6.5.1.A). As a consequence, the size of the particles decreases due to the break-up of the agglomerates after each cycle and, although they increase slightly in size with cooling (Figure 6.5.1.B), this is positive in terms of both stability and the improvement in efficiency.

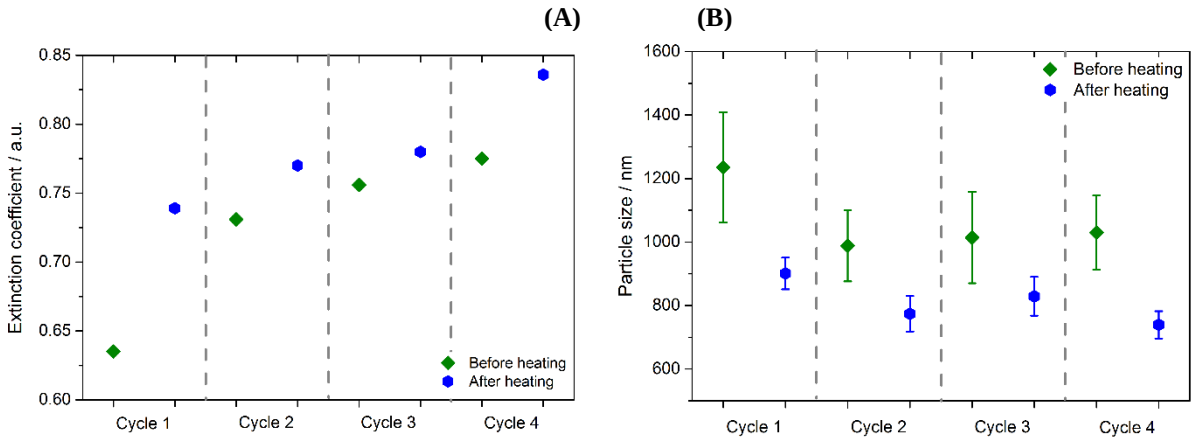

Figure 6.5.1. (A) Extinction coefficient at λ=520 nm and (B) particle size values of the gold-based nanofluid and the base fluid after each thermal cycle at 573 K.

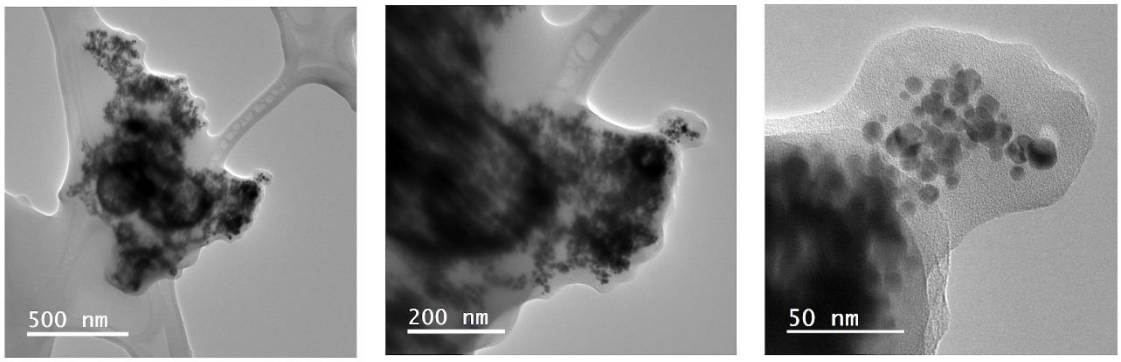

Figure 6.5.2. TEM images of the gold nanofluid obtained after the heat cycles.

The TEM images in Figure 6.5.2 show the presence of an agglomerate of gold nanoparticles of between 10 and 20 nm, with a distribution and spherical shape similar to those observed after the nanofluid preparation process (Figure 6.2.3.B), suggesting that the thermal cycles cause the nanomaterial to change shape, which is positive in terms of stability.

6.6. References

[1] Y. Hwang, J.K. Lee, C.H. Lee, Y.M. Jung, S.I. Cheong, C.G. Lee, B.C. Ku, S.P. Jang, Stability and thermal conductivity characteristics of nanofluids, Thermochimica Acta 455(1-2) (2007) 70-74.

[2] H. Chang, M.H. Tsai, Synthesis and characterization of ZnO nanoparticles having prism shape by a novel gas condensation process, Reviews on Advanced Materials Science 18 (2008) 734-743.

[3] M. Hadadian, S. Samiee, H. Ahmadzadeh, E.K. Goharshadi, Nanofluids for heat transfer enhancement – a review, Physical Chemistry Research 1 (2013) 1-33.

[4] W. Smith, T.R. Forester, DL POLY 2.0: A general-purpose parallel molecular dynamics simulation package, Journal of Molecular Graphics 14(3) (1996) 136-141.

[5] J.M. Martinez, L. Martinez, Packing optimization for automated generation of complex system's initial configurations for molecular dynamics and docking, Journal of Computational Chemistry 24(7) (2003) 819-825.

[6] M. Allen, D. Tildesley, Computer Simulation of Liquids (Clarendon Press, Oxford, 1987).

[7] F. Duarte, P. Bauer, A. Barrozo, B.A. Amrein, M. Purg, J. Aqvist, S.C.L. Kamerlin, Force field independent metal parameters using a nonbonded dummy model, Journal of Physical Chemistry B 118(16) (2014) 4351-4362.

[8] C. Campana, R.E. Miller, Physical properties of liquid hexane and derived polar by-products of hexane autoxidation: molecular dynamics calculations using the TraPPE-UA force field, Molecular Simulation 39(11) (2013) 882-894.

[9] T.T. Trinh, T.J.H. Vlugt, S. Kjelstrup, Thermal conductivity of carbon dioxide from non-equilibrium molecular dynamics: A systematic study of several common force fields, Journal of Chemical Physics 141(13) (2014).

[10] H.V.R. Annapureddy, S.K. Nune, R.K. Motkuri, B.P. McGrail, L.E.X. Dang, A combined experimental and computational study on the stability of nanofluids containing metal organic frameworks, Journal of Physical Chemistry B 119(29) (2015) 8992-8999.

[11] J. Philip, P.D. Shima, B. Raj, Enhancement of thermal conductivity in magnetite based nanofluid due to chainlike structures, Applied Physics Letters 91(20) (2007).

[12] B. Koslowski, H.G. Boyen, C. Wilderotter, G. Kastle, P. Ziemann, R. Wahrenberg, P. Oelhafen, Oxidation of preferentially (111)-oriented Au films in an oxygen plasma investigated by Scanning Tunneling Microscopy and Photoelectron Spectroscopy, Surface Science 475(1-3) (2001) 1-10.

[13] M.P. Casaletto, A. Longo, A. Martorana, A. Prestianni, A.M. Venezia, XPS study of supported gold catalysts: the role of Au^0 and Au^+ species as active sites, Surface and Interface Analysis 38(4) (2006) 215-218.

[14] S. Mondal, U. Rana, R.R. Bhattacharjee, S. Malik, One pot green synthesis of polyaniline coated gold nanorods and its applications, Rsc Advances 4(100) (2014) 57282-57289.

[15] N.K. Sadanandhan, S.J. Devaki, Gold nanoparticle patterned on PANI nanowire modified transducer for the simultaneous determination of neurotransmitters in presence of ascorbic acid and uric acid, J. Appl. Polym. Sci. 134(1) (2017) 9.

[16] H.J. Chen, D.S. Wen, Ultrasonic-aided fabrication of gold nanofluids, Nanoscale Research Letters 6 (2011).

[17] B. Wang, X. Wang, W. Lou, J. Hao, Ionic liquid-based stable nanofluids containing gold nanoparticles, Journal of colloid and interface science 362(1) (2011) 5-14.

[18] S.K. Das, S.U.S. Choi, W. Yu, T. Pradeep, Nanofluids: science and technology John Wiley & Sons (2007).

[19] D.R. Lide, CRC Handbook of Chemistry and Physics, 90th Edition, CRC Press, Boca Raton, Florida, USA (2009).

[20] H. Chen, S. Witharana, Y. Jin, Y. Ding, C. Kim, Predicting the thermal conductivity of nanofluids based on suspension rheology, Sri Lanka (2008).

[21] J.W. Goodwin, R.W. Hughes, Rheology for chemists: an introduction, Royal Society of Chemistry (2008).

[22] S. Witharana, H.S. Chen, Y.L. Ding, Stability of nanofluids in quiescent and shear flow fields, Nanoscale Research Letters 6 (2011).

[23] M. Chandrasekar, S. Suresh, T. Senthilkumar, Mechanisms proposed through experimental investigations on thermophysical properties and forced convective heat transfer characteristics of various nanofluids - A review, Renewable & Sustainable Energy Reviews 16(6) (2012) 3917-3938.

[24] N.S.S. Mousavi, S. Kumar, Effective heat capacity of ferrofluids - Analytical approach, International Journal of Thermal Sciences, 84 (2014) 267-274.

[25] D. Cabaleiro, C. Gracia-Fernandez, J.L. Legido, L. Lugo, Specific heat of metal oxide nanofluids at high concentrations for heat transfer, International Journal of Heat and Mass Transfer 88 (2015) 872-879.

[26] D. Shin, D. Banerjee, Enhanced specific heat capacity of nanomaterials synthesized by dispersing silica nanoparticles in eutectic mixtures, Journal of Heat Transfer-Transactions of the ASME 135(3) (2013).

[27] D. Shin, D. Banerjee, Specific heat of nanofluids synthesized by dispersing alumina nanoparticles in alkali salt eutectic, International Journal of Heat and Mass Transfer 74 (2014) 210-214.

[28] M. Neek-Amal, R. Asgari, M.R.R. Tabar, The formation of atomic nanoclusters on graphene sheets, Nanotechnology 20(13) (2009).

[29] A. Naumkin, A. Kraut-Vass, S. Gaarenstroom, Powell CJ NIST Standard Reference Database 20, Version, 2012.

[30] A. Toghan, M. Khodari, F. Steinbach, R. Imbihl, Microstructure of thin film platinum electrodes on yttrium stabilized zirconia prepared by sputter deposition, Thin Solid Films 519(22) (2011) 8139-8143.

[31] D.I. Potemkin, E.Y. Filatov, A.V. Zadesenets, V.A. Sobyanin, CO preferential oxidation on $Pt_{0.5}Co_{0.5}$ and Pt-CoOx model catalysts: Catalytic performance and operando XRD studies, Catalysis Communications 100 (2017) 232-236.

[32] R.W. Wyckoff, Crystal Structures. vol. 1, Interscience Publisher (1971).

[33] F. Šebesta, V. Sláma, J. Melcr, Z. Futera, J.V. Burda, Estimation of transition-metal empirical parameters for molecular mechanical force fields, Journal of Chemical Theory and Computation 12(8) (2016) 3681-3688.

[34] J. Navas, A. Sanchez-Coronilla, E.I. Martin, M. Teruel, J.J. Gallardo, T. Aguilar, R. Gomez-Villarejo, R. Alcantara, C. Fernandez-Lorenzo, J.C. Pinero, J. Martin-Calleja, On the enhancement of heat transfer fluid for concentrating solar power using Cu and Ni nanofluids: An experimental and molecular dynamics study, Nano Energy 27 (2016) 213-224.

Chapter 7

Conclusions

7. Conclusions

In the present Doctoral Thesis, four kinds of nanofluids have been prepared, experimentally characterized and studied from a theoretical perspective. All the nanofluids were prepared using the eutectic mixture of diphenyl oxide and biphenyl as the base fluid and can be described as follows: nanofluids based on commercial silver nanoparticles and prepared following the two-step method; nanofluids based on synthesized gold nanoparticles prepared following both the one-step and two-step methods; and nanofluids based on synthesized platinum nanoparticles following the two-step method. A study was also performed of how the surfactants participate in the stability of the nanofluids and in their possible increase in efficiency in heat transfer processes.

In those cases, in which the nanomaterial was synthesized, x-ray photoelectron spectroscopy (XPS), x-ray diffraction (XRD) and transmission electron microscopy (TEM) showed that the results obtained were those desired: gold and platinum nanoparticles with a mainly spherical morphology and with optimal size distribution.

The first experimental study of the nanofluids prepared is related with monitoring their physical and chemical stability over time. In light of the results obtained, the following conclusions can be drawn:

- The addition and dispersion of metal nanoparticles does not lead to physical and chemical modifications in the base fluid.
- The use of surfactants (TOAB in the case of nanofluids based on synthesized gold nanoparticles prepared following the one-step method; and ODT for the nanofluids based on platinum nanoparticles) keeps the size of the particles constant for a few days after the nanofluids are prepared, these nanofluids presenting high ζ potential values and a slight decrease in their extinction coefficient, measured by means of UV-Vis spectroscopy. This leads to the nanofluids presenting good stability over time and is evidence of the value of using surfactants.
- The application of ultrasound treatments significantly enhances the dispersion of the nanomaterial in the heart of the base fluid. The combination of ultrasound and surfactants improves the suspension of the nanomaterial and the stability of the nanofluids.

Regarding the characterization of the nanofluids prepared, addressing their thermal and rheological properties to estimate their degree of efficiency as heat transfer fluids, it can be concluded that:

- The addition of metal nanoparticles and additives such as phase transfer agents and surfactants leads to slight increases in the density values of the nanofluids with regard to the base fluid, and the more nanomaterial added, the greater these increases.
- The addition of the components mentioned above also generates changes in the viscosity values of the nanofluids with regard to the base fluid. An increase in the viscosity of the nanofluids is undesirable in terms of efficiency; however, no significant increases in this property we obtained. The nanofluids with the highest concentrations of silver and gold nanoparticles, both prepared following the two-step method, presented the highest increases in viscosity, approximately 4.5% and 4.3% respectively.
- In general, nanofluids show enhanced isobaric specific heat values in comparison with the base fluid. The improvement is more noticeable in the cases of the nanofluids with the highest concentration of silver nanomaterial, the improvement reaching 7.4%. The nanofluid with the intermediate volume fraction of gold nanoparticles, prepared following the one-step method, also presents an improvement in this property, in this case of 5.3%.
- Regarding the thermal conductivity values, the nanofluid with the highest concentration of silver nanomaterial shows an improvement of approximately 5.7% at 350 K; in turn, the active participation of the two surfactants and the ultrasound treatment results in an improvement in the thermal conductivity of the nanofluids based on synthesized platinum nanoparticles: at 363 K, the nanofluid with the two surfactants presents an increase of 37% while the nanofluid with just one surfactant shows an improvement of 17%. In any case, the highest increase in thermal conductivity was obtained for the nanofluid with the highest volume fraction of synthesized gold nanoparticles prepared following a one-step method; it presented a dramatic increase of up to 70% at 363 K.
- Finally, the nanofluids studied were seen to show improved heat transfer coefficients with regard to the base fluid: at high temperatures, the nanofluid with the highest concentration of commercial silver nanoparticles, the nanofluid prepared following the

one-step method with the highest volume fraction of synthesized gold nanoparticles, and the nanofluid based on synthesized platinum nanoparticles prepared with two surfactants and treated with ultrasound showed increases in efficiency of 5.3 %, 36% and 20%, respectively.

In light of the results obtained, considering the method of preparation, the nanofluids prepared following the one-step method presented greater stability than those prepared in two steps, proof of which is a comparison of the nanofluid systems based on synthesized gold nanoparticles. Furthermore, the combination of using surfactants with ultrasound treatment generates increased dispersion and suspension of the nanomaterial, as shown by the nanofluids based on synthesized platinum nanoparticles.

Regarding their thermal and rheological properties and their degree of efficiency, the gold nanofluids prepared using the one-step method show the largest increase in thermal conductivity and a significant increase in isobaric specific heat; in turn, incorporating nanomaterial and surfactant leads to an admissible increase in viscosity and there is, therefore, an interesting improvement in the heat transfer coefficient. Thus, this nanofluid system can be considered to be the one offering the biggest advantages for its future application as a heat transfer fluid in concentrating solar power plants. In addition, the study of these nanofluids after successive heat cycles reaching 573 K shows that degradation of the nanofluid does not occur after the increase in temperature and that the particle size remains constant, suggesting that its use in this technology is perfectly viable.

Finally, the theoretical study using Molecular Dynamics simulations of the nanofluid systems leads to the following conclusions:

- The calculation of thermal and transport properties shows a trend that is in line with the results obtained experimentally. The theoretical calculation of the isobaric specific heat of the gold and silver nanofluids and the base fluid follows the same sequence as that obtained in the experimental characterization: the nanofluids present higher isobaric specific heat values than the base fluid. In turn, by calculating the diffusion coefficient, thermal conductivity values were calculated for the same nanofluids, an identical trend being observed to that obtained experimentally: the gold and silver nanofluids present higher thermal conductivity values than the base fluid.

- The analysis of the radial and spatial distribution functions shows that nanofluids behave like dynamic systems, movement of the molecules of the base fluid and surfactant being produced with changes in temperature.
- The possible improvement in thermal properties and the degree of efficiency in heat transfer is associated with the number of diphenyl oxide molecules belonging to the base fluid arranged around the metallic nanoparticle, which generates order in the system. Thus, when the temperature of the system rises, the same tendency is observed in the case of the gold and platinum nanofluids: the number of diphenyl oxide molecules increases leading to enhanced thermal properties. The experimental comparison performed of the improvement in the degree of efficiency of copper and nickel nanofluids reported in the literature with the silver and gold nanofluids, all prepared following the two-step method, leads to a relationship between this improvement and the number of diphenyl oxide molecules around the metal; the more diphenyl oxide molecules, the higher the degree of improvement in the efficiency.
- The role played by the surfactants in the nanofluid systems studied is fundamental. In the case of the gold nanofluid system, the TOAB surfactant is arranged around the gold nanoparticle, preventing the agglomeration of the nanoparticles and making the system stable. As the temperature increases, there is a decrease in the number of surfactant molecules around the nanoparticle, thus allowing for the entry of diphenyl oxide molecules, which, as mentioned above, improves the heat transfer processes. In the case of the two surfactants used in the platinum-based nanofluids, the analysis of their structural properties shows that, even at high temperatures, closed structures are generated when there is only DDA in the system. However, the incorporation of the second surfactant (ODT) produces competition between the two, which causes or enables the diphenyl oxide molecules to move closer to the metal, generating an improvement in thermal properties.

Summing up these conclusions, we can show that nanofluids based on metal nanoparticles with optimal temporal stability have been designed and prepared. Their characterization, both experimental and theoretical, by means of Molecular Dynamics simulations, has shown that nanofluids were produced with dramatically improved thermal properties and heat transfer coefficient with regard to the base fluid, which was a thermal oil commonly used in concentrating solar power plants at high temperature. Therefore, the

nanofluids analysed show great potential for use as new heat transfer fluids in this kind of thermosolar plants, justifying the starting hypothesis and satisfactorily achieving the main objective of this Doctoral Thesis.

Recently, within the field of nanofluids, graphene- and carbon-based nanomaterials such as carbon nanotubes have burst onto the scene. They have generated a great deal of interest and the opportunity has arisen to combine a wide range of nanomaterials to produce nanofluids with enhanced thermal properties. In this section and following the line established in this Doctoral Thesis, it is worth pointing out that a possible task for the future is the preparation of nanofluids based on boron nitride nanotubes using the eutectic mixture of diphenyl oxide and biphenyl as the base fluid. Boron nitride nanotubes are generating a great deal of interest in all fields of science thanks to their promising thermal properties, such as high thermal conductivity values due to the preferential heat conduction in the dimensions of space defined by their morphology. Thus, boron nitride nanotubes are emerging as a promising nanomaterial for the preparation of nanofluids. Initial progress in this respect was made during a pre-doctoral stay in the Université Rennes I under the supervision of Dr. Patrice Estellé. During this stay, the characterization was performed of the rheological properties of nanofluids based on boron nitride nanotubes using Dowtherm-A as the base fluid and Triton X-100 as the surfactant. The results obtained suggest that it would be of great interest to continue researching this nanomaterial with the aim of producing stable nanofluids with improved performance for future application in the high temperature thermosolar industry.

List of figures

Figure 6.5.2. TEM images of the gold nanofluid obtained after the heat cycles. 158

List of tables

Annex 1

CSP in Spain

Province	Name	Company	Year	Technology
Alicante	Enerstar	Pleniuam/FCC/Mitsui	2013	PTC
Badajoz	La Risca	Acciona/Mitsubishi Corp.	2009	PTC
	Extresol-1	COBRA	2009	
	Extresol-2		2010	
	Extresol-3		2013	
	Casablanca			
	La Florida	Renovables SAMCA	2010	
	La Dehesa			
	Astexol II	Elecnor/Eiser/Aries	2012	
	Olivenza 1	Ibereolica	2012	
	Orellana	Acciona	2012	
	Termosol 1	Nextera-FPL	2012	
	Termosol 2		2013	
Cáceres	Majadas	Acciona/Mitsubishi Corp.	2010	PTC
	Solaben 2	Abengoa Solar	2012	
	Solaben 3			
	Solaben 1		2013	
	Solaben 6			
Cádiz	Valle-1	Torresol Energy	2011	PTC
	Valle-2			
Ciudad Real	Ibersol	Iberdrola	2009	PTC
	Manchasol-1	COBRA	2010	
	Manchasol-2		2011	
	ASTE 1A	Elecnor/Eiser/Aries	2012	
	ASTE 1B			
	Helios 1	Abengoa Solar	2012	
	Helios 2			

Córdoba	Palma del Río II	Acciona/Mitsubishi Corp.	2010	PTC
	Palma del Río I		2011	
	Solarcor 1	Abengoa Solar/JGC Corp.	2012	
	Solarcor 2			
	Guzmán	Pleniuam/FCC/Mitsui	2012	
	La Africana	Ortiz/TSK/Magtel	2012	
Granada	Andasol 1	RREEF/ANTIN/COBRA	2008	PTC
	Andasol 2		2009	
	Andasol 3	S.Millenium/Ferrostaal/Rhein.E	2011	
Lleida	Termosolar Borges	Abantia/Comsa EMTE	2012	PTC+Biomass
Murcia	Puerto Errado I	Novatec	2008	PTC
	Puerto Errado II		2012	Fresnel
Sevilla	PS 10	Abengoa Solar	2007	Solar Tower with saturated steam
	PS 20		2009	
	Solnova 1		2010	PTC
	Solnova 3			
	Solnova 4			
	Gemasolar	Torresol Energy	2010	Solar Tower with molten salts
	Lebrija 1	Valoriza/Siemens	2011	PTC
	Helioenergy 1	Abengoa Solar/EON	2011	
	Helioenergy 2		2012	
	Morón	Ibereolica	2012	
	Arenales	RREEF/STEAG/OHL	2013	

PTC: Parabolic trough collectors or concentrators.

Annex 2

Ag-based nanofluidic system to enhance heat transfer fluids for concentrating solar power: Nano-level insights

Applied Energy 194 (2017) 19–29

Contents lists available at ScienceDirect

Applied Energy

journal homepage: www.elsevier.com/locate/apenergy

Ag-based nanofluidic system to enhance heat transfer fluids for concentrating solar power: Nano-level insights

Roberto Gómez-Villarejo [a], Elisa I. Martín [b], Javier Navas [a,*], Antonio Sánchez-Coronilla [c,*], Teresa Aguilar [a], Juan Jesús Gallardo [a], Rodrigo Alcántara [a], Desiré De los Santos [a], Iván Carrillo-Berdugo [a], Concha Fernández-Lorenzo [a]

[a] Departamento de Química Física, Facultad de Ciencias, Universidad de Cádiz, E-11510 Puerto Real, Cádiz, Spain
[b] Departamento de Ingeniería Química, Facultad de Química, Universidad de Sevilla, E-41012 Sevilla, Spain
[c] Departamento de Química Física, Facultad de Farmacia, Universidad de Sevilla, E-41012 Sevilla, Spain

HIGHLIGHTS

- Ag-based nanofluid improves the heat transfer process in Concentrating Solar Power.
- The isobaric specific heat and thermal conductivity were improved.
- MD calculations were performed to reach a better understanding of the nanofluid.
- The arrangement of the base fluid around the nanoparticles is revealed from MD results.

GRAPHICAL ABSTRACT

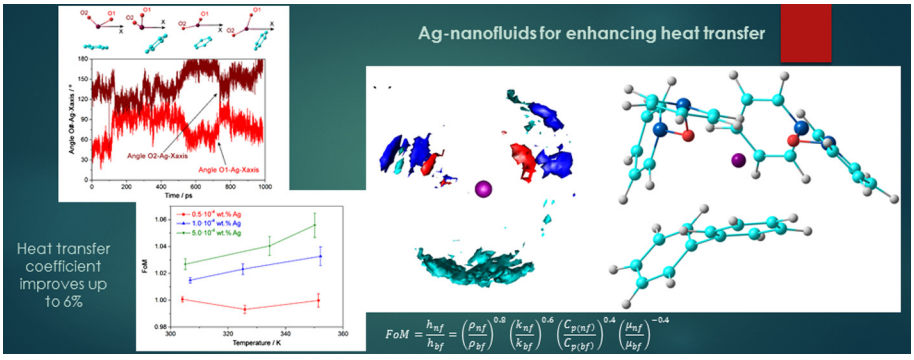

ARTICLE INFO

Article history:
Received 6 October 2016
Received in revised form 21 February 2017
Accepted 2 March 2017

Keywords:
Concentrating solar power
Nanofluidics
Heat transfer process
Molecular dynamics

ABSTRACT

One of the possible research lines for improving the Concentrated Solar Power (CSP) technology is the enhancement of the thermophysical properties of the Heat Transfer Fluids (HTF) used. This enhancement leads to reduce costs for producing electricity using this technology. So, this study presents the preparation of nanofluids in which Ag nanoparticles were added to a base fluid composed of a eutectic mixture of diphenyl oxide and biphenyl. The base fluid is a heat transfer fluid commonly used in concentrating solar power plants. The nanofluids were shown to have improved thermal properties, the heat transfer coefficient increasing by up to 6% compared with the base fluid. Thus, their use could lead to enhancements in the overall efficiency of CSP plants. Accordingly, nanofluids were prepared with varying nanoparticle concentrations and their properties were characterized, including their physical and chemical stability, viscosity, isobaric specific heat and thermal conductivity. In addition, molecular dynamic calculations were performed to reach a better understanding of the nanofluid system at a molecular level. The isobaric specific heat and thermal conductivity values followed the same experimental tendency. An analysis of the radial distribution functions (RDFs) and spatial distribution functions (SDFs) shows that there is a first layer of base fluid molecules around the metal in which the oxygen atoms play an important role. This first layer encourages the directionality of the movement in the heart of the nanofluid, which leads to enhanced thermal properties.

* Corresponding authors.
E-mail addresses: javier.navas@uca.es (J. Navas), antsancor@us.es (A. Sánchez-Coronilla).

http://dx.doi.org/10.1016/j.apenergy.2017.03.003
0306-2619/

1. Introduction

One of the challenges facing society today is the need to meet the growing demand for energy while minimalizing the environmental impact on the planet [1]. Solar energy is a renewable source of energy that can be used to a large extent to this end [2]. In fact, global solar radiation flux can reach values of *c.a.* 900–1000 W/m^2 on summer days [3]. In this regard, the conversion of solar energy into electricity is of interest, and concentrating solar power (CSP) systems play an important role as the thermal energy converters used in electric power generation [4,5]. To do this, high temperatures (400–500 °C or higher) must be reached and CSP systems achieve this by concentrating solar radiation on special receivers, converting solar radiation into thermal energy [2,6]. The different kinds of receivers are designed to capture the maximum amount of radiation reaching them, and they can be classified according to their focus geometry as point- and line-focus concentrators. Examples of focus concentrators are solar tower systems and parabolic dishes, while line-focus concentrators include linear Fresnel and parabolic-trough collectors (PTCs) [6,7]. Among these, PTCs are the systems generating the most commercial interest [4,7]. The PTC solar field can be integrated in a steam turbine plant either directly, through a direct steam generator (DSG technology), or indirectly, by heating thermal oil for generating steam in a heat exchanger (HTF technology) [6].

As a result, different lines of research are trying to improve the global efficiency of the plants by taking on board the new knowledge gained. One line of research is related with improving the thermal properties of the heat transfer fluid (HTF) used in CSP plants based on parabolic cylinder collectors. These collectors are responsible for storing and transporting the heat generated [7–9]. Improving the thermophysical properties of the fluids used is of particular interest for enhancing the heat transfer processes that take place in these plants as this should result in an increase in their overall efficiency. In this sense, the use of nanofluids has been shown to be an interesting option for enhancing the thermal properties of base fluids [7–14]. Nanofluids are colloidal suspensions of nanometric particles in a base fluid. Suspending nanoparticles in an HTF has been shown to improve such properties as its thermal conductivity, heat transfer coefficient or isobaric specific heat [10,11,15–18]. In turn, an increase in thermal conductivity is known to make HTFs more efficient. However, there are not many studies in the literature about nanofluids based on the HTFs used in CSP plants because most of the studies are based on fluids for low-temperature applications such as water or ethylene glycol. Furthermore, with the HTFs used in CSPs it is necessary to use low concentrations of nanoparticles. These analyses are not common in the literature since heat transfer may take place through particle-particle contact [19] and so high concentrations of nanoparticles are normally used. But the use of high concentrations also has the drawback of significant increases in viscosity.

Thus, the review of the literature reveals that CSP is one of the most interesting alternatives to conventional energy sources nowadays, and that there are advantages to be gained from the use nanofluids in CSP for high temperature applications. In this sense, the study of new nanofluids prepared with heat transfer fluids other than water or ethylene glycol is of great interest, particularly if these fluids are to have a future commercial use. The use of nanofluids within the heat transfer energy market is forecast to increase by over 2 billion dollars in the future, making it a promising field of study [20,21]. Thus, effective nanofluids that can optimise the use of a resources such as solar energy are candidates for consideration as value-added materials that produced a decreased impact on the environment [22,23].

This study has used nanofluids based on a eutectic mixture of biphenyl ($C_{12}H_{10}$) and diphenyl oxide ($C_{12}H_{10}O$), a HTF used in CSP plants. These fluids are not usually studied, unlike conventional ones, such as water or ethylene glycol (typical heat transfer fluids) [24]. Commercial Ag was used in three low concentrations. Metal nanoparticles were chosen because several studies have reported that they increase thermal conductivity [10,15,25–28], while low concentrations were used to prevent significant increases in viscosity. Also, several studies have reported improvements in some thermal properties of nanofluids with low concentrations of metal nanoparticles. For example, Patel et al. reported a significant increase in the effective thermal conductivity of nanofluids with Au, using toluene as the base fluid [26]. To determine how adding nanoparticles affected the base fluid, some properties of the nanofluids prepared were characterized, including their chemical and physical stability, density, viscosity, isobaric specific heat and thermal conductivity. In addition, to understand the molecular behaviour of this kind of nanofluid systems, molecular dynamics simulations were performed. The highest experimental concentration of Ag in the base fluid ($5.0 \cdot 10^{-4}$ wt.%) was chosen. The isobaric specific heat, diffusivity and thermal conductivity values were obtained and compared with the experimental values, a good correlation being observed. Finally, the structural properties of the nanofluid system were obtained by analysing their radial distribution functions (RDF) and spatial distribution functions (SDF). The analysis of the theoretical results showed that the interaction between the metal and base fluid plays an important role in enhancing the thermal properties of these systems. The synergy between the experimental and theoretical results in order to understand the thermal behaviour in the nanofluid system is a new approach for the study of this kind of systems. Clearly, this approach is original, and the explanation of the macroscopic properties based on nano-level interactions is a real advance in the analysis of nanofluids.

2. Material and methods

2.1. Experimental

The nanofluids used in this study were prepared following a two-step method [29]. The first step involves synthesizing the nanomaterial to be used and the second consists of dispersing the nanomaterial in the fluid base. The base fluid was a commercial heat transfer fluid composed of the eutectic mixture of biphenyl ($C_{12}H_{10}$, 26.5%) and diphenyl oxide ($C_{12}H_{10}O$, 73.5%), supplied by The Dow Chemical Company©, model Dowtherm A. These compounds have practically the same vapour pressures so the mixture can be treated as if it were a single compound. The nanomaterials used were commercial Ag nanoparticles (purity ≥99%, density 10,490 kg m^{-3} at 298 K, Sigma-Aldrich) with a particle size of <100 nm.

To prepare the nanofluids, an initial nanofluid was prepared with a mass concentration of 0.01 wt.%. They were prepared using 100 mL of the base fluid, the quantity of nanoparticles to obtain the stated concentration and the same amount of polyethylene glycol (PEG, MW: 400, Sigma-Aldrich). A sonication method was used to obtain the colloidal suspension of nanoparticles. It was applied for 3 h (∼50 W output power) using a Sonics Vibra Cell VCX 750 sonicator, controlling the evaporation of the base fluid. Aliquots were taken from the initial nanofluid to prepare nanofluids with a mass concentration of $0.5 \cdot 10^{-4}$, $1.0 \cdot 10^{-4}$ and $5.0 \cdot 10^{-4}$ wt.%, adding base fluid until reaching 100 mL. Next, the nanoparticles were dispersed again following the procedure described above.

Several properties of the nanofluids prepared were characterized. Their chemical stability was analysed using Vis-NIR

spectroscopy. The spectra were recorded in the visible range using an equipment assembled in our laboratory. The system was composed of a halogen lamp (model DH-2000-BAL) supplied by Ocean Optics© as the illumination source, and a USB2000+ spectrometer supplied by Ocean Optics©. The NIR absorption spectra were recorded using a system assembled in our laboratory. The system consisted of an incandescent lamp emitting as a black body at 2400 K as the illumination source; a DK240 monochromator, supplied by CVI-Spectral Products©; and a Ge photodiode as a detector. The physical stability of the nanofluids was also analysed by means of particle size measurements using the dynamic light scattering technique. The measurements were recorded for about a week. Several measurements were performed each day, each one in triplicate. A Malvern© zetasizer Nano Z system was used to perform these measurements.

To assess whether the base fluid was enhanced by adding the nanoparticles, the ratio of the heat transfer coefficients (h) was used as the Figure of Merit (*FoM*). This ratio was calculated using the Dittus-Boelter correlation, according to the equation

$$FoM = \frac{h_{nf}}{h_{bf}} = \left(\frac{\rho_{nf}}{\rho_{bf}}\right)^{0.8}\left(\frac{k_{nf}}{k_{bf}}\right)^{0.6}\left(\frac{C_{p(nf)}}{C_{p(bf)}}\right)^{0.4}\left(\frac{\mu_{nf}}{\mu_{bf}}\right)^{-0.4} \quad (1)$$

where h is the heat transfer coefficients, ρ is the density, k the thermal conductivity, C_p is the isobaric specific heat, and μ is the dynamic viscosity [15,30,31]. The subscripts *nf* and *bf* refer to the nanofluid and base fluid, respectively. Typically, when $h_{nf}/h_{bf} > 1$, the efficiency of the system is considered to improve. Thus, the properties required to obtain this *FoM* were measured. The density was measured using a pycnometer and a Select© thermal bath to control the temperature. The dynamic viscosity was also measured using Malvern© SV-10 viscometer. Both density and viscosity measurements were performed in triplicate. The isobaric specific heat measurements were performed using a Temperature Modulated Differential Scanning Calorimeter (TMDSC), supplied by TA Instruments©, model Q-20. A program was created to perform the measurements and can be summarized as: (i) the temperature was equilibrated at 341 K to remove contaminants and kept isothermal for 10 min; (ii) the samples were equilibrated at 301 K and then (iii) ramped to 391 K at 1 K/min; (iv) a modulation was programmed around the studied temperatures with an amplitude of ±1 K and a period of 120 s; (v) finally, cooling was performed at 1 K/min. The isobaric specific heat of the base fluid was measured to test the method used with regard to the values reported by the supplier. In addition, the thermal conductivity was measured using the Laser Flash technique (LFA 1600 equipment, supplied by Linseis Thermal Analysis©). This technique measures thermal diffusivity, which is the thermo-physical property that defines the speed of heat propagation by conduction during changes of temperature; the higher the thermal diffusivity, the faster the heat propagation. Thermal diffusivity (D) is related to thermal conductivity, isobaric specific heat and density, according to

$$k(T) = D(T)\cdot C_p(T)\cdot \rho(T) \quad (2)$$

All the thermal measurements were performed in triplicate.

2.2. Computational methods

2.2.1. Force field

The TraPPE-EH force field [32,33] was used to describe the intra- and intermolecular interactions of the HTF (diphenyl oxide/biphenyl blend). It treats aromatic rings and directly connected atoms as rigid entities. The phenyl rings were treated as rigid but were allowed to rotate with regards to each other around the C1—C1′ bond of the biphenyls. The parameters used in our simulations to describe the metal nanoparticle were adopted from the literature [34] and were adapted to a Non-Bonded Dummy Model [35,36] consisting of six particles, referred to as 'dummy atoms', placed around a central metal particle in an octahedral geometry. The geometry of the dummy complex itself is kept rigid by the imposition of large force constants on the metal-dummy bonds. However, as there are no bonds between the dummy complex and the surrounding ligands, overall rotation of the six-centre frame about the nucleus is possible, and no internal forces are associated with such rotation. Therefore, the coordination geometry is not constrained to the geometry of the dummy model used, but rather, the system is free to exchange ligands.

The TraPPE-EH force field and the Non-Bonded Dummy Model use Lennard-Jones (LJ) and Coulomb potentials to represent the non-bonded interactions

$$u(r_{ij}) = 4\varepsilon_{ij}\left[\left(\frac{\sigma_{ij}}{r_{ij}}\right)^{12} - \left(\frac{\sigma_{ij}}{r_{ij}}\right)^{6}\right] + \frac{q_i q_j}{4\pi\varepsilon_0 r_{ij}} \quad (3)$$

where r_{ij}, ε_{ij}, σ_{ij}, q_i, q_j, and ε_0 are the distance between interaction sites i and j, the LJ well depth, the LJ diameter, the partial charges on interaction sites i and j, and the permittivity of vacuum, respectively. The Lorentz-Berthelot combining rules were used to determine LJ parameters for unlike interactions.

2.2.2. Simulation details

Molecular dynamics simulations were performed with the DLPOLY code [37] in the canonical ensemble (NVT) using a Nose-Hoover thermostat and periodic boundary conditions. The initial configurations are constructed with the PACKMOL code [38] providing cubic boxes in which the length of the box sides are chosen to keep the density of the experimental HTF at 298 K (1056 kg m^{-3}). In each of the simulations performed, the box contained a metal nanoparticle, 117 diphenyl oxides and 48 biphenyls.

A time step of 0.5 fs was used and the simulation runs lasted for 1 ns. For the trajectory analysis, structures were saved every 100 time steps. A cut-off distance of 9 Å was applied in all cases and the Ewald sum methodology [39] applied to account for the electrostatic interactions.

Finally, structure images were obtained using ChemCraft 1.6 [40].

3. Results and discussion

3.1. Nanofluid stability

The analysis of the physical stability of these nanofluids is a great interest for the typical applications of these systems and for concentrating solar power. Hence, the physical stability of the nanofluids was studied by measuring their particle sizes using the dynamic light scattering (DLS) technique. These measurements were performed for approximately one week, taking several measurements each day and in triplicate. The results are shown in Fig. 1. The values recorded were higher than the nominal values of the nanoparticles because with the DLS technique the particle size obtained corresponds to the hydrodynamic diameter, which is determined as the sum of the particle diameter and the Debye length. The Debye length is the thickness of the diffuse layer, a layer of species between the surface of the nanoparticle and the slipping plane that moves with the nanoparticle within the base fluid. For this reason, the value obtained using this technique always overestimates the size of the particles [41]. In this sense, the particle size increased quickly but then remained practically stable, except in the case of the nanofluid with the highest concentration. This nanofluid started with a higher value at time zero and a steadier increase was produced. The final size recorded was proportional to the concentration of nanoparticles. Particles bigger

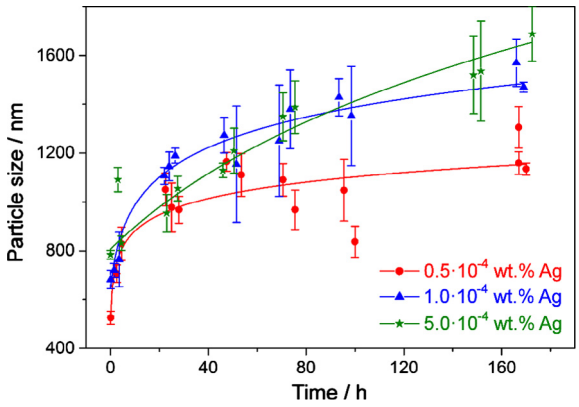

Fig. 1. Particle size measurements using the dynamic light scattering technique for the nanofluids prepared.

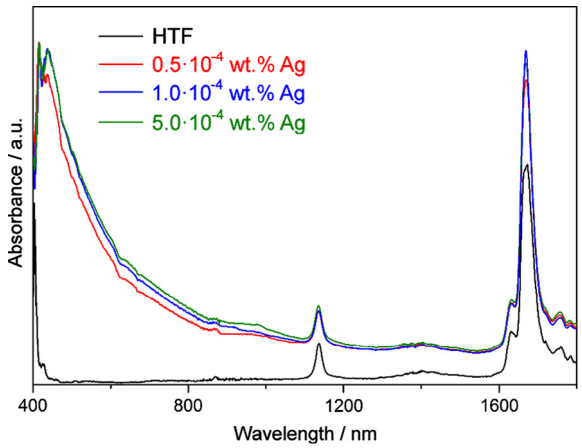

Fig. 2. Vis-NIR spectra for the nanofluids prepared and the base fluid.

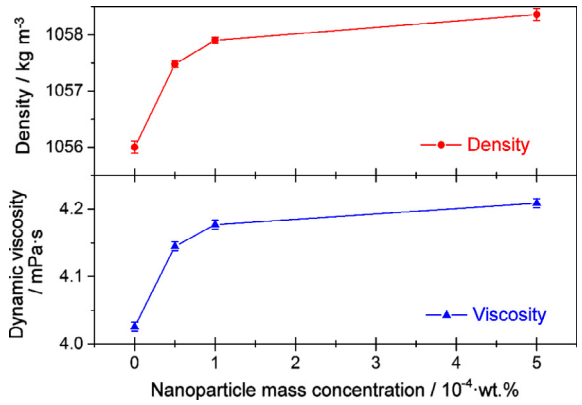

Fig. 3. Density and viscosity values obtained for nanofluids prepared versus nanoparticle mass concentration.

than those shown in Fig. 1 were not recorded for any of the nanofluids. Thus, these results suggest that the nanoparticles added to the base fluid agglomerate after a certain time and then remain stable, except for the fluid with the highest concentration, which the data obtained would suggest is less stable.

The chemical stability of the nanofluids was also analysed. That is, whether adding nanoparticles led to any chemical modification in the nanoparticles themselves or in the base fluid. To study this, Vis-NIR spectra were recorded in a range between 400 and 1800 nm and are shown in Fig. 2. It shows that the nanofluids have a wide band up to approximately 700 nm, which is typical for colloidal suspension systems, in which it is common for light to be dispersed when it strikes the nanoparticles. Furthermore, this process is known to mainly take place at short wavelengths [42,43]. All the spectra show two bands at approximately 1135 and 1679 nm. These bands are observed in the spectrum for the base fluid so they can be assigned to the fluid itself, the addition of nanoparticles having no effect. No other bands are observed in the spectra. So, this suggests that no chemical changes took place in the samples because the effects observed in the spectra of the nanofluids are assigned to the dispersion of the light due to the presence of the nanoparticles.

3.2. Density

The density of nanofluids has a significant effect on their thermal properties. For example, high density materials are known to make heat transfer more efficient [44]. Thus, the density of the nanofluids was measured in accordance with the nanoparticle mass concentration. The density of the base fluid used was also measured to check the goodness of the method followed. A deviation below 0.1% was found between the mean value (1056 kg m^{-3}) and the value provided by the supplier (1055.7 kg m^{-3}). Fig. 3 shows the density values obtained. It shows an increase in the density of up to 0.23% for the nanofluid with the highest nanoparticle content.

3.3. Viscosity

The viscosity values of a heat transfer fluid are vital data. In the case of nanofluids, incorporating nanoparticles into a fluid would be expected to lead to an increase in viscosity. This is counterproductive in terms of the efficiency of the processes involved as it can affect matters such as the pumping pressure or lead to possible drops in pressure. Therefore, it is necessary to control any possible increase in viscosity. Thus, the viscosity of the nanofluids prepared was measured to establish its influence on their heat transfer efficiency. The viscosity of the base fluid was also measured to check the goodness of the method followed. A deviation below 0.7% was found between the mean value ($4.03 \cdot 10^{-3}$ kg m^{-1} s^{-1}) and the value provided by the supplier ($4.06 \cdot 10^{-3}$ kg m^{-1} s^{-1}). Fig. 3 shows the viscosity values obtained for the nanofluids prepared. They show an increase of up to 4.5% for the fluid with the highest concentration of Ag. In turn, an increase in viscosity is observed with higher concentrations of nanoparticles, which is coherent with results reported in the literature [45]. This often occurs because a greater number of nanoparticles increases the interaction between them, producing an increase in viscosity [46]. It is worth noting that the increase in viscosity with the nanoparticle concentration is not linear, as the Einstein model predicts [47], especially for the nanofluids with low concentrations of nanoparticles. This behaviour implies some particle-particle interaction, which is not considered in the Einstein viscosity model.

3.4. Isobaric specific heat

The isobaric specific heat values for the nanofluids prepared were measured between approximately room temperature and 360 K to determine how the presence of Ag nanoparticles affected the base fluid. Fig. 4A shows that an increase in the isobaric specific heat was observed for all the nanofluids prepared. The increase was as high as 7.4% for the nanofluid with the highest concentration of nanoparticles. In this sense, it is known that the specific

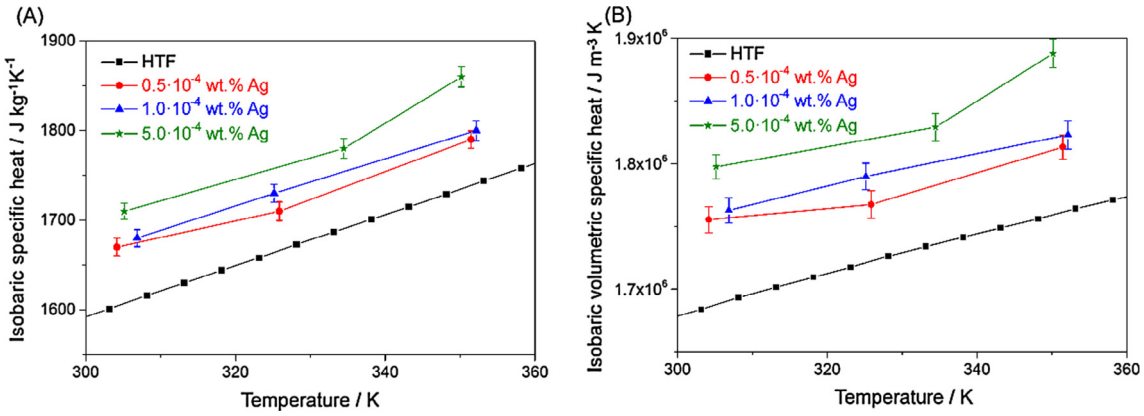

Fig. 4. (A) Isobaric specific heat values measured for the nanofluids versus temperature and nanoparticle mass concentration and (B) isobaric volumetric specific heat values calculated.

heat of solids is lower than that of liquids, so the specific heat of the nanofluids would be expected to be lower than that of the base fluid [44,48,49], and decreases expected at higher nanoparticle mass concentrations [44,45,50–54]. But set against this reasoning, cases have been reported where the opposite behaviour is observed. That is, the specific heat increases with the concentration of nanoparticles [51,52,55–57], as is the case here when adding Ag nanoparticles to the base fluid (see Fig. 4A). In this regard, Shin et al. [58,59] suggested that this behaviour is due to the formation of an internal structure within the nanofluid due to the interaction between the nanoparticles and the base fluid and depending on the nature of both, as we will demonstrate here by means of theoretical molecular dynamics calculations.

As reported previously, the heat transfer rate, $\dot{q}$, in a heat exchanger depends on the temperature gradient, ΔT, on the volumetric flux, $\dot{V}$, and on the isobaric volumetric specific heat, C_{pV}, according to $\dot{q} = \dot{V} C_{pV} \Delta T$. Thus, to determine how the incorporation of the Ag nanoparticles affected the heat transfer of the base fluid, the isobaric volumetric specific heat was determined from $C_{pV} = \rho C_p$, and measuring the density, ρ. Due to the low concentration of nanoparticles in the nanofluids, the evolution of the isobaric volumetric specific heat values was similar to that of the isobaric specific heat values, as Fig. 4B shows. There was an increase of 7.6% for the nanofluid with the highest concentration of nanoparticles.

3.5. Thermal conductivity

The thermal conductivity of the nanofluids was measured at different temperatures using the Laser Flash technique, which measures thermal diffusivity and estimates the conductivity from the density and isobaric specific heat values, as is shown above (see Eq. (2)). The thermal conductivity of the base fluid was also measured to check the goodness of the method used. A difference of round 1.5% was found between the base fluid value at room temperature (0.136 W m^{-1} K^{-1}) and the value given by the supplier (0.138 W m^{-1} K^{-1}). The thermal conductivity values obtained for the nanofluids are shown in Fig. 5A together with the data given by the supplier for the base fluid. It shows a clear increase in the thermal conductivity of the nanofluids. It is also possible to observe that the base fluid and nanofluids followed a similar tendency in that the thermal conductivity values decreased as the temperature increased, possibly due to the low concentrations of nanoparticles used. In addition, the thermal conductivity values increased with the concentration of nanoparticles, which is coherent with other studies in the literature [60].

To perform a quantitative assessment of the increase in the thermal conductivity of the nanofluids, the thermal conductivity enhancement was determined (*TCE*, %) according to the equation, $TCE\ (\%) = 100[(k_{nf} - k_{bf})/k_{bf}]$, where k is the thermal conductivity and the sub-indexes *nf* and *bf* refer to the nanofluid and the base fluid. The values used for the base fluid were calculated at the exact temperature at which the thermal conductivity of the nanofluids was calculated using the values supplied by the supplier. Fig. 5B shows the values obtained for the enhancement of the thermal conductivity. The enhancement is slight for the nanofluids with a low concentration of nanoparticles, but much greater as the concentration increases, and also greater at higher temperatures. The enhancement in the thermal conductivity reached around 6.0% in the case of the nanofluids with a nanoparticle mass concentration of $5.0 \cdot 10^{-4}$ wt.%. In this case, the increase in the thermal conductivity values of the Ag nanofluids has two possible explanations. The first is the high thermal conductivity of the silver nanoparticles compared with other metals (k = 429 W m^{-1} K^{-1} at 298.15 K) [61]. The second is the presence of the nanoparticles themselves since, as reported previously, this is an even more important factor than the thermal conductivity of the nanoparticles [10,62], if there are interactions between the particles. These interactions were also observed by means of the viscosity values reported, which do not follow a linear tendency with the concentration of nanoparticles, which suggests that there are interactions between particles. It is also possible to relate the values measured with interactions between the fluid base and the nanoparticles, as will be shown below using theoretical molecular dynamics calculations.

3.6. Performance of the nanofluids

To analyse the possible enhanced efficiency of the nanofluids, the Dittus-Boelter equation was used as the *Figure of Merit*, as stated above. This *FoM* offers the ratio between the heat transfer coefficient of the nanofluid and the base fluid (h_{nf}/h_{bf}), as is shown in Eq. (1). Values for this ratio above 1 imply enhanced efficiency of the nanofluid compared with the base fluid. Thus, the *FoM* was calculated for the nanofluids at the temperatures at which the isobaric specific heat and the thermal conductivity were measured. The density and viscosity values were estimated from the evolution with temperature of the values reported by the supplier and considering the values measured for the nanofluids at around room temperature. Fig. 6 shows the values obtained for the nanofluids. It shows that the efficiency of the nanofluids improved in nearly all cases, with the exception of the lowest concentration which, shows values around 1 and a different tendency to the others. The nanofluid with the highest nanoparticle concentration showed the

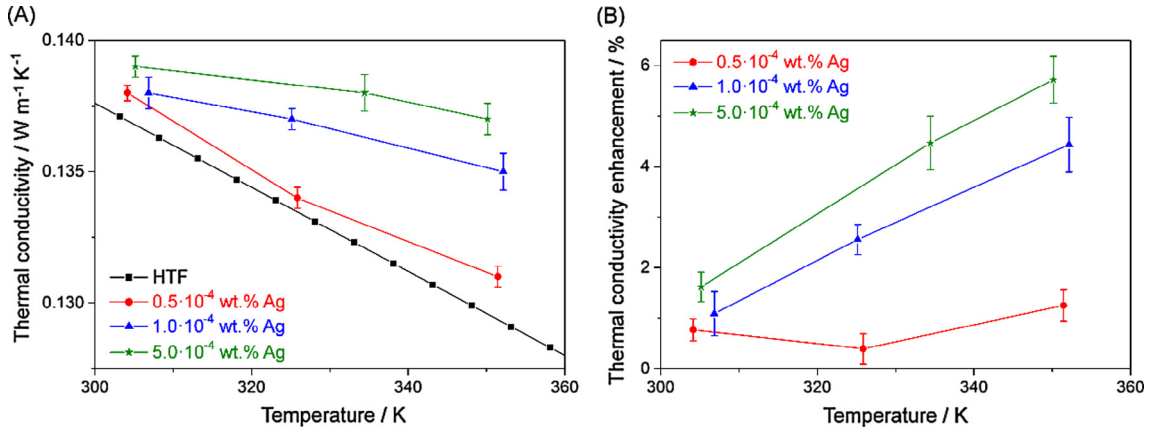

Fig. 5. (A) Thermal conductivity values measured and (B) thermal conductivity enhancement for the nanofluids versus temperature and nanoparticle mass concentration.

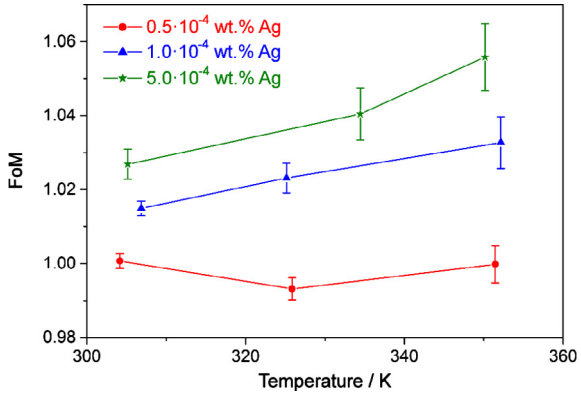

Fig. 6. Values of the ratio of the heat transfer coefficients (*FoM*) of the nanofluids.

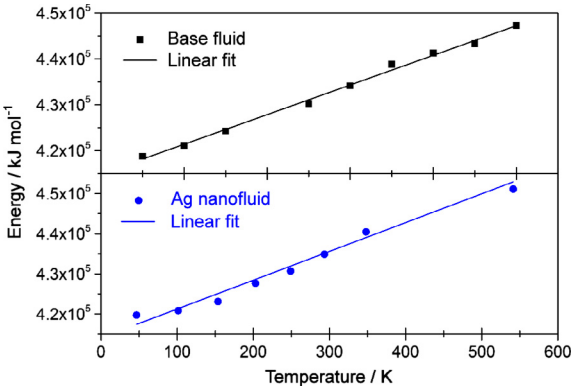

Fig. 7. Plot of the energy *vs* temperature for the base fluid (black) and Ag-nanofluid (blue). (For interpretation of the references to colour in this figure legend, the reader is referred to the web version of this article.)

greatest enhancement, up to 6%, although it was also the least stable. The efficiency of the intermediate nanofluid improved by over 3%. The efficiency increased as the temperature rose until around 350 K, and this nanofluid also had good stability, as was shown above.

Thus, the nanofluids prepared can be tested in a CSP system for their use in this kind of solar energy technology. To reduce the cost of producing electricity with CSP technology is one known strategy to increase the overall efficiency of the plants. One way of achieving this is to improve the thermophysical properties of the HTFs used in the solar field. Our nanofluids improve the thermophysical properties of the base fluid, such as its thermal conductivity, isobaric specific heat, and heat transfer process, leading to an enhanced efficiency and a reduction in the costs of the CSP plants. Therefore, testing the nanofluids for use in CSP plants would seem very worthwhile.

3.7. Theoretical analysis: isobaric specific heat

Based on the results of the experimental characterization, a theoretical study of the Ag-nanofluid system and an analysis of its behaviour with regard to the base fluid were considered of great interest. Thus, molecular dynamics calculations were performed with the experimental nanoparticle mass concentration of $5.0 \cdot 10^{-4}$ wt.% for Ag. This concentration was chosen to ensure the representativeness of the nanoparticle in the nanofluid taking into account the cost of the computation.

The molecular dynamics calculations were performed in a temperature range of *c.a.* 50–500 K for the calculation of the isobaric specific heat. The plot of the total energy versus temperature (Fig. 7) shows a linear tendency for both the base fluid and the Ag-nanofluid system. The isobaric specific heat values deduced from the slopes of these plots were $2.15 \cdot 10^3$ and $1.94 \cdot 10^3$ J kg^{-1} K^{-1} for the Ag-nanofluid and the base fluid, respectively. These values are slightly higher than those obtained experimentally but follow the same qualitative tendency, $C_{p(\text{Ag-nanofluid})} > C_{p(\text{base fluid})}$. Comparing the isobaric specific heat values obtained would suggest that the Ag-nanofluid system is more likely to produce efficient heat transfer processes than the base fluid, possibly because the structural reorganization of the base fluid molecules around the Ag plays an important role, as will be discussed below.

3.8. Theoretical analysis: diffusivity and thermal conductivity

The translational diffusion coefficients of the base fluid and Ag-nanofluid were computed according to the Einstein relation by calculating the mean square displacement (MSD). This translational diffusion coefficient is the thermal diffusivity used typically in experimental studies, as is discussed above. Thus, the diffusion coefficients are obtained by the following equation:

$$D_i = \lim_{t\to\infty} \frac{\langle |\vec{r}_i(t) - \vec{r}_i(0)|^2 \rangle}{6t} \tag{4}$$

where $\langle |\vec{r}_i(t) - \vec{r}_i(0)|^2 \rangle$ is the mean square displacement (MSD).

The plot of the mean square displacement (MSD) versus time for the base fluid and the Ag-nanofluid at 300 K is shown in Fig. 8, as well as their components in the x, y, and z directions. After

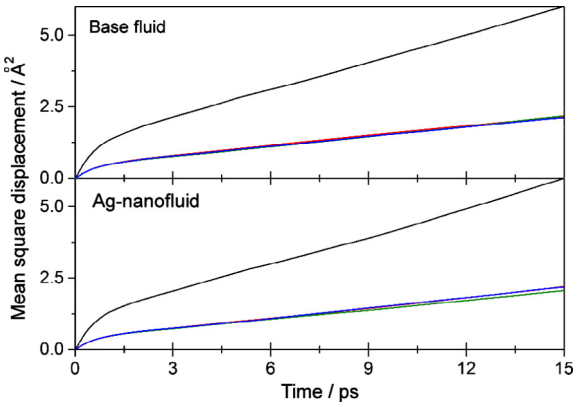

Fig. 8. Plot of the mean square displacement (MSD) *vs* time for the system modelled. The MSD components in the x, y and z directions are shown in red, green and blue, respectively. (For interpretation of the references to colour in this figure legend, the reader is referred to the web version of this article.)

approximately 3 ps the mean square displacement varies in line with time for the systems. The diffusion coefficients are obtained from the slope of this plot and by applying Eq. (4). The thermal conductivity was obtained using Eq. (2) from the values for the diffusion coefficient, the density and the isobaric specific heat, obtaining 0.125 and 0.107 W m^{-1} K^{-1} for the Ag-nanofluid and the base fluid, respectively. These thermal conductivity values are lower than those obtained experimentally (see Fig. 5), an underestimation that has been reported before in studies involving TraPPE force fields in molecular dynamics simulations [63,64]. Therefore, qualitatively, our thermal conductivity results can be considered to follow the same experimental tendency $k_{(\text{Ag-nanofluid})} > k_{\text{Base fluid}}$, confirming again that this thermal property is enhanced by the presence of silver.

Thus, both the thermal conductivity and the isobaric specific heat values obtained by classical molecular dynamics follow the same tendency and coincide with the experimental results, which validates the theoretical method proposed.

3.9. Theoretical analysis: structural properties

To gain a better understanding of the nanofluid system at a molecular level, the radial distribution function (RDF) and spatial distribution function (SDF) were analysed. A detailed analysis of these functions makes it possible to identify and discuss the interaction sites between the Ag and the base fluid.

The analysis of the RDFs of the Ag—O, Ag—C and Ag—H pairs showed very little variation with regard to temperature. Fig. 9A is shown as an example of the RDFs for the Ag—O pair in the temperature range from 100 to 500 K. For greater clarity, the inset in this figure shows the superimposed RDFs at the different temperatures and in all of them the peak is centred at approximately 2.2 Å. There are no significant modifications with temperature so for the discussion of RDFs and SDFs, the trajectories corresponding to the nanofluid systems at 300 K were chosen.

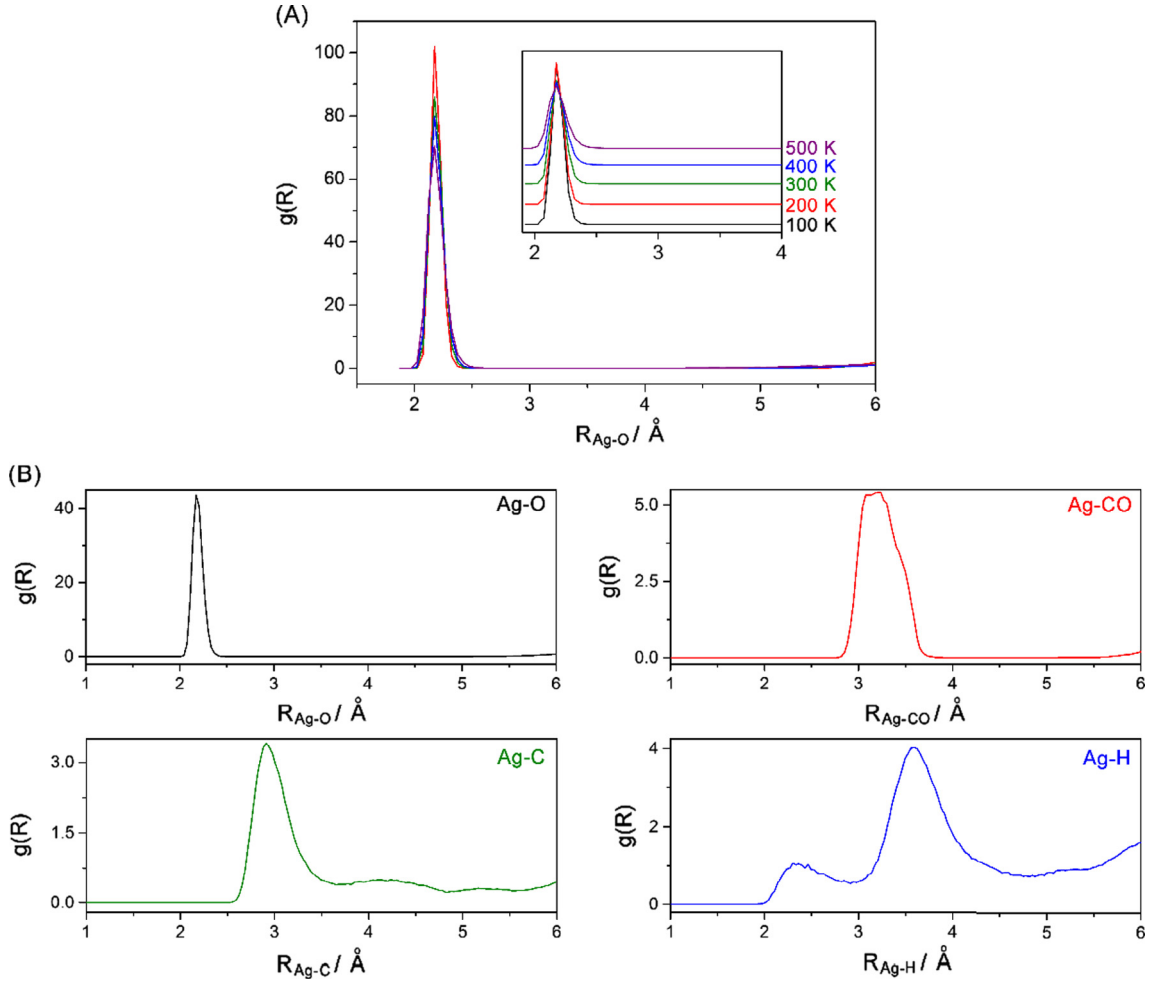

Fig. 9. (A) RDF for Ag—O in the range 100–500 K. (B) RDFs between the Ag—O, Ag—CO, Ag—C and Ag—H pairs in the Ag-nanofluid system.

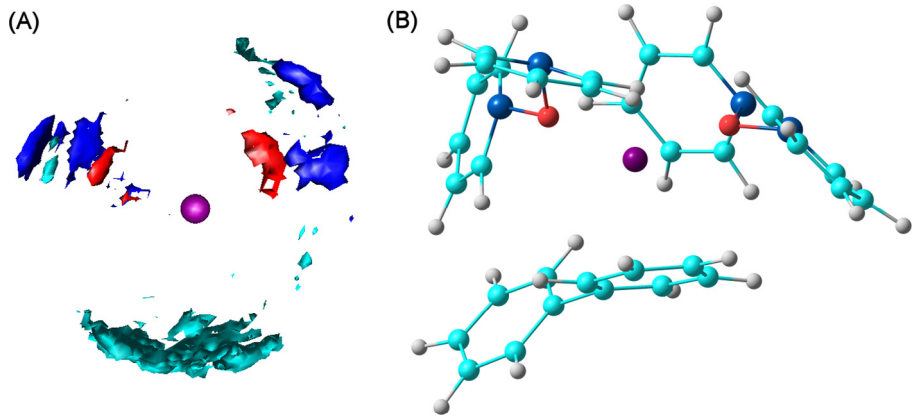

Fig. 10. (A) SDFs from the Ag-nanofluid. (B) Structure around the Ag in the nanofluid system.

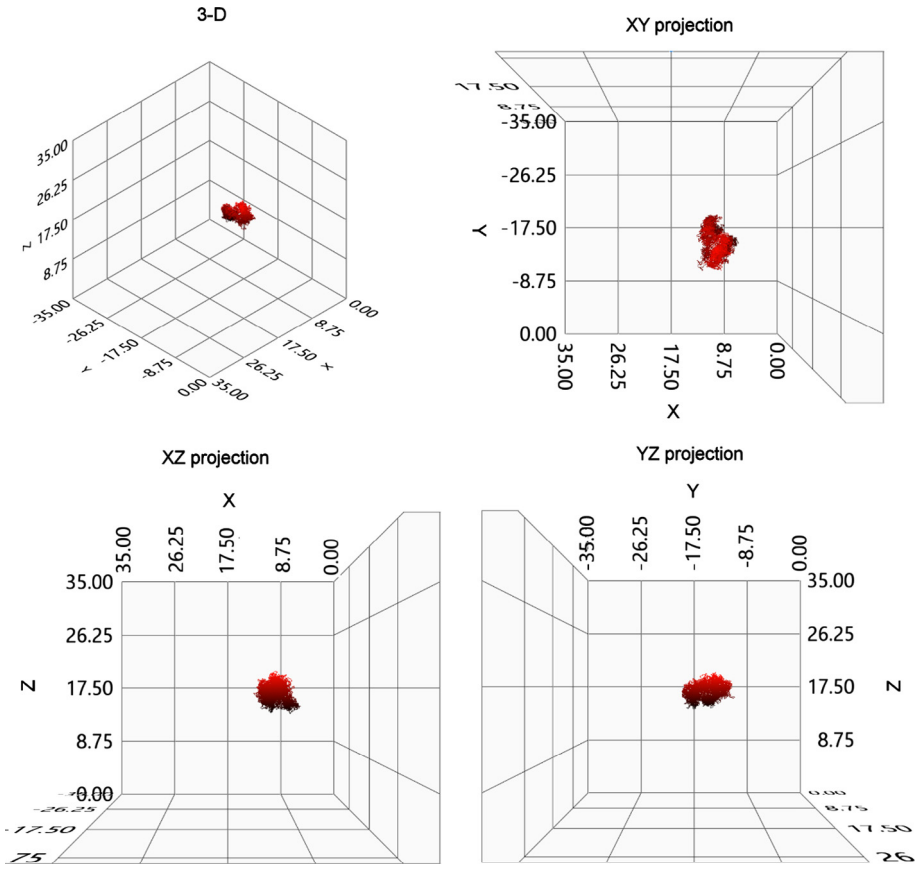

Fig. 11. Trajectory in three dimensions and the projection of the trajectory to XY, YZ, and XZ planes.

For the Ag-nanofluid system, the analysis of the RDF of the Ag—O pair shows an intense and well-defined peak centred around 2.2 Å (Fig. 9B) due to two O atoms belonging to two diphenyl oxide molecules. This intense peaks indicates strong orientation binding [65]. Regarding the C atoms, two types of C can be distinguished. The C atoms linked to the O atoms of the diphenyl oxide (CO) and the ring carbons (C), from the diphenyl oxide and the biphenyl. In this regard, for the Ag—CO pair (Fig. 9B), a fairly wide, intense peak is observed at 3.2 Å that integrates to 4 C atoms; that is, two C atoms for each diphenyl oxide. On the other hand, for the Ag—C pair (Fig. 9B), the RDF shows a more intense peak and two less intense shoulders centred at 2.9, 4.2 and 5.2 Å that correspond with 8, 16 and 8 C atoms, respectively. Regarding the analysis of the RDF of the Ag—H (Fig. 9B), two peaks and a shoulder appear centred at 2.4, 3.8 and 5.4 Å, respectively. The first low intensity peak at 2.4 Å corresponds to one H atom and the remaining peaks to 31 atoms, so these peaks correspond to 32 ring H atoms. It is noteworthy that the integration is calculated until 6 Å. At distances beyond 6 Å, wide low-intensity peaks appear so the discussion was based on the first layer of base fluid molecules around the metal.

By analysing the SDF it is possible to determine how the base fluid molecules are arranged around the Ag. Fig. 10A shows the SDF for the Ag-nanofluid system in a radius of 4 Å with the Ag in the centre (purple colour[1]). This range was chosen to enable a

[1] For interpretation of color in Fig. 10, the reader is referred to the web version of this article.

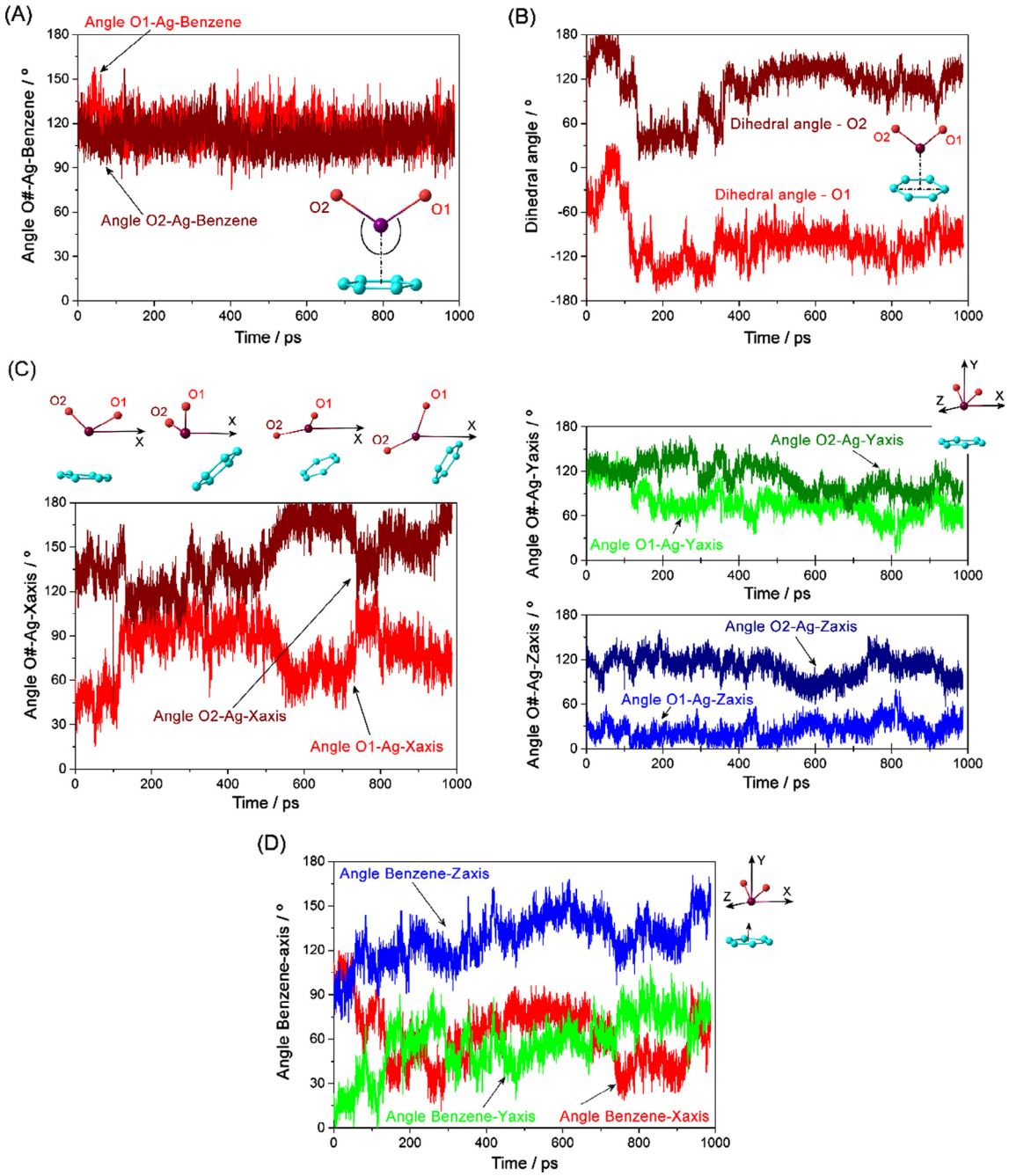

Fig. 12. (A) Angle formed by each oxygen with the metal and the centre of the ring. (B) Dihedral angle formed by each oxygen with the metal, the centre of the ring of biphenyl, and one of their C atoms. (C) Angle formed by each oxygen with regard to the metal and the x, y and z axes. (D) Angle formed between the benzene ring of the biphenyl and the x, y and z axes along its trajectory.

greater clarity of the image of the first layer around the Ag. The red coloured spatial distribution is assigned to O atoms, blue corresponds to the C atoms linked to the O atoms of the diphenyl oxide (CO), and the sky-blue SDFs correspond to the ring C atoms from the benzene rings of diphenyl oxide and biphenyl. The H atoms were not included in the analysis of the SDF to keep the image clear. Fig. 10A shows that the two O atoms (red) from the diphenyl oxide molecules are oriented towards the Ag in the centre. In this sense, it follows that the first layer of base fluid molecules around the metal is composed of two diphenyl oxide molecules, with the oxygen atoms oriented towards the Ag, which is on a benzene ring of the biphenyl (Fig. 10B and multimedia Video 1). It may be considered that this two-molecule layer of diphenyl oxide and a ring of biphenyl wrap around the Ag forming a cluster that provides stability to the nanofluid system (see multimedia Video 1). It would therefore seem reasonable to think that the arrangement of the first layer of base fluid molecules around the metal is responsible for the enhanced thermal properties of the nanofluid. This structural arrangement (Fig. 10B) must generate a directionality of movement that involves effective heat transport, leading to increased thermal conductivity compared with the base fluid [66], as was shown experimentally.

3.10. Theoretical analysis: trajectory and internal movements

To test the hypothesis of the directionality of movement, the trajectory of the Ag in the nanofluid system was plotted. Fig. 11 shows the trajectory in three dimensions and the projection of

the trajectory to XY, YZ, and XZ planes. It is possible to observe that the movement is slightly longer in the Y axis than in the Z and X axes.

Similarly, this trajectory is associated with an internal movement of the particles of this first-layer cluster, which is analysed below. This analysis focuses on the rotation of the O atoms of the two diphenyl oxide molecules with regard to the metal, and on the torsion with regard to the benzene ring of the biphenyl molecule. To study the rotation with regard to the metal, Fig. 12A shows the histogram of the angle formed by each oxygen (O1 and O2 in the inset in Fig. 12A) with the metal and the centre of the ring. It shows that the angles fluctuate around the mean value along the whole trajectory, in a range between 120–150° for O1 and 110–130° for O2, which would describe a slight fluttering movement of the O atoms (see inset Fig. 12A). Regarding the torsion of the O atoms with respect to the benzene ring, Fig. 12B shows the histogram of the dihedral angle formed by each O atom with the metal, the centre of the ring of biphenyl, and one of their C atoms (inset Fig. 12B). As this figure shows, the angles of rotation of the O atom around the metal range between 50 and 150° for O1 and −50 and 150° for O2. A comparison of the range of rotation and torsion, *c.a.* 20° and 100° respectively, indicates that rotation of the O atoms around the metal is more restricted in the direction of the benzene ring. The fact that the O atoms cannot displace the benzene ring in its rotational movement around the metal reveals the stability of this first-layer cluster. Finally, Fig. 12C shows the histogram of the angle formed by each O atom with regard to the metal and the x, y and z axes of the box. It shows that on the x axis (Fig. 12C) bigger jumps are produced in the angle of rotation of both O atoms as a consequence of the more limited movement of the first-layer cluster through the nanofluid system in this spatial direction. Focussing on O1, the O—Ag-(x-axis) angle is seen to alternate between 60 and 100°, while the O2, in a complementary manner, varies between 140 and 120° at the beginning of the trajectory and alternates with 170°. However, the jumps in the angle of rotation with regard to the y and z axes are more attenuated. On the y axis (Fig. 12B), the O—Ag-(y-axis) angles vary between *c.a.* 120 until 60° for the O1, while for the O2 the variation is from *c.a.* 130 to 100°. Regarding the z axis (Fig. 12C), the O—Ag-(z-axis) angle for the O1 during most of the trajectory remains around 30°, while for O2 it is 110° decreasing to 70° in the 500–700 ps interval.

Finally, an analysis was performed of the angle formed between the benzene ring of the biphenyl and the x, y and z axes along its trajectory (Fig. 12D). The aperture of the angles with the y and z axes increases constantly along the trajectory, reaching nearly 70° in both cases. However, besides not showing a constant aperture along the trajectory, the angle with regard to the x axis only changes *c.a.* 20°. This result suggests that during the trajectory, the benzene ring should swing around the metal and its range of movement must be limited by the presence of two diphenyl oxide molecules. Consequently, this result is consistent with the discussion above and highlights the stability of the first-layer cluster.

Two multimedia files have been included in the Supplementary Material to help clarify all the internal movements of the first-layer cluster and its movement with regard to the coordinates system of the box.

The results in Figs. 11 and 12 and the structural results of the SDFs and RDFs make it possible to establish that the first layer encourages the directionality of the movement in the heart of the nanofluid. This movement, preferably in one direction, can favour effective heat transport and an increase in the thermal conductivity of the nanofluid with regard to the base fluid. To our knowledge, this is the first time that an analysis of this kind has been performed on this type of nanofluid systems.

4. Conclusions

In this study, nanofluids based on a heat transfer fluid composed of a eutectic mixture of diphenyl oxide and biphenyl and Ag nanoparticles were prepared. These systems were analysed from both theoretical and experimental perspectives.

The characterization revealed that no chemical changes were produced in the base fluid when nanoparticles were added. An increase in density and viscosity was also observed in all the nanofluids prepared. Regarding their thermal properties, the nanofluids showed an increase in both isobaric specific heat and thermal conductivity. In turn, the heat transfer coefficient was improved by up to 6% with regard to the base fluid according to a *FoM* based on the Dittus-Boelter correlation. Consequently, the nanofluids based on Ag nanoparticles enhance heat transfer efficiency, which could lead to the improved overall efficiency of CSP plants, in which this kind of fluids is often used as a HTF.

The molecular dynamics results follow the experimental tendency. Thus, the thermal conductivity and the isobaric specific heat follow the same tendency and coincide with the experimental results. The structural analysis showed the existence of a first-layer structure composed of two diphenyl oxide molecules and one biphenyl molecule around the Ag. This structural arrangement leads to a directionality of the movement. This movement can favour effective heat transport and an increase in thermal conductivity with regard to the base fluid. This kind of analysis has not been performed before for this kind of nanofluid systems.

The approach based on experimental and theoretical results, and the explanation of the macroscopic properties from the analysis of the nano-level interactions included in this manuscript is clearly new and original.

Finally, the thermal properties, such as thermal conductivity, isobaric specific heat, and the heat transfer process, of the nanofluids prepared in this study were improved, and consequently they could be tested in a CSP system. Their use may lead to the improved efficiency of these plants, and therefore the cost of producing electricity can be reduced.

Acknowledgements

We thank the Ministerio de Economia y Competitividad (MINECO) of the Spanish Government for funding under Grant No. ENE2014-58085-R.

We thank Torresol Energy Investments, S.A. for their support.

Calculations were made through CICA - Centro Informático Científico de Andalucía (Spain).

Antonio Sánchez-Coronilla thanks VPPI-US for the financial support.

Appendix A. Supplementary material

Supplementary data associated with this article can be found, in the online version, at http://dx.doi.org/10.1016/j.apenergy.2017.03.003.

References

[1] Khan J, Arsalan MH. Solar power technologies for sustainable electricity generation – a review. Renew Sust Energy Rev 2016;55:414–25.

[2] Devabhaktuni V, Alam M, Depuru SSSR, Green RC, Nims D, Near C. Solar energy: trends and enabling technologies. Renew Sust Energy Rev 2013;19:555–64.

[3] El Mghouchi Y, El Bouardi A, Choulli Z, Ajzoul T. Models for obtaining the daily direct, diffuse and global solar radiations. Renew Sust Energy Rev 2016;56:87–99.

[4] Desideri U, Zepparelli F, Morettini V, Garroni E. Comparative analysis of concentrating solar power and photovoltaic technologies: technical and environmental evaluations. Appl Energy 2013;102:765–84.

[5] Bijarniya JP, Sudhakar K, Baredar P. Concentrated solar power technology in India: a review. Renew Sust Energy Rev 2016;63:593–603.
[6] Fernandez-Garcia A, Zarza E, Valenzuela L, Perez M. Parabolic-trough solar collectors and their applications. Renew Sust Energy Rev 2010;14:1695–721.
[7] Mwesigye A, Huan ZJ, Meyer JP. Thermodynamic optimisation of the performance of a parabolic trough receiver using synthetic oil-Al_2O_3 nanofluid. Appl Energy 2015;156:398–412.
[8] Navas J, Sánchez-Coronilla A, Martín EI, Teruel M, Gallardo JJ, Aguilar T, et al. On the enhancement of heat transfer fluid for concentrating solar power using Cu and Ni nanofluids: an experimental and molecular dynamics study. Nano Energy 2016;27:213–24.
[9] Suganthi KS, Vinodhan VL, Rajan KS. Heat transfer performance and transport properties of ZnO-ethylene glycol and ZnO-ethylene glycol-water nanofluid coolants. Appl Energy 2014;135:548–59.
[10] Yoo DH, Hong KS, Yang HS. Study of thermal conductivity of nanofluids for the application of heat transfer fluids. Thermochim Acta 2007;455:66–9.
[11] Lee S, Choi SUS, Li S, Eastman JA. Measuring thermal conductivity of fluids containing oxide nanoparticles. J Heat Trans-T Asme 1999;121:280–9.
[12] Chen MJ, He YR, Zhu JQ, Wen DS. Investigating the collector efficiency of silver nanofluids based direct absorption solar collectors. Appl Energy 2016;181:65–74.
[13] Colangelo G, Favale E, de Risi A, Laforgia D. Results of experimental investigations on the heat conductivity of nanofluids based on diathermic oil for high temperature applications. Appl Energy 2012;97:828–33.
[14] Colangelo G, Favale E, Miglietta P, de Risi A, Milanese M, Laforgia D. Experimental test of an innovative high concentration nanofluid solar collector. Appl Energy 2015;154:874–81.
[15] Singh D, Timofeeva EV, Moravek MR, Cingarapu S, Yu WH, Fischer T, et al. Use of metallic nanoparticles to improve the thermophysical properties of organic heat transfer fluids used in concentrated solar power. Sol Energy 2014;105:468–78.
[16] Choi SUS. Nanofluids: from vision to reality through research. J Heat Trans-T Asme 2009;131:033106.
[17] Yu WH, France DM, Routbort JL, Choi SUS. Review and comparison of nanofluid thermal conductivity and heat transfer enhancements. Heat Transfer Eng 2008;29:432–60.
[18] Colangelo G, Favale E, de Risi A, Laforgia D. A new solution for reduced sedimentation flat panel solar thermal collector using nanofluids. Appl Energy 2013;111:80–93.
[19] Sreeremya TS, Krishnan A, Mohamed AP, Hareesh US, Ghosh S. Synthesis and characterization of cerium oxide based nanofluids: an efficient coolant in heat transport applications. Chem Eng J 2014;255:282–9.
[20] Wen DS, Lin GP, Vafaei S, Zhang K. Review of nanofluids for heat transfer applications. Particuology 2009;7:141–50.
[21] CEA. Nanofluids for heat transfer applications. France: Marketing Study Unit, CEA; 2007.
[22] Verma SK, Tiwari AK. Progress of nanofluid application in solar collectors: a review. Energy Convers Manage 2015;100:324–46.
[23] Mohammed HA, Al-Aswadi AA, Shuaib NH, Saidur R. Convective heat transfer and fluid flow study over a step using nanofluids: a review. Renew Sust Energy Rev 2011;15:2921–39.
[24] Murshed SMS, de Castro CAN. Conduction and convection heat transfer characteristics of ethylene glycol based nanofluids – a review. Appl Energy 2016;184:681–95.
[25] Timofeeva EV, Smith DS, Yu WH, France DM, Singh D, Routbort JL. Particle size and interfacial effects on thermo-physical and heat transfer characteristics of water-based alpha-SiC nanofluids. Nanotechnology 2010;21:215703.
[26] Patel HE, Das SK, Sundararajan T, Sreekumaran Nair A, George B, Pradeep T. Thermal conductivities of naked and monolayer protected metal nanoparticle based nanofluids: manifestation of anomalous enhancement and chemical effects. Appl Phys Lett 2003;83:2931–3.
[27] Huxtable ST, Cahill DG, Shenogin S, Xue LP, Ozisik R, Barone P, et al. Interfacial heat flow in carbon nanotube suspensions. Nat Mater 2003;2:731–4.
[28] Eastman JA, Choi SUS, Li S, Yu W, Thompson LJ. Anomalously increased effective thermal conductivities of ethylene glycol-based nanofluids containing copper nanoparticles. Appl Phys Lett 2001;78:718–20.
[29] Li YJ, Zhou JE, Tung S, Schneider E, Xi SQ. A review on development of nanofluid preparation and characterization. Powder Technol 2009;196:89–101.
[30] Dittus FW, Boelter LMK. Pioneers in heat transfer – heat transfer in automobile radiators of the turbular type. University California Publications Eng.; 1930; 2:443–61.
[31] Yu W, France DM, Timofeeva EV, Singh D, Routbort JL. Thermophysical property-related comparison criteria for nanofluid heat transfer enhancement in turbulent flow. Appl Phys Lett 2010;96:213109.
[32] Rai N, Siepmann JI. Transferable potentials for phase equilibria. 9. Explicit hydrogen description of benzene and five-membered and six-membered heterocyclic aromatic compounds. J Phys Chem B 2007;111:10790–9.
[33] Rai N, Siepmann JI. Transferable potentials for phase equilibria. 10. Explicit-hydrogen description of substituted benzenes and polycyclic aromatic compounds. J Phys Chem B 2013;117:273–88.
[34] Erkoc S. Interaction of nitric oxide with elements. J Mol Struct-Theochem 2001;574:127–32.
[35] Duarte F, Bauer P, Barrozo A, Amrein BA, Purg M, Aqvist J, et al. Force field independent metal parameters using a nonbonded dummy model. J Phys Chem B 2014;118:4351–62.
[36] Liao QH, Kamerlin SCL, Strodel B. Development and application of a nonbonded Cu^{2+} model that includes the Jahn-Teller effect. J Phys Chem Lett 2015;6:2657–62.
[37] Smith W, Forester TR. DL_POLY_2.0: a general-purpose parallel molecular dynamics simulation package. J Mol Graphics 1996;14:136–41.
[38] Martinez JM, Martinez L. Packing optimization for automated generation of complex system's initial configurations for molecular dynamics and docking. J Comput Chem 2003;24:819–25.
[39] Allen MP, Tildesley DJ. Computer simulation of liquids. Oxford: Clarendon; 1989.
[40] www.chemcraftprog.com.
[41] Song YY, Bhadeshia HKDH, Suh DW. Stability of stainless-steel nanoparticle and water mixtures. Powder Technol 2015;272:34–44.
[42] Chang H, Tsai MH. Synthesis and characterization of Zno nanoparticles having prism shape by a novel gas condensation process. Rev Adv Mater Sci 2008;18:736–45.
[43] Hwang Y, Lee JK, Lee CH, Jung YM, Cheong SI, Lee CG, et al. Stability and thermal conductivity characteristics of nanofluids. Thermochim Acta 2007;455:70–4.
[44] Chandrasekar M, Suresh S, Senthilkumar T. Mechanisms proposed through experimental investigations on thermophysical properties and forced convective heat transfer characteristics of various nanofluids – a review. Renew Sust Energy Rev 2012;16:3917–38.
[45] Namburu PK, Kulkarni DP, Dandekar A, Das DK. Experimental investigation of viscosity and specific heat of silicon dioxide nanofluids. Micro Nano Lett 2007;2:67–71.
[46] Hadadian M, Samiee S, Ahmadzadeh H, Goharshadi EK. Nanofluids for heat transfer enhancement – a review. Phys Chem Res 2013;1:1–33.
[47] Einstein A. Investigation on the theory of Brownian movement. New York: Dover; 1956.
[48] Cabaleiro D, Gracia-Fernandez C, Legido JL, Lugo L. Specific heat of metal oxide nanofluids at high concentrations for heat transfer. Int J Heat Mass Transfer 2015;88:872–9.
[49] Mousavi NSS, Kumar S. Effective heat capacity of ferrofluids – analytical approach. Int J Therm Sci 2014;84:267–74.
[50] Elias MM, Mahbubul IM, Saidur R, Sohel MR, Shahrul IM, Khaleduzzaman SS, et al. Experimental investigation on the thermo-physical properties of Al_2O_3 nanoparticles suspended in car radiator coolant. Int Commun Heat Mass 2014;54:48–53.
[51] Starace AK, Gomez JC, Wang J, Pradhan S, Glatzmaier GC. Nanofluid heat capacities. J Appl Phys 2011;110:124323.
[52] Nieh HM, Teng TP, Yu CC. Enhanced heat dissipation of a radiator using oxide nano-coolant. Int J Therm Sci 2014;77:252–61.
[53] Barbes B, Paramo R, Blanco E, Casanova C. Thermal conductivity and specific heat capacity measurements of CuO nanofluids. J Therm Anal Calorim 2014;115:1883–91.
[54] Pantzali MN, Kanaris AG, Antoniadis KD, Mouza AA, Paras SV. Effect of nanofluids on the performance of a miniature plate heat exchanger with modulated surface. Int J Heat Fluid Flow 2009;30:691–9.
[55] de Castro CAN, Murshed SMS, Lourenco MJV, Santos FJV, Lopes MLM, Franca JMP. Enhanced thermal conductivity and specific heat capacity of carbon nanotubes ionanofluids. Int J Therm Sci 2012;62:34–9.
[56] Shin D, Banerjee D. Enhancement of specific heat capacity of high-temperature silica-nanofluids synthesized in alkali chloride salt eutectics for solar thermal-energy storage applications. Int J Heat Mass Transfer 2011;54:1064–70.
[57] O'Hanley H, Buongiorno J, McKrell T, Hu LW. Measurement and model validation of nanofluid specific heat capacity with differential scanning calorimetry. Adv Mech Eng; 2012. Artn 181079.
[58] Shin D, Banerjee D. Enhanced specific heat capacity of nanomaterials synthesized by dispersing silica nanoparticles in eutectic mixtures. J Heat Trans-T Asme 2013;135:032801.
[59] Shin D, Banerjee D. Specific heat of nanofluids synthesized by dispersing alumina nanoparticles in alkali salt eutectic. Int J Heat Mass Transfer 2014;74:210–4.
[60] Sundar LS, Farooky MH, Sarada SN, Singh MK. Experimental thermal conductivity of ethylene glycol and water mixture based low volume concentration of Al_2O_3 and CuO nanofluids. Int Commun Heat Mass 2013;41:41–6.
[61] Lide DR. CRC handbook of chemistry and physics. 90th ed. Boca Raton, Florida, USA: CRC Press; 2009.
[62] Hong KS, Hong TK, Yang HS. Thermal conductivity of Fe nanofluids depending on the cluster size of nanoparticles. Appl Phys Lett 2006;88.
[63] Campana C, Miller RE. Physical properties of liquid hexane and derived polar by-products of hexane autoxidation: molecular dynamics calculations using the TraPPE-UA force field. Mol Simulat 2013;39:882–94.
[64] Trinh TT, Vlugt TJH, Kjelstrup S. Thermal conductivity of carbon dioxide from non-equilibrium molecular dynamics: a systematic study of several common force fields. J Chem Phys 2014;141:134504.
[65] Annapureddy HVR, Nune SK, Motkuri RK, McGrail BP, Dang LEX. A combined experimental and computational study on the stability of nanofluids containing metal organic frameworks. J Phys Chem B 2015;119:8992–9.
[66] Philip J, Shima PD, Raj B. Enhancement of thermal conductivity in magnetite based nanofluid due to chainlike structures. Appl Phys Lett 2007;91.

Annex 3

Preparation of Au nanoparticles in a non-polar medium: obtaining high-efficiency nanofluid for Concentrating Solar Power. An experimental and theoretical perspective

Journal of Materials Chemistry A

PAPER

Cite this: J. Mater. Chem. A, 2017, 5, 12483

Preparation of Au nanoparticles in a non-polar medium: obtaining high-efficiency nanofluids for concentrating solar power. An experimental and theoretical perspective†

Roberto Gómez-Villarejo,[a] Javier Navas,*[a] Elisa I. Martín,[b] Antonio Sánchez-Coronilla,*[c] Teresa Aguilar,[a] Juan Jesús Gallardo,[a] Desiré De los Santos,[a] Rodrigo Alcántara,[a] Concha Fernández-Lorenzo[a] and Joaquín Martín-Calleja[a]

This paper presents the preparation of Au nanoparticles in a non-polar medium, which is a fluid composed of the eutectic mixture of biphenyl and diphenyl oxide commonly used in Concentrating Solar Power (CSP) plants. The nanofluids prepared showed enhanced thermal properties, presenting thermal conductivity values 70% higher than those of base fluids, and isobaric specific heat values up to 10% higher. In turn, an increase of up to 36% was observed in their heat transfer coefficient, which is their efficiency as a heat transfer fluid (HTF). Also, the stability of the nanofluids was analysed using UV-vis spectroscopy, and particle size and ζ potential. The nanofluids with lower concentrations agglomerate slowly, which is considered stable for this application. Thus, these nanofluids are a promising, interesting alternative to the HTF often used in CSP plants. Also, molecular dynamics calculations were performed to better understand how the Au-nanofluid behaves in the presence of a surfactant within a temperature range between 50 and 600 K. The isobaric specific heat and thermal conductivity values followed the same experimental tendency. The analysis of the radial distribution functions (RDFs) and spatial distribution functions (SDFs) showed that, as the temperature rose, an exchange took place between the surfactant and diphenyl oxide molecules in the first layer of molecules around the metal. This movement incorporated a directionality that may play a part in the enhanced thermal properties. The surfactant participates as an active component within the Au-nanofluid, contributing to efficient heat transfer processes.

Received 31st January 2017
Accepted 12th May 2017

DOI: 10.1039/c7ta00986k

rsc.li/materials-a

1. Introduction

One of the main goals of modern society is to find solutions for the growing demand for energy while minimizing the impact that energy sources have on the environment.[1] To this effect, one of the options generating most interest is Concentrating Solar Power (CSP).[2,3] One line of research aimed at improving the efficiency of this kind of plants involves improving the thermal properties of the HTF used in CSP plants, which will lead to improvements in the heat transfer processes taking place. In this sense, the use of nanofluids seems to be an interesting alternative for improving the thermal properties of base fluids.[4–6] Many studies of nanofluids have reported improvements in properties such as isobaric specific heat[5,7–11] or thermal conductivity.[5,8,12–14] However, there are few studies about nanofluids using the typical HTFs used in CSP applications as a base fluid.

Therefore, this study involved the preparation of nanofluids based on the HTF used in CSP plants, which is the eutectic

[a]Departamento de Química Física, Facultad de Ciencias, Universidad de Cádiz, E-11510 Puerto Real (Cádiz), Spain. E-mail: javier.navas@uca.es
[b]Departamento de Ingeniería Química, Facultad de Química, Universidad de Sevilla, E-41012 Sevilla, Spain
[c]Departamento de Química Física, Facultad de Farmacia, Universidad de Sevilla, E-41012 Sevilla, Spain. E-mail: antsancor@us.es

† Electronic supplementary information (ESI) available: General XPS spectrum of the Au nanoparticles synthesized (Fig. S1). Na 1s and O 1s signals obtained from the XPS measurements performed for the Au nanoparticles synthesized (Fig. S2). UV-vis spectra obtained for the nanofluids at zero time and absorbance values at λ = 520 nm for the nanofluids prepared according to the nanoparticle weight percentage (Fig. S3). UV-vis spectra obtained for the nanofluid with a nominal concentration of 0.005 wt% subjected to heating/cooling cycles (Fig. S4). Density values of the nanofluids prepared *versus* the nanoparticle weight percentage (Fig. S5). Parameters of the Hamilton–Crosser conduction model with a Brownian motion driven convection model. β and $f(T,\phi)$ values for the plots in Fig. 8C in the main article (Table S1). $f(T,\phi)$ values obtained for the simulated values of thermal conductivity (Fig. S6). Mo_{nf}/Mo_{bf} ratio values for the nanofluids prepared (Fig. S7). Mean square displacement of the Au-nanofluid and the base fluid at several temperatures, and the diffusion coefficient estimated from the mean square displacement (Fig. S8). See DOI: 10.1039/c7ta00986k

mixture of biphenyl ($C_{12}H_{10}$) and diphenyl oxide ($C_{12}H_{10}O$). Gold nanoparticles were used to prepare the nanofluids because metal nanoparticles are known to increase the thermal conductivity of base fluids.[5,11,13–15] Au nanoparticles were synthesized within the fluid itself using a phase transfer surfactant to provide the nanofluid with greater stability. The synthesized nanoparticles were characterised to check the method followed, and an analysis was performed to determine the physical and chemical stability of the nanofluids. Properties related to the performance of the nanofluids such as density, viscosity, isobaric specific heat and thermal conductivity were also analysed, a huge increase in thermal conductivity of about 70% and the heat transfer coefficient up to 36% being observed. In addition, to gain an insight into the molecular behaviour of this kind of nanofluid systems with the inclusion of the surfactant, molecular dynamics simulations were performed. Thermophysical properties were estimated and compared with the experimental values, a good qualitative correlation being observed. The structural properties of the Au-nanofluid system were obtained by analysing their radial distribution function (RDF) and spatial distribution function (SDF). The exchange of the surfactant and diphenyl oxide molecules in the first layer of molecules around the metal plays an important role in enhancing the thermal properties of the system.

2. Methods

2.1. Preparation of Au nanoparticles and nanofluids

Au-nanofluids were prepared by a one-step method based on the synthesis of Au nanoparticles in the base fluid used, following the following chemical reactions in solution:[16]

$$AuCl_4^- (aq) + N(C_8H_{17})_4^+ (bf) \rightarrow N(C_8H_{17})_4^+AuCl_4^- (bf)$$

$$mAuCl_4^- (bf) + 3me^- (bf) \rightarrow mCl_4^- (bf) + Au_m (bf)$$

An initial nanofluid with a nanoparticle mass concentration of 0.01 wt% was prepared through a one-step method which involves dissolving a certain amount of tetraoctylammonium bromide ($(C_8H_{17})_4NBr$, TOAB, purity > 98%, supplied by Sigma-Aldrich) in 100 mL of a commercial heat transfer fluid (HTF) used as a base fluid, an eutectic mixture of biphenyl ($C_{12}H_{20}$, 26.5%) and diphenyl oxide ($C_{12}H_{10}$, 73.5%) supplied by Dowtherm©. The commercial name of this fluid is Dowtherm A.

This solution was treated with 5 mL of aqueous chloroauric acid ($HAuCl_4$, assay 99.9%, Sigma-Aldrich) solution (10 mM) and left under magnetic stirring for 30 minutes. Double the amount by weight of TOAB compared with $HAuCl_4$ was added to achieve the maximum phase transfer of $AuCl_4^-$ from the aqueous phase to the HTF. Then, the aqueous phase was collected and discarded. Next, 10 mL of aqueous sodium borohydride ($NaBH_4$, purity > 98%, Fluka Sigma-Aldrich) solution (50 mM) was added slowly to the organic phase for the reduction of $AuCl_4^-$ for obtaining metallic Au nanoparticles inside the organic phase, which is the base fluid of the nanofluid. The mixture was magnetically stirred again for one hour and later, the organic phase containing nanofluids was extracted. A change of colour was observed in the nanofluid from dark green to brown. Nanofluids with a different concentration of gold nanoparticles were obtained by changing the concentration of $HAuCl_4$ in the solution. The nominal weight percentages of Au with regard to the base fluid for the nanofluids prepared were 0.0025 wt%, 0.005 wt%, and 0.01 wt%. These percentages will be used in this paper for naming the nanofluids.

In order to characterize the nanoparticles synthesized, the nanofluids were centrifuged, and the supernatant liquid was discarded, resulting in a black dust which was cleaned with acetone in successive extractions.

2.2. Characterization of nanoparticles and nanofluids

In order to corroborate the synthesis of gold nanoparticles in the base fluid, several techniques were required. The chemical state bonding and the oxidation states of the solid extracted from the nanofluids were studied by X-ray photoelectron spectroscopy (XPS). Also, Transmission Electron Microscopy (TEM) was used to observe the size and shape of the nanoparticles. In turn, X-ray diffraction (XRD) was used to determine the crystalline phases in the solid extracted from the nanofluids. The details of the characterization of solid gold nanoparticles are shown in the ESI.†

Stability is one of the key concepts in nanofluids because their thermal properties depend heavily on whether they are stable or unstable. Several techniques were used for monitoring the temporal stability of the nanofluids prepared. UV-vis spectroscopy (UV-vis) can provide a measurable characterization of stability by evaluating the absorbance of a suspension.[17] To this end, UV-vis spectra were recorded in the wavelength range of 400–880 nm for analysing the sedimentation process. Also, ζ potential measurements were performed. Particle size and size distribution were also measured, using the principle of Dynamic Light Scattering (DLS) as a simple method for analysing suspension stability and particle size measurements in solution.[18,19] The details of the stability characterization are shown in the ESI.†

Density, viscosity, isobaric specific heat and thermal conductivity were determined to characterize the performance of nanofluids, taking into consideration their application as a new class of heat transfer fluids in solar collectors in CSP. Density was estimated using a pycnometer controlling the temperature. Dynamic viscosity was measured using a SV-10 viscometer supplied by Malvern Instruments Ltd. Density and viscosity measurements were performed five times to calculate the average values. The isobaric specific heat measurements were performed using a Temperature Modulated Differential Scanning Calorimeter (TMDSC), supplied by TA Instruments©, model Q-20. To perform the measurements, a program was created which can be summarized as follows: the temperature was equilibrated at 341 K to remove contaminants and kept isothermal for 10 min; then the samples were equilibrated at 301 K and then ramped to 391 K at 1 K min^{-1}. A modulation was programmed around the studied temperatures with an amplitude of ± 1 K in a period of 120 seconds. Finally, cooling was

performed at 1 K min^{-1}. The isobaric specific heat of the base fluid was measured to test the method used with regard to the values reported by the supplier. Finally, the thermal conductivity of the nanofluids was measured at several temperatures using the laser flash technique (LFA 1600 equipment, supplied by Linseis Thermal Analysis©). This technique really measures thermal diffusivity, which is the thermophysical property that defines the speed of heat propagation by conduction during changes in temperature. According to Standard ASTM E 1461-01 the relationship between both properties is given by the equation:

$$k(T) = D(T)C_P(T)\rho(T) \quad (1)$$

where k is the thermal conductivity, D the thermal diffusivity, C_P is the isobaric specific heat and ρ is the density. All thermal measurements were performed in triplicate.

2.3. Computational methods

Force field. The Transferable Potentials for Phase Equilibria-Explicit-Hydrogen (TraPPE-EH) force field[20,21] was used to describe the intra and intermolecular interactions of the HTF fluid (diphenyl oxide/biphenyl blend). The TraPPE-EH force field treats aromatic rings and the directly connected atoms as rigid entities. The phenyl rings were treated as rigid but were allowed to rotate with regard to each other around the C1–C1′ bond of the biphenyls.

The intra and intermolecular interactions of the TOAB surfactant were described by using the Transferable Potentials for Phase Equilibria-United-Atom (TraPPE-UA) force field.[22–24] For the alkyl groups, a fully flexible model based on single interaction sites (pseudo-atoms) was used to represent a carbon atom together with all of its bonded hydrogen atoms (CH_3 and CH_2). Meanwhile, the polar nitrogen atom and the carbon atoms bonded to it were treated as explicit interaction sites in a rigid unit. Also, the simulation of the metal nanoparticles was performed using a rigid unit cell of 14 gold atoms with the point group $Fm\bar{3}m$. The parameters used in our simulations to describe the non-bonded force field of the metal nanoparticle were adopted from (ref. 25).

The Transferable Potentials for Phase Equilibria (TraPPE-EH and TraPPE-UA) and the non-bonded force field of the metal nanoparticle use Lennard–Jones (LJ) and Coulomb potentials to represent the non-bonded interactions

$$u(r_{ij}) = 4\varepsilon_{ij}\left[\left(\frac{\sigma_{ij}}{r_{ij}}\right)^{12} - \left(\frac{\sigma_{ij}}{r_{ij}}\right)^{6}\right] + \frac{q_i q_j}{4\pi\varepsilon_0 r_{ij}} \quad (2)$$

where r_{ij}, ε_{ij}, σ_{ij}, q_i, q_j, and ε_0 are the distance between interaction sites i and j, the LJ well depth, the LJ diameter, the partial charges on interaction sites i and j, and the permittivity of vacuum, respectively. The Lorentz–Berthelot combining rules were used to determine LJ parameters for unlike interactions.

Simulation details. Molecular dynamics simulations were performed with the DLPOLY code[26] in the canonical ensemble (NVT) using a Nose–Hoover thermostat and periodic boundary conditions. The initial configurations were built with the PACKMOL code[27] providing cubic boxes in which the length of the box sides is chosen to keep the density of the experimental HTF at 298 K (1059 kg m^{-3}). A time step of 0.5 fs was employed and simulation runs lasted for 1 ns. For the trajectory analysis, structures were saved every 100 time steps. A cut-off distance of 9 Å was applied in all the cases and the Ewald sum methodology[28] was applied to account for the electrostatic interactions.

3. Results and discussion

3.1. Characterisation of gold nanoparticles

In order to test the formation of gold nanoparticles, a solid was extracted from the nanofluids prepared. This solid was characterized by means of XPS, XRD and TEM, as described above. XPS was used to analyse the oxidation state of Au to determine whether Au^0 nanoparticles were synthesized. Fig. 1A shows the Au 4f spectrum obtained. The binding energy (BE) of the Au $4f_{7/2}$ and Au $4f_{5/2}$ was around 83.8 and 87.5 eV, respectively. These values are typical for pure metallic Au^0 nanoparticles,[29–31] which show a slightly shifted Au $4f_{7/2}$ signal with regard to the typical value of 84.0 eV. According to the literature, the Au $4f_{7/2}$ signal is shifted for other oxidation states, 1.3 and 2.0 eV towards higher binding energies for Au^+ and Au^{3+} species. Thus, the presence of this oxidized species was negligible. Also, the separation observed for the spin–orbit components was about 3.7 eV, which is also typical for metallic Au^0. Thus, the XPS results confirmed the presence of metallic Au nanoparticles and consequently the presence of zero-valent gold formed in the nanofluid. Also, we can see that the peaks are wide, probably due to the residual presence of TOAB, the phase transfer agent used. The presence of a residual amount of TOAB is confirmed by the signal of N 1s obtained from XPS, as is observed in the general X-ray photoelectron spectrum shown in Fig. S1 in the ESI.†

Fig. S1 in the ESI† shows the general X-ray photoelectron spectra and the basic assignment of the peaks found. The XPS analysis also shows the presence of Na and O. The Na 1s signal shows two contributions at BEs of about 1070.4 and 1069.0 eV. The O 1s signal shows contributions at BEs of about 531.7 and 528.1 eV. These values can be assigned to different sodium (hydr)oxides species, such as sodium oxide, sodium hydroxide[32,33] or sodium peroxide.[34] The source of the Na is $NaBH_4$, the reducing agent used in the synthesis. Fig. S2 in the ESI† shows the Na 1s and O 1s spectra obtained.

To obtain information about the crystal structure of the Au nanoparticles synthesized, X-ray diffraction analysis was performed. The XRD pattern obtained is shown in Fig. 1B, and it shows three peaks at 2θ = 38.26, 44.45 and 64.67°, which are characteristic peaks of metallic gold. These peaks can be assigned to the (111), (200) and (220) crystal planes of gold for cubic structures with a $Fm\bar{3}m$ space group.[35,36] Finally, the TEM images of the gold nanoparticles synthesized reveal a spherical shape for the nanoparticles, as is reported in the literature.[37] An image considered to be representative is shown in Fig. 2A. A wide statistical study shows a non-uniform size distribution in the samples, the size-distribution of the gold nanoparticles being found to range between 5 and 25 nm, as is shown in

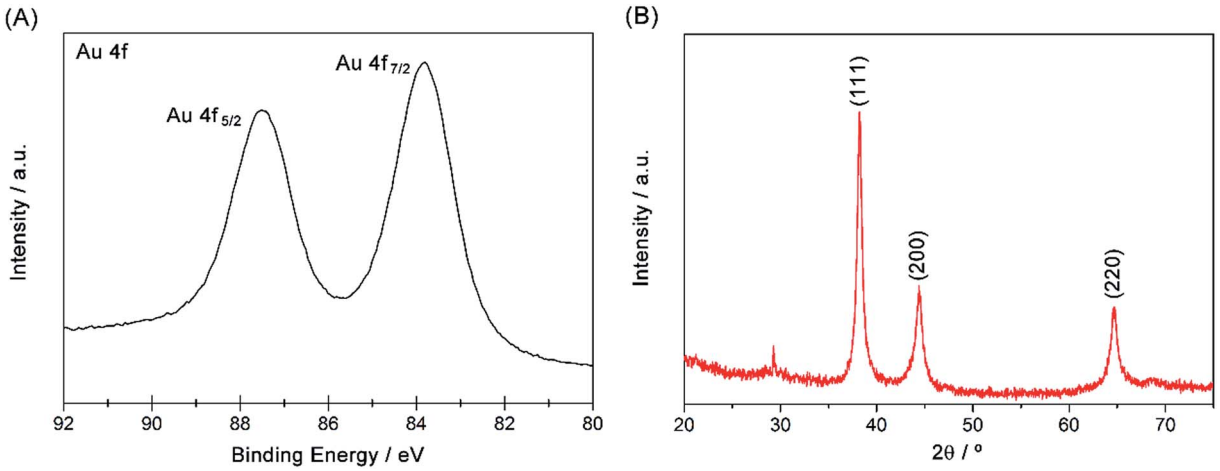

Fig. 1 (A) Au 4f signal obtained from the X-ray photoelectron spectrum. (B) XRD pattern of the nanoparticles synthesized in the base fluid.

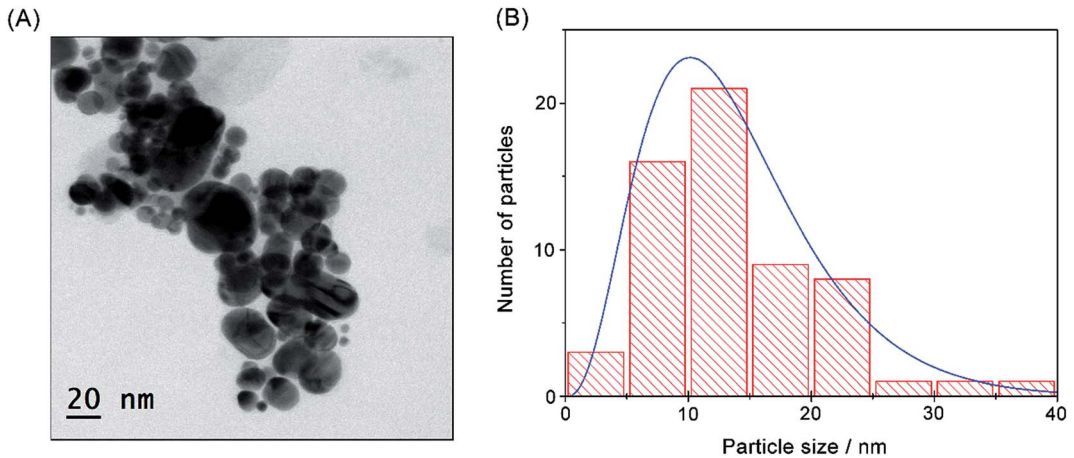

Fig. 2 (A) TEM image of the Au nanoparticles. (B) Particle size distribution obtained from the TEM images.

Fig. 2B. Some nanoparticles show size outside this range, but their amount is clearly lower.

3.2. Nanofluid stability

Nanofluids are considered to be stable when the concentration or particle size remains constant.[38] After preparation, nanofluids logically behave dynamically: nanoparticles tend to agglomerate due to attraction between them, resulting in clusters with a high weight that tend to precipitate and sediment. Particle agglomeration was found to be detrimental to the stability of the nanofluids and therefore to their thermal properties.[39,40]

UV-vis spectroscopy is one of the techniques used to analyse the stability of the nanofluids and the sedimentation process that can occur. Fig. S3A in the ESI† shows the UV-vis spectra of the nanofluids prepared at zero time, just after they were prepared. The high absorbance of up to 550–600 nm for the nanofluids with respect to the base fluid is due to the scattering process generated by the nanoparticles in the colloidal suspension, which is higher at lower wavelengths, as reported previously.[41,42]

To evaluate the stability of the nanofluids prepared, UV-vis spectra were recorded. Changes in the absorbance were studied at $\lambda = 520$ nm *versus* time, because this value is reasonable in function of the particle size and dielectric environment in the nanofluids prepared. At least four spectra were recorded every day for each nanofluid and the changes in absorbance were analysed for a week. Fig. 3 shows the absorbance values for the nanofluids prepared. At 520 nm, both photonic absorption and light scattering processes take place due to the presence of nanoparticles in suspension, so a decrease in the absorbance recorded means a decrease in the number of nanoparticles in suspension; that is, sedimentation of the nanoparticles in suspension takes place. This sedimentation process is faster for the two nanofluids with higher nanoparticle concentrations. After three days, these nanofluids are considered to remain stable.

The stability of the nanofluids prepared was analysed by measuring the particle sizes using the DLS technique. The

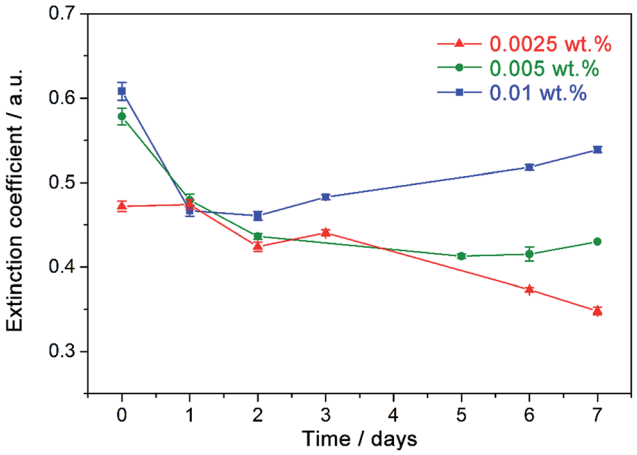

Fig. 3 Absorbance values at $\lambda = 520$ nm *versus* time for the nanofluids prepared.

measurements were recorded for a week, with several measurements performed each day. Each measurement was performed in triplicate. Fig. 4 shows the results obtained. Thus, the nanofluid with a nominal 0.0025 wt% of Au nanoparticles showed less dispersion in each particle size measurement, but we can see a slight tendency to agglomerate very slowly. This result is coherent with the results from UV-vis spectroscopy, which give us the idea that the nanofluid system is still changing after seven days. In turn, the nanofluid with an Au nanoparticle concentration of 0.01 wt% showed an increase in the particle size, and then a decrease. Possibly due to the high concentration of nanoparticles, agglomerations formed tend to agglomerate with each other and then sediment, or the big agglomerates break up to form smaller ones. As a result, more small agglomerates (450 nm on day 7, approximately) are in suspension, which increase the light scattering process, which, as mentioned above, increases at smaller wavelengths. This result explains the increase in the absorbance produced in the 0.01 wt% nanofluid after day 3. Finally, the 0.005 wt% nanofluid showed a greater dispersion in the measurements compared with the other two nanofluids, the particles being bigger too. The greater dispersion in the measurements may be a result of regions coexisting where larger agglomerates are formed that remain stable and regions in which the sedimentation of large agglomerates is produced, with only smaller sized agglomerates remaining. It is significant how agglomerates were detected between 900 nm and 1100 nm on day 7. Thus, it is possible to conclude that the nanofluid with 0.0025 wt% has a concentration that is low enough for the agglomerates to form slowly; the concentration of the 0.005 wt% nanofluid means that it is on the limit of what the system can support and for this reason some agglomerates precipitate but other larger ones do not, possibly because there is not a higher concentration of nanoparticles. Meanwhile, the nanofluid with the highest concentration clearly causes the high sedimentation rate due to this high concentration.

Also, ζ potential measurements are used for obtaining information about the stability of colloidal suspensions. Higher values of $|\zeta|$ lead to a high repulsion potential and therefore to a high stability of the colloidal system analysed. However, if the particles have low ζ potential values, there is no force to prevent the particles from agglomerating. According to the literature, the stability threshold of a colloidal-nanoparticle solution in terms of the ζ potential is ±30 mV.[43] Other authors state that nanofluids with a high ζ potential – positive or negative in the range of 40–60 mV – are considered electrically stable, and colloids with low ζ tend to coagulate or agglomerate.[18,44,45] Therefore, the greater the ζ potential, the greater the stability will be. Thus, the ζ potential of the nanofluids was measured for a week, several measurements were taken each day, and each measurement was performed in triplicate. Fig. 5 shows the results obtained. It is possible to observe that the $|\zeta|$ values are always higher for the nanofluid with the lowest nanoparticle

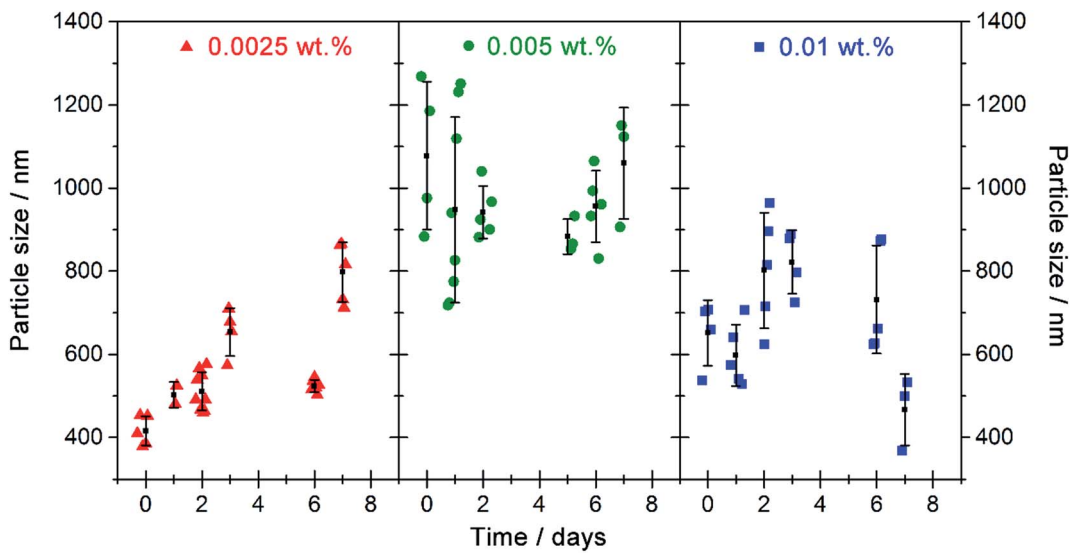

Fig. 4 Particle size obtained using the DLS technique *versus* time for the nanofluids prepared.

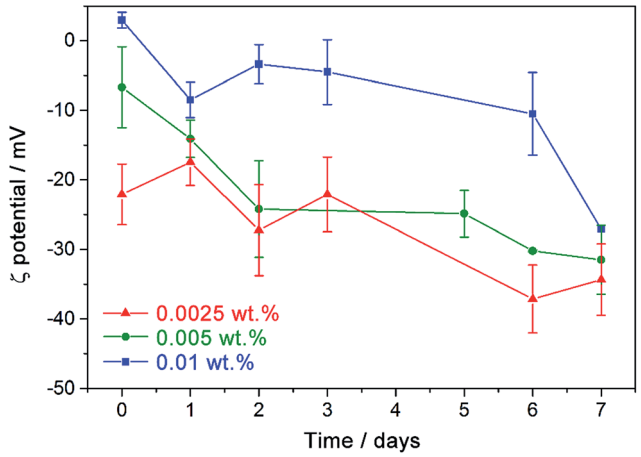

Fig. 5 ζ potential values obtained *versus* time for the nanofluids prepared.

concentration; therefore, it tends to agglomerate more slowly than the other two nanofluids, which is coherent with UV-vis and the particle size measurements shown above. In turn, the $|\zeta|$ values were lower for the nanofluid with the highest nanoparticle concentration for the measurement time. In this case, the $|\zeta|$ values increased during the last few days, which is coherent with the sedimentation produced and the fact that more stable agglomerates remain in suspension, as was discussed in the section on particle size measurements. Thus, Fig. 5 confirms that the nanofluid under consideration becomes much more stabilized with time. In fact the ζ potential for all the different concentrations approach the stabilized range of 30–40 mV.[43]

On the other hand, these nanofluids were prepared for use in CSP, which is a high temperature application. For this reason, a test of the stability with temperature was performed. The nanofluid with a nominal concentration of 0.005 wt% was heated for 5 hours controlling the evaporation of the fluid at 573 K without stirring. The UV-vis spectra of this nanofluid were registered before and after the heating process. At a high temperature, several undesired processes can occur, such as the degradation of the surfactant which could lead to a loss of stability, increasing the sedimentation process. This would be observed as a decrease in the extinction coefficient of the nanofluid. Fig. 6A shows the spectra obtained before and after the heating process. We can observe how there is no decrease in the extinction coefficient, but a slight increase occurs, which could be due to an increase in light scattering. This would be positive for the stability of the nanofluids. On the other hand, other tests were performed in order to analyse the stability of the nanofluids. Four thermal cycles (heating and cooling) to simulate daily solar irradiation were performed using the nanofluid with a nominal concentration of 0.005 wt%. The nanofluid was heated for 5 hours controlling the evaporation of the fluid, and it was allowed to cool to room temperature. The UV-vis spectra and particle size measurements were registered before and after the heating process. Also, the TEM images were registered at the end of the experiment for testing the stability observed in the nanofluid. Fig. S4 in the ESI† shows the UV-vis spectra registered in this test. No change in the spectra is observed after the thermal cycles, thus no chemical change occurs in the nanofluid. In turn, Fig. 6B shows the values of the extinction coefficient obtained from these spectra at λ = 520 nm. As in the previous test (see Fig. 6A), an increase of the

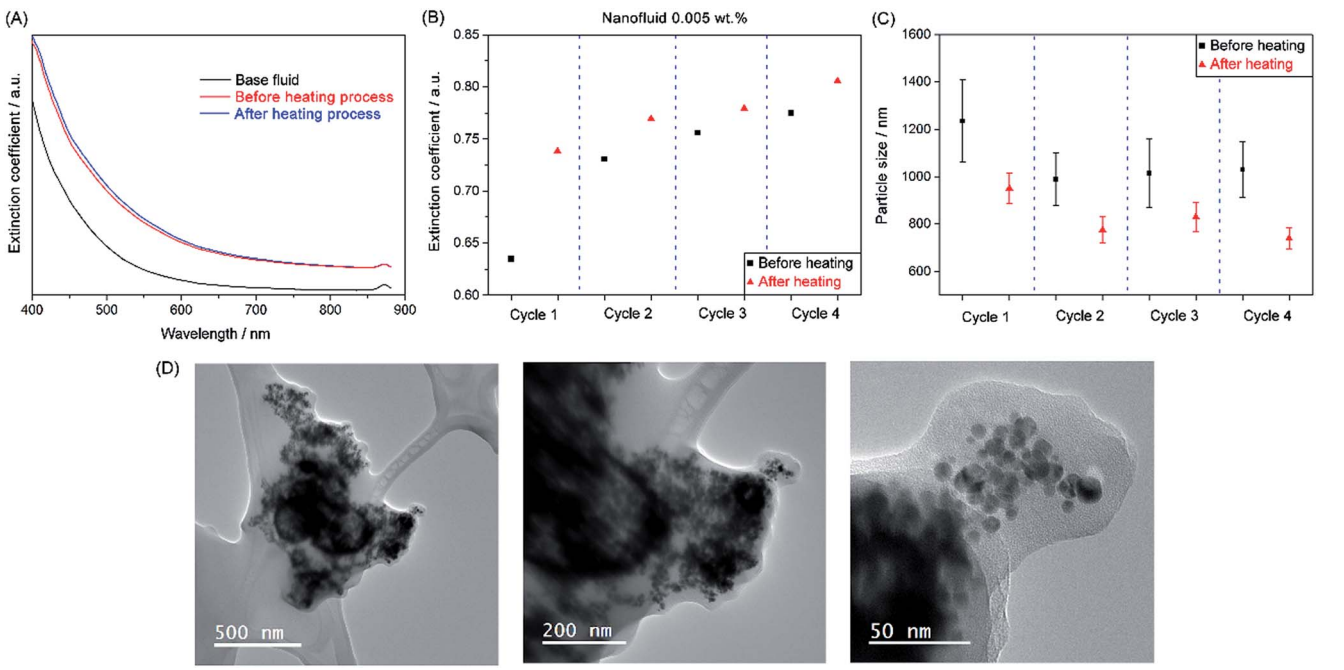

Fig. 6 (A) UV-vis spectra registered before and after the heating process at 573 K for the nanofluid with a nominal concentration of 0.005 wt%. (B) Extinction coefficient at λ = 520 nm; and (C) particle size, before and after thermal cycles. (D) TEM images obtained after thermal cycles.

extinction coefficient after the heating process is observed in each cycle, and for all the cycles. This fact could be due to an increase in light scattering, that is, the heating of the nanofluids helps to disperse the nanoparticles inside the base fluid. This is also coherent with the results from particle size measurements, which are shown in Fig. 6C. It is possible to observe a tendency for the particle size to decrease after the heating process. This would be positive for the stability of the nanofluids. Finally, Fig. 6D shows the TEM images obtained after the four thermal cycles. We can observe a cluster of hundreds of nanometers, which is composed of tens of nanometers of nanoparticles, and no changes are observed in the nanoparticles with respect to the TEM image obtained when the nanofluid was prepared (see Fig. 2). So, the TEM images support the conclusion of the stability of the nanofluids after the heating process obtained from UV-vis spectroscopy and particle size measurements.

3.3. Nanofluid performance

Several properties were characterized to evaluate the performance of the nanofluids prepared, such as density, viscosity, isobaric specific heat and thermal conductivity.

The density of the nanofluids affects the efficiency of the heat transfer fluids, studies having shown an increase in efficiency when the density increases.[12] Consequently, the density of the nanofluids was measured, and the results are shown in Table 1. The evolution of the density values with regard to the nominal Au weight percentage is shown in Fig. S5 in the ESI.† A slight increase in the density values is observed at higher nanoparticle concentrations. This may be due to the interface effects on the bulk fluid properties produced by the solid nanoparticle surface, or even due to the interactions between the nanoparticles.[46] From density values, it is possible to obtain the values of the nanoparticle volume fraction (ϕ) for the nanofluids, according to $\phi = (\rho_{nf} - \rho_{bf})/(\rho_{np} - \rho_{bf})$, where ρ is the density and the subscripts nf, bf and np refer to the nanofluid, base fluid and nanoparticles ($\rho_{np} = 19\,380$ kg m^{-3} (ref. 47)). But, the nanofluids prepared in this study are clearly made up of agglomerates or aggregates of nanoparticles, and in this case an effective volume fraction can define the systems more appropriately as it is possible to assume that these agglomerates cannot easily be broken up into the initial nanoparticles and so they are the units responsible for the transport properties.[48] The effective volume fraction (ϕ_{eff}) can be estimated according to fractal theory as $\phi_{eff} = \phi(a_a/a)^{3-D}$, where a_a is the radius of aggregates, a is the radius of primary nanoparticles, and D is the fractal index, usually 1.8 for nanofluids.[48–50] The values of a_a and a used were obtained from particle size measurements and TEM analysis, respectively, both shown above. Table 1 shows the value of ϕ and ϕ_{eff} for the nanofluids.

Table 1 Density and dynamic viscosity values measured and the values of the volume fraction and effective volume fraction for the nanofluids prepared

Nominal wt%	ρ/kg m^{-3}	ϕ/vol%	ϕ_{eff}/vol%	μ/mPa s
0	1059.5 ± 0.3	0	0	3.71 ± 0.03
0.0025	1059.9 ± 0.3	0.0022	0.34	3.76 ± 0.04
0.005	1060.5 ± 0.2	0.0079	1.55	3.82 ± 0.04
0.01	1061.2 ± 0.3	0.0098	0.86	3.78 ± 0.03

The viscosity values of a HTF are vital in heat transfer applications because they affect important parameters such as pumping power or possible drop in pressure. Particles in suspension increase the viscosity of the base fluid. Therefore, it is necessary to control the increase in viscosity. Thus, the dynamic viscosity of the nanofluids was measured, and the values obtained are shown in Table 1. It is possible to observe that the viscosity values increase with the effective volume fraction. There are several classic models to predict the effective viscosity of colloidal suspensions. The typical model for dynamic viscosity for suspensions with low nanoparticle concentrations is the Einstein model,[51] which considers spherical particles and not the interaction between nanoparticles. Considering in our case the effective nanoparticle volume fraction, the Einstein model can be expressed as $\mu_{nf} = \mu_{bf}(1 + 2.5\phi_{eff})$, where μ is the dynamic viscosity and the remaining variables and subscripts have been defined previously. In turn, Brinkman[52] generalized the Einstein model for more concentrated systems. Using the effective volume fraction, the Brinkman model is defined as $\mu_{nf} = \mu_{bf}/(1 - \phi_{eff})^{2.5}$. Fig. 7 shows the plot of the dynamic viscosity values obtained for the nanofluids and the plot of the Einstein and Brinkman models considering the effective nanoparticle volume fraction, implying that the system is composed of agglomerates and they are the transport units in the system. It is possible to observe how the experimental data agree with both the models when effective volume fractions are used. Also, for the highest value of ϕ_{eff}, the viscosity seems to deviate from both the models, reaching a slightly lower value, possibly due to the higher volume fraction and more particle–particle interactions taking place, these not being included in the Einstein and Brinkman models.

Furthermore, the suspension of nanoparticles in a HTF is known to lead to an increase in its thermal conductivity,[8,14] and

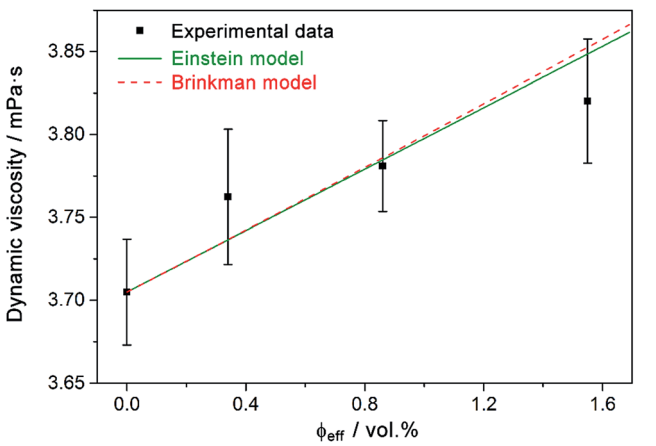

Fig. 7 Dynamic viscosity values of the nanofluids prepared and the plot of the Einstein and Brinkman models.

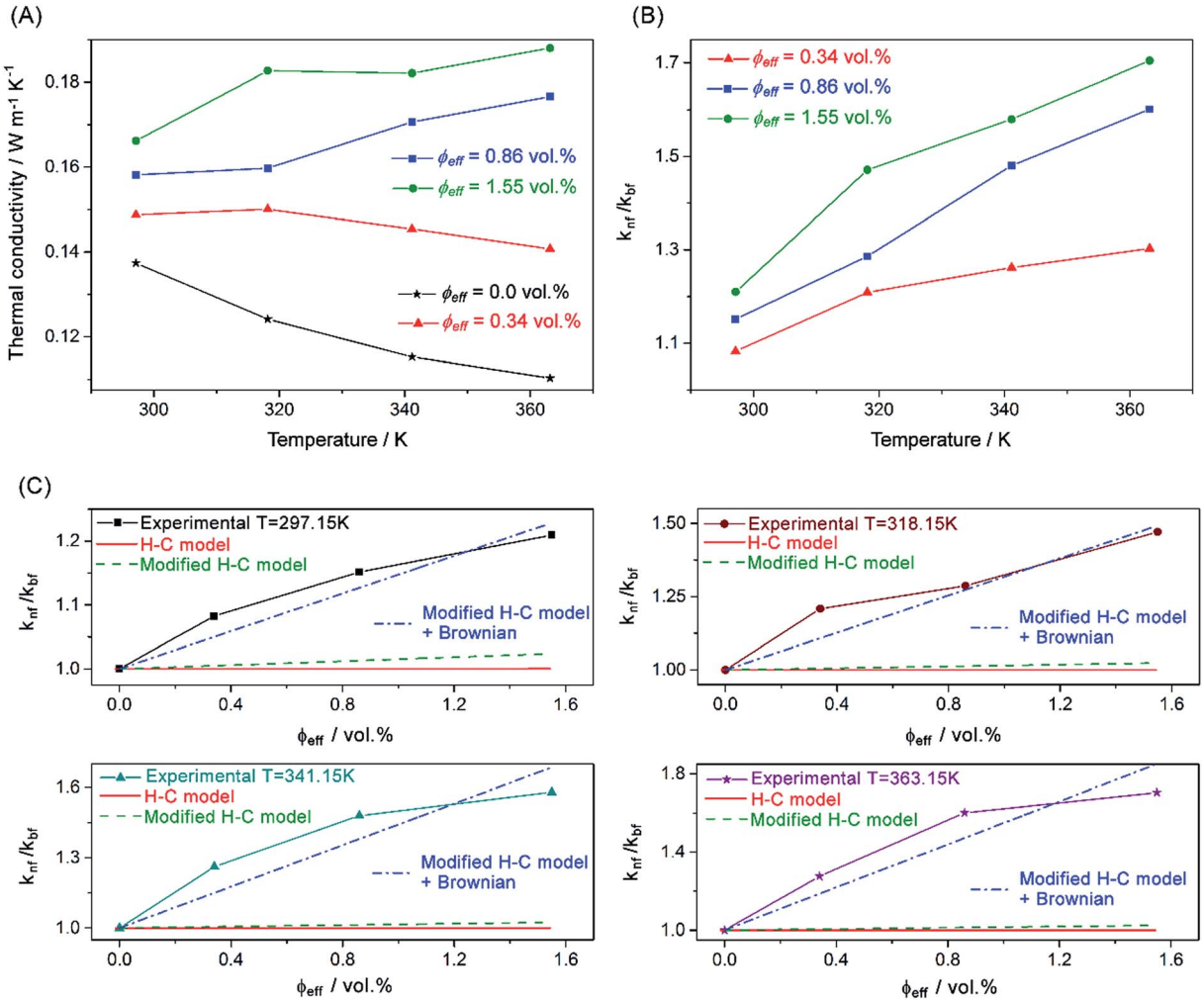

Fig. 8 (A) Thermal conductivity values, (B) ratio k_{nf}/k_{bf}, obtained for the nanofluids prepared, and (C) predicted values for this ratio using the H–C model, the modified H–C model, and the model described according to eqn (7).

materials with high thermal conductivity show better heat transfer efficiency.[12,13] For this reason, the thermal conductivity of the nanofluids was measured at different temperatures following the procedure described above. Fig. 8A shows the thermal conductivity values for the nanofluids and the base fluid. Also, Fig. 8B shows the ratio k_{nf}/k_{bf}, which gives an idea of the increased thermal conductivity values. A drastic increase of up to 70% in thermal conductivity can be seen for the nanofluid with an effective volume fraction of 1.55 vol% at 363 K.

It is interesting to analyse this drastic increase in thermal conductivity by means of the models that assess thermal conductivity in accordance with the nanoparticle volume fraction. The classic model for thermal conduction is that of Hamilton–Crosser (H–C).[53]

In turn, the conventional H–C model can be modified to predict the effective thermal conductivity of nanofluids for nanoparticles in the form of aggregates.[48] In this model, the effective volume fraction and the thermal conductivity of aggregates are included. Fig. 8C shows the plot of the thermal conductivity values *versus* the effective volume fraction and the values predicted by both models. It shows that neither model is able to predict the experimental values, a much greater increase in thermal conductivity being obtained than those predicted by the two models. Thus, a model able to predict the experimental data obtained must include another contribution to the thermal conductivity. Koo and Kleinstreuer introduced a new kind of model for spherical particles that combines the Hamilton–Crosser conduction model with a Brownian motion driven convection model[54,55]

$$k_{nf} = \frac{k_p + 2k_{bf} - 2\phi(k_{bf} - k_p)}{k_p + 2k_{bf} + \phi(k_{bf} - k_p)} k_{bf} + 5 \times 10^4 \beta \phi \rho_{bf} C_{P,bf} \sqrt{\frac{\kappa T}{\rho_p d_p}} f(T, \phi) \quad (3)$$

where k_p is the thermal conductivity of the nanoparticles, $C_{P,bf}$, is the isobaric specific heat of the base fluid, ρ_p and d_p are the density and diameter of the nanoparticle, and κ is the Boltzmann constant. The factors $\beta y f(T,\phi)$ can be adjusted to the experimental data. β is a function of ϕ and depends on the type of nanoparticles. $f(T,\phi)$ is a function of $Ty\phi$. The first term in eqn

(3) represents the static conductivity, while the second is the dynamic part that predicts the increase in conductivity due to the Brownian motion. In turn, due to the presence of aggregates in the nanofluids in this study, the modified Hamilton–Crosser model was included in the Koo and Kleinstreuer one to model the conduction process. This took into account the effective volume fraction, the thermal conductivity of aggregates (k_a, which is defined in the ESI†) and the diameter of the aggregates (d_a) obtained using the DLS technique for the nanofluid studied, as has been shown previously. Thus, the mathematical expression for the model proposed is

$$\frac{k_{nf}}{k_{bf}} = \frac{k_a + 2k_{bf} - 2\phi_{eff}(k_{bf} - k_a)}{k_a + 2k_{bf} + \phi_{eff}(k_{bf} - k_a)} + \frac{1}{k_{bf}} 5 \times 10^4 \beta \phi_{eff} \rho_{bf} C_{P,bf} \sqrt{\frac{\kappa T}{\rho_p d_a}} f(T, \phi) \quad (4)$$

Fig. 8C shows the values obtained by this model (eqn (4)). In this case, the model predicts values that are closer to those found experimentally at the temperatures measured. But, the model predicts values with a near-linear dependence with the effective volume fraction, while the experimental values show a sub-linear dependence. It is possible that for higher effective volume fractions, other interactions occur in the nanofluids which hinder the heat transfer, and this is the reason why the experimental values show a sub-linear dependence. In turn, the values obtained for β and $f(T,\phi)$ are close to those reported previously.[56] It can also be seen that β does not change and $f(T,\phi)$ increases with the temperature, as the model predicts. The ESI† includes a more detailed discussion of these parameters. In turn, β gives an idea of the volume fraction of liquid travelling with a particle,[56] and thus depends on the interactions between the nanoparticles/aggregates and the surfactant and base fluid used. These interactions are analysed below based on molecular dynamics calculations.

Isobaric specific heat is vital in the study of heat transfer fluids so the values for the nanofluids prepared were measured at several temperatures between room temperature and 370 K, approximately. Fig. 9 shows the values measured with regard to temperature and effective volume fraction. It is possible to observe that the nanofluids behave randomly. The isobaric specific heat increased with regard to the base fluid for the nanofluid with an intermediate effective volume fraction. This makes us think that there is an optimum effective volume fraction. The isobaric specific heat of solids is typically lower than that of the fluids, values for nanofluids would be expected to be lower than that of the base fluid.[12,57,58] However, the opposite behaviour has been reported on occasions whereby the isobaric specific heat in the nanofluids increases.[7,9,10] In this regard, Shin *et al.* suggested that this behaviour is due to the formation of a kind of internal structure in the heart of the nanofluid generated by the specific interaction between the nanoparticle and the base fluid.[10,59] This interaction depends on the characteristics of both and consequently will also influence the concentration of nanoparticles as it will affect the number of interactions produced and also the nanoparticle agglomerates formed in the heart of the fluid, as discussed earlier. For this reason, it is possible that certain concentrations lead to the most optimal situation in the system for obtaining the highest isobaric specific heat values, as is shown in Fig. 9.

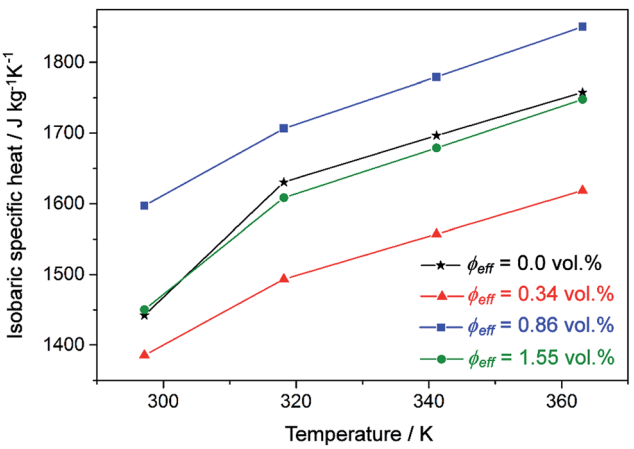

Fig. 9 Isobaric specific heat values for the nanofluids prepared.

Finally, different Figures of Merit (FoM) can be used to assess the improvement in the heat transfer processes of the nanofluid with regard to the base fluid. Two FoMs were analysed to take into account laminar and turbulent flow conditions. Under laminar flow conditions, the nanofluid is considered to improve the working conditions when the dynamic viscosity increase (DVI) is less than four times the thermal conductivity enhancement (TCE),[60] expressed mathematically as

$$\frac{\text{DVI}}{\text{TCE}} = \frac{(\mu_{nf} - \mu_{bf})/\mu_{bf}}{(k_{nf} - k_{bf})/k_{bf}} \leq 4 \quad (5)$$

In turn, under turbulent flow conditions, it is possible to analyse the ratio of the heat transfer coefficients. According to the Dittus–Boelter correlation, this heat transfer coefficient ratio is given by[61]

$$\frac{h_{nf}}{h_{bf}} = \left(\frac{\rho_{nf}}{\rho_{bf}}\right)^{0.8} \left(\frac{k_{nf}}{\rho k_{bf}}\right)^{0.6} \left(\frac{C_{P,nf}}{C_{P,bf}}\right)^{0.4} \left(\frac{\mu_{nf}}{\mu_{bf}}\right)^{-0.4} \quad (6)$$

where the variables have been defined above. The efficiency of the heat transfer process is usually considered to have improved when this ratio is greater than 1. Other figures of merit can be used to assess the improvement in the case of turbulent flow, such as the ratio of the Mouromtseff number, which provides similar results. An analysis of the ratio of the Mouromtseff number is shown in the ESI.† Thus, the FoMs were estimated for the nanofluids prepared at the temperatures at which the thermal conductivity and isobaric specific heat were measured. The dynamic viscosity and density values were estimated at the same temperatures. Fig. 10 shows the values obtained for the FoMs for laminar and turbulent flows, eqn (5) and (6), respectively. For laminar flows, all the nanofluids prepared achieve the condition shown in eqn (5), as is shown in Fig. 10A. Also, for the

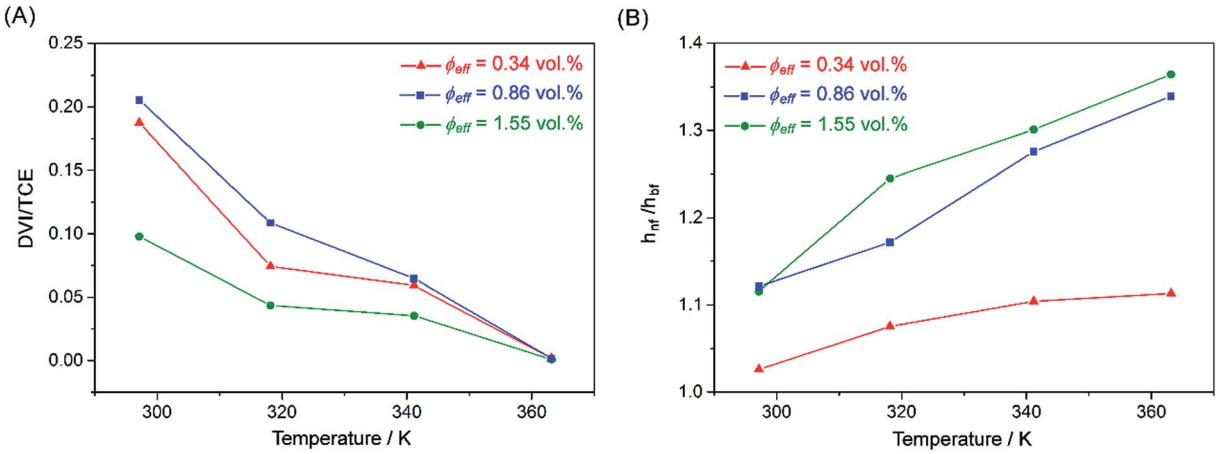

Fig. 10 (A) Ratio between the dynamic viscosity increase and the thermal conductivity enhancement. (B) Values of the ratio of the heat transfer coefficient of the nanofluids.

turbulent flows, the most interesting case for concentrating solar power applications, it is seen that there are improvements in the efficiency of the heat transfer process for all the nanofluids at all the temperatures assessed (see Fig. 10B). The nanofluid with the highest effective volume fraction showed the greatest enhancement – up to 36.5% – with regard to the base fluid. Thus, it can be concluded that the thermal properties of the nanofluids prepared are a drastic improvement over those of the base fluid and they could be a promising alternative as heat transfer systems in concentrating solar power applications.

3.4. Theoretical analysis: thermophysical properties

Taking into account the experimental results, a theoretical molecular dynamics study is an interesting way to study the behaviour of the Au-nanofluid system in the presence of a surfactant, something that, to our knowledge, has never been performed before. To this end, the Au-nanofluid system with the surfactant was studied and compared with the base fluid in a temperature range of *ca.* 50–600 K. Thus, the molecular dynamics calculations were performed in a temperature range of *ca.* 50–600 K. For the calculations, the mass concentration of 10.0×10^{-4} wt% for Au was chosen to ensure the representativeness of the nanoparticles in the nanofluid, taking into account the cost of the computation.

Fig. 11A shows the plot of the total energy *versus* temperature for the base fluid and for the Au-nanofluid system. Both systems reveal a linear tendency and the isobaric specific heat can be deduced from the slope (Fig. 11A). The isobaric specific heat values were 3.70×10^3 and 1.94×10^3 J kg^{-1} K^{-1} for the Au-nanofluid and the base fluid, respectively. However these values are higher than the experimental ones, which is typical when TraPPE force fields are used in molecular dynamics simulations, as reported elsewhere for Cu, Ni and Ag nanofluids.[5,62] The values obtained for isobaric specific heat for Au-nanofluids follow the same experimental trend in which $C_{p(\text{Au-nanofluid})} > C_{p(\text{base fluid})}$ in the case of the highest mass concentration of Au (see Fig. 9), which makes it possible to validate and continue using the theoretical model qualitatively.

Fig. 11B shows the thermal conductivity values *versus* temperature. The thermal conductivity was obtained using eqn (1) from the values of the diffusion coefficient, density and the

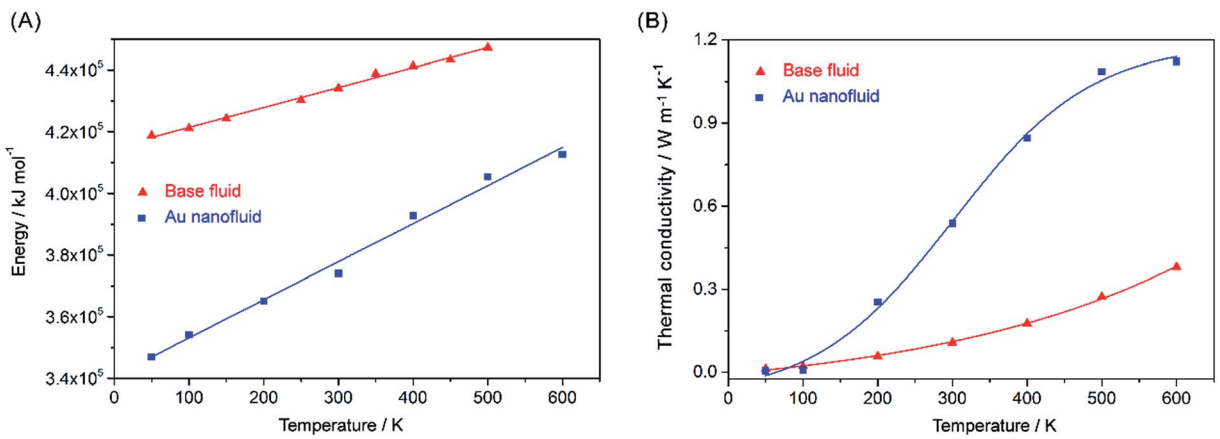

Fig. 11 (A) Plot of the energy *vs.* temperature, and (B) thermal conductivity *vs.* temperature for the base fluid (red) and Au-nanofluid (blue).

isobaric specific heat. A description related to the calculation of the diffusion coefficient is shown in the ESI.†

The thermal conductivity values obtained for the Au-nanofluid system at different temperatures appear to follow sigmoid dependence, while for the base fluid an exponential dependence is produced with temperature (Fig. 11B). Regarding the thermal conductivity, the greatest changes were produced between 300 and 600 K. Within this temperature range (300–600 K), the thermal conductivity values for the Au-nanofluid system were four times higher than those of the base fluid (Fig. 11B). High thermal conductivity values (Fig. 11B) are mainly associated with the high isobaric specific heat in the Au-nanofluid system, according to eqn (1). In this sense, the Brownian motion should play an important role in the increase of thermal conductivity with temperature, which is coherent with the experimental results shown before. This leads to the reasonable conclusion that the surfactant in these nanofluid systems must impede the freedom of movement of the gold in the base fluid at low temperatures. As a result, interparticle collisions are less frequent and so more energy is needed to increase the temperature of the system, which would explain the high isobaric specific heat value obtained (3.70×10^3 J kg^{-1} K^{-1}). As the temperature increases (300–600 K) the surfactant separates in a certain grade from the gold facilitating the movement of the system increasing the diffusivity and transport properties. This will be seen more clearly through the study of the structural properties below. This can be the reason for the increase of the thermal conductivity with temperature as shown from the experimental results, which is the opposite tendency to that observed for the base fluid (see Fig. 8A).

The theoretical results for thermal conductivity follow the same qualitative trend observed experimentally whereby the Au-nanofluid improves this property considerably. Thus, the results obtained from the classical molecular dynamics at low temperatures are in good agreement with the experimental tendency, which validates the model used.

3.5. Theoretical study: structural properties

To gain a clearer, molecular-level view of the Au-nanofluid and the role played by the surfactant, the radial distribution function (RDF) and spatial distribution function were analysed. For greater clarity, the RDFs and SDFs at the interaction sites have been recorded with regard to the centre of mass of the gold unit cell. Thus, any reference to Au in the discussion means the centre of mass of the unit cell.

To understand how the surfactant affects the Au-nanofluid system, a description will be given of the analysis corresponding to the interaction of the gold with the central N of the surfactant. Thus, the number of N atoms will give an account of the number of surfactant molecules around the gold, and it will be possible to see how this number changes as the temperature increases. Fig. 12A includes the RDF for the Au–N pair in the 50 to 600 K temperature range. At 50 K, the analysis of the RDF for the Au–N pair shows two defined peaks centred around 7.4 and 8.5 Å that integrate 2 N atoms (Fig. 12A). In the 50–200 K range, the two peaks and the values of their integrals remain, but they are shifted towards the Au until reaching a minimum distance at 300 K. The RDF at 300 K shows a wide peak centred around 6.7 Å that corresponds to 2 N atoms (Fig. 12A). However, a different situation can be observed in the 400–600 K range, where a main peak appears that varies a little with regard to the temperature. In all three cases, the peak remains centred around 8.5 Å and integrates 1 atom of N. The analysis of the

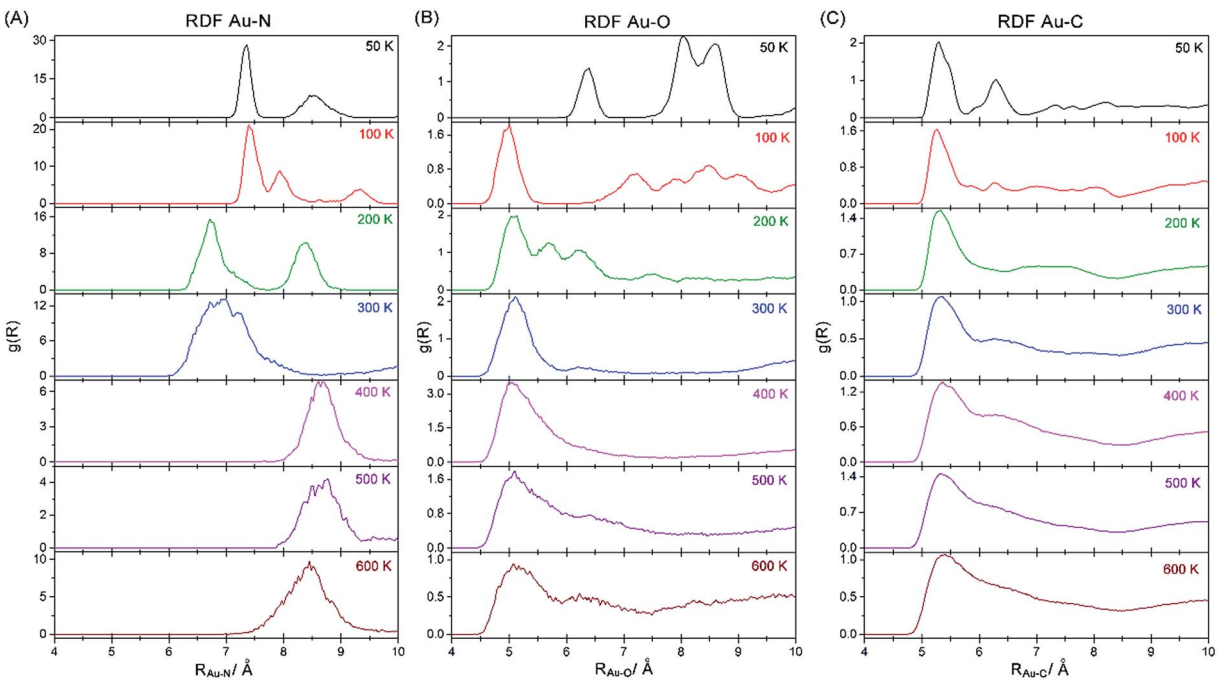

Fig. 12 RDFs of Au–N (A), Au–O (B) and Au–C (C) pairs in the 50–600 K range in the Au-nanofluid system.

RDF for the Au–N pair leads to the deduction that as the temperature rises, two surfactant molecules first move towards the gold unit cell (50–300 K) and then move away at high temperatures, leaving only one molecule in the second layer structure that is further from the cell (400–600 K), as the SDF analysis will show.

The presence of the surfactant affects the first and second layer structure of the base fluid molecules around the Au. Fig. 12B shows the RDF analysis of the Au–O pair in the 50–600 K range. At 50 K, a first peak stands out centred around 6.5 Å that corresponds to an O atom that belongs to a diphenyl oxide molecule. This intense peak indicates strong orientation binding.[63] The wide peaks from 7.5–9 Å correspond to O atoms from diphenyl oxide molecules in the second layer around the Au. In the 50–200 K range, the integration to 1 O atom is maintained, but the peaks are seen to converge until reaching a wide peak at 300 K. This peak is centred around 5.0 Å, and integrates two O atoms that correspond to two diphenyl oxide molecules. These two diphenyl oxide molecules are located closer to the gold cell. The wide peak centred at 5.0 Å remains in the 400–600 K temperature range but integrates four O atoms. The RDFs corresponding to the Au–C in the 50–600 K temperature range have been included in Fig. 12C. At all the temperatures, a more intense peak appears that is centred around 5.8 Å and starts to lose its structure as the temperature rises but does not change its position. In fact, at 50 K only, two more defined peaks centred around 5.8 and 6.5 Å appear. When integrated up to 6 Å at all the temperatures, these peaks correspond to 18 C atoms that must belong to diphenyl oxide and biphenyl molecules. As the temperature rises, the band width after 6 Å is indicative of a dynamic system in which there is movement of the C atoms. This is related to the diphenyl oxide molecules approaching the centre of masses of gold at high temperatures, as was shown in the analysis of the RDF of the Au–O pair.

The analysis of the RDF makes it clear that as the temperature increases the Au-nanofluid system undergoes molecular restructuring. An exchange takes place between the surfactant and diphenyl oxide molecules in two areas close to the gold unit cell that can be considered to be layers around the Au. At low temperatures, two surfactant molecules are located in the first layer closer to the gold unit cell. At 300 K there are two surfactant molecules and two diphenyl oxide molecules in the first layer around the gold unit cell. As the temperature rises, the two surfactant molecules become more distanced and two diphenyl oxide molecules approach the first layer. At higher temperatures, the surfactant recedes further until only one molecule occupies the second layer and four diphenyl oxide molecules remain within the first layer. Thus, some of the energy applied when the temperature rises must be used to restructure the system, which would explain the high isobaric specific heat and thermal conductivity values. These results reveal that the surfactant, used to prepare the Au-nanofluid, plays a greater role than that of a mere stabilizer of the system. Indeed, it is an effective component within the Au-nanofluid that contributes positively to efficient heat transfer processes.

By analysing the SDF it is possible to determine how the base fluid molecules and the surfactant are arranged around the Au. Fig. 13 shows the SDF for the Au-nanofluid system in a radius of 10 Å around the centre of mass of the gold unit cell (gold colour). By way of example, the SDFs of the temperatures 50, 300

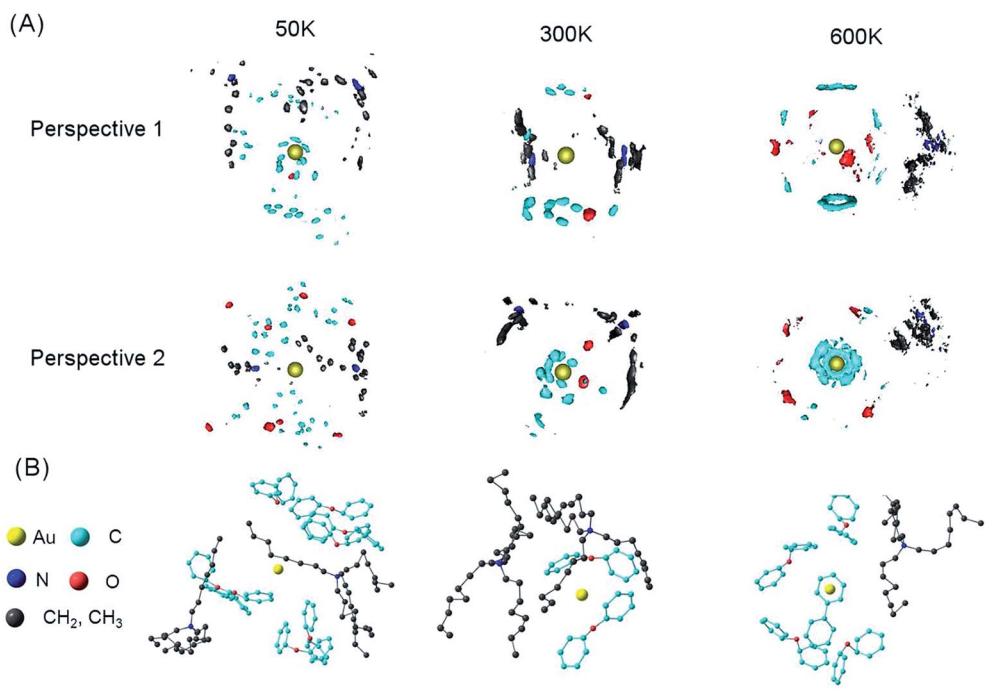

Fig. 13 (A) SDFs of the Au-nanofluid at different temperatures. Red: O atoms; sky-blue: C atoms; blue: N atoms; black: CH_2 and CH_3 groups. The hydrogen atoms were not included in the analysis of the SDF to keep the images clear. (B) Structure around the Au in the nanofluid system at different temperatures.

and 600 K were chosen as the representative of the change with temperature. This range was chosen to enable a greater clarity of the image of the first and second layer around the Au. At 50 K, it can be seen how the first layer around the centre of mass of the gold unit cell is mainly composed of two surfactant molecules (see Fig. 13), two N atoms (blue) and the carbon chains (black). They are arranged like arms around the metal. Further from the centre of mass are the O atoms (red) in an external layer (see Fig. 13). At 300 K, it is possible to see that in the first layer there are the two surfactant molecules with two O atoms (red colour) from the diphenyl oxide molecules that are oriented towards the centre. At 600 K, the surfactant occupies the second layer further from the centre of mass of the gold unit cell. Meanwhile, in the first layer four diphenyl oxide molecules remain as it is possible to see four red lobes oriented towards the centre of mass that belongs to four oxygen atoms. These are accompanied by an increase in the blue colour that corresponds to the ring C atoms, from the benzene rings of diphenyl oxide and biphenyl.

Based on all the information above, it is clear that the surfactant plays an active role in the Au-nanofluid system that contributes to more efficient heat transfer processes. Fig. 14 shows the movement of the surfactant from the first to the second layer around the Au cell in the nanofluid system as the temperature rises. It shows how the system has two surfactant molecules in the first layer around the Au cell in the 50 to 300 K temperature range. At high temperatures (400–600 K), a single surfactant molecule is located in the second layer further from the Au cell. Thus, it seems logical to think that the reorganisation of the surfactant and base fluid that occurs between the first and second layer around the Au unit cell is responsible for the enhanced thermal properties of the Au-nanofluid system. This structural arrangement (see Fig. 14) must generate a directionality of movement that involves effective heat transport, leading to increased thermal conductivity compared with the base fluid,[64] as was shown experimentally.

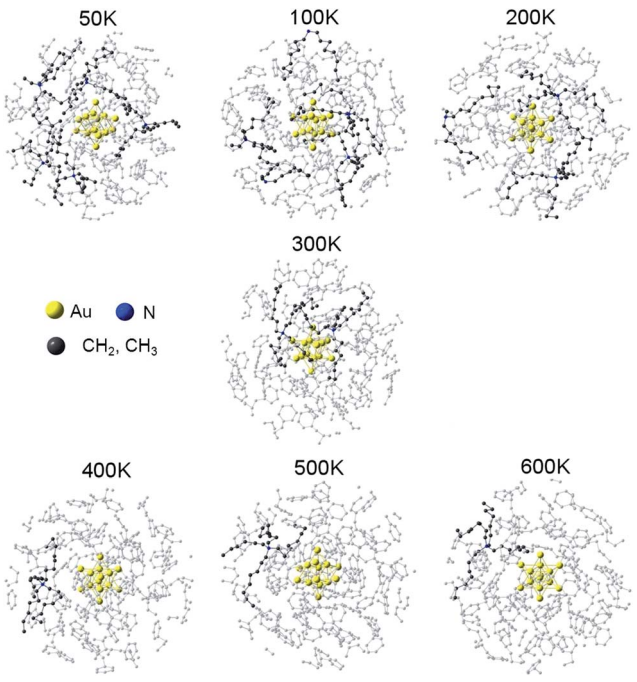

Fig. 14 Movement of the surfactant from the first to the second layer around the Au in the nanofluid system as the temperature rises.

4. Conclusions

This study presents the preparation and characterisation of Au nanoparticles and nanofluids based on these nanoparticles and on a non-polar heat transfer fluid normally used in CSP plants, composed of the eutectic mixture of biphenyl and diphenyl oxide.

The Au nanoparticles were synthesized in the heart of the HTF. The nanoparticles were characterised verifying the formation of metallic gold nanoparticles with an average size of around 10 nm. In turn, the nanofluids with varying concentrations of nanoparticles were characterised to assess their physical and chemical stability, and their thermal properties. The stability was analysed using UV-vis spectroscopy, and particle size and ζ potential measurements. It is possible to conclude that in the nanofluid with the lowest concentration the agglomerates form slowly, while at intermediate concentrations it is on the limit of what the system can support and for this reason some agglomerates precipitate but other larger ones do not, possibly because they do not have a higher concentration of nanoparticles. Finally, in the nanofluid with the highest concentration there is a high agglomeration and sedimentation rate due to the high concentration of nanoparticles.

In addition, the efficiency of the nanofluids in heat transfer processes was studied by measuring their different properties, such as density, viscosity, isobaric specific heat and thermal conductivity. The most outstanding results observed were that the thermal conductivity of the nanofluid was 70% higher than that of the base fluid, and the isobaric specific heat was also 10% higher. In turn, their efficiency in heat transfer processes was assessed by means of the Dittus–Boelter correlation, comparing the heat transfer coefficients of the nanofluids with those of the base fluid. The heat transfer coefficient was up to 36% higher in the nanofluids. These results lead us to believe that the nanofluids prepared in this study could be a promising alternative to the HTF often used in CSP plants.

The results of the molecular dynamics study show that the thermal conductivity and isobaric specific heat follow the same tendency as the experimental results. The structural analysis shows that the surfactant plays an active role in the Au-nanofluid system. It contributes positively more efficient heat transfer processes. This enhancement is the result of a structural reorganisation at the molecular level of the surfactant and the base fluid around the Au as the temperature rises. Two surfactant molecules are exchanged for four diphenyl oxide molecules in the first layer structure around the gold. This structural arrangement leads to a directionality of movement favouring effective heat transport. Furthermore, some of the energy applied when the temperature rises must be used to restructure the system, which would explain the higher isobaric specific heat and thermal conductivity values compared with

those of the base fluid. Therefore, the molecular dynamics results make it possible to extrapolate that the Au-nanofluid system could be valid for use as a high temperature fluid for CSP. To our knowledge, this is the first time an analysis of this kind that takes into account the surfactant for this kind of nanofluid systems has been performed.

Acknowledgements

We thank the Ministerio de Economia y Competitividad (MINECO) of the Spanish Government for funding under Grant No. ENE2014-58085-R. Calculations were made through CICA – Centro Informático Científico de Andalucía (Spain). Antonio Sánchez-Coronilla thanks VPPI-US for the financial support.

References

1 J. Khan and M. H. Arsalan, *Renewable Sustainable Energy Rev.*, 2016, **55**, 414–425.
2 V. Devabhaktuni, M. Alam, S. S. S. R. Depuru, R. C. Green, D. Nims and C. Near, *Renewable Sustainable Energy Rev.*, 2013, **19**, 555–564.
3 U. Desideri, F. Zepparelli, V. Morettini and E. Garroni, *Appl. Energy*, 2013, **102**, 765–784.
4 A. Mwesigye, Z. J. Huan and J. P. Meyer, *Appl. Energy*, 2015, **156**, 398–412.
5 J. Navas, A. Sánchez-Coronilla, E. I. Martín, M. Teruel, J. J. Gallardo, T. Aguilar, R. Gómez-Villarejo, R. Alcántara, C. Fernández-Lorenzo, J. C. Piñero and J. Martín-Calleja, *Nano Energy*, 2016, **27**, 213–224.
6 K. S. Suganthi, V. L. Vinodhan and K. S. Rajan, *Appl. Energy*, 2014, **135**, 548–559.
7 P. Andreu-Cabedo, R. Mondragon, L. Hernandez, R. Martinez-Cuenca, L. Cabedo and J. E. Julia, *Nanoscale Res. Lett.*, 2014, **9**, 582.
8 S. Lee, S. U. S. Choi, S. Li and J. A. Eastman, *J. Heat Transfer*, 1999, **121**, 280–289.
9 H. M. Nieh, T. P. Teng and C. C. Yu, *Int. J. Therm. Sci.*, 2014, **77**, 252–261.
10 D. Shin and D. Banerjee, *Int. J. Heat Mass Transfer*, 2014, **74**, 210–214.
11 D. Singh, E. V. Timofeeva, M. R. Moravek, S. Cingarapu, W. H. Yu, T. Fischer and S. Mathur, *Sol. Energy*, 2014, **105**, 468–478.
12 M. Chandrasekar, S. Suresh and T. Senthilkumar, *Renewable Sustainable Energy Rev.*, 2012, **16**, 3917–3938.
13 E. V. Timofeeva, W. H. Yu, D. M. France, D. Singh and J. L. Routbort, *Nanoscale Res. Lett.*, 2011, **6**, 182.
14 D. H. Yoo, K. S. Hong and H. S. Yang, *Thermochim. Acta*, 2007, **455**, 66–69.
15 J. A. Eastman, S. U. S. Choi, S. Li, W. Yu and L. J. Thompson, *Appl. Phys. Lett.*, 2001, **78**, 718–720.
16 C. X. Wang, J. Yang and Y. L. Ding, *Prog. Nat. Sci. Mater.*, 2013, **23**, 338–342.
17 W. S. Sarsam, A. Amiri, M. N. M. Zubir, H. Yarmand, S. N. Kazi and A. Badarudin, *Colloids Surf., A*, 2016, **500**, 17–31.
18 S. A. Angayarkanni and J. Philip, *Adv. Colloid Interface Sci.*, 2015, **225**, 146–176.
19 R. C. Murdock, L. Braydich-Stolle, A. M. Schrand, J. J. Schlager and S. M. Hussain, *Toxicol. Sci.*, 2008, **101**, 239–253.
20 N. Rai and J. I. Siepmann, *J. Phys. Chem. B*, 2007, **111**, 10790–10799.
21 N. Rai and J. I. Siepmann, *J. Phys. Chem. B*, 2013, **117**, 273–288.
22 M. G. Martin and J. Ilja Siepmann, *J. Phys. Chem. B*, 1998, **102**, 2569–2577.
23 M. G. Martin and J. Ilja Siepmann, *J. Phys. Chem. B*, 1999, **103**, 4508–4517.
24 C. D. Wick, J. M. Stubbs, N. Rai and J. Ilja Siepmann, *J. Phys. Chem. B*, 2005, **109**, 18974–18982.
25 M. Neek-Amal, R. Asgari and M. R. Rahimi Tabar, *Nanotechnology*, 2009, **20**, 135602.
26 W. Smith and T. R. Forester, *J. Mol. Graphics*, 1996, **14**, 136–141.
27 J. M. Martinez and L. Martinez, *J. Comput. Chem.*, 2003, **24**, 819–825.
28 M. P. Allen and D. J. Tildesley, *Computer Simulation of Liquids*, Clarendon, Oxford, 1989.
29 M. P. Casaletto, A. Longo, A. Martorana, A. Prestianni and A. M. Venezia, *Surf. Interface Anal.*, 2006, **38**, 215–218.
30 B. Koslowski, H. G. Boyen, C. Wilderotter, G. Kastle, P. Ziemann, R. Wahrenberg and P. Oelhafen, *Surf. Sci.*, 2001, **475**, 1–10.
31 A. K.-V. A. V. G. Naumkin, S. W. Gaarenstroom and C. J. Powell, in *NIST Standard Reference Database 20, Version 4.1*, Gaithersburg, 2012.
32 V. Bondarenka, Z. Martunas, S. Kaciulis and L. Pandolfi, *J. Electron Spectrosc. Relat. Phenom.*, 2003, **131**, 99–103.
33 D. Briggs, R. A. Marbrow and R. M. Lambert, *Surf. Sci.*, 1977, **65**, 314–324.
34 Q. H. Wu, A. Thissen and W. Jaegermann, *Appl. Surf. Sci.*, 2005, **252**, 1801–1805.
35 S. Mondal, U. Rana, R. R. Bhattacharjee and S. malik, *RSC Adv.*, 2014, **4**, 57282–57289.
36 N. K. Sadanandhan and S. J. Devaki, *J. Appl. Polym. Sci.*, 2017, 44351, DOI: 10.1002/APP.44351.
37 H.-J. Chen and D. Wen, *Nanoscale Res. Lett.*, 2011, **6**, 198.
38 W. Yu and H. Q. Xie, *J. Nanomater.*, 2012, **2012**, 435873.
39 S. Chakraborty, I. Sarkar, K. Haldar, S. K. Pal and S. Chakraborty, *Appl. Clay Sci.*, 2015, **107**, 98–108.
40 H. T. Zhu, Y. S. Lin and Y. S. Yin, *J. Colloid Interface Sci.*, 2004, **277**, 100–103.
41 Y. Hwang, J. K. Lee, C. H. Lee, Y. M. Jung, S. I. Cheong, C. G. Lee, B. C. Ku and S. P. Jang, *Thermochim. Acta*, 2007, **455**, 70–74.
42 B. G. Wang, X. B. Wang, W. J. Lou and J. C. Hao, *J. Colloid Interface Sci.*, 2011, **362**, 5–14.
43 S. K. Das, S. U. S. Choi, W. Yu and T. Pradeep, *Nanofluids: Science and Technology*, John Wiley & Sons, Inc., Hoboken, New Jersey, USA, 2008.
44 L. Fedele, L. Colla, S. Bobbo, S. Barison and F. Agresti, *Nanoscale Res. Lett.*, 2011, **6**, 300.

45 S. S. Pati, V. Mahendran and J. Philip, *J. Nanofluids*, 2013, **2**, 94–103.
46 M. J. Pastoriza-Gallego, C. Casanova, R. Paramo, B. Barbes, J. L. Legido and M. M. Pineiro, *J. Appl. Phys.*, 2009, **106**, 064301.
47 D. R. Lide, *CRC Handbook of Chemistry and Physics*, CRC Press, Boca Raton, Florida, USA, 90th edn, 2009.
48 H. Y. Chen, S. Witharana, Y. Jin, Y. L. Ding and C. Kim, *Predicting the thermal conductivity of nanofluids based on suspension rheology*, Sri Lanka, 2008.
49 J. W. Goodwin and R. W. Hughes, *Rheology for Chemists: an Introduction*, The Royal Society of ChemistrY, Cambridge, UK, 2nd edn, 2008.
50 S. Witharana, H. S. Chen and Y. L. Ding, *Nanoscale Res. Lett.*, 2011, **6**, 231.
51 A. Einstein, *Ann. Phys.*, 1906, **19**, 289–306.
52 H. C. Brinkman, *J. Chem. Phys.*, 1952, **20**, 571.
53 R. L. Hamilton and O. K. Crosser, *Ind. Eng. Chem. Fundam.*, 1962, **1**, 187–191.
54 J. Koo and C. Kleinstreuer, *J. Nanopart. Res.*, 2004, **6**, 577–588.
55 R. S. Vajjha and D. K. Das, *Int. J. Heat Mass Transfer*, 2012, **55**, 4063–4078.
56 R. S. Vajjha and D. K. Das, *Int. J. Heat Mass Transfer*, 2009, **52**, 4675–4682.
57 D. Cabaleiro, C. Gracia-Fernandez, J. L. Legido and L. Lugo, *Int. J. Heat Mass Transfer*, 2015, **88**, 872–879.
58 N. S. S. Mousavi and S. Kumar, *Int. J. Therm. Sci.*, 2014, **84**, 267–274.
59 D. Shin and D. Banerjee, *J. Heat Transfer*, 2013, **135**, 032801.
60 R. Prasher, D. Song, J. L. Wang and P. Phelan, *Appl. Phys. Lett.*, 2006, **89**, 133108.
61 F. W. Dittus and L. M. K. Boelter, *Univ. Calif. Publ. Eng.*, 1930, **2**, 443–461.
62 R. Gomez-Villarejo, E. I. Martín, J. Navas, A. Sánchez-Coronilla, T. Aguilar, J. J. Gallardo, R. Alcántara, D. M. De los Santos, I. Carrillo-Berdugo and C. Fernández-Lorenzo, *Appl. Energy*, 2017, **194**, 19–29.
63 H. V. R. Annapureddy, S. K. Nune, R. K. Motkuri, B. P. McGrail and L. E. X. Dang, *J. Phys. Chem. B*, 2015, **119**, 8992–8999.
64 J. Philip, P. D. Shima and B. Raj, *Appl. Phys. Lett.*, 2007, **91**, 203108.

Annex 4

Towards the improvement of the global efficiency of Concentrating Solar Power plants by using Pt-based nanofluids: The internal molecular structure effect

Applied Energy 228 (2018) 2262–2274

Contents lists available at ScienceDirect

Applied Energy

journal homepage: www.elsevier.com/locate/apenergy

Towards the improvement of the global efficiency of concentrating solar power plants by using Pt-based nanofluids: The internal molecular structure effect

Roberto Gómez-Villarejo[a], Elisa I. Martín[b], Antonio Sánchez-Coronilla[c,*], Teresa Aguilar[a], Juan Jesús Gallardo[a], Paloma Martínez-Merino[a], Iván Carrillo-Berdugo[a], Rodrigo Alcántara[a], Concha Fernández-Lorenzo[a], Javier Navas[a,*]

[a] Departamento de Química Física, Facultad de Ciencias, Universidad de Cádiz, E-11510 Puerto Real (Cádiz), Spain
[b] Departamento de Ingeniería Química, Facultad de Química, Universidad de Sevilla, E-41012 Sevilla, Spain
[c] Departamento de Química Física, Facultad de Farmacia, Universidad de Sevilla, E-41012 Sevilla, Spain

HIGHLIGHTS

- The thermal conductivity was improved up to 37%.
- The heat transfer coefficient was improved by 20%.
- Pt-based nanofluid improves the heat transfer process in Concentrating Solar Power.
- ODT and DDA was used as surfactants, playing an important role in the properties.
- The internal molecular structure is revealed from MD results.

GRAPHICAL ABSTRACT

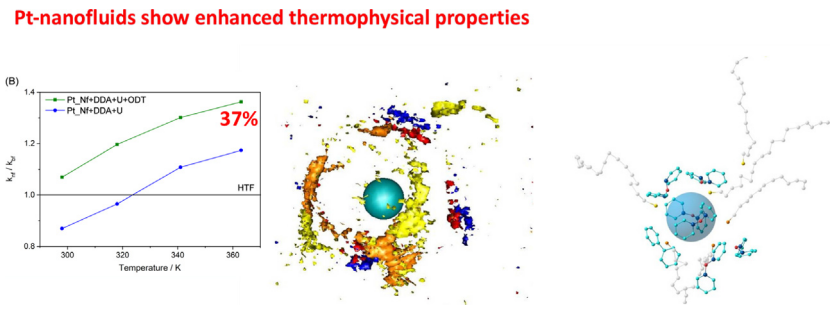

ARTICLE INFO

Keywords:
Concentrating solar power
Nanofluids
Thermophysical properties
Molecular dynamics

ABSTRACT

Nanofluids are a promising alternative to the typical heat transfer fluid (HTF) used in concentrating solar power (CSP) plants, possibly improving their global efficiency and leading to the increase the use of renewable clean energy. This study analyses nanofluids based on a typical HTF used in CSP and Pt nanoparticles. Pt nanoparticles were synthesized and dispersed in the base fluid. Dodecylamine (DDA) was used as a phase transfer and as a surfactant. Also, 1-octadecanethiol (ODT) was added as a surfactant and pulsed ultrasonication was used to disperse the nanoparticles. As the base fluid, the eutectic mixture of diphenyl oxide (73.5%) and biphenyl (26.5%) was used. This fluid is typically used in CSP plants based on parabolic through collectors. The stability of the nanofluids was analysed according to the kind of surfactant and ultrasonication process. Furthermore, to analyse the efficiency of the nanofluids, several properties were measured, including density, dynamic viscosity, isobaric specific heat and thermal conductivity. We found an increase in thermal conductivity of up to 37%, and the heat transfer coefficient also improved by up to 20%. Molecular dynamics calculations were performed to determine how the inclusion of ODT affected the system. ODT competes with DDA to interact with the Pt, forming a lattice around the Pt. The base fluid molecules, and in particular the diphenyl oxide molecules, take advantage of this competition to move closer to the Pt. This movement of molecules as the temperature rise must be Brownian in nature and enhances the heat transfer processes, improving the thermal properties of the nanofluids with both ODT and DDA compared with those prepared only with DDA. Thus, nanofluids with ODT and DDA would appear to be of interest for use in CSP.

* Corresponding authors.
E-mail addresses: antsancor@us.es (A. Sánchez-Coronilla), javier.navas@uca.es (J. Navas).

https://doi.org/10.1016/j.apenergy.2018.07.062
Received 6 March 2018; Received in revised form 27 June 2018; Accepted 14 July 2018

1. Introduction

Today's ever-growing society requires increasing amounts of energy, while being committed to reducing environmental problems, pollution, global warming, etc. [1]. Given the possible imminent end to the age of fossil fuels for electricity generation, renewable energy sources have grown in importance due to their social acceptance and capacity to generate sustainable energy to cater for the world's electricity requirements. In this sense, solar energy is an important option and being the most available energy source on the planet concentrating solar power (CSP) has emerged as an attractive source of clean and renewable energy [2,3]. In this technology, high temperatures must be reached and CSP systems achieve this by focussing solar radiation on the receivers, transforming solar radiation into thermal energy [3,4]. Several kinds of receivers have been designed to collect the maximum radiation. They are classifying with regard to the focus geometry as point- and line-focus concentrators. Solar tower system is an example of point focus concentrations, while linear Fresnel and parabolic-trough collectors (PTC) are typical line-focus concentrators [4,5]. Thus, PTCs are one of the systems generating the most commercial interest [2,5]. Typically, the PTC solar field is integrated in a steam turbine plant indirectly, by heating thermal oil (a Heat Transfer Fluid, HTF) for generating steam in a heat exchanger (HTF technology) [4].

In recent years, nanofluids have received considerable attention as a promising alternative to the heat transfer fluids (HTF) commonly used in CSP because the colloidal suspension of nanosized particles in a base fluid enhances its thermal properties such as thermal conductivity [6–10] or isobaric specific heat [8,11–13]; it also improves heat transfer processes [8,13–16]. Recently, nanofluids are being used as another kind of selectively absorber material for spectral splitting PV/T application or as direct absorber for CSP. Some researchers have been performed on direct absorption solar collectors using nanofluids [17,18]. Mu et al. [19] reported the use of nanoparticles, such as SiO_2, TiO_2, ZrC, AlN and TiN, as the base fluid spectral splitting filter. Furthermore, An et al. studied that the particle concentration in spectral splitting PV/T system affects the efficiency, obtaining an enhancement in the global efficiency at about 13.3% for hybrid PV/T system with a low concentration polypyrrole nanofluid filter [20], and about 17.9% with Cu_9S_5 nanofluid filter [21]. Regarding nanofluids as HTF in CSP applications, there are many studies in the literature about nanofluids based on water and ethylene glycol as a base fluid but comparatively few articles about nanofluids using the typical HTFs used in CSP as a base fluid. Some studies based on metallic nanoparticles [8,13–15] or metal oxide nanoparticles [5,22,23] showing improved thermal properties for nanofluids prepared using a typical HTF of CSP plants have been reported.

Thus, the review of the literature reveals that CSP is one of the most promising alternatives to conventional energy sources nowadays, and that the use of nanofluids can improve the global efficiency of this technology. The use of nanofluids within the heat transfer energy market is forecast to increase by over 2 billion dollars in the future, making it a promising field of study [24]. Thus, effective nanofluids are candidates for being considered as value-added materials that produce a decreased impact on the environment [25,26].

Therefore, this study analyses nanofluids based on a HTF typically used in CSP plants. This HTF is a eutectic mixture of two stable compounds: biphenyl ($C_{12}H_{10}$, 26.5%) and diphenyl oxide ($C_{12}H_{10}O$, 73.5%). Platinum nanoparticles were used as the nanomaterial to prepare the nanofluid. Metal nanoparticles are known to increase the thermal conductivity of base fluid [8–10,13,15,27]. Low concentrations were used since, apart from significantly enhancing thermal properties, they can also lead to increases in viscosity, an undesirable property. Moreover, the addition of surfactants and the use of ultrasound power for preparing nanofluids were analysed. Both actions were studied independently and collectively in the nanofluids prepared, which were characterized for their chemical and physical stability, density, viscosity, isobaric specific heat and thermal conductivity. The surfactants used were dodecylamine ($CH_3(CH_2)_{11}NH_2$, DDA), and 1-octadecanothiol ($CH_3(CH_2)_{17}SH$, ODT). The DDA surfactant was incorporated in all the systems studied and the use of ultrasound power was found to improve their stability. Likewise, Pt nanofluids prepared with ODT showed enhanced thermal properties. Bearing these results in mind, molecular dynamics studies were performed to obtain a molecular understanding of the effect of the ODT on the nanofluids. To this end, a comparison was performed of the system solely with DDA and the one with both DDA and ODT to see how their internal structures varied at different temperatures. The results obtained show the existence of a molecular lattice in which the ODT surfactant plays an important role allowing the diphenyl oxide molecules to approach the Pt cell, thus enhancing the heat flow. This system permits greater heat transfer, which is involved in the enhanced thermal properties of these systems for their use in CSP. Therefore, the main novelty of this work is the significant improvement in heat transfer processes using a specific configuration considering the base fluid, the nanomaterial, the surfactants and the preparation process. Also, the analysis of the effect of the surfactants in thermal properties leads to understand the behaviour of the nanofluid systems prepared.

2. Materials and methods

2.1. Preparation of Pt nanoparticles and nanofluids

The nanofluids were prepared following a two-step method [28]: the first step involves the synthesis of nanosized material, and second step the dispersion of this nanomaterial into a base fluid.

For the synthesis of the Pt nanoparticles, chloroplatinic acid hydrate (H_2PtCl_6, 38% Pt basis, Sigma-Aldrich) was used as a Pt precursor. This precursor was reduced by the reducing agent, sodium borohydride ($NaBH_4$, purity > 98%, Fluka Sigma-Aldrich) to produce Pt nanoparticles [29–31]. A volume of 10 mL of aqueous sodium borohydride solution (27 mM) was added slowly to 5 mL of aqueous chloroplatinic acid hydrate (14 mM). The reaction was carried out in a low-power ultrasonic bath. Next, this solution was added to 100 mL of a commercial heat transfer fluid (HTF) used as a base fluid, a eutectic mixture of biphenyl ($C_{12}H_{10}$, 26.5%) and diphenyl oxide ($C_{12}H_{10}O$, 73.5%) supplied by Dowtherm©. This fluid is typically used in CSP plants based on parabolic through collectors. Also, dodecylamine ($(CH_3(CH_2)_{11}NH_2)$, DDA, purity > 98%, Sigma-Aldrich) was added to the base fluid as a phase transfer agent in a 2:1 ratio with regard to the initial amount of Pt. The mixture was left magnetically stirring for one hour and the aqueous phase was discarded. Phase transfer may be considered to be complete when the aqueous solution changes colour from the black of the initial solution containing platinum to the transparent aqueous phase, which is discarded.

Three nanofluids were prepared following this method, two with the addition of the surfactant. 1-Octadecanothiol ($(CH_3(CH_2)_{17}SH)$, ODT, purity > 98%, Sigma-Aldrich) was added in a 3:1 ratio with regard to the initial amount of Pt, and subsequently stirred for one hour. One of these nanofluids was treated under pulse ultrasonication at 30% output power for 45 min. The other nanofluid was not treated with sonication in order to analyse the effect of the sonication process. Finally, the third nanofluid was prepared without surfactant and was treated with sonication following the same procedure described above. Table 1 shows information for each nanofluid in more detail.

Finally, the nominal Pt concentration for all the nanofluids was 0.005 wt.%.

2.2. Characterization of nanoparticles and nanofluids

Concerning the characterization of the nanoparticles synthesized, the nanofluids were centrifuged and the supernatant liquid was eliminated. The black dust obtained was cleaned with acetone in successive

Table 1
Identification and treatment of each nanofluid.

Identification	Base fluid + DDA	ODT	Ultrasonic power
Pt_Nf + DDA + ODT	✓	✓	X
Pt_Nf + DDA + U	✓	X	✓
Pt_Nf + DDA + U + ODT	✓	✓	✓

extractions. X-ray photoelectron spectroscopy (XPS) was used to check the chemical state bonding and the oxidation state of the nanoparticles extracted. In addition, the size and morphology of the nanoparticles was studied by transmission electron microscopy (TEM). Finally, X-ray diffraction (XRD) pattern was obtained to study the crystalline structure.

The improvement in the overall efficiency of nanofluids is a result of significantly enhancing their thermal properties. However, this efficiency also depends on their stability. Several techniques were used to analyse the chemical and physical stability of the nanofluids over time. UV–Vis spectroscopy allows for the evaluation of the sedimentation process and therefore the stability of nanofluids [32]. To this end, UV–Vis spectra were recorded in the wavelength range from 350 to 880 nm to analyse the presence of Pt nanoparticles in suspension. A system was used composed of a halogen lamp, model DH-2000-BAL, supplied by Ocean Optics©, as the illumination source, and a USB200 + spectrometer supplied by Ocean Optics©. The particle size and size distribution were measured by dynamic light scattering (DLS), a common technique for analysing colloidal systems [33,34]. Also, ζ potential measurements were performed to evaluate and understand the interactions between the particles in suspension and therefore the agglomeration process. A zetasizer Nano ZS system supplied by Malvern© was used to perform both measurements.

Several properties were analysed to evaluate the efficiency of the nanofluids prepared. Density was determined using a pycnometer and dynamic viscosity was measured by a SV-10 Viscometer supplied by Malvern Instruments Ltd. The density and viscosity measurements were performed five times at room temperature to calculate the average values. Isobaric specific heat measurements were performed using a temperature modulated differential scanning calorimeter (TMDSC), model Q-20, supplied by TA Instruments©. To perform the measurements, a program was created that can be summed up as: the temperature was equilibrated at 341 K to remove contaminants and kept isothermal for 10 min; then the samples were equilibrated at 301 K and then ramped to 391 at a rate of 1 K/min. A modulation was programmed around the studied temperatures with an amplitude of ± 1 K and a period of 120 s. Finally, cooling was performed at 1 K/min. The isobaric specific heat of the base fluid was measured to verify the method used with regard to the values reported by the supplier. Thermal conductivity was measured by the laser flash technique (LFA) using the 1600 model supplied by Linseis Thermal Analysis©. To be precise, this technique measures thermal diffusivity, which is another thermophysical property that defines the speed of heat propagation by conduction during changes of temperatures or how quickly a material reacts to a change in temperature. According to Standard ASTM E 1461-01, thermal conductivity may be calculated by the equation:

$$k(T) = D(T)\cdot C_P(T)\cdot \rho(T) \quad (1)$$

where k is the thermal conductivity, D is the thermal diffusivity, C_P is the isobaric specific heat and ρ is the density.

2.3. Computational framework

The Transferable Potentials for Phase Equilibria (TraPPE) force field were used. The transferable potentials for phase equilibria-explicit-hydrogen (TraPPE-EH) force field [35,36] were used to describe the intra- and intermolecular interactions of the molecules of the base fluid (diphenyl oxide/biphenyl blend). This force field considers aromatic ring and directly linked atoms as rigid entities. The phenyl rings were treated as rigid but were allowed to rotate with regards to each other around the C2C1–C1′C2′ bond of the biphenyls (see Tables S1 and S2 in the Supplementary Material). The Transferable Potentials for Phase Equilibria-United Atom force field (TraPPE-UA) [37–39] was used for describing both intramolecular and intermolecular interactions of the DDA and ODT surfactants. TraPPE-UA force field treats the alkyl groups as a fully flexible model based on single interaction sites (pseudo-atoms). A pseudo-atom represents a carbon atom together with all of its bonded hydrogen atoms (CH_x = CH_2 or CH_3) and treats the nitrogen, sulphur and the carbon atoms as explicit interaction sites in a rigid unit (see Table S3 in the Supplementary Material).

A rigid unit cell of 14Pt atoms with the space group *Fm*-3*m* was used to perform the simulation of the metal nanoparticle [40]. The non-bonded force field was described from adopting the setting parameters reported elsewhere [41].

The TraPPE-EH and TraPPE-UA force fields and the non-bonded force field of the metal nanoparticle use Lennard-Jones (LJ) and Coulomb potentials to represent the non-bonded interactions

$$u(r_{ij}) = 4\varepsilon_{ij}\left[\left(\frac{\sigma_{ij}}{r_{ij}}\right)^{12} - \left(\frac{\sigma_{ij}}{r_{ij}}\right)^{6}\right] + \frac{q_i q_j}{4\pi\varepsilon_0 r_{ij}} \quad (2)$$

where r_{ij}, ε_{ij}, σ_{ij}, q_i, q_j, and ε_0 are the distances between interaction sites i and j, the LJ well depth, the LJ diameter, the partial charges on interaction sites i and j, and the permittivity of vacuum, respectively. The

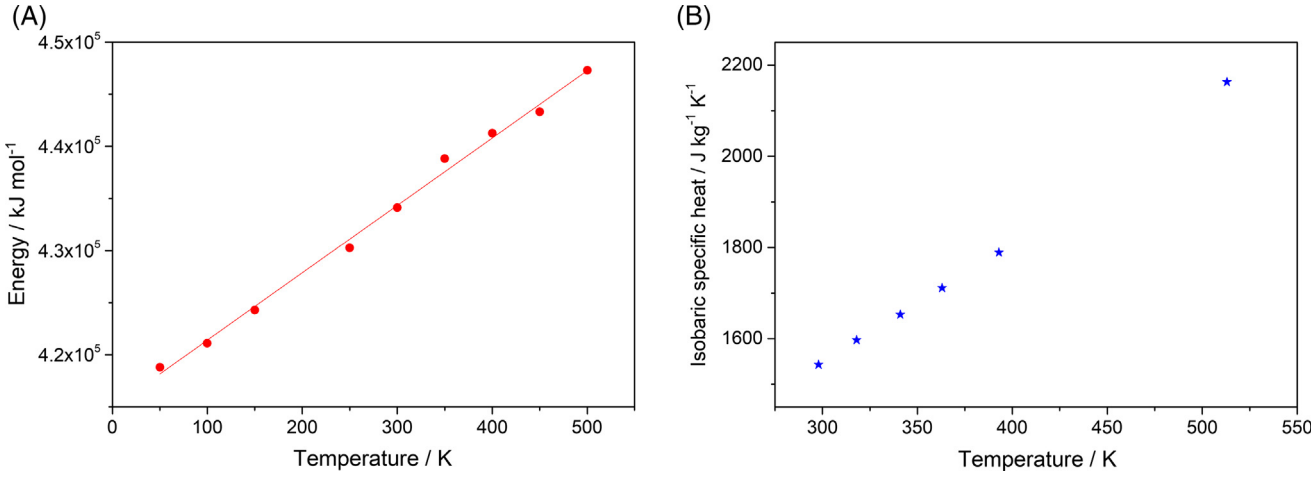

Fig. 1. Plot of energy versus temperature (A), and plot of experimental isobaric specific heat at different working temperatures (B).

Lorentz-Berthelot combining rules were used to determine LJ parameters for unlike interactions (see Table S4 in the Supplementary Material).

The DLPOLY code [42] was used to carry out the molecular dynamics simulations. The canonical ensemble (NVT) was applied in all the simulations performed by using periodic boundary conditions and a Nose-Hoover thermostat. A cubic box providing the initial configuration was built with the PACKMOL code [43]. The length of the box sides was chosen to keep the density of the experimental HTF at 298 K. The Ewald sum methodology [44] was applied to account for electrostatic interactions using a cut-off distance of 9 Å in all the cases. The simulations run lasted for 1 ns employing a time step of 0.5 fs and the structures were saved every 100 time steps for analysing the trajectory. For validate the system, molecular dynamic calculations were performed at different temperatures ranging from *c.a.* 50–500 K for the HTF used as a base fluid (diphenyl oxide/biphenyl blend). Fig. 1A shows the plot the total energy versus temperature from molecular dynamic simulations while Fig. 1B shows the experimental isobaric specific heat values at different working temperatures. These values agree with the data described in technical datasheet of the heat transfer fluid [45]. From Fig. 1A, the slope of the plot of total energy versus temperature led to the isobaric specific heat value of $1.94{\cdot}10^3\,J\,kg^{-1}\,K^{-1}$. This value, although slightly higher, is in good agreement with the average value of the experimental HTF up to 500 K (c.a. $1.74{\cdot}10^3\,J\,kg^{-1}\,K^{-1}$) obtained from the data of Fig. 1B which validates both the proposed model and the election of TraPPE force fields indicated for the prediction of thermophysical properties [35–39,45]. The slight overestimation of the isobaric specific heat values as compared to the experimental ones have also been reported for other systems when TraPPE force fields are used in molecular dynamics simulations [8,14,15,46].

3. Results and discussion

3.1. Characterization of Pt nanoparticles

Several techniques were used to determine whether Pt nanoparticles were obtained, including XRD, XPS and TEM. The XRD pattern obtained is shown in Fig. 2A. It revealed three peaks at 2θ = 40.25, 46.81 and 68.36°, which are representative of Pt nanoparticles. These peaks are assigned to the reflection of the planes (1, 1, 1), (2, 0, 0) and (2, 2, 0) belonging to *Fm3m* space group of cubic structures from metallic Pt [47,48]. Fig. 2B shows the signal for Pt 4f obtained from the X-ray photoelectron spectrum. The signal for Pt $4f_{7/2}$ appears at a binding energy (BE) at about 70.8 eV, which is coherent with presence of metallic Pt [49]. As reported previously, the Pt $4f_{7/2}$ signal for Pt (II) and Pt(IV) in oxide form appears typically at about 72.4 eV and 74.9 eV [49]. Also, the separation of the spin-orbit components obtained is 3.4 eV, which is coherent with the typical value in the literature (3.35 eV) [49]. Therefore, XPS shows a majority presence of Pt(0) in the solid synthesized. Finally, the particle size distribution is obtained from TEM images (see Fig. 2C and D). The size-distribution of the Pt nanoparticles was found to be non-uniform, sizes ranging between 5 and 35 nm, as Fig. 2D shows. The size of some nanoparticles fell outside this range.

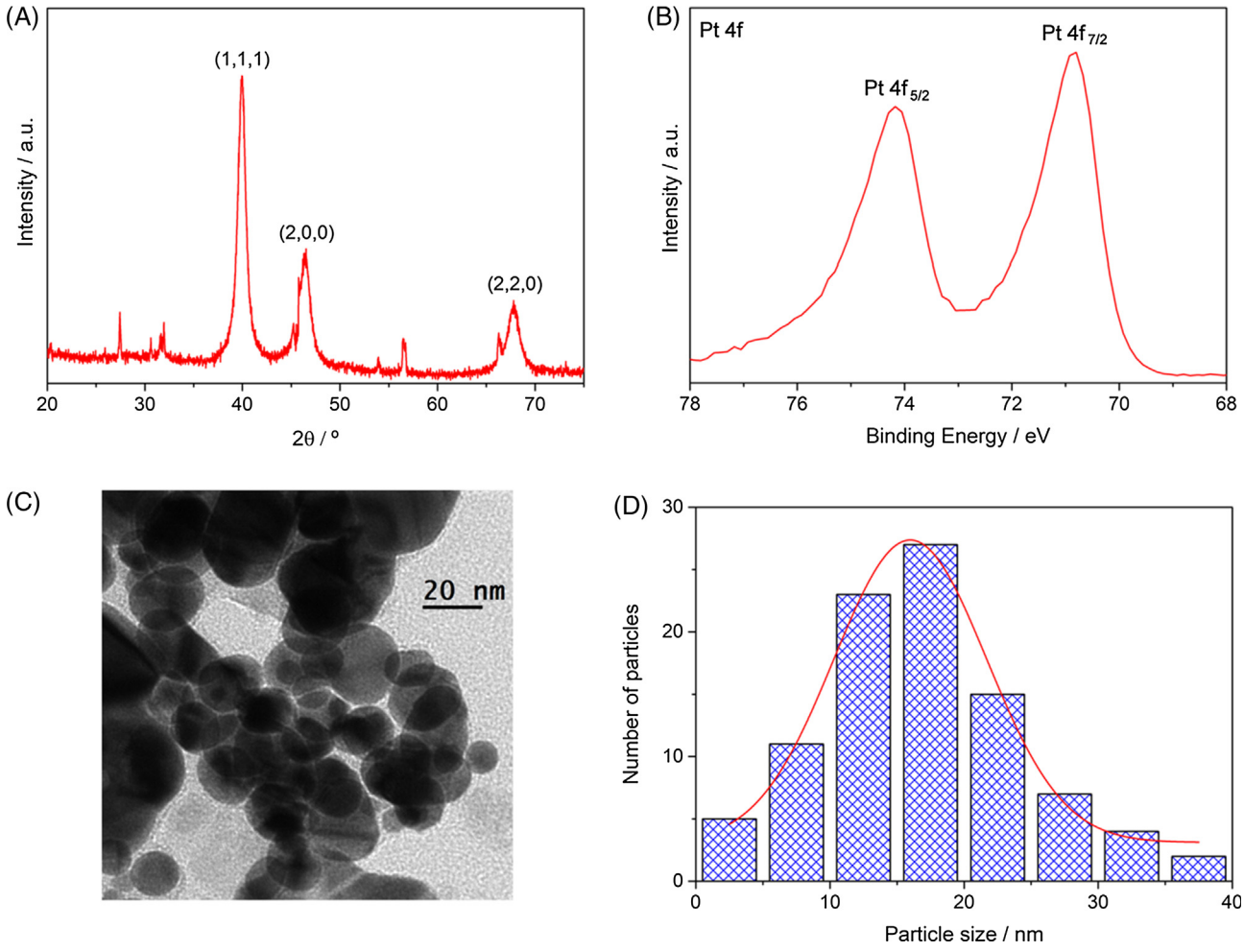

Fig. 2. XRD pattern (A), X-ray photoelectron spectrum for Pt 4f (B), TEM image (C), and particle size distribution from TEM analysis (D) for Pt nanoparticles synthesized.

3.2. Nanofluid stability

In terms of stability, nanofluids are considered to be stable when the nanoparticle concentration in suspension remains constant [50]. Due to the tendency of nanoparticles to agglomerate and precipitate, instability after preparation is logical. The subsequent formation of sediment is a problem for the application of nanofluids in concentrating solar power plants. Thus, studying the stability of the nanofluids is essential [51,52].

UV–Vis spectroscopy is a technique used to analyse the stability of nanofluids. Fig. 3A shows the UV–Vis spectra for each nanofluid just after preparation. The nanofluids treated with ultrasound presented high absorbance of around 390–500 nm, due to the scattering process generated by the presence of nanoparticles suspended in the base fluid, which is higher at lower wavelengths [53,54]. The nanofluids without ultrasound treatment (Pt_Nf + DDA + ODT) presented a weak signal for the presence of nanoparticles. This may be the settling of agglomerated nanoparticles that were not separated. This suggests that applying ultrasound can lead to more homogeneous nanofluid systems, and thus, a good dispersion of nanoparticles. No significant differences are observed between the spectra of the nanofluids and the base fluid. This suggests that there are no chemical changes in the base fluid due to the presence of the nanoparticles.

To assess the stability of the nanofluids, changes in the extinction coefficient values at $\lambda = 390$ nm were studied from UV–vis spectra. Three spectra were recorded every day for one week. Fig. 3B shows the extinction coefficient values for each nanofluid with respect to time. The nanofluid with ultrasound treatment and the addition of ODT (Pt_Nf + DDA + U + ODT) reached certain stability two days after its preparation, and the nanofluid that only underwent ultrasound treatment (Pt_Nf + DDA + U) also reached certain stability at around the same time, but the decrease in the extinction coefficient value was more pronounced during the first two days. This big difference observed may be due to the presence of the surfactant, whose function is to prevent an abrupt sedimentation process and to enable the nanofluid to quickly reach a stable state. After three days, both nanofluids were considered to remain stable and the values obtained after seven days were similar. The nanofluid with only ODT (Pt_Nf + DDA + ODT) did not show nanoparticles in suspension. The sedimentation of nanoparticles occurred immediately and changes in absorbance values were not appreciated. Therefore, the sonication process was necessary to disperse the nanoparticles into the base fluid.

Also, the physical stability of the nanofluids was determined by particle size measurements using the DLS technique. The measurements were recorded for a week, multiple measurements being performed daily. Fig. 4 shows the results obtained.

The nanofluid with only ODT, Pt_Nf + DDA + ODT, showed a wide range of particle size, values being observed from 500 to 2000 nm after five days. Thus, the presence of the surfactant did not result in nanoparticles of a constant size, their continuous agglomeration and sedimentation leading to an unstable nanofluid. This is in line with the results obtained by UV–Vis spectroscopy. Moreover, ultrasound power application generated nanoparticle size smaller than 900 nm. In turn, in the case of the nanofluid with ODT and treated with ultrasound power (Pt_Nf + DDA + U + ODT), the particle size was greater than in the case of that treated only with ultrasound due to the presence of the surfactant, which increased its hydrodynamic ratio. In addition, the Pt_Nf + DDA + U + ODT nanofluid showed a lower dispersion of nanoparticle size over time. Agglomeration and precipitation processes were observed in the first few days due to this dispersion and after three days the nanoparticle sizes remained stable, which is coherent with the UV–Vis results. The Pt_Nf + DDA + U nanofluid, without ODT, presented agglomeration processes before the second day, and then less dispersion; that is, the particle sizes remained stable over time. The difference in nanoparticle sizes between the first and second day is coherent with the abrupt decrease in extinction coefficient values observed above (see Fig. 3B).

To complete the analysis of the stability of the nanofluids, ζ potential measurements were performed several times each day for a week. ζ potential is related to steric repulsions or electrostatic interactions between particles present in a solution. A nanofluid is considered stable when its ζ potential is higher than 30 mV in absolute value [55]. Generally, ζ potential values of ± 30–50 mV are sufficient to ensure good colloidal stability. Fig. 5 shows the results obtained.

The measurements of ζ potential for the nanofluid with only ODT (Pt_Nf + DDA + ODT) were incoherent and it was not possible obtain enough information each day. Despite this, values of ζ potential around ± 10 mV were obtained for this nanofluid, which corroborates its instability. Regarding the ζ potential of the other nanofluids, they may be considered stable because they show values in a range of 30–80 mV. Thus, ultrasonic power treatment caused an increase in ζ potential values, these becoming less disperse over time. The presence of the surfactant may confer extra stability, so the ζ potential values of the nanofluid with ODT were higher than those in the nanofluid without ODT. Therefore, these results confirm the stability of the nanofluids with ultrasound power treatment, which is coherent with the UV–Vis spectroscopy analysis and particle size results. The nanofluid with only ODT (Pt_Nf + DDA + ODT), without ultrasound power treatment, presented absorbance values very similar to the base fluid, and its particle size values were not in accordance with a colloidal system such as a nanofluid. In addition, the ζ potential values confirmed these results, so this nanofluid was considered totally unstable and

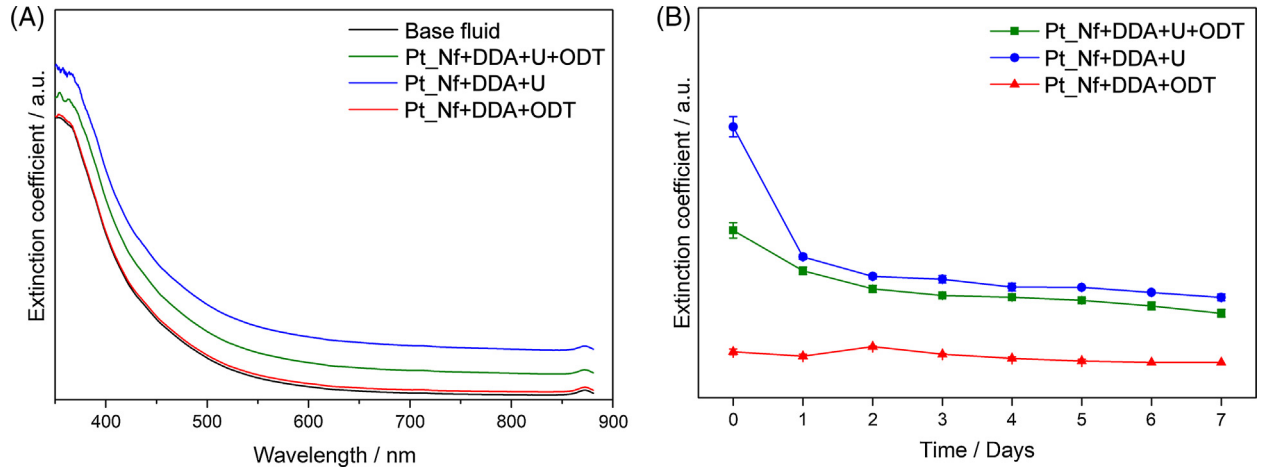

Fig. 3. (A) UV–vis spectra recorded at zero time for the nanofluids prepared. (B) Extinction coefficient values recorded at $\lambda = 390$ nm for one week.

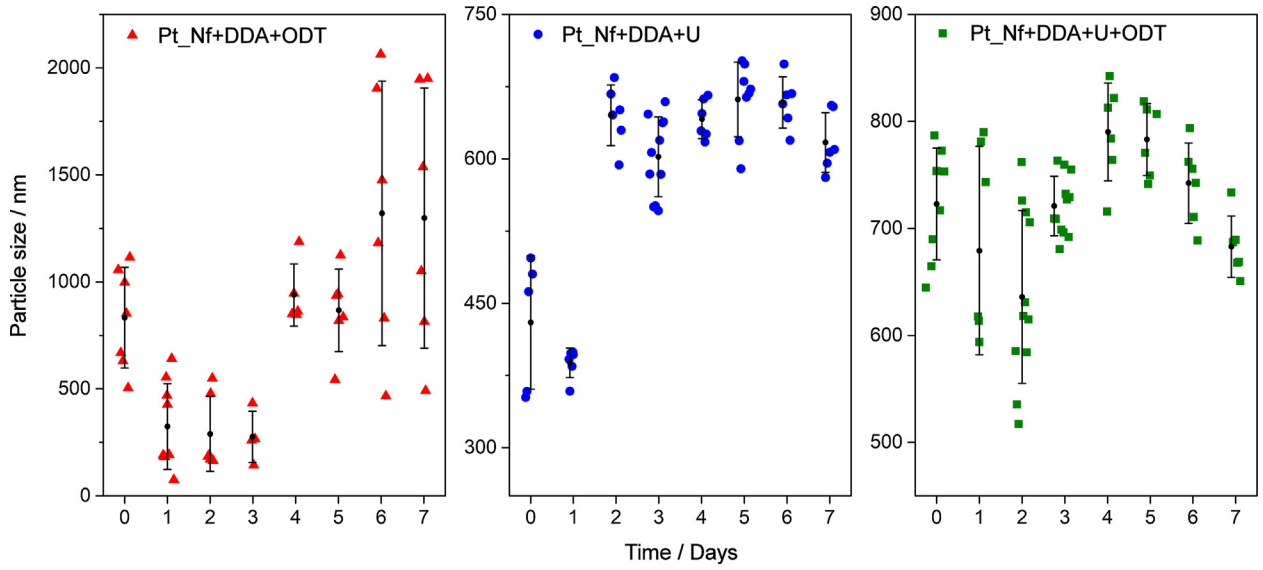

Fig. 4. Particle size measured using dynamic light scattering technique for the nanofluids prepared.

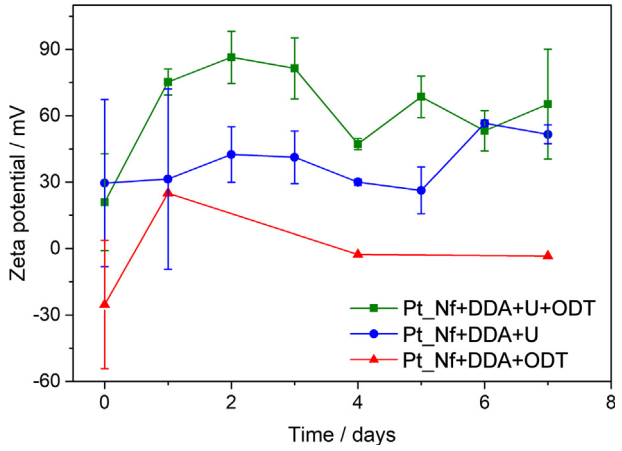

Fig. 5. ζ potential values for the nanofluids prepared.

consequently, it was ruled out for thermal characterization.

3.3. Nanofluid performance

The heat transfer coefficient can be generally expressed as a function of the properties of a fluid and is given by $h = (k^a \rho^b C_P^c)/(\mu^d \sigma^e)$, where k is thermal conductivity, ρ the density, C_P the isobaric specific heat, μ the dynamic viscosity and σ the surface tension [6]. Also, a, b, c, d, e are empirical or theoretical constants that depend on different boundary and geometrical conditions, and e is normally zero for convections without phase change [24]. Therefore, density, viscosity, isobaric specific heat and thermal conductivity were characterized in order to evaluate the performance of the nanofluids.

Density is a thermal property that plays an important role because a slight increase in its values can significantly enhance the efficiency of the heat transfer process [8]. Viscosity is the factor that limits the efficiency of nanofluids for their application in concentrating solar power plants because a slight increase can have a dramatic effect on efficiency, according to the heat transfer coefficient equation. It may also cause problems in elements such as pumps and ducts, or lead to drops in pressure [56]. Table 2 shows the density and dynamic viscosity values obtained for the base fluid and for the two nanofluids studied. The platinum concentration added for all the nanofluids was $5 \cdot 10^{-3}$ wt.%, so the same platinum concentration is considered for both nanofluids. An increase in the values of both properties was expected due to the addition of nanoparticles to base fluid.

Isobaric specific heat is an essential thermal property with regard to the efficiency of nanofluids so the values for those prepared were measured in a range of temperatures between room temperature and approximately 370 K. Fig. 6 shows the results of the isobaric specific heat measured for the two nanofluids prepared and the base fluid. The isobaric specific heat increased slightly with regard to base fluid for the nanofluid with ultrasound power treatment and ODT as a surfactant. However, a sharp decrease was observed for the nanofluid treated with ultrasound power and DDA. It is known that the isobaric specific heat of solids is commonly lower than that of fluids so it is reasonable to expect the values for the nanofluid to be lower than that of the base fluid [6,57,58]. However, some studies have reported an increase in isobaric specific heat with regard to the base fluid [8,13]. This increase may be due to the formation of an internal structure inside the nanofluid caused by interactions between the nanoparticles and base fluid [12,59]. Internal structure is created around the nanoparticle that give rise to aggregates that have semi-solid properties that cause, in this case, an increase in isobaric specific heat. The surfactant must play an important role in this kind of structure, as the molecular dynamics study will show below.

Finally, thermal conductivity is a vital property of nanofluids used as a heat transfer fluid. Thermal conductivity was measured in the same temperature range. Fig. 7A shows the thermal conductivity values obtained for the nanofluids and the base fluid. It is possible to observe that thermal conductivity of the nanofluids are higher than those of the base fluid, so ultrasonic power treatment would appear to result in an enhancement in this property for both nanofluids at high temperature. Fig. 7B shows the ratio between the thermal conductivity of the nanofluids with regard to base fluid. It is possible to observe an increase in thermal conductivity of up to 37% for the nanofluid with ODT and sonication treatment and of up to 17% for the nanofluid with sonication treatment but without ODT. Thus, ODT has a positive effect on the

Table 2
Values of the density and dynamic viscosity.

Sample	Density/kg m^{-3}	Viscosity/mPa s
HTF (base fluid)	1058.8 ± 0.8	3.76 ± 0.03
Pt_Nf + DDA + U	1060.8 ± 0.4	3.88 ± 0.03
Pt_Nf + DDA + U + ODT	1060.3 ± 0.6	3.91 ± 0.02

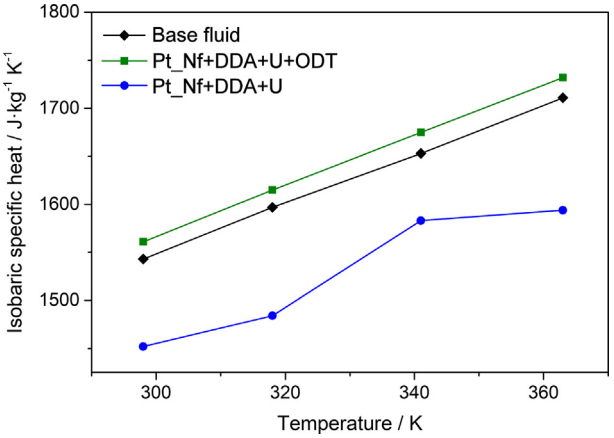

Fig. 6. Isobaric specific heat values obtained for the nanofluids prepared.

thermal properties of the nanofluids prepared using Pt nanoparticles and the base fluid.

Finally, in order to analyse the efficiency of the heat transfer process, two *Figure of Merits* have been analysed. Under laminar flow conditions, a nanofluid is considered more efficient than the base fluid when the ratio between the dynamic viscosity increase (*DVI*) and thermal conductivity enhancement (*TCE*) is less than four [60]. Mathematically, this is expressed by:

$$\frac{DVI}{TCE} = \frac{\frac{(\mu nf - \mu bf)}{\mu bf}}{\frac{(knf - kbf)}{kbf}} \leqslant 4 \tag{3}$$

where the variables have been defined previously, and the subscripts *bf* and *nf* refer to the base fluid and nanofluid, respectively. On the other hand, under turbulent conditions the relationship between the heat transfer coefficient (*h*) for the nanofluids prepared and the base fluid was considered as a *Figure of Merit*, which is known as the Dittus-Boelter equation. Mathematically, it is given by [61]

$$FoM = \frac{h_{nf}}{h_{bf}} = \left(\frac{\rho_{nf}}{\rho_{bf}}\right)^{0.8}\left(\frac{k_{nf}}{k_{bf}}\right)^{0.6}\left(\frac{C_{P,nf}}{C_{P,bf}}\right)^{0.4}\left(\frac{\mu_{nf}}{\mu_{bf}}\right)^{-0.4} \tag{4}$$

where the variables have been defined above. If this ratio is higher than 1, an improvement in the efficiency of the heat transfer process is obtained. In terms of the efficiency of the heat transfer process, an increase in dynamic viscosity is considered a disadvantage because it can affect different elements inside solar plants; however, an increase in density, isobaric specific heat and thermal conductivity values are beneficial.

Thus, the *FoM* for both laminar and turbulent conditions were estimated for the nanofluids at the temperature at which the isobaric specific heat and thermal conductivity were measured. Their density and the dynamic viscosity were estimated at these temperatures. Fig. 8 shows the values obtained for the *FoMs* for the laminar and turbulent flows obtained. Under laminar flow conditions, all the nanofluids showed values below 4 (see Fig. 8A), which means the nanofluid is more efficient than the base fluid. However, in some cases this *FoM* gives negative values because the thermal conductivity of the nanofluid is lower than that of the base fluid. In these cases, the efficiency of heat transfer processes is not improved. On the other hand, the most interesting case for concentrating solar power applications is the analysis under turbulent flows conditions. In this case, the Dittus-Boelter equation was used as a *FoM*. Fig. 8B shows the values obtained for the nanofluids prepared. It is possible to observe that the improvement in the efficiency of the heat transfer process is greater for the nanofluid prepared using sonication treatment and ODT as a surfactant. For this nanofluid, the improvement obtained is about 20%. In the case of the nanofluid without ODT, the improvement in the heat transfer process obtained is about 5%. Thus, the ODT clearly affected the performance of the nanofluid. When ODT was used the efficiency of the heat transfer process improved at all the temperatures and the enhancement was up to 20%, as is shown in Fig. 8B.

In turn, the effect of the use of nanofluids on the efficiency of the collectors used in CSP plants can be studied from the outlet temperature. The heat flux from the surface of the receiver to the heat transfer fluid is defined as $q_s'' = h\Delta T = h(T_s - T_{m,o})$, where T_s is the temperature on the surface of the pipe, and $T_{m,o}$ is the mean temperature of the base fluid at the pipe outlet. For a constant solar irradiance of 1000 W m^{-2}, q_s'' and T_s are considered, and thus ΔT for the base fluid and for the nanofluids can be compared. Mathematically, this can be expressed as $(\Delta T_{nf}/\Delta T_{bf}) = (h_{bf}/h_{nf})$. Then, if $(\Delta T_{nf}/\Delta T_{bf}) < 1$, $T_{m,o}$ is higher when the nanofluid is used, and the efficiency of the collector is improved, because the outlet temperature rises. So, Fig. 8C shows the values of $(\Delta T_{nf}/\Delta T_{bf})$ obtained. It is possible to observe that using ODT as a surfactant led to an increase of the outlet temperature, and therefore an increase in the efficiency of the solar collectors.

Thus, it can be concluded that the thermal properties of the nanofluid with ODT were drastically better than those of the base fluid and could therefore be a promising alternative as a heat transfer system in concentrating solar power applications. This nanofluid could be tested in CSP systems with the aim of reducing the cost of producing electricity and improving the global efficiency of the plants.

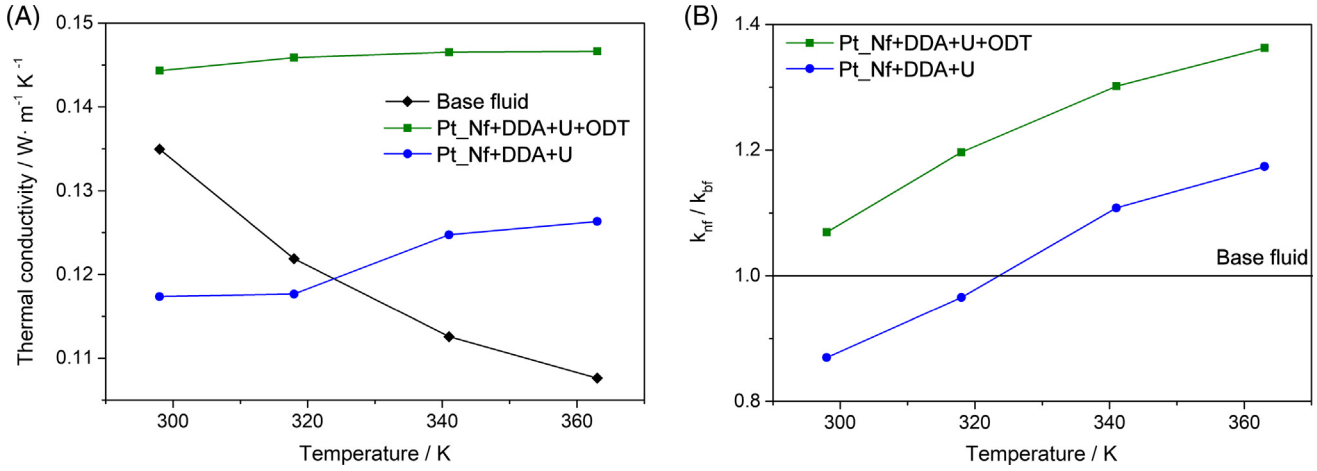

Fig. 7. (A) Thermal conductivity values obtained, and (B) the improvement in thermal conductivity with regard to the base fluid for the nanofluid prepared.

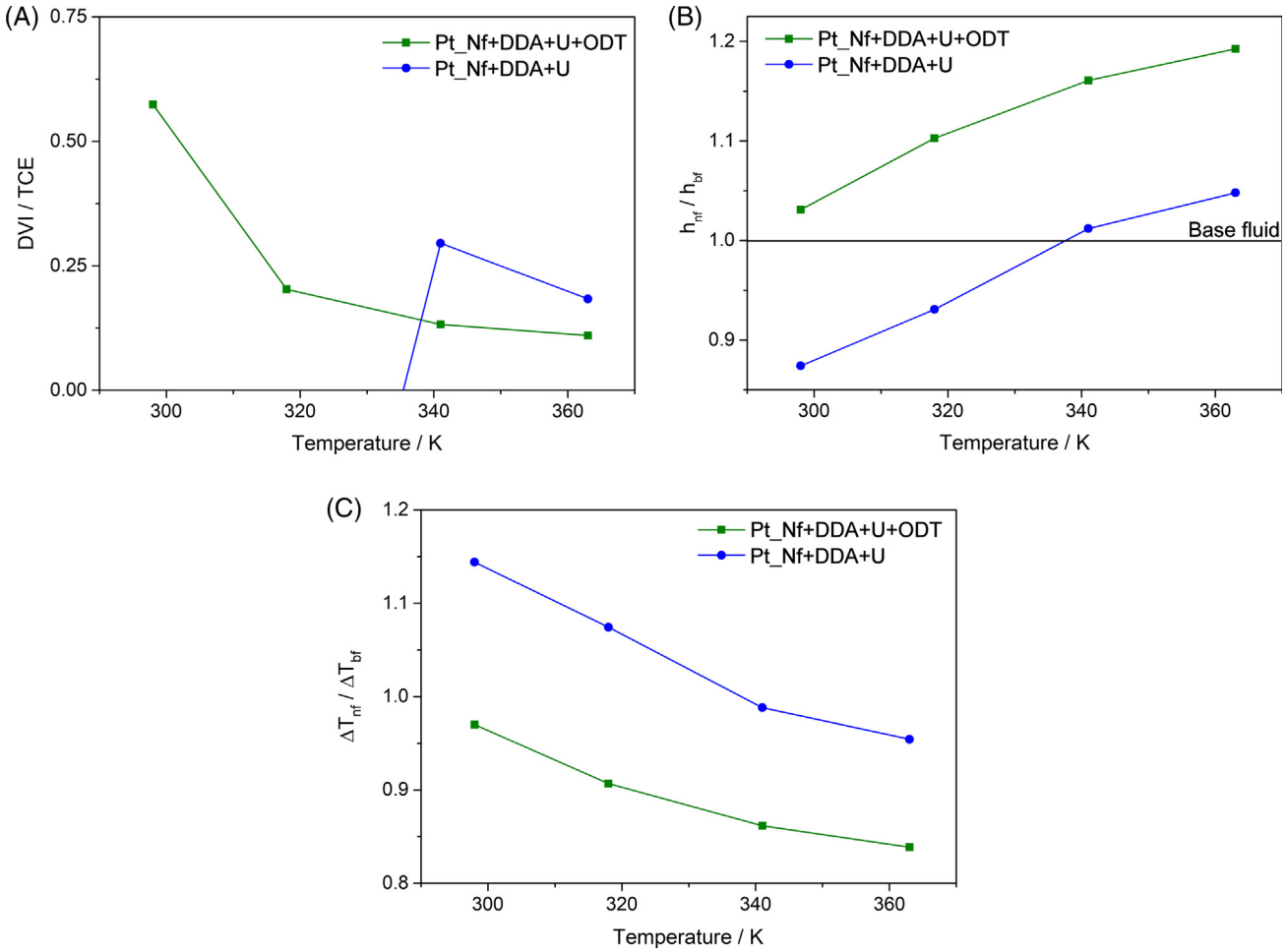

Fig. 8. (A) Ratio between dynamic viscosity increase (*DVI*) and thermal conductivity enhancement (*TCE*) used as a *FoM* for laminar flow conditions, (B) the ratio between the heat transfer coefficient of the nanofluid with regard to base fluid, used as a *FoM* under turbulent flow conditions, and (C) analysis of the outlet temperature in solar collectors.

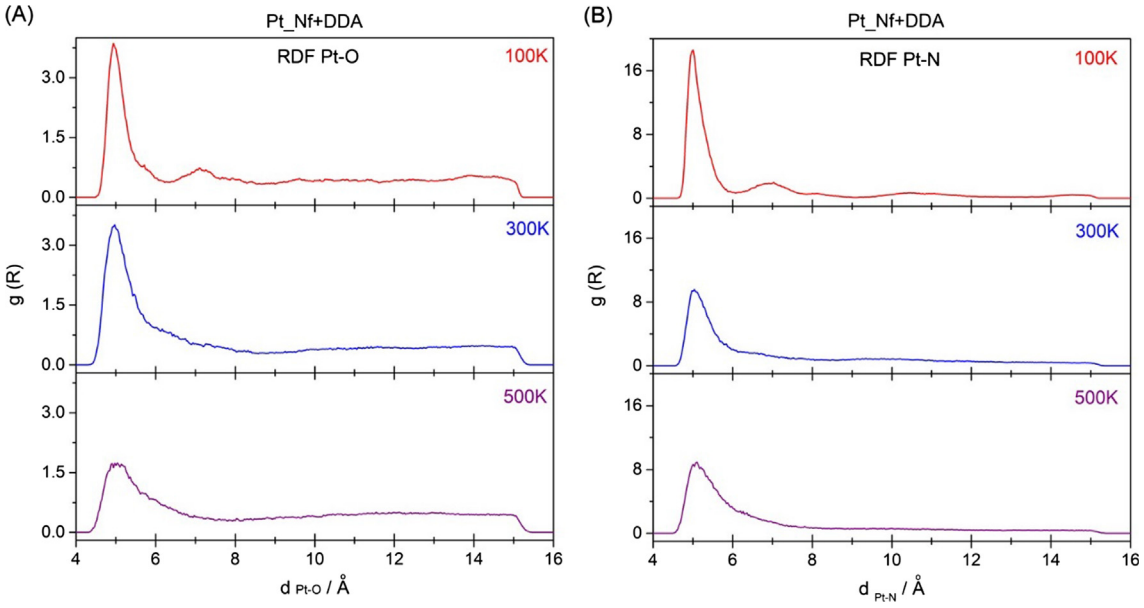

Fig. 9. RDFs for Pt-O (A), Pt-N (B) at 100, 300 and 500 K in the Pt_Nf + DDA system.

3.4. Molecular dynamics: structural properties

The experimental results shown above reveal that the presence of ODT as a surfactant in the nanofluid improves the efficiency of the heat transfer processes. In this sense, it is of interest to explore the internal structure and layout of the molecules around the nanoparticle as they must play an important role in this enhanced performance. Thus, a molecular dynamics study was performed to determine how the presence of DDA and ODT affects the Pt nanofluid at a molecular level. To this end, the Pt_Nf + DDA and Pt_Nf + DDA + ODT systems were compared at 100, 300 and 500 K. In this study, theoretical Pt_Nf + DDA and Pt_Nf + DDA + ODT systems are referred to the experimental Pt_Nf + DDA + U and Pt_Nf + DDA + U + ODT systems, respectively. The analysis were performed with regard to the centre of mass of the Pt cell, so, unless stated otherwise, any reference to Pt in the discussion means the centre of mass of the unit cell.

3.4.1. Pt_Nf + DDA system

Fig. 9 shows the radial distribution functions (RDFs) for the Pt_Nf + DDA system at different temperatures. Analysing the RDFs of the Pt-O pair makes it possible to deduce the number of O atoms around the Pt cell that belong to diphenyl oxide molecules from the base fluid. Fig. 9A shows the presence of a peak centred around 5 Å that begins to lose intensity and widens as the temperature increases. At 100 K there is a small peak centred around 7 Å that is not present at 300 K; it combines with the first peak at 5 Å making it wider. Integration up to 8.5 Å reveals the presence of 6 and 7 atoms at 100 and 300 K, respectively. However, at 500 K the integral shows the presence of 5 O atoms that belong to 5 diphenyl oxide molecules.

For the description of the interaction between the Pt and the DDA, the N of the DDA was taken for reference to be indicative of the number of molecules around the nanoparticle. Fig. 9B shows the RDFs for the Pt-N pair at different temperatures. In general, as occurred with the Pt-O pair, a peak is observed centred at 5 Å that becomes less intense and wider at 500 K. Integrating the RDFs up to 8.5 Å, at 100 and 300 K, six DDA molecules can be seen in the first layer around the Pt. Meanwhile, at 500 K, another molecule is incorporated, making 7 molecules, which must occupy a larger area of space between a first layer and a second one further from the Pt cell.

Analysing spatial distribution functions (SDFs) also makes it possible to determine how the base fluid and DDA molecules are arranged around the Pt and to see how the system evolves with changes in temperature. Fig. 10 shows the SDF for the system in a radius of 9 Å around the centre of mass of the Pt cell (Fig. 10A) and the structure associated with it (Fig. 10B). The hydrogen and carbon atoms from the rings, and the surfactant chains were not included in the analysis of the SDF to keep the images clear. An initial look at Fig. 10A shows a loss of definition of the spatial distributions as the temperature rises, which is indicative of a dynamic system. At 100 K (Fig. 10A), six O atoms (red[1] lobes) from the diphenyl oxide molecules can be seen oriented towards the central Pt atom. The blue lobes are C atoms attached to the O atoms of the diphenyl oxide (CO). Six orange lobes can be seen around the Pt that correspond to the N atoms of the DDA. At 300 K a decrease in the definition of the SDF is observed and the red (O atoms) and orange colours that occupy an inner layer around the Pt stand out. Meanwhile, at 500 K the presence of orange lobes corresponding to DDA molecules is of particular note. This result is coherent with the widening and long tails of the RDFs of the Pt-O and Pt-N pairs, indicative of a dynamic system in which exchanges take place between diphenyl oxide and DDA molecules as the temperature increases. At low temperatures (100 K), there are 6 diphenyl oxide molecules in the inner layer around the Pt cell and another molecule is incorporated at room temperature (Fig. 10B). However, at high temperatures (500 K) one of the diphenyl oxide molecules moves away from the Pt cell and occupies a position in a second layer further from the nanoparticle (Fig. 10B). This movement of diphenyl oxide molecules at 500 K is accompanied by a DDA molecule being incorporated into the inner layer around the Pt cell, resulting in 7 DDA molecules (Fig. 10B). This result is also in agreement with wide peaks being observed in the RDFs as the temperature rises. When only DDA is found in the nanofluid, the presence of an inner layer of molecules around the nanoparticles is to be expected due to the favourable interaction between Pt and N [62].

3.4.2. Pt_Nf + DDA + ODT system

Fig. 11 includes the RDFs for the Pt_Nf + DDA + ODT system at 100, 300 and 500 K. Fig. 11A shows the RDFs for the Pt-O pair. At 100 K, the RDF shows an intense, well-defined peak at around 5 Å that integrates two O atoms and is accompanied by other less intense peaks, totalling seven O atoms when integrated up to *c.a.* 9 Å. As the temperature rises, the first peak becomes less intense, broader and its tail longer. The integral of the RDFs up to 9 Å at 300 and 500 K indicates that there are 6 and 7 oxygen atoms, respectively. The RDFs for the Pt-N pair (Fig. 11B) are very similar to that of the Pt_Nf + DDA system. At 100 K there is an intense peak centred at 5 Å and another centred at 8 Å that integrate to 2 and 1 N atoms, respectively. As the temperature rises the peak centred at 5 Å becomes less intense and broader. The integral of this peak up to 9 Å corresponds to 3 and 2 N atoms, at 300 and 500 K, respectively. This means that, at high temperatures, a DDA molecule distances itself from the inner layer around the Pt, unlike what occurred in the Pt_Nf + DDA system. Fig. 11C includes the RDF for the description of the interaction between the Pt and the S atom of the ODT surfactant at 100, 300 and 500 K. The S atom was chosen as representative of the ODT molecule. At 100 K, a well-defined peak is observed centred at 5.4 Å that integrates 3 S atoms corresponding to 3 ODT molecules. This peak is indicative of strong orientation binding [15,63]. As the temperature increases, the peak loses its intensity and structure, a shoulder appearing around 7 Å and a tail. At 300 and 500 K, the peak centred at 5.4 Å integrates 2 and 1 S atom, respectively. However, when integrated under the long tail of the RDF including the low intensity peak centred at 10 Å, there are a total of 3 and 2 S atoms at 300 and 500 K, respectively. The long tails of these RDFs suggest that there is movement of ODT molecules from an inner to an outer layer of the Pt unit cell. This movement of ODT molecules and the increased number of diphenyl oxide molecules favours the generation of a lattice around the nanoparticle, as the SDF study will show below; this is linked with an increase in the isobaric specific heat.

Fig. 12A and B show the SDFs of the Pt_Nf + DDA + ODT system and its associated structures. As with Fig. 10, the H and C atoms from the rings, and the surfactant chains were not included in the analysis of the SDF to keep the images clear. As the temperature rises, the spatial distributions become less defined, indicative of a dynamic system in which movement of molecules must take place, as was the case with the Pt_Nf + DDA system (Fig. 10A). At 100 K, three yellow and orange lobes can be seen in an inner layer around the Pt that belong to three ODT and DDA molecules, respectively. There are also 7 red lobes (O atoms) with their respective blue lobes of the C atoms linked to the O atoms (CO) of the diphenyl oxide (Fig. 12A). At 300 K, there are six diphenyl oxide molecules but the three ODT and DDA molecules remain, although the yellow and orange lobes are broader, which is indicative of movement of the molecules around the Pt cell, making it quite labile. So much so that at 500 K only two ODT and DDA molecules remain in the inner layer close to the Pt cell (Fig. 12B). This decrease in the number of ODT and DDA molecules involves diphenyl oxide molecules moving nearer to the Pt at high temperatures (Fig. 12B), which is in agreement with the width and long tail of the RDFs of the Pt-O, Pt-S and Pt-N pairs (Fig. 11).

Finally, although the C atoms from the biphenyl molecule were not included in the SDFs, they were included in their associated structures

[1] For interpretation of color in Figs. 10 and 12, the reader is referred to the web version of this article.

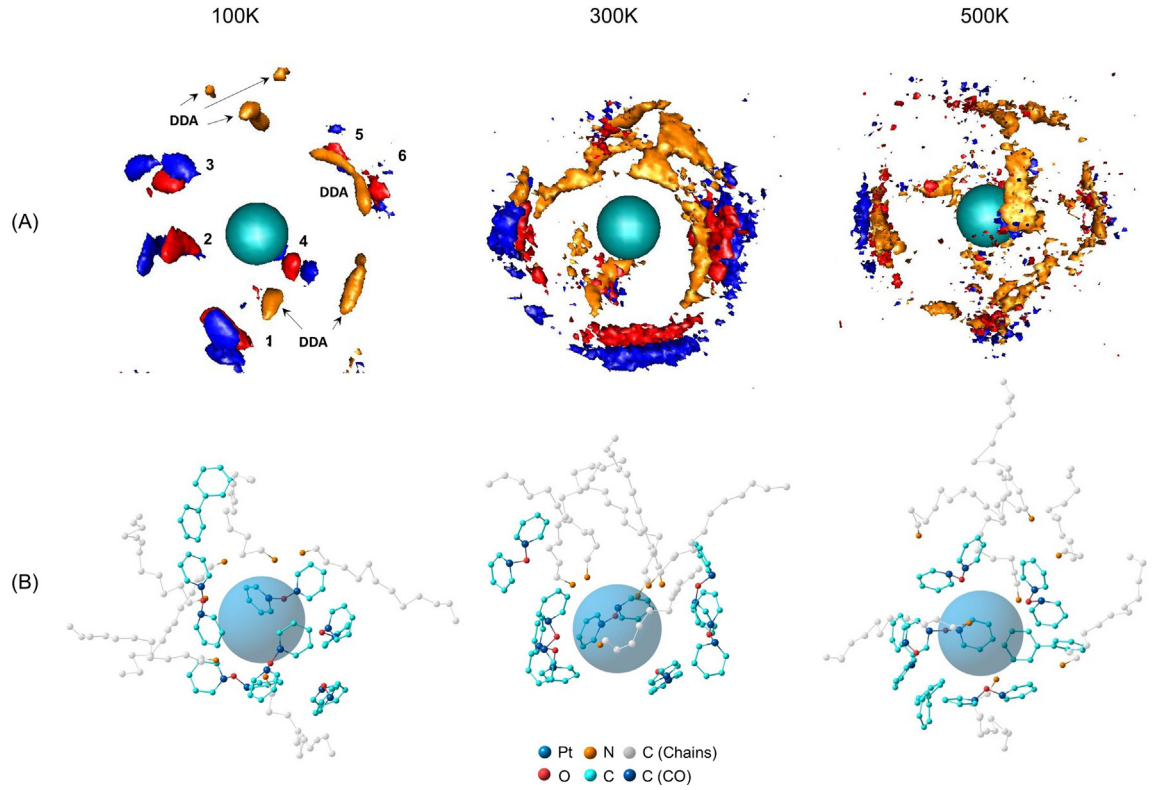

Fig. 10. (A) SDFs from the Pt_Nf + DDA nanofluid at different temperatures. (B) Structure around the Pt in the nanofluid system at 100, 300 and 500 K.

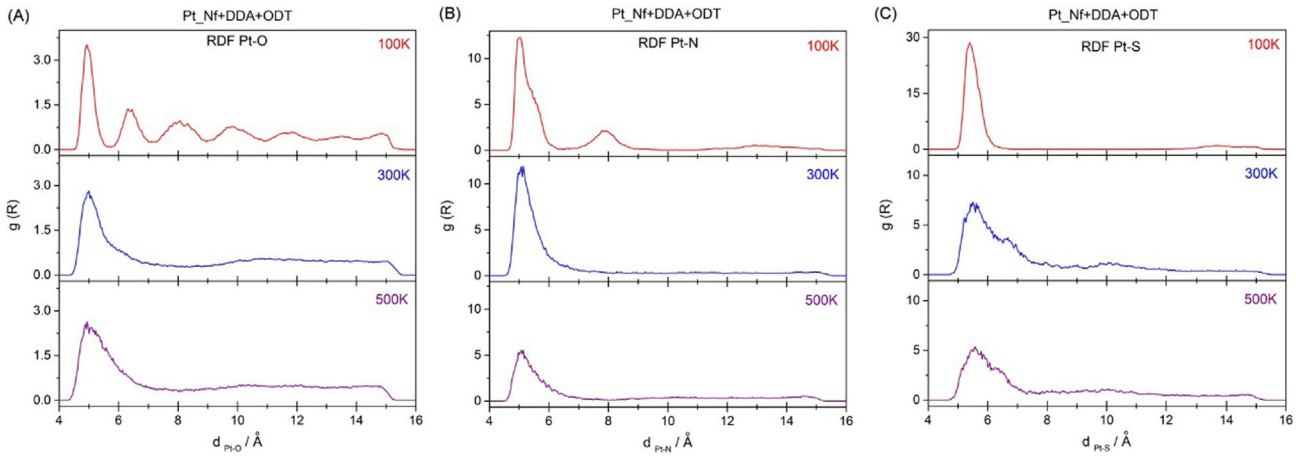

Fig. 11. RDFs for Pt-O (A), Pt-N (B) and Pt-S (C) pairs in the 100–500 K range in the Pt_Nf + DDA + ODT system.

(Figs. 10B and 12B). Figs. 10B and 12B are clear evidence that the biphenyl molecules play a less significant role than the diphenyl oxide molecules in the first layer around the Pt, a feature that has been observed previously for other systems [8,14,15].

3.4.3. *Pt_Nf + DDA vs Pt_Nf + DDA + ODT systems*

A comparison of the Pt_Nf + DDA and Pt_Nf + DDA + ODT systems makes it possible to see how the ODT affects the nanofluid. Fig. 13 shows the layout of the surfactants around the Pt cell for the Pt_Nf + DDA and Pt_Nf + DDA + ODT systems as the temperature increases. When only DDA is present in the system (Fig. 13A), a large number of DDA molecules are found around the Pt. These molecules and their respective chains, along with well-established stability of Pt-N [62], must generate steric hindrance that impedes the diphenyl oxide molecules from approaching the metal, limiting the heat flow.

However, a more favourable situation with regard to heat transfer is found when there are both ODT and DDA in the system (Fig. 13B). In that regard, it is important to remember that ODT molecules have a longer carbon chain than DDA molecules. In the Pt_Nf + DDA + ODT system, as the temperature rises, the presence of ODT and DDA creates a more flexible lattice between the first and second layers around the Pt, which must facilitate the exchange of particles due to Brownian movement. The ODT and DDA molecules must compete to interact with the Pt, resulting, at high temperatures, in a decrease in the number of surfactant molecules around the metal in comparison with the Pt_Nf + DDA system. Likewise, the base fluid takes advantage of this possible competition between the two surfactants to incorporate more diphenyl oxide molecules into the first layer, which, as mentioned above, is related with producing nanofluids with enhanced thermal capabilities [8,14,15]. In this sense, the molecular lattice generated in the Pt_Nf + DDA + ODT system will reduce the number of collisions between particles, favouring energy transfer and increasing thermal conductivity

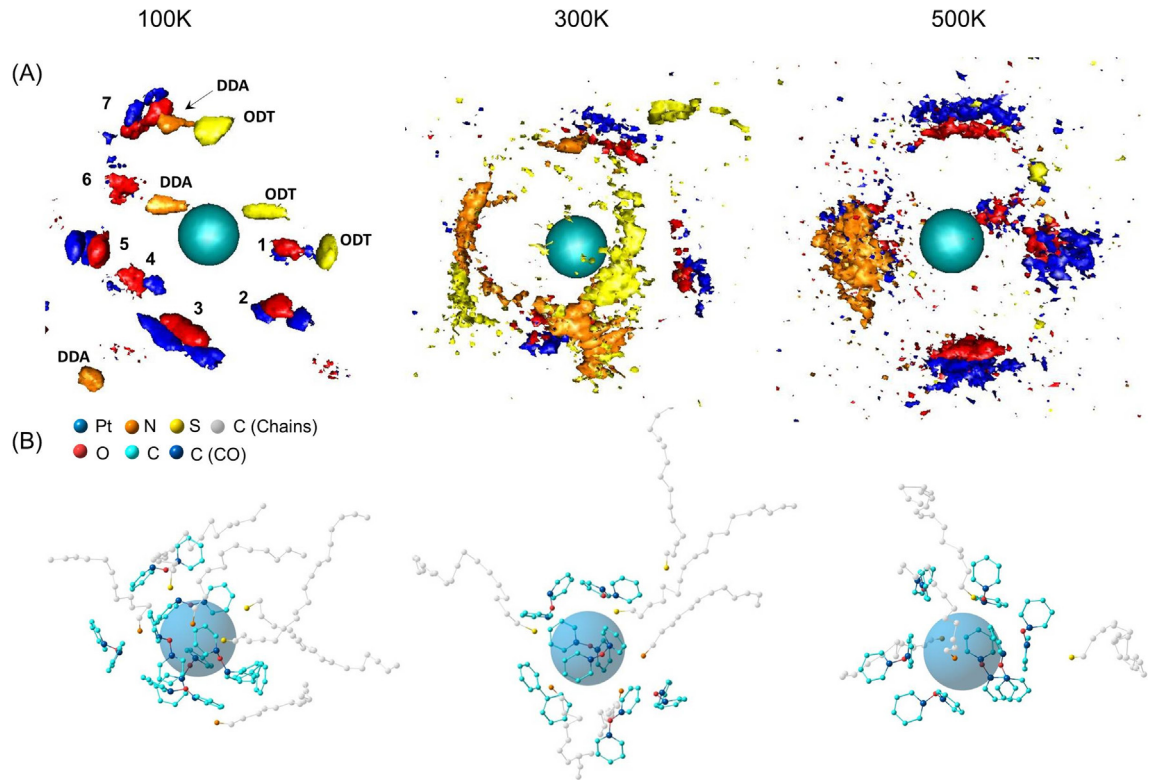

Fig. 12. (A) SDFs from the PT_Nf + DDA + ODT at different temperatures. (B) Structure around the Pt in the PT_Nf + DDA + ODT system at 100, 300 and 500 K.

[33]. In short, the presence of ODT leads to competition with the DDA to interact with the metal and results in the incorporation of more diphenyl oxide molecules into the first layer around the Pt as the temperature rises. This result is a molecular explanation of the effect of ODT on the experimental performance observed in the Pt_Nf + DDA + ODT system.

4. Conclusions

This study presents the performance of nanofluids based on Pt nanoparticles for use in CSP applications. As the base fluid, the eutectic mixture of diphenyl oxide (73.5%) and biphenyl (26.5%) was used. This fluid is typically used in CSP plants based on parabolic through

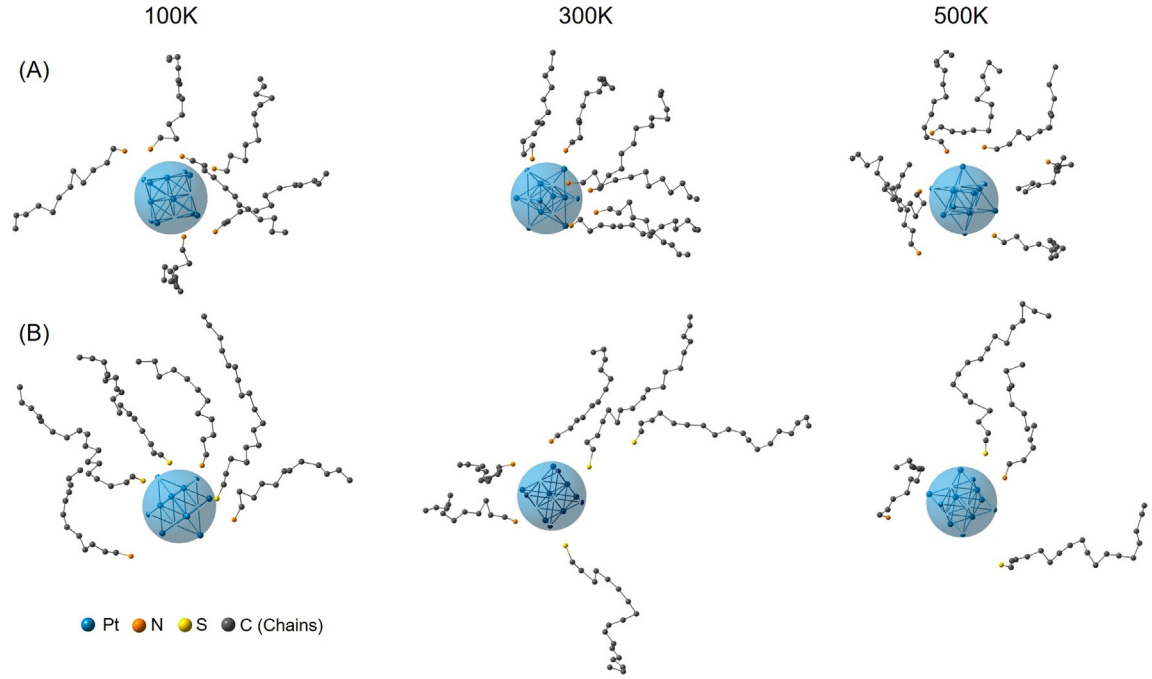

Fig. 13. Structures of the surfactant molecules around the Pt cell in the PT_Nf + DDA (A) and PT_Nf + DDA + ODT (B) systems at 100, 300 and 500 K.

collectors. In turn, Pt nanoparticles were synthesized and dispersed in a HTF typically used in CSP plants. The Pt nanoparticles were characterized using TEM, XRD and XPS. The presence of metallic Pt nanoparticles was confirmed.

The Pt nanoparticles were transferred to the base fluid using DDA as a phase transfer agent. DDA takes the role of the surfactant too. The nanoparticles were dispersed using ultrasonication with two nanofluids and without sonication in the case of another. An analysis was also performed of the addition of another surfactant, namely ODT. The stability of the nanofluids was analysed by means UV–vis spectroscopy, particle size and ζ potential measurements. The nanofluids treated with ultrasonication were more stable, implying that sonication is needed to disperse the nanoparticles effectively. Furthermore, density, dynamic viscosity, isobaric specific heat and thermal conductivity were measured to analyse the performance of the nanofluids. The density and dynamic viscosity values increased slightly, by up to 0.25% and 4% respectively. The isobaric specific heat increased slightly for the nanofluid treated with sonication and incorporating ODT, but decreased for the nanofluid without ODT. Moreover, increased thermal conductivity was found for all the nanofluids. This increase was up to 37% for the nanofluid with ODT and up to 17% for the nanofluid without. These properties were included in a FoM to analyse the enhancement of the heat transfer process. For the nanofluid with ODT, the heat transfer process increased by up to 20%, and for the nanofluid without the increase was by up to 5%. So, the nanofluid prepared with sonication and with ODT presented good stability and enhanced thermal properties and would seem to be a promising alternative to the typical HTF used in CSP plants.

In addition, to determine the effect of the presence of ODT on the systems and its effect at different temperatures, molecular dynamics calculations were performed at 100, 300 and 500 K. In the Pt_Nf + DDA + ODT system, ODT and DDA molecules appear to compete to interact with the Pt, which facilitates the entry of base fluid molecules into the layer closer to the metal. It can be seen that increases in temperature favour a flexible lattice formed of ODT and DDA chains around the Pt; the ODT chains are longer than the DDA ones. This lattice enables diphenyl oxide molecules to move closer to the metal, which favours heat transfer and consequently enhances the thermal properties of the nanofluid. In the DDA system, increasing the temperature favours the interaction between the Pt and the N atoms of the DDA, there being 7 DDA molecules around the Pt, which hinders the flow of heat in comparison with the Pt_Nf + DDA + ODT system.

For this reason, the Pt_Nf + DDA + ODT system presents favourable conditions for use as a nanofluid in CSP.

Acknowledgements

This work was supported by the Ministerio de Economia y Competitividad (MINECO) of the Spanish Government [Grant No. ENE2014-58085-R and Grant No. UNCA15-CE-2945].

Calculations were made through CICA - Centro Informático Científico de Andalucía (Spain).

Appendix A. Supplementary material

Supplementary data associated with this article can be found, in the online version, at https://doi.org/10.1016/j.apenergy.2018.07.062.

References

[1] Khan J, Arsalan MH. Solar power technologies for sustainable electricity generation - a review. Renew Sustain Energy Rev 2016;55:414–25.
[2] Desideri U, Zepparelli F, Morettini V, Garroni E. Comparative analysis of concentrating solar power and photovoltaic technologies: technical and environmental evaluations. Appl Energy 2013;102:765–84.
[3] Devabhaktuni V, Alam M, Depuru SSSR, Green RC, Nims D, Near C. Solar energy: trends and enabling technologies. Renew Sustain Energy Rev 2013;19:555–64.
[4] Fernandez-Garcia A, Zarza E, Valenzuela L, Perez M. Parabolic-trough solar collectors and their applications. Renew Sustain Energy Rev 2010;14:1695–721.
[5] Mwesigye A, Huan ZJ, Meyer JP. Thermodynamic optimisation of the performance of a parabolic trough receiver using synthetic oil-Al2O3 nanofluid. Appl Energy 2015;156:398–412.
[6] Chandrasekar M, Suresh S, Senthilkumar T. Mechanisms proposed through experimental investigations on thermophysical properties and forced convective heat transfer characteristics of various nanofluids - a review. Renew Sustain Energy Rev 2012;16:3917–38.
[7] Lee S, Choi SUS, Li S, Eastman JA. Measuring thermal conductivity of fluids containing oxide nanoparticles. J Heat Trans-T Asme 1999;121:280–9.
[8] Navas J, Sanchez-Coronilla A, Martin EI, Teruel M, Gallardo JJ, Aguilar T, et al. On the enhancement of heat transfer fluid for concentrating solar power using Cu and Ni nanofluids: an experimental and molecular dynamics study. Nano Energy 2016;27:213–24.
[9] Timofeeva EV, Yu WH, France DM, Singh D, Routbort JL. Nanofluids for heat transfer: an engineering approach. Nanoscale Res Lett 2011;6.
[10] Yoo DH, Hong KS, Yang HS. Study of thermal conductivity of nanofluids for the application of heat transfer fluids. Thermochim Acta 2007;455:66–9.
[11] Andreu-Cabedo P, Mondragon R, Hernandez L, Martinez-Cuenca R, Cabedo L, Julia JE. Increment of specific heat capacity of solar salt with SiO_2 nanoparticles. Nanoscale Res Lett 2014:9.
[12] Shin D, Banerjee D. Specific heat of nanofluids synthesized by dispersing alumina nanoparticles in alkali salt eutectic. Int J Heat Mass Transf 2014;74:210–4.
[13] Singh D, Timofeeva EV, Moravek MR, Cingarapu S, Yu WH, Fischer T, et al. Use of metallic nanoparticles to improve the thermophysical properties of organic heat transfer fluids used in concentrated solar power. Sol Energy 2014;105:468–78.
[14] Gomez-Villarejo R, Martin EI, Navas J, Sanchez-Coronilla A, Aguilar T, Gallardo JJ, et al. Ag-based nanofluidic system to enhance heat transfer fluids for concentrating solar power: nano-level insights. Appl Energy 2017;194:19–29.
[15] Gomez-Villarejo R, Navas J, Martin EI, Sanchez-Coronilla A, Aguilar T, Gallardo JJ, et al. Preparation of Au nanoparticles in a non-polar medium: obtaining high-efficiency nanofluids for concentrating solar power. an experimental and theoretical perspective. J Mater Chem A 2017;5:12483–97.
[16] Yu WH, France DM, Routbort JL, Choi SUS. Review and comparison of nanofluid thermal conductivity and heat transfer enhancements. Heat Transfer Eng 2008;29:432–60.
[17] Otanicar T, Phelan P, Prasher R, Rosengarten G, Taylor R. Nanofluid-based direct absorption solar collector. J Renew Sustain Energy 2010;2. 033102-1-13.
[18] Taylor R, Phelan P, Otanicar T, Adrian R, Prasher R. Nanofluid optical property characterization: towards efficient direct absorption solar collectors. Nanoscale Res Lett 2011;6. 225-1-11.
[19] Mu L, Zhu Q, Si L. Radiative properties of nanofluids and performance of a direct solar absorber using nanofluids. In: ASMEeditor. ASME 2009 second international conference on micro/nanoscale heat and mass transfer. Shanghai: ASME; 2009. p. 549-53.
[20] An W, Zhang J, Zhu T, Gao N. Investigation on a spectral splitting photovoltaic/thermal hybrid system based on polypyrrole nanofluid: preliminary test. Renew Energy 2016;86:633–42.
[21] An W, Wu J, Zhu T, Zhu Q. Experimental investigation of a concentrating PV/T collector with Cu9S5 nanofluid spectral splitting filter. Appl Energy 2016;184:197–206.
[22] Aguilar T, Navas J, Sánchez-Coronilla A, Martín EI, Gallardo JJ, Martínez-Merino P, et al. Investigation of enhanced thermal properties in NiO-based nanofluids for concentrating solar power applications: a molecular dynamics and experimental analysis. Appl Energy 2018;211:677–88.
[23] Yasinskiy A, Navas J, Aguilar T, Alcantara R, Gallardo JJ, Sanchez-Coronilla A, et al. Dramatically enhanced thermal properties for TiO_2-based nanofluids for being used as heat transfer fluids in concentrating solar power plants. Renew Energy 2018;119:809–19.
[24] Wen DS, Lin GP, Vafaei S, Zhang K. Review of nanofluids for heat transfer applications. Particuology 2009;7:141–50.
[25] Mohammed HA, Al-Aswadi AA, Shuaib NH, Saidur R. Convective heat transfer and fluid flow study over a step using nanofluids: a review. Renew Sustain Energy Rev 2011;15:2921–39.
[26] Verma SK, Tiwari AK. Progress of nanofluid application in solar collectors: a review. Energy Convers Manage 2015;100:324–46.
[27] Eastman JA, Choi SUS, Li S, Yu W, Thompson LJ. Anomalously increased effective thermal conductivities of ethylene glycol-based nanofluids containing copper nanoparticles. Appl Phys Lett 2001;78:718–20.
[28] Li YJ, Zhou JE, Tung S, Schneider E, Xi SQ. A review on development of nanofluid preparation and characterization. Powder Technol 2009;196:89–101.
[29] Kinoshita K, Stonehart P. Modern aspect of electrochemisty. New York: Plenum Press; 1996.
[30] Klabunde KJ, Mohs C. Chemistry of advance materials. New York: Wiley-VCH; 1998.
[31] Park KW, Choi JH, Kwon BK, Lee SA, Sung YE, Ha HY, et al. Chemical and electronic effects of Ni in Pt/Ni and Pt/Ru/Ni alloy nanoparticles in methanol electrooxidation. J Phys Chem B 2002;106:1869–77.
[32] Sarsam WS, Amiri A, Zubir MNM, Yarmand H, Kazi SN, Badarudin A. Stability and thermophysical properties of water-based nanofluids containing triethanolamine-treated graphene nanoplatelets with different specific surface areas. Colloid Surf A 2016;500:17–31.
[33] Angayarkanni SA, Philip J. Review on thermal properties of nanofluids: recent developments. Adv Colloid Interf 2015;225:146–76.
[34] Murdock RC, Braydich-Stolle L, Schrand AM, Schlager JJ, Hussain SM.

Characterization of nanomaterial dispersion in solution prior to In vitro exposure using dynamic light scattering technique. Toxicol Sci 2008;101:239–53.
[35] Rai N, Siepmann JI. Transferable potentials for phase equilibria. 9. explicit hydrogen description of benzene and five-membered and six-membered heterocyclic aromatic compounds. J Phys Chem B 2007;111:10790–9.
[36] Rai N, Siepmann JI. Transferable potentials for phase equilibria. 10. Explicit-hydrogen description of substituted benzenes and polycyclic aromatic compounds. J Phys Chem B 2013;117:273–88.
[37] Martin MG, Siepmann JI. Transferable potentials for phase equilibria. 1. United-atom description of n-alkanes. J Phys Chem B 1998;102:2569–77.
[38] Martin MG, Siepmann JI. Novel configurational-bias Monte Carlo method for branched molecules. Transferable potentials for phase equilibria. 2. United-atom description of branched alkanes. J Phys Chem B 1999;103:4508–17.
[39] Wick CD, Stubbs JM, Rai N, Siepmann JI. Transferable potentials for phase equilibria. 7. Primary, secondary, and tertiary amines, nitroalkanes and nitrobenzene, nitriles, amides, pyridine, and pyrimidine. J Phys Chem B 2005;109:18974–82.
[40] Wyckoff RWG. Crystal structures. 2nd ed. New York: Interscience Publishers; 1963.
[41] Sebesta F, Sláma V, Melcr J, Futera Z, Burda JV. Estimation of transition-metal empirical parameters for molecular mechanical force fields. J Chem Theo Comput 2016;12:3681–8.
[42] Smith W, Forester TR. DL_POLY_2.0: a general-purpose parallel molecular dynamics simulation package. J Mol Graphics. 1996;14:136–41.
[43] Martinez JM, Martinez L. Packing optimization for automated generation of complex system's initial configurations for molecular dynamics and docking. J Comput Chem 2003;24:819–25.
[44] Allen MP, Tildesley DJ. Computer simulation of liquids. Clarendon, Oxford; 1989.
[45] Company TD. Dowtherm A. Heat transfer fluid. Product Technical Data. VLL0-V0100-MA-001; 1997.
[46] Martin EI, Sanchez-Coronilla A, Navas J, Gomez-Villarejo R, Martinez-Merino P, Alcantara R, et al. Revealing at the molecular level the role of the surfactant in the enhancement of the thermal properties of the gold nanofluid system used for concentrating solar power. PCCP 2018;20:2421–30.
[47] Potemkin DI, Filatov EY, Zadesenets AV, Sobyanin VACO. preferential oxidation on Pt0.5Co0.5 and Pt-CoOx model catalysts: catalytic performance and operando XRD studies. Catal Commun 2017;100:232–6.
[48] Toghan A, Khodari M, Steinbach F, Imbihl R. Microstructure of thin film platinum electrodes on yttrium stabilized zirconia prepared by sputter deposition. Thin Solid Films 2011;519:8139–43.
[49] Naumkin AK-VAVG, W S, Powell CJ. NIST Standard Reference Database 20, Version 41, Gaithersburg; 2012.
[50] Yu W, Xie HQ. A review on nanofluids: preparation, stability mechanisms, and applications. J Nanomater 2012.
[51] Chakraborty S, Sarkar I, Haldar K, Pal SK, Chakraborty S. Synthesis of Cu-Al layered double hydroxide nanofluid and characterization of its thermal properties. Appl Clay Sci 2015;107:98–108.
[52] Zhu HT, Lin YS, Yin YS. A novel one-step chemical method for preparation of copper nanofluids. J Colloid Interf Sci 2004;277:100–3.
[53] Hwang Y, Lee JK, Lee CH, Jung YM, Cheong SI, Lee CG, et al. Stability and thermal conductivity characteristics of nanofluids. Thermochim Acta 2007;455:70–4.
[54] Wang BG, Wang XB, Lou WJ, Hao JC. Ionic liquid-based stable nanofluids containing gold nanoparticles. J Colloid Interf Sci 2011;362:5–14.
[55] Das SK, Choi SUS, Yu W, Pradeep T. Nanofluids: science and technology. Hoboken, New Jersey, USA: John Wiley & Sons, Inc.; 2008.
[56] Gupta M, Singh V, Kumar R, Said Z. A review on thermophysical properties of nanofluids and heat transfer applications. Renew Sustain Energy Rev 2017;74:638–70.
[57] Cabaleiro D, Gracia-Fernandez C, Legido JL, Lugo L. Specific heat of metal oxide nanofluids at high concentrations for heat transfer. Int J Heat Mass Transf 2015;88:872–9.
[58] Mousavi NSS, Kumar S. Effective heat capacity of ferrofluids - analytical approach. Int J Therm Sci 2014;84:267–74.
[59] Shin D, Banerjee D. Enhanced specific heat capacity of nanomaterials synthesized by dispersing silica nanoparticles in eutectic mixtures. J Heat Trans-T Asme 2013;135.
[60] Prasher R, Song D, Wang JL, Phelan P. Measurements of nanofluid viscosity and its implications for thermal applications. Appl Phys Lett 2006;89.
[61] Dittus FW, Boelter LMK. Pioneers in heat-transfer - heat-transfer in automobile radiators of the tubular type (Reprinted from University of California Publications in Engineering, Vol 2, Pg 443–461, 1930. Int Commun Heat Mass. 1985;12:3–22.
[62] Greenwood NN, Earnshaw A. Chemistry of the elements. Oxford, United Kingdom: Butterworth-Heinemann; 1997.
[63] Annapureddy HVR, Nune SK, Motkuri RK, McGrail BP, Dang LEX. A combined experimental and computational study on the stability of nanofluids containing metal organic frameworks. J Phys Chem B 2015;119:8992–9.

Annex 5

Experimental characterization and theoretical modelling of Ag and Au-nanofluids: A comparative study of their thermal properties

AMERICAN SCIENTIFIC PUBLISHERS

Journal of Nanofluids
Vol. 7, pp. 1–10, 2018
(www.aspbs.com/jon)

ARTICLE

Experimental Characterization and Theoretical Modelling of Ag and Au-Nanofluids: A Comparative Study of Their Thermal Properties

R. Gómez-Villarejo[1,*], E. I. Martín[2], A. Sánchez-Coronilla[3], T. Aguilar[1], M. Teruel[1], R. Alcántara[1], I. Carrillo-Berdugo[1], C. Fernández-Lorenzo[1], and J. Navas[1]

[1]*Departamento de Química Física, Facultad de Ciencias, Universidad de Cádiz, E-11510 Puerto Real (Cádiz), Spain*
[2]*Departamento de Ingeniería Química, Facultad de Química, Universidad de Sevilla, E-41012 Sevilla, Spain*
[3]*Departamento de Química Física, Facultad de Farmacia, Universidad de Sevilla, E-41012 Sevilla, Spain*

This article reports the preparation and characterization of nanofluids based on the heat transfer fluid (HTF) commonly used in concentrating solar power (CSP) plants. Nanofluids were prepared with commercial Ag nanoparticles and synthesized Au nanoparticles which were dispersed into a base fluid composed by a eutectic mixture of two stable compounds: diphenyl oxide and biphenyl. Both sets of nanofluids were characterized attending to its physical and chemical stability and the possible improvement on thermal properties respect to base fluid. Moreover, a theoretical analysis was achieved by Molecular Dynamics simulations to obtain a greater knowledge about this kind of systems through the study of the different interactions between the metal and the molecules of the base fluid. The results showed that the incorporation of Ag nanoparticles into a base fluid improves significantly thermal properties such as isobaric specific heat and thermal conductivity, giving an enhancement of its heat transfer coefficient. Theoretical analysis revealed that the arrangement of molecules of base fluid around the Ag nanoparticle favors the improvement of thermal properties. On his part, addition of Au nanoparticles into the base fluid did not produce any increment of thermal properties with regard to base fluid, and the theoretical analysis showed a minor participation of diphenyl oxide molecules in a first layer of Au nanoparticle.

KEYWORDS: Nanofluid, Concentrating Solar Power, Heat Transfer Process, Molecular Dynamics.

1. INTRODUCTION

During last decades heat transfer management has been introduced in most industrial processes and the development of high performance thermal systems for heat transfer have become a primary challenge. Due to an accelerated population and industrial growth, the daily consumption of energy forces society to look for alternative energies that may replace fossil-based energy sources and it allows us to respond to a huge world demand without generating an environmental impact on the planet.[1,2] Renewable sources such as solar, eolic and geothermal energies are excellent alternatives due to their good availability and environmental innocuousness so that they can be used to a large extent.[3–6] Particularly, solar energy is considered as the energy of our future and concentrating solar power (CSP) has emerged as an attractive option due to its potential to meet base load applications.[7] The operating mechanism of CSP is based on focusing solar radiation by using parabolic mirrors to concentrate radiation towards an absorbing tube that may be in solar tower systems or parabolic dishes, where the heat is collected by a thermal energy carrier called heat transfer fluid (HTF).[8–11] HTF can operate directly as a driver towards a turbine to produce power or, more commonly, to be combined with a heat exchanger in a secondary cycle with other fluid.[11–13] This type of devices can reach temperatures about 400–500 °C and it possible to capture sunlight efficiently during winter thanks to the geometrical configuration of mirrors.[7]

Improving heat transfer efficiency in CSP plants is one of the keys to obtain a better performance of these systems.[2] One of the effective methods that has opened a wide field of research is to replace the working HTF with fluid containing nanoparticles that improve the thermophysical properties of the original HTF. This type of fluids are called nanofluids.[14–16]

Nanofluids are a new type of HTF that are formed by the colloidal suspension of nano-sized particles within a

*Author to whom correspondence should be addressed.
Email: roberto.gomezvi@uca.es
Received: 30 January 2018
Accepted: 14 March 2018

base fluid. Previous reports showed thermal conductivity enhancements up to 40% for copper-based nanofluids[17] and about 18% for silver-based nanofluids[18] using ethylene glycol as base fluid in both cases. In addition, metal oxide nanoparticles such as Al_2O_3, TiO_2 or WO_3 also enhance thermal conductivity values.[19–20] Water or ethylene glycol are typically used as base fluid for its application in low temperatures systems. In contrast, a smaller fraction of the published researches are focused on those fluids commonly used in CSP plants. This type of HTF, usually organic oils, can be thermally stable at the operating temperature range of 70–550 °C.[21]

This report aims to compare Ag-based and Au-based nanofluids from both experimental and theoretical points of view. Nanofluids have been prepared in a commonly used HTF for CSP plants, which is an eutectic mixture of biphenyl ($C_{12}H_{10}$) and diphenyl oxide ($C_{12}H_{10}O$). Recent studies showed an improvement of thermal properties for copper-based[22] and gold-based nanofluids[23] using this type of base fluid. Ag commercial nanoparticles and Au synthesized nanoparticles have been used to prepare three nanofluids of each metal in three different mass fractions. Each set of nanofluids has been characterized to check its physical and chemical stability and to confirm any possible improvement in thermal properties with respect to the base fluid caused by the addition of metal nanoparticles. Properties such as density, viscosity, isobaric specific heat and thermal conductivity were measured. The comparison of both kind of nanofluids prepared following the same procedure is really interesting in order to compare their efficiencies as HTF. In addition, to understand the behavior of these nanofluids at the molecular level, the study of structural properties was carried out by Molecular Dynamics simulations. Radial distribution functions (RDF) and spatial distribution functions (SDF) were calculated to compare both systems and to study the interactions between the metal and the molecules of base fluid. This rationalization the behavior of the nanofluid systems is of great interest in order to understand the thermal properties found.

2. METHODS

2.1. Preparation of Nanofluids

Nanofluids studied in this work were prepared following a two-step method.[24] This method is extensively used in the preparation of nanofluids by mixing the base fluid with nanopowders obtained from different mechanical, physical and chemical routes. Au nanoparticles were synthesized by the citrate reduction method, using sodium citrate ($C_6H_5Na_3O_7 \cdot 2H_2O$, purity >99.0%, supplied by PanReac AppliChem©) as reduction agent, and using tetrachloroauric acid ($HAuCl_4$, assay 99.9%, Sigma-Aldrich©) as Au precursor agent. This reduction method constitutes the first step in the nanofluid preparation. In the case of Ag nanofluid, we have used commercial nanoparticles (purity ≥99%, density 10.490 kg m^{-3} at 298 K, Sigma-Aldrich©) with a particle size lower than 100 nm. The second step consists on dispersing the nanomaterial in the base fluid. In this study, a commercial heat transfer fluid was used as base fluid, it is composed of the eutectic mixture of biphenyl ($C_{12}H_{10}$, 26.5%) and diphenyl oxide ($C_{12}H_{10}O$, 73.5%), supplied by the Dow Chemical Company©, model DowthermA. Both compounds show practically the same vapor pressure, consequently, the mixture can be treated as if it was a single compound.

Three nanofluids of each metal, with a mass nanoparticle concentration of $0.5 \cdot 10^{-4}$, $1.0 \cdot 10^{-4}$ and $5.0 \cdot 10^{-4}$ wt.% were prepared by dilution of other nanofluid with 0.01 wt.% and the same amount of polyethylene glycol (PEG, average molecular: 5000–7000, supplied by PanReac AppliChem©). All nanofluids were prepared using 100 mL of the base fluid. A sonication method was used in all of them to obtain the dispersion of nanoparticles. It was applied for 3 hours (~50 W output power) using a Sonics Vibra Cell VCX 750 sonicator, controlling the temperature at 293 K in a thermal bath.

2.2. Characterization of Nanofluids

Several properties of nanofluids prepared were characterized to prove the possible enhancement of heat transfer process for its application in Concentrating Solar Power (CSP) plants.

To determine the chemical and physical stability of nanofluids, two properties were studied. Chemical stability was analyzed by visible spectroscopy. Spectra were recorded in the visible range using a system mounted in our laboratory composed of a halogen lamp (model DH-2000-BAL) as illumination source and a USB2000+ spectrometer, both supplied by OceanOptics©. Moreover, physical stability was analyzed by particle size measurements using the Dynamic Light Scattering (DLS) technique supplied by Malvern© zetasizer Nano-Z system. Measurements of particle size were recorder for one week.

Four properties were measured to verify the possible enhancement of heat transfer process of nanofluids with regard to base fluid by means the determination of the ratio of the heat transfer coefficients of nanofluids and base fluid using the Dittus-Boelter equation:

$$FoM = \frac{h_{nf}}{h_{bf}} = \left(\frac{\rho_{nf}}{\rho_{bf}}\right)^{0.8} \left(\frac{k_{nf}}{k_{bf}}\right)^{0.6} \left(\frac{C_{p(nf)}}{C_{p(bf)}}\right)^{0.4} \left(\frac{\mu_{nf}}{\mu_{bf}}\right)^{-0.4} \quad (1)$$

where h is the heat transfer coefficient, ρ is the density, k the thermal conductivity, C_P is the isobaric specific heat and μ is the dynamic viscosity,[22,25,26] and the subscripts nf and bf refer to the nanofluid and base fluid, respectively. We note that there is an improvement in the efficiency of the system whether the ratio $h_{nf}/h_{bf} > 1$. Thus, density was estimated by a pycnometer and dynamic viscosity was measured using a SV-10 viscometer supplied by Malvern Instruments Ltd. Both properties were measured in a thermal bath to control the temperature and

they were performed in triplicate. The isobaric specific heat measurements were performed using a Temperature Modulated Differential Scanning Calorimeter (TMDSC), supplied by Netzsch© model DSC214Polyma. A standard procedure was created to perform the measurements and can be summarized in the following points: the temperature was equilibrated at 341 K to remove contaminants and kept isothermal for 10 min; then the samples were equilibrated at 288 K and the ramped to 373 K at 1 K/min. A modulation around the studied temperatures with an amplitude of ± 1 K and a period of 120 s was programmed. Finally, cooling was performed freely. Finally, thermal conductivity was measured using the light flash technique, using a LFA467 HyperFlash equipment, supplied by Netzsch©. This technique really measures thermal diffusivity (D) which is defined as the speed of heat propagation by conduction during changes of temperature. This property is related to thermal conductivity, isobaric specific heat and density by the following equation:

$$k(T) = D(T) \cdot C_p(T) \cdot \rho(T) \tag{2}$$

2.3. Computational Methods

2.3.1. Force Field

The TraPPE-EH force field[27,28] was used to describe inter- and intramolecular interactions between the molecules of diphenyl oxide and biphenyl that compound the base fluid. The TraPPE-EH force field treats aromatic rings and directly linked atoms as rigid entities. Phenyl rings were allowed to rotate with regard to each other around the C1–C1′ bond of the biphenyl. Parameters used in our simulations to study the metal nanoparticle were adapted to a Non-Bonded Dummy Model,[29,30] consisting on six dummy atoms distributed around a central metal particle in an octahedral geometry. The geometry of the dummy complex itself is kept rigid by the imposition of large force constants for the metal-dummy bonds. However, as there are no bonds between the dummy complex and the surrounding ligands, the overall rotation of the octahedral frame around the nucleus is plausible since no internal forces are associated. Therefore, the coordination geometry is not restricted to the geometry of the dummy model used but rather the system has the freedom to exchange ligands.

The TraPPE-EH force field and the Non-Bonded Dummy Model use Lennard-Jones (LJ) and Coulomb potential functions to represent the non-bonding interactions:

$$u(r_{ij}) = 4\varepsilon_{ij}\left[\left(\frac{\sigma_{ij}}{r_{ij}}\right)^{12} - \left(\frac{\sigma_{ij}}{r_{ij}}\right)^{6}\right] + \frac{q_i q_j}{4\pi\varepsilon_0 r_{ij}} \tag{3}$$

where r_{ij}, ε_{ij}, σ_{ij}, q_i, q_j, and ε_0 are the distance between interaction sites i and j, the LJ well depth, the LJ diameter, the partial charges on interaction sites i and j, and the permittivity of vacuum, respectively. The Lorentz-Berthelot combining rules were used to determine LJ parameters for different interactions.

2.3.2. Simulation Details

Molecular Dynamics simulations were performed with the DLPOLY code[31] in the canonical ensemble (NVT) using a Nose-Hoover thermostat and periodic boundary conditions. The initial configurations are constructed with de PACKMOL code[32] providing cubic simulation environments with a side length chosen to keep the density of the experimental HTF at 298 K (1056 kg m^{-3}). In each and every simulation performed, the box contained a metal nanoparticle, 117 diphenyl oxide molecules and 48 biphenyl molecules.

A time step of 0.5 fs was used and the overall simulation runs lasted for 1.0 ns. For the trajectory analysis, structures were saved every 100 time steps. A cut-off distance of 9.0 Å was applied in all cases and the Ewald summation methodology[33] applied to account for the long-range electrostatic interactions.

Lastly, structural images were computed using ChemCraft 1.6.

3. RESULTS AND DISCUSSION

3.1. Nanofluids Stability

Stability of nanofluids is an essential and interesting parameter to study in order to consider nanofluids as a promising alternative in real applications. So, chemical stability was analyzed to verify whether the addition of nanoparticles causes chemical changes in the base fluid. To study this, spectra were recorded in a range 400–800 nm and they are shown in Figure 1(A). Ag and Au-based nanofluids show a wide band up centered at 400–500 nm, which is typical for colloidal suspension systems, since the light is dispersed when it collides against nanoparticles. Besides, this phenomenon occurs typically at lower wavelengths.[34,35] Bands at 630 and 870 nm appear both in Au-nanofluids and the base fluid, and they can be assigned to the fluid itself. In the case of Ag-nanofluids, it appears only a soft peak at 870 nm, which also corresponds to the base fluid. Consequently, no chemical modification in the base fluid is observed due to the nanoparticles incorporation.

Likewise, physical stability of nanofluids was analyzed from particle size measurements using Dynamic Light Scattering (DLS) technique. Measurements were performed for one week, registering several measurements each day. Results obtained are shown in Figure 1(B). Particle size values obtained were higher than the nominal values for the nanoparticles because of DLS technique gives information about the hydrodynamic diameter, which is determined as the sum of the particle diameter and the thickness of the diffuse layer known as Debye length.[36] But also, for both sets of nanofluids, particle size increased rapidly for few hours after the preparation, and after it

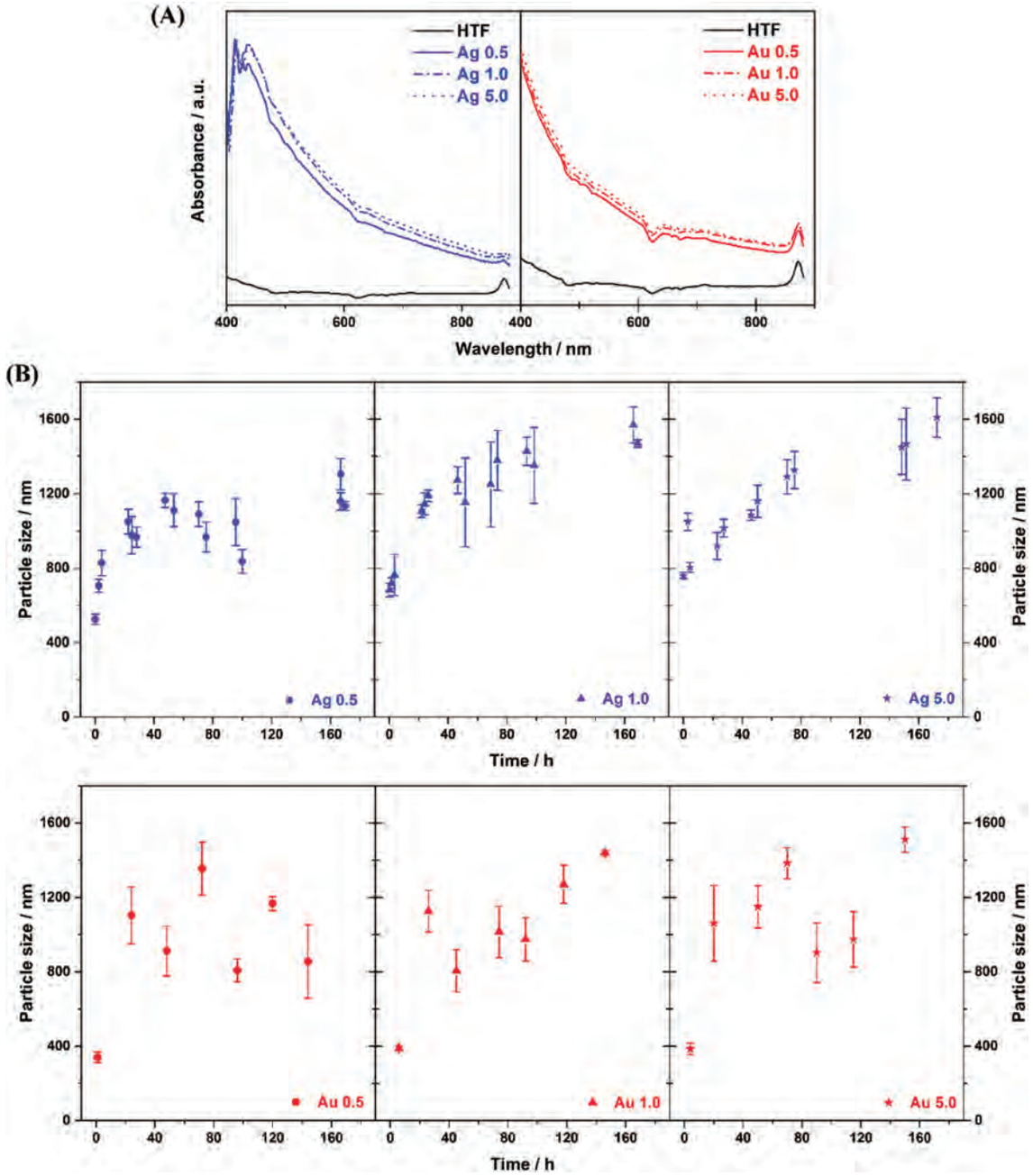

Fig. 1. (A) Visible spectra for both sets of Ag and Au nanofluids and base fluid. (B) Particle size measurements using DLS technique for Ag and Au nanofluids.

remained practically stable. The growth of the particle size was due to agglomeration phenomena that occur after the preparation, for several hours. After, the particle size was considered stable over time.

3.2. Density

Density is a property that affects significantly to heat transport. It is well-known that high density materials enhance heat transfer process.[37] Density of nanofluids was measured in accordance with the nanoparticle mass concentration. The density of the base fluid was also measured to verify the workability of the method followed, which showed a deviation below 0.1% of mean value (1056 ± 0.7 kg m^{-3}) regarding to the value provided by the supplier (1055.7 kg m^{-3}). Figure 2(A) shows density values obtained for nanofluids and base fluid. An increase

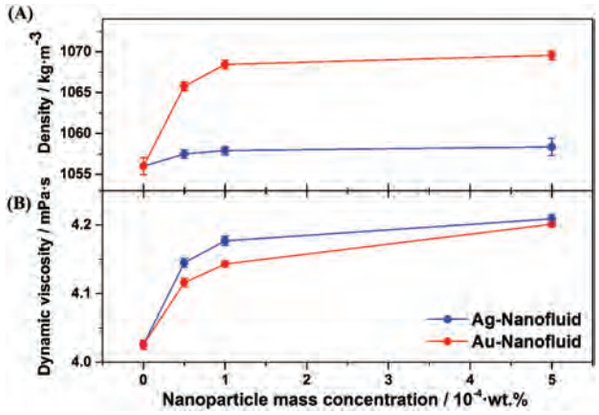

Fig. 2. Density (A) and dynamic viscosity (B) values versus nanoparticle mass concentration of Ag and Au nanofluids.

in the density of up to 1.3% for the nanofluid with the high nanoparticle content in the case of Au nanofluids, and an increase up to 0.23% for Ag nanofluid were found.

3.3. Viscosity

Viscosity plays an important role in the heat transfer process. It would be expected that the addition of nanoparticles into a base fluid causes an increase in viscosity values, and this increase is detrimental in terms of efficiency because it can affect different elements in a solar plant such as the pumping pressure or to lead to possible drops in pressure. Therefore, it is essential to control any possible increase in viscosity. Thus, viscosity was measured to correlate its influence in the heat transfer process. Viscosity of the base fluid was also measured to check the goodness of the method used. A deviation below 0.9% was found between the value obtained of base fluid (4.030 ± 0.004 mPa · s) and the value provided by the supplier (4.060 mPa · s). Figure 2(B) shows the viscosity values obtained for all of nanofluids prepared. An increase of up to 4.3% for the Au nanofluid with highest concentration of nanoparticle, and an increase of up to 4.5% in the case of Ag nanofluid with the same amount of nanoparticle were found. In addition, the results of viscosity are coherent with previous results, where viscosity increases when nanoparticles are added. The number of interactions between the nanoparticles inside the fluid considerably increasing, producing higher viscosity values.[38,39] On the other hand, the relation between viscosity and nanoparticle mass concentration is not linear for both kind of nanofluids, as the Einstein model predicts for nanofluids with low concentrations of nanoparticles.[40] This suggests the existence of particle–particle interactions, which is not considered in the Einstein model for viscosity.

3.4. Isobaric Specific Heat

Isobaric specific heat values for Au and Ag nanofluids prepared were measured in the temperature range 300–360 K following the procedure described above. Figure 3(A) shows the results obtained for both nanofluid and for the base fluid. All nanofluids incorporating Ag nanoparticles improve the isobaric specific heat values regarding to base fluid. In fact, Ag nanofluid with the highest concentration of nanoparticles shows an improvement about 7%. In the case of Au nanofluids, the values of the isobaric specific heat are close to the values for the base fluid. Only slight changes were found. To understand these results, it is necessary to know that the isobaric specific heat for solids is lower than for liquids. Thus, it would be expected that isobaric specific heat is lower for nanofluids with respect to the base fluid,[41,42] and also it decreases when the nanoparticle mass concentration increases.[46–48] Thus, fact occurs in Au nanofluid. By contrast, cases where the isobaric specific heat increase when nanoparticles are added have been reported,[44,45,49] which is the same behavior found for Ag nanofluids in this work. In this regard, Shin et al.[50,51] suggest the existence of an internal structure within the nanofluid generated by the specific interaction between the nanoparticle and the base fluid, which depends on nature and concentration of the components of the nanofluid.

3.5. Thermal Conductivity

Thermal conductivity of nanofluids prepared was measured at different temperature and the measurements were performed using the light flash technique as is described above. This technique really measures the thermal diffusivity, which is related with thermal conductivity by the Eq. (2). The thermal conductivity values obtained are shown in Figure 3(B). Ag nanofluids show an enhancement of thermal conductivity regarding to the base fluid. The highest increase, up to 6%, is found for the nanofluid incorporating the highest nanoparticle mass concentration. This result is coherent with previous reports.[52] Also, thermal conductivity for Ag nanofluids decrease as the temperature increased, following a similar tendency to the base fluid. For the case of Au nanofluid, the improvement of thermal conductivity appears significantly at high temperature, giving an enhancement up to 3% for the nanofluid with highest nanoparticle concentration.

Moreover, thermal conductivity of Ag nanofluids increased as nanoparticle mass concentration increases. Probably the interaction between base fluid/nanoparticle is the responsible of the behavior found. The nature of all the components in the nanofluid system is an important variable. The base fluid used in this work is clearly different to other typically used due to the low polarity, and therefore the interactions between the components depends on the nature of the base fluid. Also, the formation of aggregates affects to the properties of the nanofluids prepared. As reported previously, effective hear conduction through nanoparticle agglomerates leads to enhanced thermal conductivity.[53] Also, the increase in thermal conductivity for Ag nanofluids can be explained using several

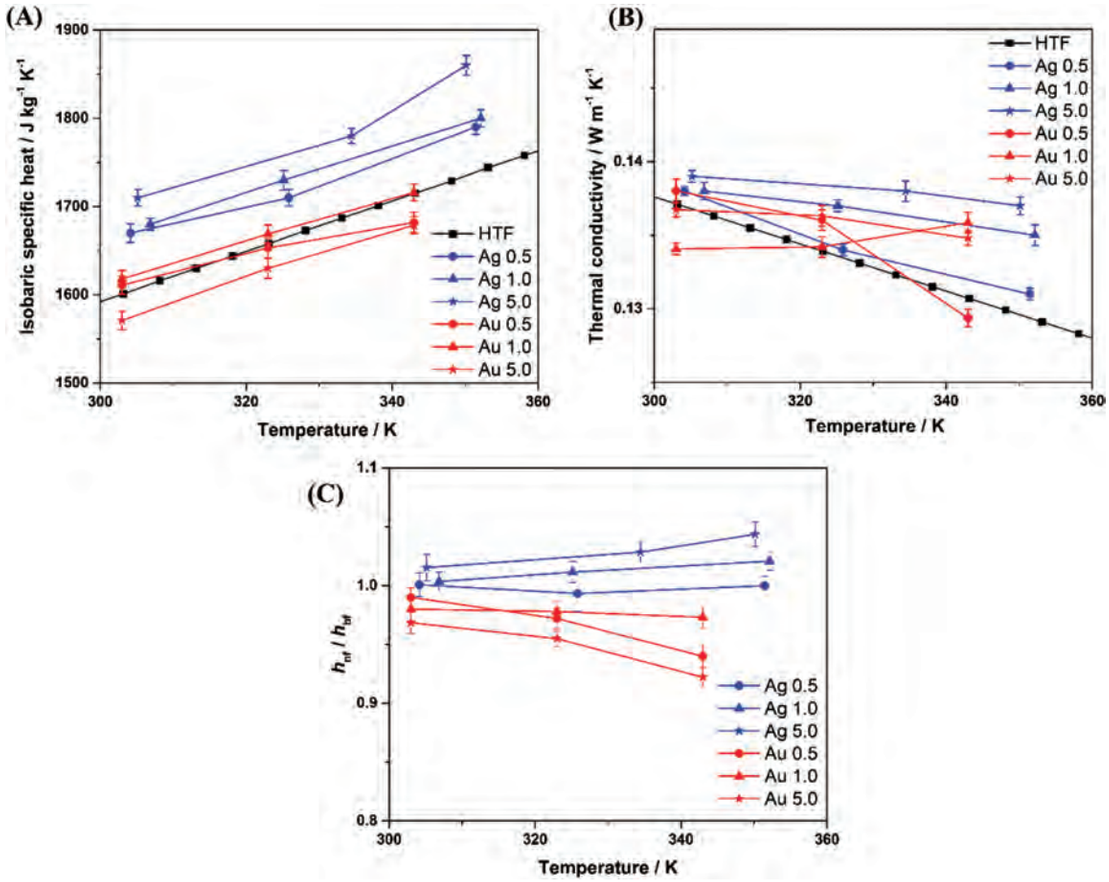

Fig. 3. (A) Isobaric specific heat and (B) thermal conductivity values for Ag and Au nanofluids. Values of base fluid reported by the supplier have been included for comparison purposes. (C) Values of the ratio of the heat transfer coefficient obtained for Ag and Au nanofluids.

factors. First, the high thermal conductivity of Ag nanoparticles with respect to the base fluid. Second, other important reason is the presence of nanoparticles themselves because of the interactions between the particles, which were also observed by means of the viscosity results shown above. Third, the interactions between nanoparticles and the molecules of the base fluid could be the origin of the Brownian motion, as reported previously.[54]

3.6. Performance of the Nanofluids

To analyze the efficiency of the nanofluids in heat transfer applications, the ratio between the heat transfer coefficient of nanofluids and the base fluid is estimated by the Dittus-Boelter correlation (see Eq. (1)). Values for this ratio above 1 ($h_{nf}/h_{bf} > 1$) imply an enhancement in the efficiency of the nanofluid with regard to base fluid. The ratio of heat transfer coefficient was estimated at temperature at which isobaric specific heat and thermal conductivity were measured. Density and viscosity values were estimated using the evolution of the values reported by the supplier and considering the values measured for the nanofluids at around temperature. Thus, Figure 3(B) shows the values obtained for Ag and Au nanofluids. For Ag nanofluids, an enhancement up to 6% was obtained for the nanofluid with the highest nanoparticle mass concentration. However, Au-nanofluid did not showed a significant improvement in no case.

Therefore, Ag nanofluids would be consider as an interesting alternative to the typical fluid used as heat transfer fluid in CSP plants. Ag-nanofluids improve the thermal properties without causing modifications in nature of base fluid. Au-nanofluids do not present an improvement in the heat transfer coefficient, consequently, their application in CSP would not be logical. However, recent publications[55] report a greatest enhancement of heat transfer coefficient when Au-nanofluids are stabilizers by a surfactant. In any way, presence of surfactant allows an effective stabilization of gold nanoparticles that provides an improvement in their thermal properties. As a result, the role of surfactant is very important in the stabilization of nanofluids and it open the possibility to applicate Au-nanofluids in CSP systems.

3.7. Theoretical Analysis: Structural Properties

The study at molecular level of the nanofluidic systems was achieved by Molecular Dynamics, in order to

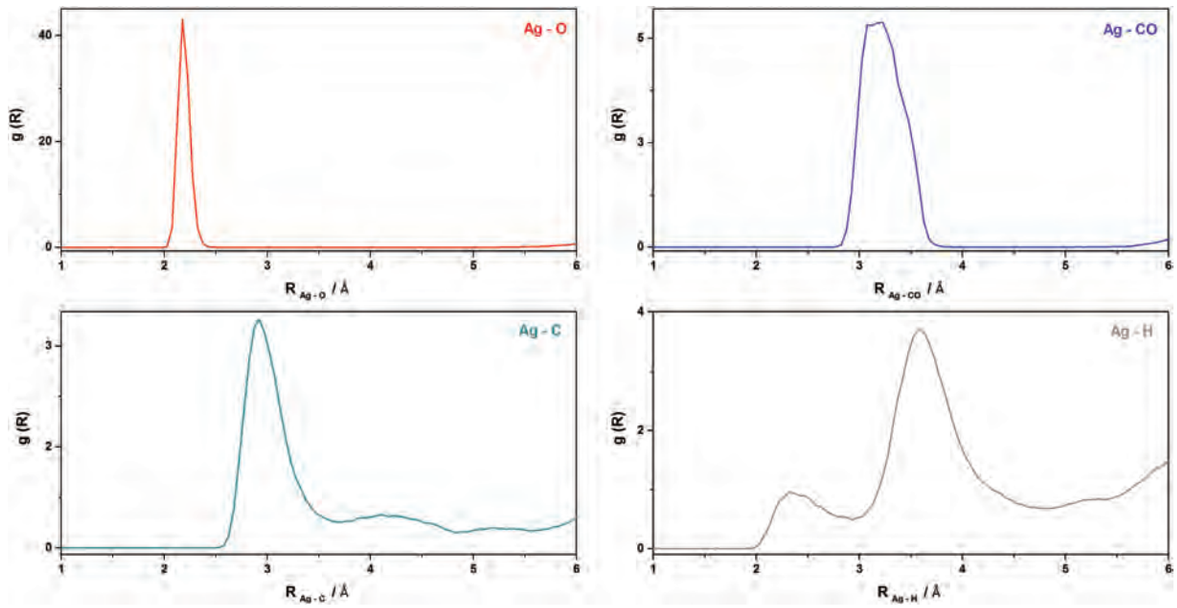

Fig. 4. Radial distribution functions between the Ag–O, Ag–CO, Ag–C and Ag–H pairs in Ag-nanofluid system.

obtain information about how the base fluid molecules are arranged around the metallic nanoparticle and the interactions between them. Radial distribution functions (RDF) and spatial distribution functions (SDF) are powerful tools to gain greater knowledge about the nanofluid systems at molecular scale. Through an extracted information of these function is possible to identify the interaction between the metal frameworks and the base fluid. For comparing both nanofluids, performing calculations at 300 K was chosen.

Interactions between metallic nanoparticle and molecules of base fluid were analyzed from radial distribution functions, in particular those interactions between silver and gold with four different atoms of the base fluid molecules: O atoms of diphenyl oxide, C atoms of biphenyl oxide linked to an O atom, C atoms of aromatic ring and aromatic H atoms. Figure 4 shows the analysis of the RDFs of the Ag–O, Ag–CO, Ag–C and Ag–H pairs. For Ag–O interactions, the analysis of his RDF shows an intense peak centered around 2.2 Å, which integrates for two O atoms belonging to two diphenyl oxide molecules. The small width of the peak means clearly that two molecules of diphenyl oxide are localized very close to the Ag atom. Consequently, the peak of the interaction between Ag and C linked to O in diphenyl oxide molecules is located at 3.2 Å and it integrates to four atoms; that is, two C atoms for each molecule of diphenyl oxide. For Ag–C interactions, three peaks are observed in the RDF results. The first peak is intense and it appears around 2.9 Å. It corresponds with eight C atoms. The other two peaks appear at 4.2 and 5.2 Å, and they integrate to 16 and 8 C atoms, respectively. Finally, in the case of Ag–H, another three peaks can be distinguished: a very intense peak centered at 3.8 Å and two smoother peaks at 2.4 and 5.4 Å. The integration of these peaks corresponds to 32 H atoms. With all this information, a first layer of base fluid around the silver nanoparticles may be described as two molecules of diphenyl oxide and one molecule of biphenyl around the Ag nanoparticle.

This arrangement can be better understood by the analysis of the SDF. Figure 5(A) shows the SDFs for the Ag-nanofluid system at a distance of 4.0 Å, with the silver atom in the center (green color). Red and blue spatial distributions correspond to O atoms and C atoms linked to O atoms, while C atoms from aromatic rings were assigned

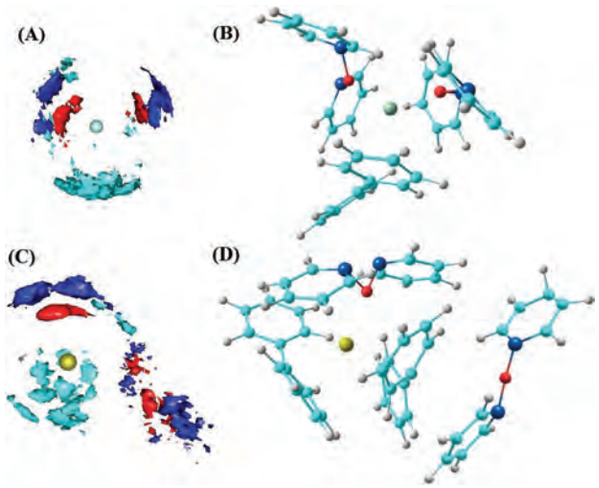

Fig. 5. Spatial distribution functions for the Ag-nanofluid (A) and Au-nanofluid (C). Structures around the Ag (B) and Au (D) in the nanofluidic systems.

with sky-blue color. H atoms were not included in order to clarify the image. Figure 5(B) shows a representation of the SDF in order to clarify the position of the atoms and molecules. Figures 5(A) and (B) show two molecules of diphenyl oxide oriented towards Ag atom, being O atoms close to Ag, and a molecule of biphenyl located around Ag. These molecules build a cluster that possibly stabilizes the system and causes an enhancement on thermal properties of the nanofluid due to the directionality of movement that may favor a heat transport.

For Au nanofluids, Figure 6 shows the results of RDFs for Au–O, Au–CO, Au–C and Au–H interactions. The intense peak observed on the Au–O pair is also centered at 2.2 Å, but it integrates only an O atom belonging to one diphenyl oxide molecule. A weak peak appears at 5.7 Å, which corresponds to an O atom from another diphenyl oxide molecule. For the interaction of Au–CO, the peak integrates two C atoms, corresponding to one diphenyl oxide molecule. Besides, a weak peak from 5.8 Å is observed, and it is assigned to the second molecule of diphenyl oxide. On the other hand, Ag–C interaction shows a intense peak at 2.9 Å that integrates eight C atoms and two less intense peaks at 4.2 and 5.7 Å, which correspond to 16 and 10 C atoms, respectively. Finally, an analysis of the RDF of the Ag–H interaction reveals a weak signal at 2.9 Å and a wide peak at 3.5 Å. Both integrate 1 and 15 H atoms that is a total of 16 H atoms. Last peak at 5.8 Å corresponds to other 16 H atoms.

Although the analysis of RDF for Ag and Au-nanofluid systems were calculated until 6.0 Å, in the case of Au-nanofluid is interesting to discuss the signals appearing around 5.5–6.0 Å to verify the existence of a second molecule of diphenyl oxide. Describing the atoms with the same colors previously assigned, Figures 5(C) and (D) show the SDF for the Au-nanofluid system and a representation of the molecules in a radius of 6.0 Å with the Au atom in the center (golden color). In this case, only one molecule of diphenyl oxide and one molecule of biphenyl are located around the Au atom, constituting the first layer around the metal. This layer is not totally closed, so a second molecule of diphenyl oxide appears close to this layer.

This arrangement is not enough to approximate a ratio of 2:1 of diphenyl oxide/biphenyl for Au-nanofluid as it was for the Ag-nanofluid. For that, the first layer around de Au does not cause an enhancement in thermal properties due to the number of molecules of diphenyl oxide. Literature reports that thermal properties of nanofluids have increased considerably when the distribution of molecules of base fluid around the metal nanoparticle is 3:1 of diphenyl oxide/biphenyl, which is the same proportion of the eutectic mixture that composes the base fluid.[56] In our case, Ag-nanofluids show a ratio of 2:1 and improve moderately the thermal properties of base fluid. In turn, Au-nanofluid present an intermediate ratio between 1:1 and 2:1 and it does not cause significant modifications in thermal properties of base fluid.

For instance, isobaric specific heat was calculated by Molecular Dynamics from 50 to 600 K for both nanofluids and for the base fluid, by means of the plot of the total energy versus temperature (Fig. 7). The values estimated from the slopes in these plots were $2.15 \cdot 10^3$ J kg^{-1} K^{-1} for the Ag-nanofluid; $2.01 \cdot 10^3$ J kg^{-1} K^{-1} for the Au-nanofluid and $1.94 \cdot 10^3$ J kg^{-1} K^{-1} for the base fluid. These results are in accordance with the experimental results obtained, so that follow the same qualitative

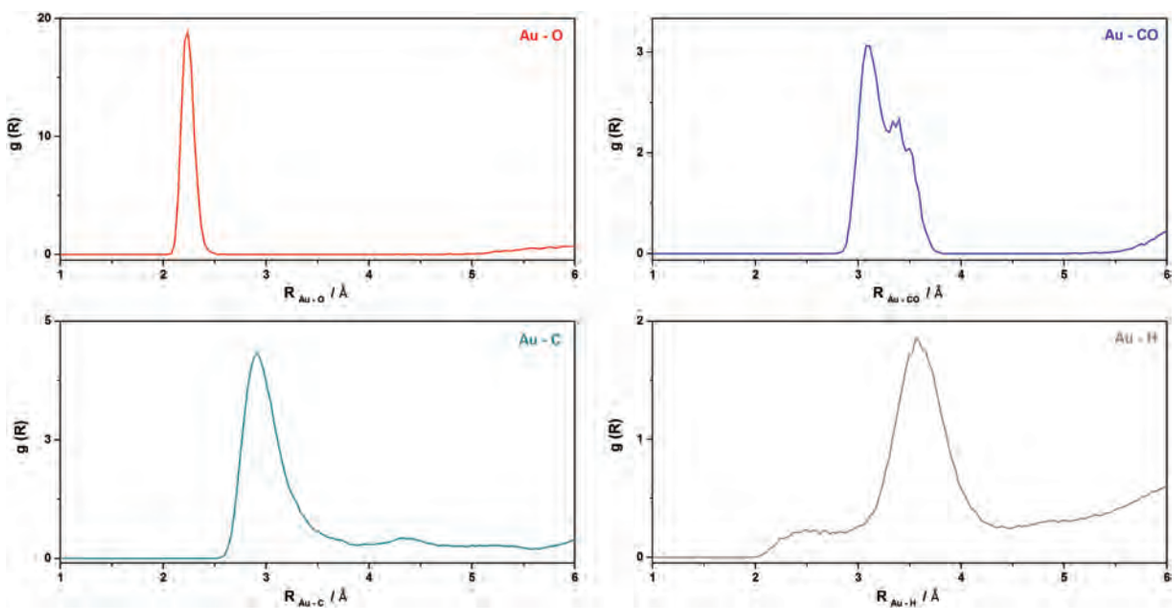

Fig. 6. RDFs between the Au–O, Au–CO, Au–C and Au–H pairs in Au-nanofluid system.

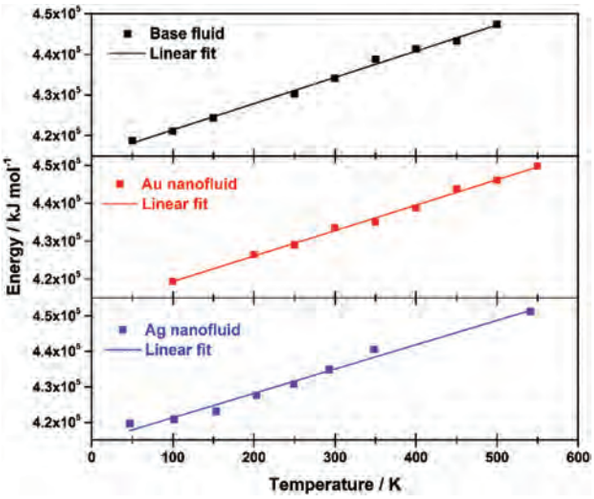

Fig. 7. Plot of the total energy versus temperature for the base fluid (black), Au nanofluid (red) and Ag nanofluid (blue).

tendency, $C_{p(Ag\text{-}nanofluid)} > C_{p(Au\text{-}nanofluid)} > C_{p(basefluid)}$, and this is an evidence of the possible participation from diphenyl oxide molecules in the enhancement of thermal properties.

Moreover, most recent studies show the importance of the use of surfactants in this type of systems, not only from a stability point of view but also from its capability to reorganize the system and improve thermal processes. In fact, Au-nanofluid shows a remarkable improvement on thermal properties regard to the base fluid when surfactant is added in the preparation process.[55]

4. CONCLUSIONS

In this study, nanofluids based on a heat transfer fluid composed of a eutectic mixture of diphenyl oxide and biphenyl with Ag and Au nanoparticles were prepared. Both sets of nanofluids were analyzed from an experimental and theoretical perspective.

The addition of metallic nanoparticles did not cause chemical changes in the base fluid. An increase in density and viscosity was observed for all the nanofluids prepared. Regarding to the thermal properties, Ag-nanofluids showed an increase in both isobaric specific heat and thermal conductivity. It was obtained an improve by up to 6% of heat transfer coefficient for Ag-nanofluid with regard to the base fluid according to an *FoM* based on the Dittus-Boelter correlation. Consequently, the nanofluids based on Ag nanoparticles enhance heat transfer efficiency, and therefore the application of this kind of nanofluids as HTF in CSP plants can be promising. However, Au-nanofluids did not produce neither increase in the thermal properties cited above, so its application such as HTF would be dismissed.

By the study of the radial distribution functions (RDF) and spatial distribution functions (SDF), the structural analysis around the Ag nanoparticle showed the existence of a first-layer structure composed of two diphenyl oxide molecules and one biphenyl molecule. Only a molecule of diphenyl oxide and two molecules of biphenyl were found around the Au nanoparticle. These different structures could explain the enhancement of thermal properties in the case of Ag-nanofluids, due to the better re-ordering of base fluid around the metal atom that seems to be favored and leads to an increase of thermal properties.

NOMENCLATURE

ρ	Density $kg \cdot m^{-3}$
μ	Dynamic viscosity $mPa \cdot s$
h	Heat transfer coefficient a.u.
k	Thermal conductivity $W \cdot m^{-1} \cdot K^{-1}$
D	Thermal diffusivity $m^2 \cdot s^{-1}$
C_p	Isobaric specific heat $J \cdot kg^{-1} \cdot K^{-1}$
T	Temperature K.

Subscripts

bf	Base fluid
nf	Nanofluid.

ABBREVIATIONS

HTF	Heat Transfer Fluid
CSP	Concentrating Solar Power
RDF	Radial Distribution Function
SDF	Spatial Distribution Function
FoM	Figure of Merit
DLS	Dynamic Light Scattering
TMDSC	Temperature Modulated Differential Scanning Calorimetry
LFA	Light Flash Analysis.

Acknowledgments: We thank the Ministerio de Economia y Competitividad (MINECO) of the Spanish Government for funding under Grant No. ENE2014-58085-R. We thank Torresol Energy Investments, S.A. for their support. Calculations were made through CICA—Centro Informático Científico de Andalucía (Spain).

References and Notes

1. J. Khan and M. H. Arsalan, *Renew. Sust. Energy Rev.* 55, 414 **(2016)**.
2. A. H. Elsheikha, S. W. Sharshirc, Mohamed E. Mostafad, F. A. Essac, and Mohamed Kamal Ahmed Alif, *Renew. Sust. Energy Rev.* 82, 3483 **(2018)**.
3. V. Devabhaktuni, M. Alam, SSSR. Depuru, R. C. Green, D. Nims, and C. Near, *Renew. Sust. Energy Rev.* 19, 555 **(2013)**.
4. A. E. Barkaoui, S. Boldyryev, N. Duic, G. Krajacic, and Z.Guzović, *Appl. Energy* 184, 1343 **(2016)**.
5. M. Mussard, *Renew. Sustain. Energy Rev.* 74, 733 **(2017)**.
6. A. A. Prasad, R. A. Taylor, and M. Kay, *Appl. Energy* 190, 354 **(2017)**.
7. K. Vignarooban, X. Xu, A. Arvay, K. Hsu, and A. M. Kannan, *Appl. Energy* 146, 383 **(2015)**.

ARTICLE

8. Y. El Mghouchi, A. El Bouardi, Z. Choulli, and T. Ajzoul, *Renew. Sust. Energy Rev.* 56, 87 **(2016)**.
9. U. Desideri, F. Zepparelli, V. Morettini, and E. Garroni, *Appl. Energy* 102, 765 **(2013)**.
10. J. P. Bijarniya, K. Sudhakar, and P. Baredar, *Renew. Sust. Energy Rev.* 63, 593 **(2016)**.
11. A. Fernandez-Garcia, E. Zarza, L. Valenzuela, and M. Perez, *Renew-SustEnergy Rev.* 14, 1695 **(2010)**.
12. H. L. Zhang, J. Baeyens, J. Degreve, and G. Caceres, *Renew. Sust. Energy Rev.* 22, 466 **(2013)**.
13. D. Barlev, R. Vidu, and P. Stroeve, *Sol. Energy Mater. Sol. Cells* 95, 2703 **(2011)**.
14. S. Lee, S. U. S. Choi, S. Li, and J. A. Eastman, *J. Heat Trans.-T Asme* 121, 280 **(1999)**.
15. W. H. Yu, D. M. France, J. L. Routbort, and S. U. S. Choi, *Heat Transfer Eng.* 29, 432 **(2008)**.
16. S. U. S. Choi, *J. Heat Trans.-T Asme* 131, 033106 **(2009)**.
17. J. A. Eastman, S. U. S. Choi, S. Li, W. Yu, and L. J. Thomson, *Appl. Phys. Lett.* 78, 718 **(2001)**.
18. T. Cho, I. Baek, J. Lee, and S. Park, *J. Ind. Eng. Chem.* 11, 400 **(2005)**.
19. D. H. Yoo, K. S. Hong, and H. S. Yang, *ThermochimActa* 455, 66 **(2007)**.
20. G. Colangelo, E. Favale, P. Miglietta, A. de Risi, M. Milanese, and D. Laforgia, *Appl. Energy* 154, 874 **(2015)**.
21. D. Beretta, F. C. Loveless, and W. Nudenberg, Use of synthetic hydrocarbon oils as heat transfer fluids, US Patent 4239638 **(1980)**.
22. D. Singh, E. V. Timofeeva, M. R. Moravek, S. Cingarapu, W. H. Yu, and T. Fischer, *Sol. Energy* 105, 468 **(2014)**.
23. C. X. Wang, J. Yang, and Y. L. Ding, *Prog. Nat. Sci. Mater.* 23, 338 **(2013)**.
24. Y. J. Li, J. E. Zhou, S. Tung, E. Schneider, and S. Q. Xi, *Powder Technol.* 196, 89 **(2009)**.
25. F. W. Dittus and L. M. K. Boelter, Pioneers in Heat Transfer-Heat Transfer in Automobile Radiators of the Tubular Type, University California Publications Eng. **(1930)**, Vol. 2, pp. 443–61.
26. W. Yu, D. M. France, E. V. Timofeeva, D. Singh, and J. L. Routbort, *Appl. Phys. Lett.* 96, 213109 **(2010)**.
27. N. Rai and J. I. Siepmann, *J. Phys. Chem. B* 111, 10790 **(2007)**.
28. N. Rai and J. I. Siepmann, *J. Phys. Chem. B* 117, 273 **(2013)**.
29. F. Duarte, P. Bauer, A. Barrozo, B. A. Amrein, M. Purg, and J. Aqvis, *J. Phys. Chem. B* 118, 4351 **(2014)**.
30. Q. H. Liao, S. C. L. Kamerlin, and B. Strodel, *J. Phys. Chem. Lett.* 6, 2657 **(2015)**.
31. W. Smith and T. R. Forester, *J. Mol. Graphics* 14, 136 **(1996)**.
32. J. M. Martinez and L. Martinez, *J. ComputChem.* 24, 819 **(2003)**.
33. M. P. Allen and D. J. Tildesley, Computer Simulation of Liquids, Clarendon, Oxford **(1989)**.
34. H. Chang and M. H. Tsai, *Rev. Adv. Mater. Sci.* 18, 736 **(2008)**.
35. Y. Hwang, J. K. Lee, C. H. Lee, Y. M. Jung, S. I. Cheong, and C. G. Lee, *ThermochimActa* 455, 70 **(2007)**.
36. Y. Y. Song, H. K. D. H. Bhadeshia, and D. W. Suh, *Powder Technol.* 272, 34 **(2015)**.
37. M. Chandrasekar, S. Suresh, and T. Senthilkumar, *Renew. Sust. Energy Rev.* 16, 3917 **(2012)**.
38. P. K. Namburu, D. P. Kulkarni, A. Dandekar, and D. K. Das, *Micro Nano Lett.* 2, 67 **(2007)**.
39. M. Hadadian, S. Samiee, H. Ahmadzadeh, and E. K. Goharshadi, *Phys. Chem. Res.* 1, 1 **(2013)**.
40. A. Einstein, Investigation on the Theory of Brownian Movement, Dover, New York **(1956)**.
41. D. Cabaleiro, C. Gracia-Fernandez, J. L. Legido, and L. Lugo, *Int. J. Heat Mass Transfer* 88, 872 **(2015)**.
42. N. S. S. Mousavi and S. Kumar, *Int. J. ThermSci.* 84, 267 **(2014)**.
43. M. M. Elias, I. M. Mahbubul, R. Saidur, M. R. Sohel, I. M. Shahrul, and S. S. Khaleduzzaman, *IntCommun. Heat Mass* 54, 48 **(2014)**.
44. A. K. Starace, J. C. Gomez, J. Wang, S. Pradhan, and G. C. Glatzmaier, *J. Appl. Phys.* 110, 124323 **(2011)**.
45. H. M. Nieh, T. P. Teng, and C. C. Yu, *Int. J. ThermSci.* 77, 252 **(2014)**.
46. B. Barbes, R. Paramo, E. Blanco, and C. Casanova, *J. Therm. Anal. Calorim.* 115, 1883 **(2014)**.
47. M. N. Pantzali, A. G. Kanaris, K. D. Antoniadis, A. A. Mouza, and S. V. Paras, *Int. J. Heat Fluid Flow* 30, 691 **(2009)**.
48. C. A. N. de Castro, S. M. S. Murshed, M. J. V. Lourenco, F. J. V. Santos, M. L. M. Lopes, and J. M. P. Franca, *Int. J. ThermSci.* 62, 34 **(2012)**.
49. H. O'Hanley, J. Buongiorno, T. McKrell, and L. W. Hu, *AdvMechEng.* 181079 **(2012)**.
50. D. Shin and D. Banerjee, *J. Heat Trans.-T Asme* 135, 032801 **(2013)**.
51. D. Shin and D. Banerjee, *Int. J. Heat Mass Transfer* 74, 210 **(2014)**.
52. L. S. Sundar, M. H. Farooky, S. N. Sarada, and M. K. Singh, *Int-Commun. Heat Mass* 41, 41 **(2013)**.
53. J. Philip, P. D. Shima, and B. Taj, *Appl. Phys. Lett.* 91 **(2007)**.
54. T. Aguilar, J. Navas, A. Sanchez-Coronilla, E. I. Martın, J. J. Gallardo, P. Martinez-Merino, R. Gomez-Villarejo, J. C. Piñero, R. Alcantara, and C. Fernandez-Lorenzo, *ApplEnergy* 211, 677 **(2018)**.
55. R. Gomez-Villarejo, J. Navas, E. I. Martın, A. Sanchez-Coronilla, T. Aguilar, J. J. Gallardo, D. De los Santos, R. Alcantara, C. Fernandez-Lorenzo, and J. Martin-Calleja, *J. Mater. Chem. A* 5, 12483 **(2017)**.
56. J. Navas, A. Sanchez-Coronilla, E. I. Martin, M. Teruel, J. J. Gallardo, and T. Aguilar, *Nano Energy* 27, 213 **(2016)**.

Consent of the co-authors

We, the undersigned co-authors of the scientific article entitled "*Ag-based nanofluidic system to enhance heat transfer fluids for concentrating solar power: Nano-level insights*" and published in Applied Energy, under reference number *Appl Energ, 194, (2017), 19-29*; declare that, D. **Roberto Gómez Villarejo** has taken an active role in producing and drafting of the aforementioned article, making the following contributions:

- Design and preparation of the silver nanofluids.
- Monitoring over time the stability of the silver nanofluids prepared.
- Experimental characterization of the silver nanofluids, taking into account their thermal and rheological properties.
- Estimation of the efficiency of the silver nanofluids for use as heat transfer fluids.
- Theoretical study using Molecular Dynamics simulations of the nanofluid system to calculate thermal and transport properties.
- Theoretical study using Molecular Dynamics simulations of structural properties to analyse the molecular organisation and distribution of the nanofluid system.

And we give our consent for the aforementioned article to form a part of the Doctoral Thesis entitled **"*Nanofluids based on metal nanoparticles with optimized thermal properties for being used in thermosolar industry*"** and explicitly and formally waive the right for this article to be cited as part of any other Doctoral Thesis.

Cádiz, 12 December, 2018.

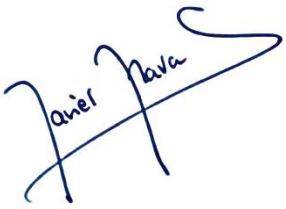

Dra. Dª. Elisa Isabel Martín Fernández Dr. D. Francisco Javier Navas Pineda

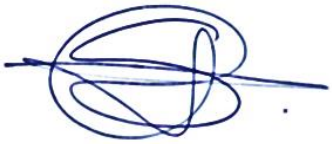

Dr. D. Antonio Sánchez Coronilla

Dra. Dª. María Teresa Aguilar Sánchez

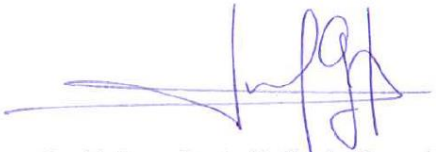

Dr. D. Juan Jesús Gallardo Bernal

Dr. D. Rodrigo Alcántara Puerto

Dra. Dª. Desiré De los Santos Martínez

D. Iván Carrillo Berdugo

Dra. Dª. Concepción Fernández Lorenzo

We, the undersigned co-authors of the scientific article entitled "*Preparation of Au nanoparticles in a non-polar medium: obtaining high-efficiency for Concentrating Solar Power. An experimental and theoretical perspective*" and published in the Journal of Materials Chemistry A, under reference number *J. Mater. Chem. A, 5, (2017), 12483*; declare that, D. **Roberto Gómez Villarejo** has taken an active role in producing and drafting of the aforementioned article, making the following contributions:

- Synthesis and characterization of gold nanoparticles.
- Design and preparation of the gold nanofluids.
- Monitoring over time the stability of the gold nanofluids prepared.
- Study of possible physical and chemical changes in the gold nanofluids prepared after the application of thermal cycles.
- Experimental characterization of the gold nanofluids, taking into account their thermal and rheological properties.
- Estimation of the efficiency of the gold nanofluids for use as heat transfer fluids.
- Theoretical study using Molecular Dynamics simulations of the nanofluid system to calculate thermal and transport properties.
- Theoretical study using Molecular Dynamics simulations of structural properties to analyse the molecular organisation and distribution of the nanofluid system, paying particular attention to the role of the surfactant.

And we give our consent for the aforementioned article to form a part of the Doctoral Thesis entitled **"*Nanofluids based on metal nanoparticles with optimized thermal properties for being used in thermosolar industry*"** and explicitly and formally waive the right for this article to be cited as part of any other Doctoral Thesis.

Cádiz, 12 December, 2018.

Dr. D. Francisco Javier Navas Pineda Dra. Dª. Elisa Isabel Martín Fernández

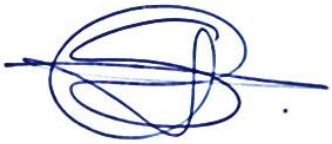

Dr. D. Antonio Sánchez Coronilla

Dra. Dª. María Teresa Aguilar Sánchez

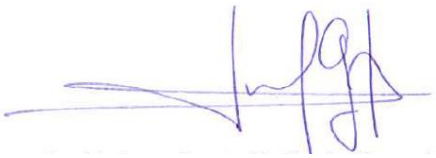

Dr. D. Juan Jesús Gallardo Bernal

Dra. Dª. Desiré De los Santos Martínez

Dr. D. Rodrigo Alcántara Puerto

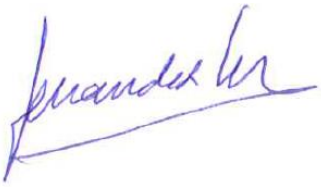

Dra. Dª. Concepción Fernández Lorenzo

Dr. D. Joaquín Martín Calleja

We, the undersigned co-authors of the scientific article entitled "*Towards the improvement of the global efficiency of concentrating solar power plants by using Pt-based nanofluids: The internal molecular structure effect*" and published in Applied Energy, under reference number *Appl.Energ, 228, (2018), 2262-2274*; declare that, D. **Roberto Gómez Villarejo** has taken an active role in producing and drafting of the aforementioned article, making the following contributions:

- Synthesis and characterization of platinum nanoparticles.
- Design and preparation of the platinum nanofluids.
- Monitoring over time the stability of the platinum nanofluids prepared, taking into account the possible effects of surfactants and ultrasound treatment.
- Experimental characterization of the platinum nanofluids, taking into account their thermal and rheological properties.
- Estimation of the efficiency of the platinum nanofluids for use as heat transfer fluids.
- Theoretical study using Molecular Dynamics simulations of structural properties to analyse the molecular organisation and distribution of the nanofluid system, paying particular attention to the role of each surfactant

And we give our consent for the aforementioned article to form a part of the Doctoral Thesis entitled **"*Nanofluids based on metal nanoparticles with optimized thermal properties for being used in thermosolar industry*"** and explicitly and formally waive the right for this article to be cited as part of any other Doctoral Thesis.

Cádiz, 12 December, 2018.

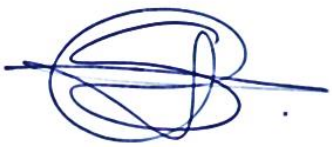

Dra. Dª. Elisa Isabel Martín Fernández Dr. D. Antonio Sánchez Coronilla

Dra. Dª. María Teresa Aguilar Sánchez

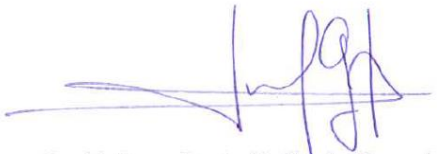

Dr. D. Juan Jesús Gallardo Bernal

Dª. Paloma Martínez Merino

D. Iván Carrillo Berdugo

Dr. D. Rodrigo Alcántara Puerto

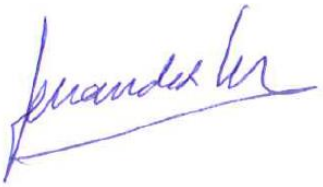

Dra. Dª. Concepción Fernández Lorenzo

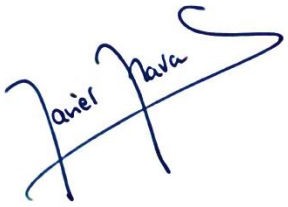

Dr. D. Francisco Javier Navas Pineda

We, the undersigned co-authors of the scientific article entitled "*Experimental characterization and theoretical modelling of Ag and Au-nanofluids: a comparative study of their thermal properties*" and published in the Journal of Nanofluids, under reference number *J.Nanofluids, 7, (2018), 1-10*; declare that, D. **Roberto Gómez Villarejo** has taken an active role in producing and drafting of the aforementioned article, making the following contributions:

- Synthesis of gold nanoparticles.
- Design and preparation of the gold nanofluids.
- Monitoring over time the stability of the gold nanofluids prepared.
- Experimental characterization of the gold nanofluids, taking into account their thermal and rheological properties.
- Estimation of the efficiency of the gold nanofluids for use as heat transfer fluids.
- Theoretical study using Molecular Dynamics simulations of the nanofluid system to calculate thermal properties.
- Theoretical study using Molecular Dynamics simulations of structural properties to analyse the molecular organisation and distribution of the nanofluid system.

And we give our consent for the aforementioned article to form a part of the Doctoral Thesis entitled **"*Nanofluids based on metal nanoparticles with optimized thermal properties for being used in thermosolar industry*"** and explicitly and formally waive the right for this article to be cited as part of any other Doctoral Thesis.

Cádiz, 12 December, 2018.

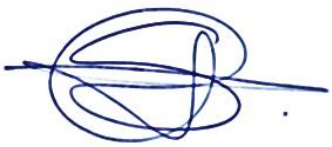

Dra. Dª. Elisa Isabel Martín Fernández Dr. D. Antonio Sánchez Coronilla

Dra. Dª. María Teresa Aguilar Sánchez

Dª. Miriam Teruel Sibón

Dr. D. Rodrigo Alcántara Puerto

D. Iván Carrillo Berdugo

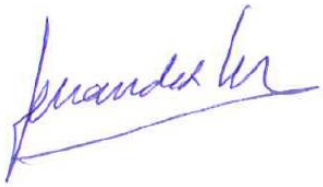

Dra. Dª. Concepción Fernández Lorenzo

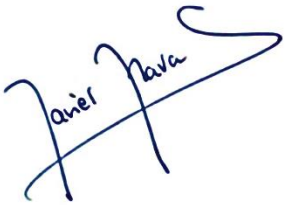

Dr. D. Francisco Javier Navas Pineda